AD-A032 130 SYRACUSE UNIV N Y DEPT OF ELECTRICAL AND COMPUTER E--ETC F/G 9/5
SOLID STATE ARRAY STUDIES RELEVANT TO OTP REGULATIONS. PART 1. --ETC(U)
AUG 76 D W GRIFFIN F30602-75-C-0121
UNCLASSIFIED RADC-TR-76-241-PT-1 NL

1 OF 3
AD A032130

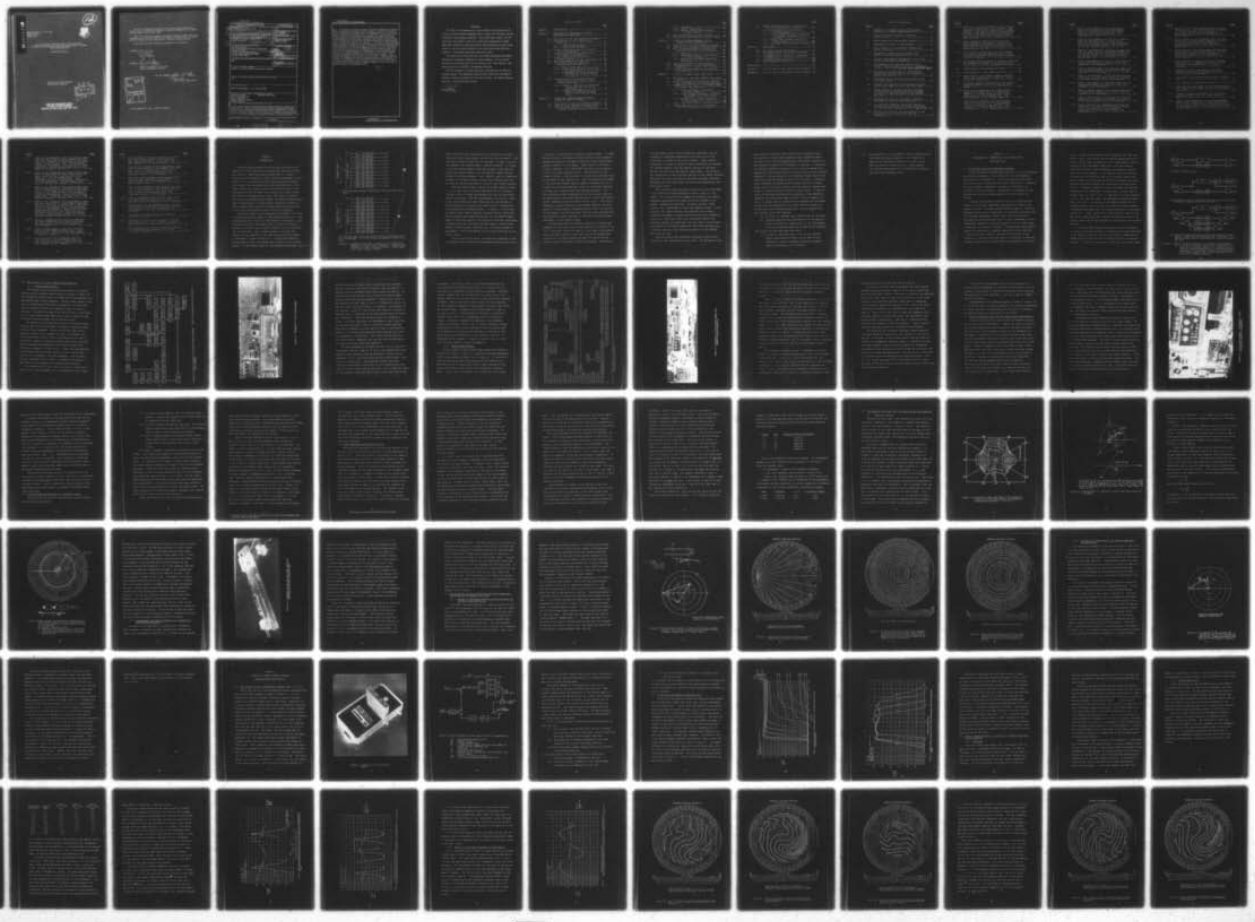

12

RADC-TR-76-241, Pt 1 (of two)
Interim Report
August 1976

SOLID STATE ARRAY STUDIES RELEVANT TO OTP REGULATIONS
Evaluation of Amplitude and Phase Characteristics of Microwave Solid State Amplifier

Syracuse University

ROME AIR DEVELOPMENT CENTER
AIR FORCE SYSTEMS COMMAND
GRIFFISS AIR FORCE BASE, NEW YORK 13441

Some of the charts in this report are of poor quality reproduction. However, this is unimportant because the relevant information on the charts is sufficiently clear to the reader.

This report has been reviewed by the RADC Information Office (OI) and is releasable to the National Technical Information Service (NTIS). At NTIS it will be releasable to the general public, including foreign nations.

This report has been reviewed and approved for publication.

APPROVED: R H Chilton

R. H. CHILTON
Project Engineer

APPROVED: Rudolf C Paltauf

RUDOLF C. PALTAUF, Lt Col, USAF
Chief, Surveillance Division

FOR THE COMMANDER: John P. Huss

JOHN P. HUSS
Acting Chief, Plans Office

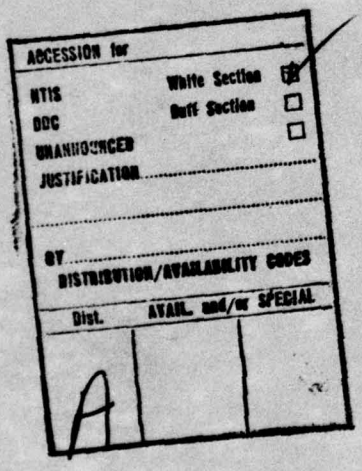

Do not return this copy. Retain or destroy.

UNCLASSIFIED

SECURITY CLASSIFICATION OF THIS PAGE (When Data Entered)

REPORT DOCUMENTATION PAGE

READ INSTRUCTIONS BEFORE COMPLETING FORM

1. REPORT NUMBER: RADC-TR-76-241, Pt-1 (of two)	2. GOVT ACCESSION NO.
3. RECIPIENT'S CATALOG NUMBER	
4. TITLE (and Subtitle): SOLID STATE ARRAY STUDIES RELEVANT TO OTP REGULATIONS. Evaluation of Amplitude and Phase Characteristics of Microwave Solid State Amplifier. Part 1.	5. TYPE OF REPORT & PERIOD COVERED: Interim Report. Sep 74 — Feb 76
	6. PERFORMING ORG. REPORT NUMBER: N/A
7. AUTHOR(s): Donald W. Griffin	8. CONTRACT OR GRANT NUMBER(s): F30602-75-C-0121
9. PERFORMING ORGANIZATION NAME AND ADDRESS: Syracuse University, Dept of Electrical and Computer Engineering, Syracuse NY 13210	10. PROGRAM ELEMENT, PROJECT, TASK AREA & WORK UNIT NUMBERS: 62702F 95670003 17 00
11. CONTROLLING OFFICE NAME AND ADDRESS: Rome Air Development Center (OCTE), Griffiss AFB NY 13441	12. REPORT DATE: August 1976
	13. NUMBER OF PAGES: 226 (12) 222 p.
14. MONITORING AGENCY NAME & ADDRESS (if different from Controlling Office): Same	15. SECURITY CLASS. (of this report): UNCLASSIFIED
	15a. DECLASSIFICATION/DOWNGRADING SCHEDULE: N/A

16. DISTRIBUTION STATEMENT (of this Report)

Approved for public release; distribution unlimited.

17. DISTRIBUTION STATEMENT (of the abstract entered in Block 20, if different from Report)

Same

18. SUPPLEMENTARY NOTES

RADC Project Engineer: R. H. Chilton (OCTE)

19. KEY WORDS (Continue on reverse side if necessary and identify by block number)

Phased Array Radar
Microwave Solid State
Solid State Amplifiers
BiPolar Transistor
BiPolar Transistor Modules
TRAPATT Amplifiers

20. ABSTRACT (Continue on reverse side if necessary and identify by block number)

A study has been made of microwave amplifier modules designed for phased array antenna service. Output amplitude and phase behavior have been measured under mismatched load conditions at fundamental and harmonic frequencies. A bridge has been used that is capable of being balanced at fundamental, second and third harmonics. Reference signals at these frequencies are adjusted in amplitude and phase to cancel the corresponding components produced by the amplifier under

DD FORM 1 JAN 73 1473 EDITION OF 1 NOV 65 IS OBSOLETE

UNCLASSIFIED

SECURITY CLASSIFICATION OF THIS PAGE (When Data Entered)

406737

test. The amplitude and phase variations of the waves travelling out of the amplifier are measured as a function of load mismatch. A standard test load is used to present to the amplifier output, the impedances that lie on a selected series of VSWR circles on a Smith chart. The test load is not a replica of the dynamic impedance of any particular chosen element in a phased array but the data gathered can be used to provide amplitude and phase data for radiation pattern calculations if the dynamic impedance of each antenna element is known. Results obtained using the load are presented as equi-power and equi-phase contours in the overall region of load variation. L- and S-band bipolar transistor modules designed for phased array antenna service and various experimental S-band TRAPATT amplifiers have been studied. In the modules it is found that harmonic levels are below 35 dB down on the fundamental and are subject to large variations with load change. In some cases the variation of harmonic output is a function of the load impedance at the fundamental but more frequently is depends upon the impedance presented at the harmonic. In the case of TRAPATTS it has been essential to operate them in a two circulator assembly. Less variation of harmonic level is observed with load change. Levels only 23 dB down on the fundamental are found in some units whereas in others greater than 50 dB has been observed. In the former higher level case it was found that behavior was not affected greatly by changing the diode in the circuit and it is inferred from this that behavior regarding harmonic levels in the output is mainly determined by the microwave circuit.

END ABSTRACT

EVALUATION

The Office of Telecommunication's Policy Manual of Regulations and procedures for Radio Frequency Management dated 1 January 1973 contained a section pertaining to radar spectrum emissions. These regulations, agreed to by DOD could have a major impact in the use of solid state transmitters in phased array radars because the regulations had not been interpreted for phased array systems nor had the spectral emission of the solid state devices been fully evaluated. This program investigated these vital areas.

The results of the effort show that both Bipolar Transistors and TRAPATT amplifiers are reasonable candidates for array elements. Thus the initial concern over the spectral purity of the devices is not a major problem. This program was part of RADC-TPO-5, Surveillance Technology.

The work reported on in these reports was conducted under the RADC Post Doctoral Program. The experimental work was done at RADC while the computer analysis of arrays was conducted at Syracuse University. The reports complete this task of the Post Doctoral Program.

R. H. CHILTON
Project Engineer

TABLE OF CONTENTS

LIST OF ILLUSTRATIONS

CHAPTER 1

INTRODUCTION

There are many approaches to the design, construction and operation of active phased array antennas that are both possible and practical. With the coming implementation of a Manual of Regulations and Procedures for Radio Frequency Management to radar systems, it is a major task at this stage to determine whether those regulations, developed mainly from experience with conventional radars, are likely to lead to severe difficulties in the introduction of active phased array antennas into radar systems. The Office of Telecommunication Policy (OTP) Manual recognizes this point with a footnote that states, "For radars employing more than a single emitter, including certain phased-array radars, a special method may be required in establishing the maximum level of emissions and determining levels outside the bandwidth."

Of the many types of active phased array antennas, this study is concerned with those types of array that incorporate solid state microwave amplifiers that drive the elements of the antenna. Such amplifiers operate at high power levels and their efficiency of operation is a prime factor in their selection for the application from the beginning. Thus, a simple example of an array that incorporates one amplifier of the type studied with each element of the antenna is shown in Figure 1.1. A module may comprise a digital phase shifter, a microwave power amplifier and an antenna element. In the example shown, ten such modules are employed. (Ref. 1)

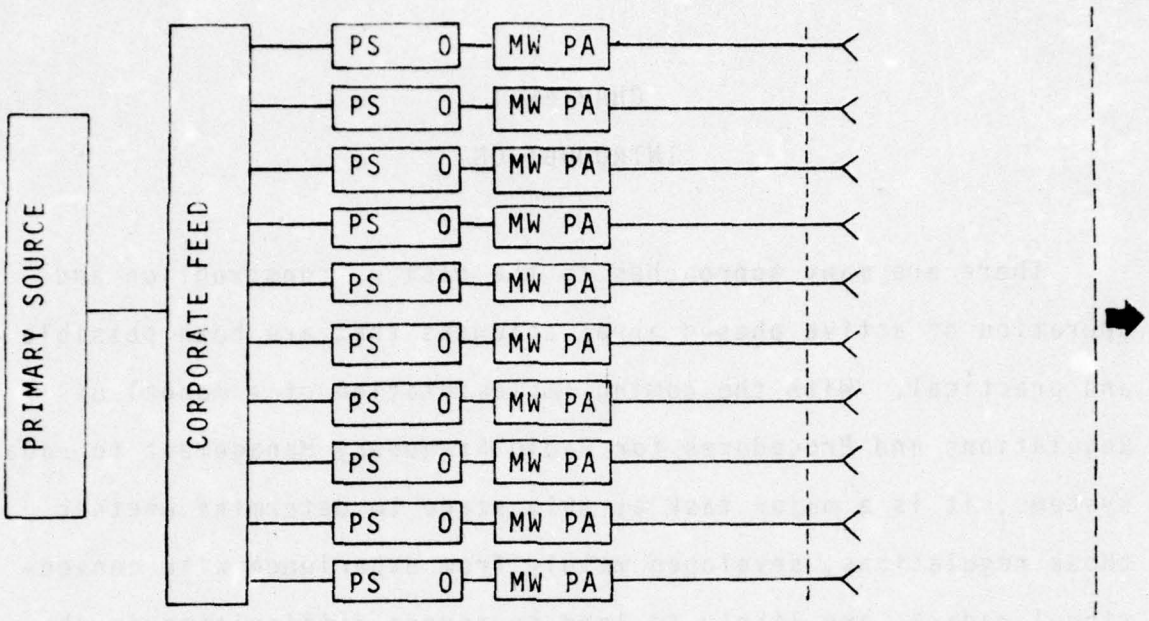

(a) Radiated beam steered broadside; all phase shifters set to zero.

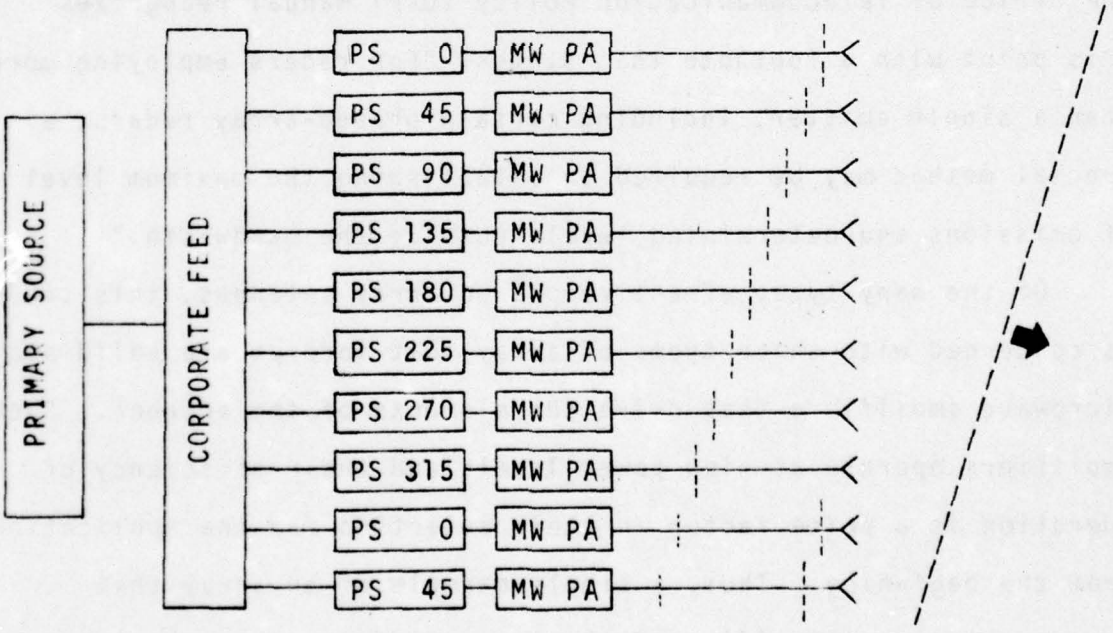

(b) Radiated beam deflected through maximum angle; phase shifters incremented 1 bit (45°) from one element to next adjacent.

Figure 1.1 Example of the type of phased array antenna preferred for highest power operation. A module compromises a three bit phase shifter, a power amplifier and an antenna element.

Power from the primary source would be divided into ten equal amplitude, equal phase signals, one for driving each module. With the digital phase shifters all set the same, in Figure 1.1(a) to zero degrees, the radiated beam is steered broadside. In Figure 1.1(b) the radiated beam is deflected through a large angle by setting the phase shifters 1 bit (45 degrees) larger from one element to the next adjacent. Thus, ideally, phase is controlled by means of the phase shifter only and the microwave amplifier provides the desired amplitude of drive for each antenna element.

There are several ways in which the simple scheme of Figure 1.1 is an ideal that can only be approached and not precisely realized, and it is these shortcomings that must be held within certain tolerances if the OTP requirements are to be met. Many of the shortcomings have been recognized and incorporated in specifications for the design and construction of experimental active phased array antenna systems. It applies, in particular, to modules using state-of-the-art microwave bipolar transistors. Other microwave semiconducting devices, such as TRAPATT diodes, appear to have the potential for service as efficient, high power, microwave amplifiers, but have not been tested in phased array antenna systems and are, therefore, at a less mature stage of development. Their shortcomings for this application may not be as well known.

A basic problem that occurs in phased array antennas is that the impedance seen looking into any elemental antenna port varies

as the beam is steered over its range of spatial angles. To steer the beam in space, the phase of the excitation of each element is changed and, therefore, the power coupled to a given element from adjacent elements is also changed. Hence, what is called the "dynamic impedance," is a complicated function of the direction in which main beam radiation occurs. The excitation of the elemental antenna is the resultant of incident and reflected waves on the feeder at the antenna port. Thus, the magnitude and phase of the excitation depends upon the dynamic impedance and, as it changes from a matched condition, errors in excitation amplitude and phase occur compared with ideal matched operation. This basic problem has been recognized and the only control that can be exercised over the errors that may result, is for the range of dynamic impedance to be held within certain limits. This can be regarded as a design problem for the antenna engineer, and each array will exhibit dynamic impedance behavior that is a function of the geometry from the feed ports into the array, together with the excitation strategy employed in steering the radiation beam throughout its total angular range.

The microwave amplifier designer identifies a varying load impedance for the final stage of amplification as a threat to its life. Transistor failure can result if the output line standing wave ratio (SWR) exceeds a level specified by the manufacturer. A three-port circulator between the amplifier output and the antenna input is introduced to serve two purposes. Reflections

from the antenna input, under transmitting conditions, can be absorbed in a matching termination on the third port of the circulator, or simply it acts as an isolator. Under receive conditions, it serves to transmit signals received by the antenna via transmit-receive (T-R) and channel switches to the phase shifter and then on to the receiver input stages. Specification and construction of the circulator and the T-R and channel switches should be such that, not only are the above-described functions performed, but also errors that can arise from imperfections are held within limits.

This raises difficulties that are not minor as will be shown in the studies of various amplifiers given in detail in this report. For a specific active phased array antenna, the dynamic impedance range needs to be known and the performance of the module, incorporating amplifier, circulator switches, phase shifter, etc., determined for that load impedance range. A wide range of tests under matching load conditions are already a customary requirement in module manufacture and are an expensive part of it. Additional tests under simulated mismatch load conditions would incur additional cost and require justification. The studies in this report demonstrate the nature and magnitude of effects that may occur and provide details of test methods that could be used.

Operation within the fundamental frequency range has been implicit in the introduction to this point. The OTP Manual places

upper bounds on emission levels outside the fundamental band. Each amplifier in each module generates these components which are more or less radiated depending upon the dynamic impedance of each elemental antenna at the frequency in question. To determine the complete radiation characteristics of an active phased array antenna the relative amplitude and relative phase of each frequency component in the excitation of each elemental antenna needs to be known along with the geometric details of the array. A companion report addresses the computational problems that occur, taking proper account of mutual coupling using the method of moments and given all of the excitation statistics stated above. If specific values of amplitude and phase can be measured at each important frequency from each module then the task is at its simplest, at least in concept, but all modules must be measured and the amount of data would be comparable to or exceed that which takes up a significant part of manufacturing costs. Such an approach was not followed in this work because,

(i) an array or a complete set of modules was not available

(ii) resources would not have permitted all of the measurements to be made on a large array, of say, 100 modules, nor for an automated measuring assembly to be developed.

The studies that have been made show that,

(i) the task as described above is not at its simplest because amplitudes and phases are all more or less dependent on dynamic impedance in practical modules despite the presence of a circulator

(ii) data measured on a large number of modules under matching load conditions may be subject to such large errors, compared with the correct operational values, as to make the effort and resources used, largely wasted. This applies particularly to the prediction of harmonic and out-of-band radiation levels.

CHAPTER 2

MEASUREMENT OF HARMONICALLY RELATED AMPLITUDE AND PHASE DATA

2.1 Principles of the Instrumentation Assembly

In well designed microwave power amplifiers it is most probable that the main components in the output will be the fundamental excitation and its harmonics. It has been explained that determination of relative amplitude and relative phase data is necessary for each frequency component if the spatial distribution of radiation is to be calculated. Conventional instruments are not suitable for making such measurements for various reasons as follows.

Advanced test equipment assemblies exist for measuring the behavior of microwave components, subassemblies or modules and complete systems. Microwave network analyzers measure scattering parameters and provide a simple means of completely characterizing the microwave performance of both active and passive devices provided that the devices are linear or that a knowledge of their fundamental response to sinusoidal signals within a linear range of behavior is all that is required. Microwave spectrum analyzers measure the amplitude of frequency components and by comparison of input and output signals, a measure of the effects of non-linearity in producing additional spectral components is obtained. Microwave sampling oscilloscopes measure the waveforms of periodic

signals in the microwave region and by comparison of input and output signals, they can be used to identify mechanisms giving rise to various types of departure from linear behavior. Fourier analysis of the time-domain output will yield the relative amplitude and phase of the fundamental and harmonics present. There is a limit, however, to the accuracy with which the data on harmonics can be obtained and for the harmonic levels that are of concern in conforming with the OTP requirements on radar emissions the method appears too inaccurate to give any useful results. Microwave bridges are usually assembled from discrete components in the laboratory in various ways. A basic type of bridge, shown in Figure 2.1(a), is operated at a single frequency in such a way that the signal that propagates through the device under test (DUT) is nulled out in the detector shown here as a spectrum analyzer (SA), by means of a reference signal adjusted in amplitude and phase with a calibrated attenuator (A) and phase shifter (P). Either insertion loss and electrical length of the DUT can be determined or the relative amplitude and phase of the output signal from the DUT measured as a function of some variable quantity.

It has been found that sensitive and accurate measurements of relative amplitude and phase of harmonically related components in the output of amplifier modules can be made by combining the bridge balancing principle with the sensitivity of the spectrum analyzer. Of particular relevance is that this can be done under

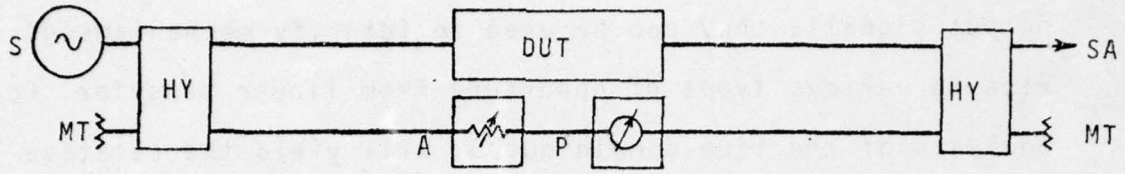

(a) Basic microwave bridge.

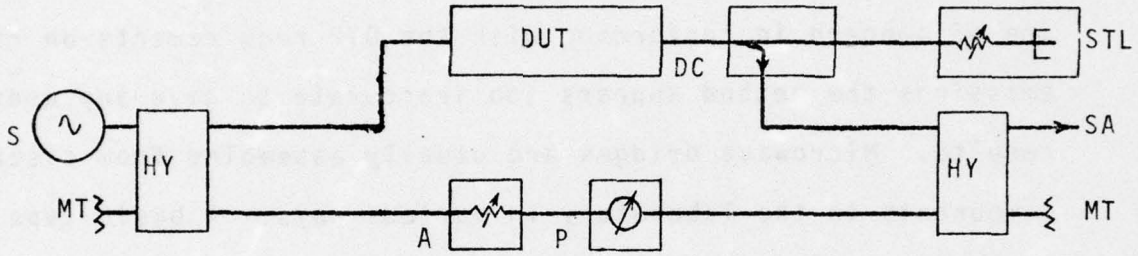

(b) Bridge for measuring amplifier behaviour under various load conditions. Used at L-band in this work.

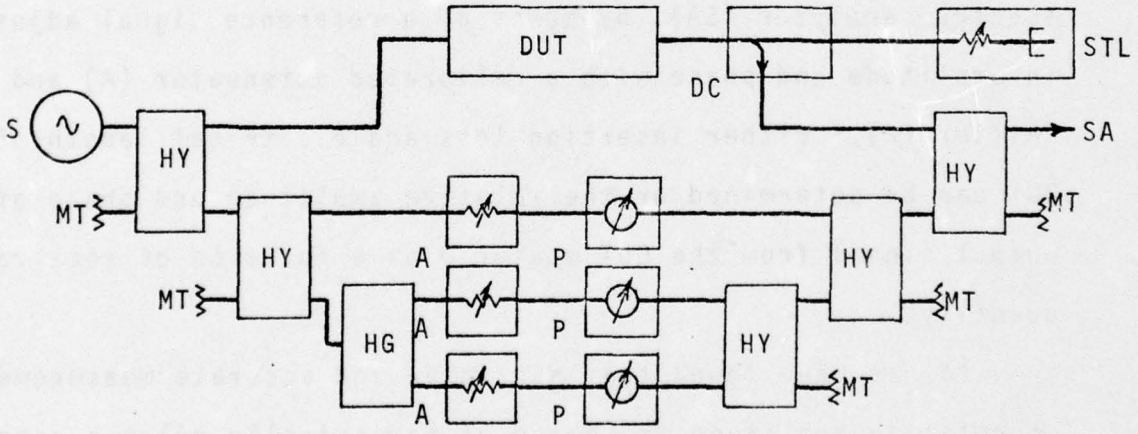

(c) Bridge for measuring relative amplitude and phase of fundamental, second and third harmonics from the output of an amplifier under various load conditions. Used at S-band in this work.

Figure 2.1 Simplified block diagrams of L-band and S-band bridges.
Key: S, source; HY, hybrid; DUT, device or amplifier under test; DC, directional coupler; STL, standard test load; MT, matched termination; A, calibrated variable attenuator; P, calibrated variable phase shifter(usually line stretcher); HG, harmonic generator and filtering; SA, spectrum analyser.

conditions of any mismatch termination as the load for the amplifier output. Figure 2.1(b) shows the simple modifications to the basic bridge that are necessary to allow measurements at the fundamental frequency. The gain in the amplifier, which is the DUT, results in an output signal level which cannot be balanced by the reference path. A directional coupler with a coupling factor about equal to the amplifier gain provides a fraction of the output suitable for combining with the reference channel. Most of the output remains in the main line through the coupler and can be fed to any termination. In fact, a standard test load is used in this work and it can be set to correspond almost any point on the Smith chart. An important point to note as one of the operating principles of this assembly is that relative amplitude and phase measurements are made on the wave that travels forward from the amplifier output port to the load. If the load is a matching termination, this wave corresponds to the power absorbed by the load. Under mismatch conditions this assembly can be used to study the way in which the forward wave at the amplifier output varies with load conditions. Thus, effects arising within practical modules can be measured separately from the effects that reflection from the load have on the resultant quantities at the load.

Figure 2.1(c) illustrates how this principle can be extended to permit balancing of second and third harmonic that may be present along with the fundamental at the output of the amplifier.

The directional coupler must be sufficiently wideband to preserve the correct relative amplitude and phase of components in the coupled path as in the wave travelling toward the STL. Three reference signals are produced, independently controlled in amplitude and phase, and then combined with each other and the components from the DUT. Thus, there are signal and reference components at fundamental and second and third harmonics at the input to the spectrum analyzer. Complete balance of this harmonic bridge is obtained by successively nulling fundamental, second and finally third harmonics. Second and third harmonic reference signals are phase-locked to the fundamental. Changes in amplitude and phase data with changes in the STL can be measured with the assembly. If the phases of the harmonics need to be referred to the fundamental, then, it is necessary to establish this between the reference paths, where levels are high, with a sampling oscilloscope.

Two bridges have been assembled for evaluation of amplifier module performance, an L-band one of the simpler configuration shown in Figure 2.1(b) and an S-band one having the total capability illustrated in Figure 2.1(c). A brief description of each assembly is given to begin with, so that a grasp of the components required to achieve accurate and reasonably convenient operating procedure can be obtained. In sections that follow, details of specific aspects of each assembly are given in order to clarify important features in the design and component choice found suitable in each case.

2.2 Description of L- and S-Band Bridge Assemblies

2.2.1 L-Band Bridge Assembly

The assembly used for evaluating the behavior of L-band modules under mismatched load conditions is shown in Figure 2.2. The fundamental signal source is a sweep oscillator operated cw at the desired input signal frequency. The oscillator output is fed into a PIN modulator driven with a pulsed bias source so that 100 microsecond rf pulses at a repetition rate of 1 KHz are obtained. The peak pulse power of a few milliwatts is amplified with a travelling wave tube amplifier to give in excess of 500 milliwatts peak pulse power for driving the bridge.

The modules to be tested require only 30 to 100 milliwatts input so most of the source power is used as a reference signal in the bridge arrangement. Power to drive the input to the amplifier, which in this diagram is item 7, is provided via a 10 dB directional coupler, item 5, and monitored with item 6. Directional couplers associated with the input signal need only have a bandwidth corresponding to the range over which the excitation frequency is to be varied. Output from the amplifier is monitored with directional couplers, items 8 and 10, the latter being a wideband 1 to 4 GHz component. With it and a variable band pass filter, item 11, fundamental and harmonic amplitudes can be separately and successively monitored.

The reflection test unit, item 14, contains a directional coupler and a line stretcher and is incorporated in such a way

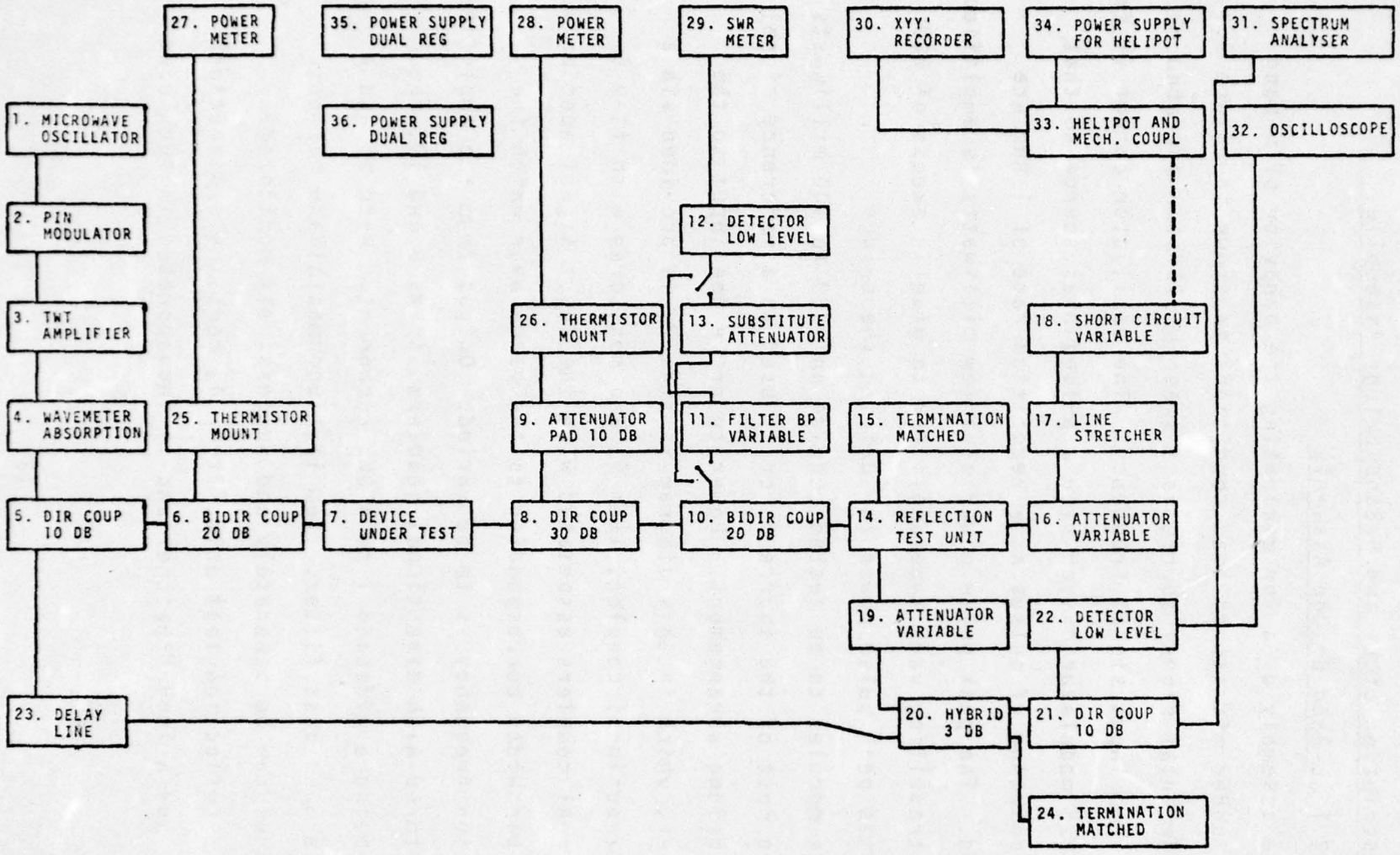

Figure 2.2 Block diagram of L-band bridge assembly. (Not all connections to electronic units shown)

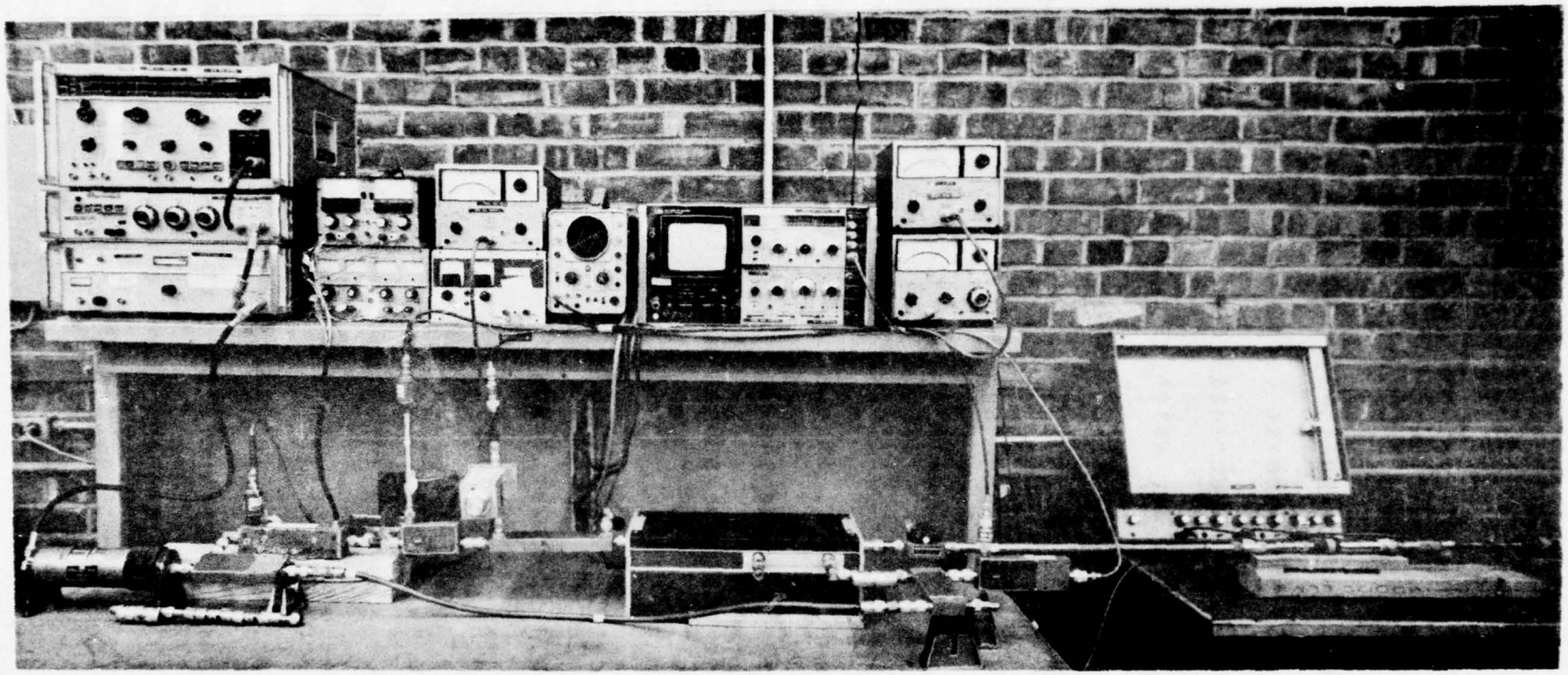

Figure 2.3 Photograph of L-band bridge assembly

that the coupled-out signal passes through the line stretcher, a variable attenuator and then to a hybrid, item 20, where it is combined with the reference signal which comes via item 23. The variable attenuator and the line stretcher are used to adjust amplitude and phase at the fundamental frequency until a null in the spectrum analyzer, item 31, which is connected to one of the hybrid's output ports via item 21, is observed. The spectrum of the reference signal is close to the ideal shape for a pulsed cw waveform which is desirable for accurate determination of bridge null conditions. Since the amplifier under test operates in class C conditions the output is independent of small variations in the input amplitude. Thus, if the device output spectrum about the fundamental is to be similar to that of the reference path, it is important that the pulsed wave envelope be as close to rectangular as practicable. The output from the amplifier will have harmonic components but only the coupling performance of item 10 need have sufficient bandwidth.

The load presented to the amplifier consists of a string of directional couplers, items 8, 10 and 14, that absorb only a few percent of the output and then an attenuator, item 16, a line stretcher, item 17, and a precision variable short circuit, item 18, on its output port. The attenuator reduces the unity reflection coefficient of the short circuit (ignoring the minus sign) to a lower value. Moving the short circuit alters the phase of the resultant reflection coefficient at the input side of the

attenuator. This type of load is such that approximately the same magnitude of reflection coefficient for a given value of attenuation is presented to every frequency component. The phase however, depends upon the distance from the output port of the module under test to the short circuit and the particular frequency component. Moving the short circuit causes the load impedance for each frequency component to move around a constant VSWR circle on the Smith chart. Because of the limited range of travel of the short circuit, a line stretcher is necessary if an overall movement of at least half a wavelength is to be achieved at L-band. A helipot is mechanically coupled to the micrometer thimble on the short circuit. This is used to provide a voltage proportional to short circuit position so that the output level at frequencies of interest can be plotted as a function of the phase of the load reflection on a XYY' recorder, item 30. A photograph of the assembly is shown in Figure 2.3 and a list of items in this assembly is given in Appendix 1.

2.2.2 S-Band Bridge Assembly

A block diagram of the S-band bridge assembly with harmonic balancing is shown in Figure 2.4. The pulse modulated fundamental signal source comprises items 1 to 6, 56 and 57. It functions in much the same way as the L-band source with the addition of a band-pass filter to prevent any harmonic power produced by this source from passing along the test and fundamental reference paths. Items 7 and 8 are hybrids for dividing the source power

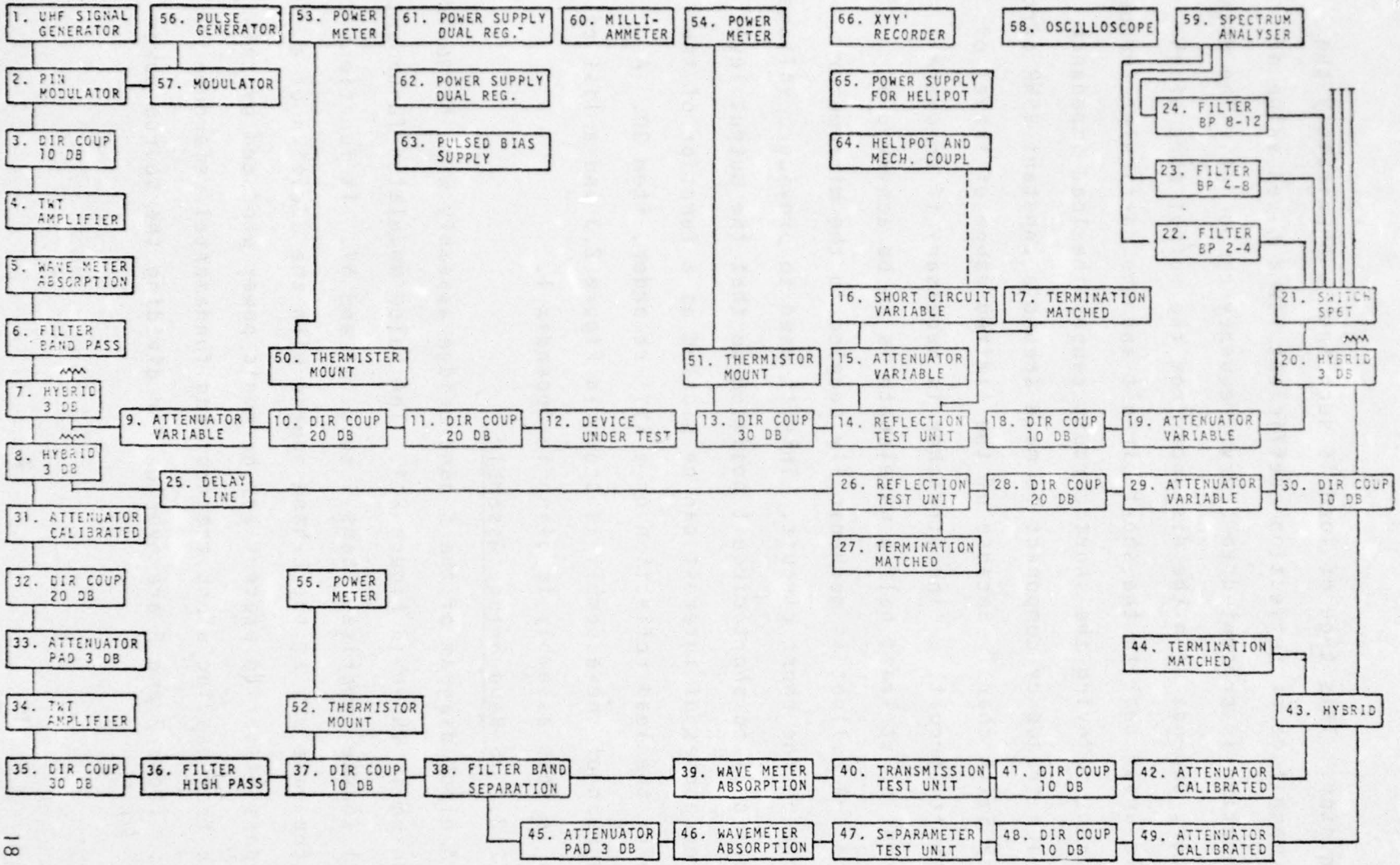

Figure 2.4 Block diagram of S-band bridge assembly with harmonic balancing. (Not all connections to electronic units shown).

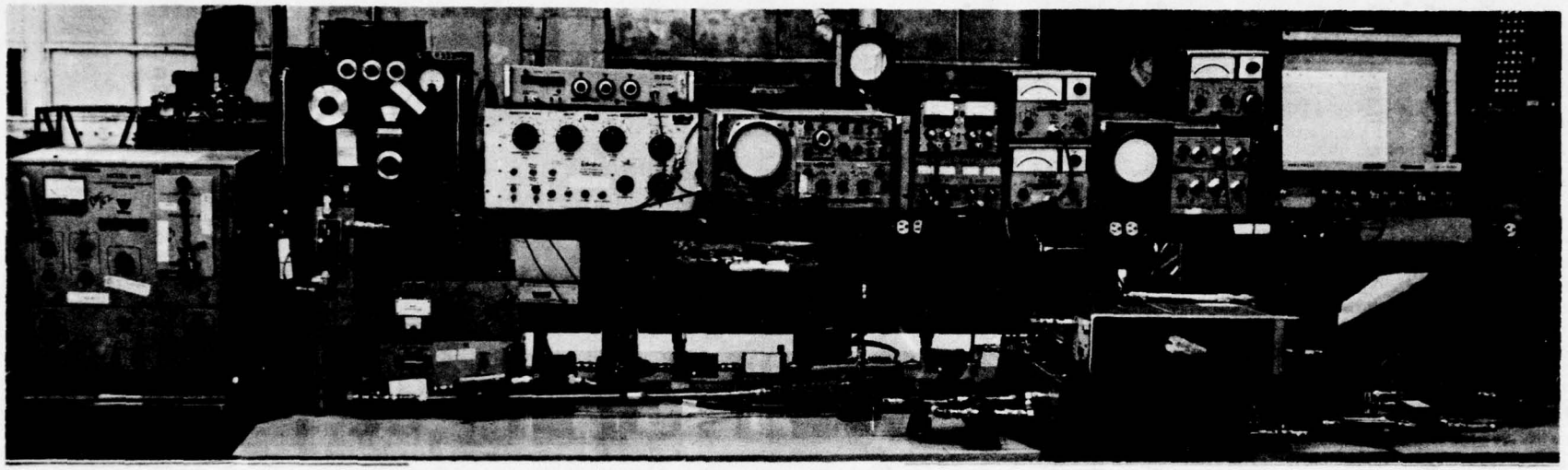

Figure 2.5 Photograph of S-band bridge assembly with harmonic balancing capability

into three parts, one half for the test path, one quarter for the fundamental reference path and one quarter for driving a harmonic generator for producing second and third harmonic reference signals.

Items 9, 10 and 11 control and monitor the power for driving the input of the amplifier, item 12 and items 13 and 14 monitor the output which passes to the load made up of items 15 and 16, the calibrated attenuator and precision short circuit used in the L-band bridge. The reflection test unit, item 14 couples a fraction of the output for combining with reference signals and gives constant amplitude dispersionless coupling over the frequency range 2 to 12.4 GHz level indication and control are possible with items 18 and 19 before the test output spectrum is combined with reference signals in item 20. The phase of all of the signal components coupled by the reflection test unit, item 14, can be shifted in phase because this unit is connected so that a precision line stretcher for 2 to 12.4 GHz carries the coupled signal to item 18.

The fundamental reference signal is obtained from item 8, passes via a delay line approximately equal in electrical length to the amplifier, item 12, to a second reflection test unit, item 26. This item is used simply for the precision line stretcher contained in it and could be replaced by such a component by itself. With it the phase of the fundamental reference can be independently adjusted and measured. Reference fundamental level

are monitored and controlled with items 28 and 29.

The remaining part of the source power from item 8 passes through control and monitor, items 31 to 33, into a travelling wave tube amplifier, item 34. This unit is nominally for operation in the 4 to 8 GHz range and when driven hard with a 3 GHz input produces second and third harmonic output which is separated from fundamental power with high-pass filter, item 36 and after monitoring the harmonics are separated from each other with item 38. Items 39 to 42 are used to check the frequency, shift the phase, monitor the level and control the amplitude of the second harmonic respectively. Items 45 to 49 perform similar functions with respect to the third harmonic. Items 40 and 47 could be replaced by precision calibrated line stretchers.

The second and third harmonic reference signals emerging from items 42 and 49 respectively, are combined in item 43 and one half of the power of each passes through item 30, where one tenth of the fundamental reference signal is combined with them. The three reference signals are now combined with fundamental and harmonics from the amplifier being tested and one half of the total of all these components passes from item 20 to a single pole six position switch for passage to the spectrum analyzer, item 50, via a chosen band pass filter from items 22 to 24. Spare positions on the switch may be used for other filters or monitoring the unfiltered resultant.

As with the L-band assembly plots of the amplitude of a chosen frequency component as a function of the phase of the load reflection can be made on item 66 with items 64 and 65 providing the voltage for x-axis deflection. Item 63 is used for TRAPATT amplifier biassing.

A photograph of the complete assembly is shown in Figure 2.5, a list of the items is given in Appendix 2 and close-up photographs of various sections of the assembly are also given in Appendix 2 to guide reassembly or duplication of the bridge.

2.3 Factors Affecting Choice of the Signal Source Sub-Assembly

For accurate operation of the bridge the fundamental source has to meet several requirements. Ideally the source should be a pure sinewave because any non-linearity in the amplifier under test will give rise to harmonics as well as the fundamental at the output. The amplifiers to be tested with the bridges that have been assembled, operate on a pulsed input signal basis with limits on the length, repetition frequency and duty cycle of the pulses. These are imposed to limit the effect of heat in the amplifier under test and it can be anticipated that some change in behavior may occur from the leading to the trailing edge of the pulse. Ideally the input pulses should have negligible rise and fall times compared with the pulse length and during the pulse there should be a simple sinewave variation. Such an input signal would appear on a spectrum analyzer as a sinc type ($\sin\theta/\theta$) distribution. A non-linear time-invariant

amplifier under test would produce spectral distributions about the fundamental and each harmonic of shape similar to that of the input. Departure from time-invariance, due to say heating, would lead to visible differences in spectral shape. The spectral distributions of signals in the reference paths should be similar to that of the source. If all distributions are similar then a null between a test and a reference signal will be possible with least ambiguity and therefore phase and amplitude measurements will have greatest accuracy.

A comparison was made between various ways of modulating different types of microwave source for the S-band bridge. The methods of modulation compared were, (i) internal pulse modulation provided within the microwave generator unit, (ii) external pulse modulation applied to the generator from a suitable pulse generator, and (iii) pulse modulating the steady output from the source with a PIN diode type modulator. The type of source compared were the backward wave oscillator and the reflex klystron type signal generator. The spectral distribution that was closest to ideal for bridge operation was that obtained from the PIN diode modulated output from a reflex klystron type signal generator. These items are shown in Figure 2.6 on the shelf above the bench. The performance obtained is dependent on the state of each instrument and should be verified from time to time. The choice indicated above is a desirable starting point for bridge accuracy.

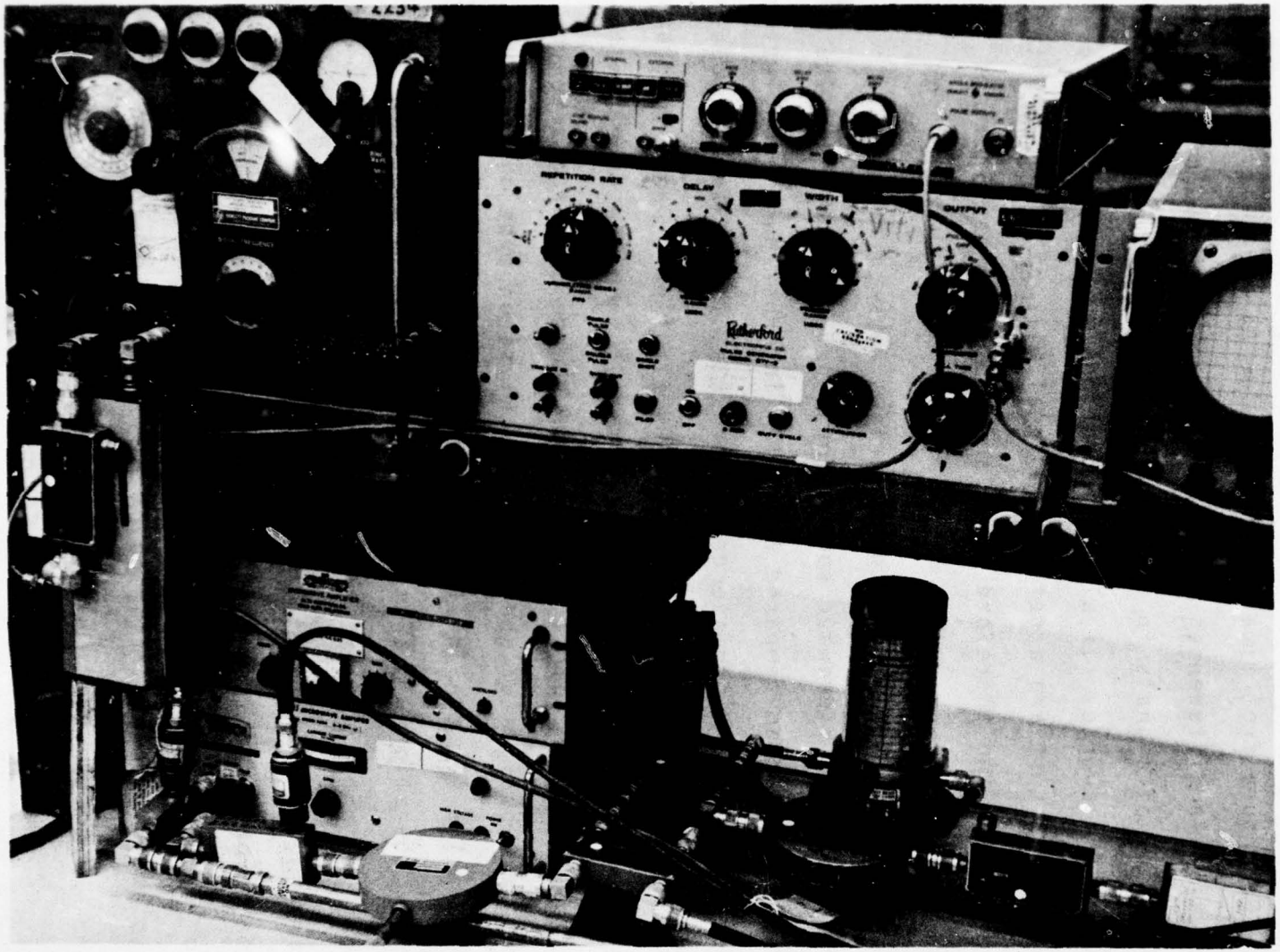

Figure 2.6 S-band bridge assembly - photograph of source and harmonic generation arrangements

2.4 Factors Affecting Bridge Sensitivity for Coherent Cancellation

In the interests of obtaining maximum sensitivity with the bridge it is desirable to work with as large an amplitude of signal from the amplifier under test as is practicable. That amplitude is not set by the available output from the amplifier under test but by the need to provide a fundamental reference signal of sufficient amplitude to allow nulling as large a fraction of the available output as possible. Thus, it is the available power from the bridge source that is the basic limitation and it is best to divide it between the test and reference paths as follows. Sufficient power must be provided to drive the input of the amplifier under test and the saturated travelling wave tube amplifier used to generate harmonics. Amplitude control is necessary on these two inputs. The rest of the available source power is used for the fundamental reference path.

The output from the amplifier under test passes to a standard test load and only a fraction of that forward travelling power can be coupled off for bridge balancing. The fraction should be such that the fundamental power in it is slightly less than the reference fundamental power, both being measured in a common line or at the spectrum analyzer. If this is done, then it also follows that the maximum practicable harmonic components from the amplifier under test will also be present for nulling with corresponding harmonic reference signals. The only way that larger harmonic components can be used is if the fundamental reference signal

(The reverse of this page intentionally left blank)

can be made as large as the fundamental component available from the amplifier under test. This is impractical for high output power amplifiers and is usually unnecessary. It also prevents testing with mismatched loads because the output is all absorbed in the termination on the output arm adjacent to the spectrum analyzer.

The other basic factor that determines sensitivity is the minimum signal level that can be accurately nulled. This depends upon the spectrum analyzer used and appears to be a signal level of the order of 10 dB above the noise level of that unit. The signal that remains when the best possible null is obtained is the difference between the spectral distributions of the test path and reference path signals about the chosen harmonic. This difference arises either because of differences between the amplitude or the phase distributions of the two signals or both differences existing simultaneously. The details of the spectral distribution of the source signal have an influence on the residual signal obtained at a null condition.

The harmonic reference paths should provide signal levels that are larger than the minimum set by the spectrum analyzer and the larger they are, the more convenient it is for measurement purposes. The range over which harmonic components from the amplifier under test can be measured will range from the minimum set by the spectrum analyzer to a maximum set by the combination of the largest harmonic reference available and the largest

amount by which the harmonic signal to be measured can be attenuated.

To realize the benefits of maximum sensitivity when nulling harmonic signals, it is necessary to prevent spurious harmonics being generated in the spectrum analyzer mixer by a signal at fundamental frequency. This is done by either, or both, of two methods in this bridge. Firstly, if the bridge is carefully balanced at the fundamental frequency then all but a small residual of the fundamentals will be absorbed by the termination on item 20 in Figure 2.4. Secondly, if a bandpass filter is switched into the path, i.e., item 23 or 24, that passes the desired harmonic, then the fundamental is prevented from reaching the spectrum analyzer input. It is reflected and will be absorbed in items 19, 17, 29, 42 and 49. This collection of absorbing items will not be an ideal termination but the residual fundamental is small and no problems appear due to re-reflections in the S-band bridge that was developed.

High sensitivity becomes particularly important when the duty cycle for pulsed operation is low. The spectral distribution is wider and the amplitude at the center where nulling is to be achieved is lower. Careful attention to the performance of the pulse modulation of the source is of greatest importance under these conditions.

2.5 Factors Affecting the Choice of a Harmonic Source

The source for the harmonic reference paths should satisfy the following requirements,

(i) it should provide adequate power at second and third harmonic to cancel the largest harmonic levels that may be produced by devices under test

(ii) it should produce the required power over the frequency range of operation of the bridge with as little adjustment or tuning of each frequency as possible

(iii) both the power output and the phase of each harmonic should remain stable to the extent that a condition of cancellation can be retained indefinitely in the bridge.

Four types of harmonic source were evaluated for use in the bridge. Mixer diodes were mounted in structures which had provision for matching the fundamental input drive and the harmonic output. A conversion loss of about 13 dB was readily achieved for second harmonic generation and about 20 dB for third harmonic generation. The drive level was limited to 5 mW and careful adjustment of the circuit was necessary when the drive frequency was changed over the test band 3.1 to 3.5 GHz. For the latter reason and also the low harmonic power this method of generation was unsatisfactory. Step recovery diodes were used instead of mixer diodes to allow higher drive levels and output levels. The need to adjust the circuit with change of frequency still applied so this modification was also unsatisfactory.

Injection locking of an oscillator was also considered but

the generation of the harmonic injection signal appeared to still leave the same basic problem. The fourth method studied was generation of harmonics with a travelling wave tube amplifier (TWTA). Though this requires expensive equipment and may appear to be a relatively inefficient "brute force" method, it satisfied all of the requirements for operating in the bridge.

Output from the fundamental source in the range 3.1 to 3.5 GHz is fed via a level setting attenuator and a directional coupler, items 31 and 32, to the input of a 4 to 8 GHz TWTA. The output is fed via a high pass (f_c = 5 GHz), item 36, which rejects any fundamental output, to a band separation filter, item 38, which accepts components in the band 4 to 12 GHz and passes those in the band 4 to 7.5 GHz to one output port and those in the band 7.5 to 12 GHz to a second output port. These output ports are the second and third harmonic ports respectively for fundamental operation extending from 2.6 to 3.7 GHz. In the studies presented in later chapters a fundamental range from 3.1 to 3.5 GHz was used. Harmonic outputs from these ports pass through line stretchers, items 40 and 47, which because they are part of special units, also introduce attenuation of 20 and 17 dB. Figure 2.7* shows the available harmonic reference path power levels at the inputs to items 42 and 49 as a function of frequency in the range 3.1 to 3.5 GHz with input power level as parameter. It is evident that the available levels range widely with input and frequency. However, if the input is held constant with frequency

* Although Figure 2.7 has been deleted from this report, the explanatory data may prove useful to the reader.

at 0.8 watts, sufficient second and third harmonic power is available for use in the reference paths. The TWT amplifier operates as a harmonic generator without perceptible change in performance, apart from average power, for duty cycles ranging from 0.001 to 0.1 in the experimental tests that were made. At the lower duty cycle tested, system sensitivity is least but for the amplifiers evaluated in this study harmonics as much as 50 dB below the fundamental could be balanced and their behavior with load change measured.

2.6 Phase Adjustment and Bridge Balancing

Reference has been made to the role that the spectral distributions of test and reference signal has in bridge balancing in section 2.2.1. Experience gained in evaluating various types of microwave amplifiers with the L- and S-band assemblies, shows that there is a technique to be learned in phase adjustment and bridge balancing. As well as observing the combined test and reference signals with the spectrum analyzer, the frequency domain view, it is important to observe the shape of the pulsed signal at various points in the system. In doing this careful consideration should be given to (i) the monitoring item response, be it directional coupler or hybrid, (ii) the detector response and (iii) the operation of the oscilloscope. The response of the monitoring item is particularly important for accurate phase measurements at harmonic frequencies. The detector response should be such that the rise and fall times of the pulse envelope

(The reverse of this page intentionally left blank)

at the output are an accurate replica of the envelope of the microwave pulse and the detector sensitivity should be constant and as high as practicable over the fundamental and harmonic frequency ranges. Careful operation of the oscilloscope is important because the output from the amplifier under test can exhibit features that may affect oscilloscope triggering. For example, in testing microwave bipolar transistor amplifiers that operate in the class C mode, the output envelope may have steps in the leading edge under certain drive conditions. If this condition of operation is not identified, then a false balance condition could be recorded by working with the spectrum analyzer display.

If a zero or null in the detector is obtained then total cancellation of all frequency components within the band fed to the detector has been achieved. In general, with a signal having a spectral distribution this does not occur. A null can often be achieved over a frequency range that is only part of the extent of the spectrum and as the relative phases of test and reference signals are altered the null may move through the total range of the spectrum. In other cases a minimum, rather than a zero, can be obtained and with phase adjustment the magnitude of the minimum and the frequency at which it occurs change. The time domain resultant displayed on an oscilloscope gives a complementary view of the behavior of the resultant near balance. It may show that a minimum resultant is being obtained at some instant during the

pulse. Thus, balancing can be observed near the leading edge or the trailing edge of the pulse output from the DUT. However, a more precise criterion of the balance condition corresponding to some chosen instant on the time scale, can usually be obtained by careful observation of the resultant spectral distribution.

The L-band assembly can only be balanced at fundamental frequency. Thus outflow power and phase behavior of amplifiers at the fundamental frequency can be studied but at second and third harmonic only outflow power behavior can be determined. The S-band assembly is more versatile and can be used to study all six aspects of S-band amplifier behavior, viz., outflow power and phase at fundamental, second and third harmonic frequencies. In Figure 2.2 item 14 is used to alter the phase of the test output signal but with only one reference signal, the fundamental, balancing and phase studies are limited to that range. In Figure 2.4 items 14, 26, 40 and 47 are used to alter phase. One item is redundant and the most convenient one to omit is item 26 in which case 14 is used for fundamental balancing and 40 and 47 for harmonic balancing.

Interpretation of changes in the settings of the line stretchers can be easily confused with consequent errors in the sign, and possibly the magnitude, of the phase change being incorporated into studies of phase behavior of amplifiers. The line stretchers used are those contained in wide band precision test units developed for use in microwave network analyzer

assemblies. Details of actual units used are contained in Appendices 1 and 2. In using them in the L- and S-band bridges a change in stretcher reading is converted to a phase change as follows. A positive change in the stretcher reading shifts a feature, say the maximum, on the microwave emerging from the reference channel output port by a distance measured in the coaxial line of twice the change in reading. The positive reading on the stretcher dial corresponds to shortening the path through the stretcher to the output port. The shift of the feature is outward from that port and if this is done to reinstate balance then it has compensated for a change that has occurred in the signal passing through the amplifier under test. In the case of item 14 in Figures 2.2 and 2.4 the stretcher shift has compensated for a change in the electrical length in the amplifier of opposite sign against the fundamental reference which is assumed fixed. In the case of item 26 in Figure 2.4 a shift in this stretcher compensates for a change in the amplifier of the same sign assuming that item 14 remains fixed. For harmonic balancing a shift in the line stretcher in item 40 or 47 compensates for a change in the amplifier of the same sign also. The stretcher in item 14 is only altered for fundamental balancing if item 26 is not used, and is not touched for harmonic balancing.

The studies reported in later sections are concerned with the effect of standard test load changes. If the internal electrical

length of an amplifier under test increases with a load change, a feature on the emerging wave moves into the amplifier and the line stretchers would be altered according to the following table to reinstate balance.

FIGURE	ITEM	STRETCHER CHANGE FOR BALANCE
2.2	14	Positive
2.4	14	Positive
2.4	26	Negative
2.4	40	Negative
2.4	47	Negative

Results are presented in electrical degrees. $+\Delta L$ centimeters change on the line stretcher dial corresponds to $(720\ \Delta Lf/c)$ electrical degrees, where

f is fundamental, second or third harmonic frequency

c is the electromagnetic wave velocity in the airfilled coaxial line stretcher taken as equal to 3.10^{10} cms per sec.

Changes in dial readings can be determined to one hundredth of a centimeter and this resolution at various frequencies of interest corresponds to the following quantities in electrical degrees.

BAND	FREQUENCY	ΔL cms	ELECTRICAL DEGREES
L-Band	1.325 GHz	0.01	0.32
S-Band	3.300 GHz	0.01	0.80

2.7 The Standard Test Load (STL) For Studying Amplifier Behavior

2.7.1 Choice of the STL

Reference has been made in the introduction to the fact that the dynamic impedance of any element in a phased array antenna varies as the radiated beem is steered in space. The instrumentation assemblies that have been described are arranged so that amplifiers for phased array antenna service can be studied under mismatched load conditions. The question to decide is the type of load to use for tests.

The dynamic impedance will be a complicated function of radiation direction for any given phased array geometry. For beam steering the phase of the excitation of each element is altered in steps and consequently the dynamic impedance will alter by stepping from one point to another on the Smith chart.(2) An example of contours of equal reflection coefficient magnitude as a function of beam steering is shown in Figure 2.8. Figure 2.9 explains how the contours are constructed. For a given direction of radiation (θ,ϕ) the magnitude of the reflection coefficient $|\Gamma|$ is calculated for the particular array. That value of $|\Gamma|$ is plotted into a plane whose coordinates are obtained by projection from the (θ,ϕ) hemisphere. The θ coordinate lines are the family of concentric circles of radius proportional to θ and the ϕ coordinate lines radiate from the common center. From a large number of calculated values of $|\Gamma|$ the contours of Figure 2.8 are drawn. The process must be repeated for each frequency of operation and quite different results might be expected at

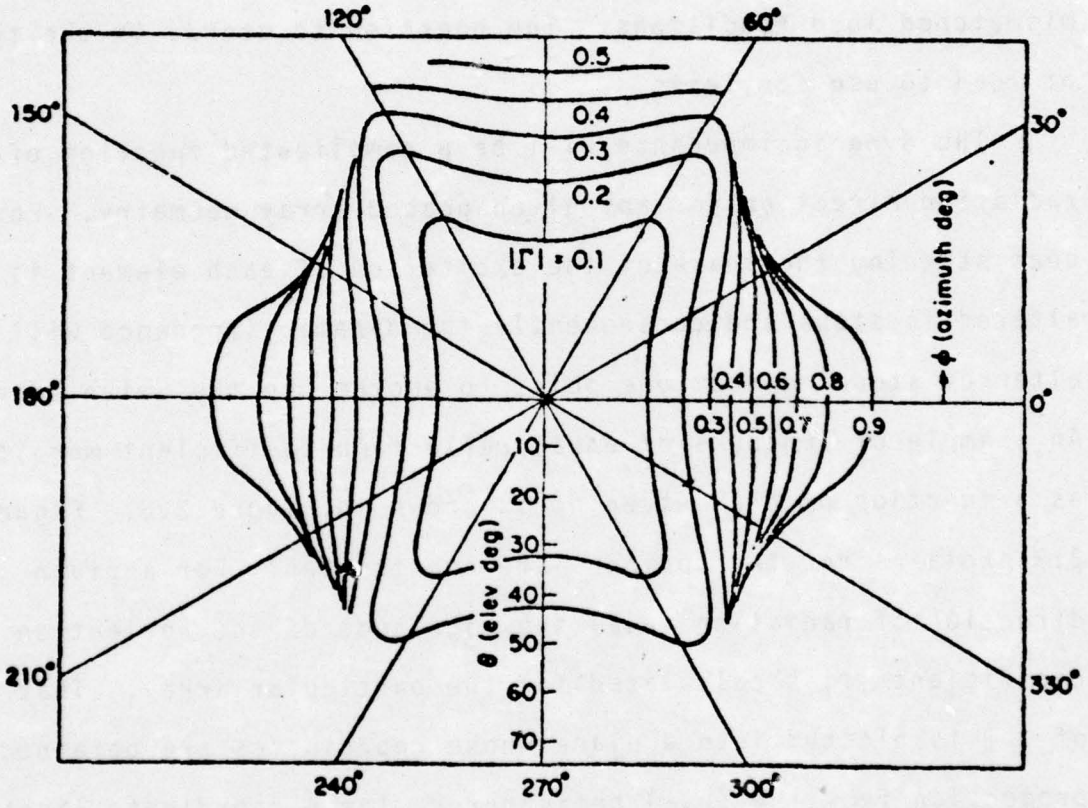

Figure 2.8 Variation of the magnitude of the reflection coefficient with scan angle at one element in a phased array antenna. (From (2).)

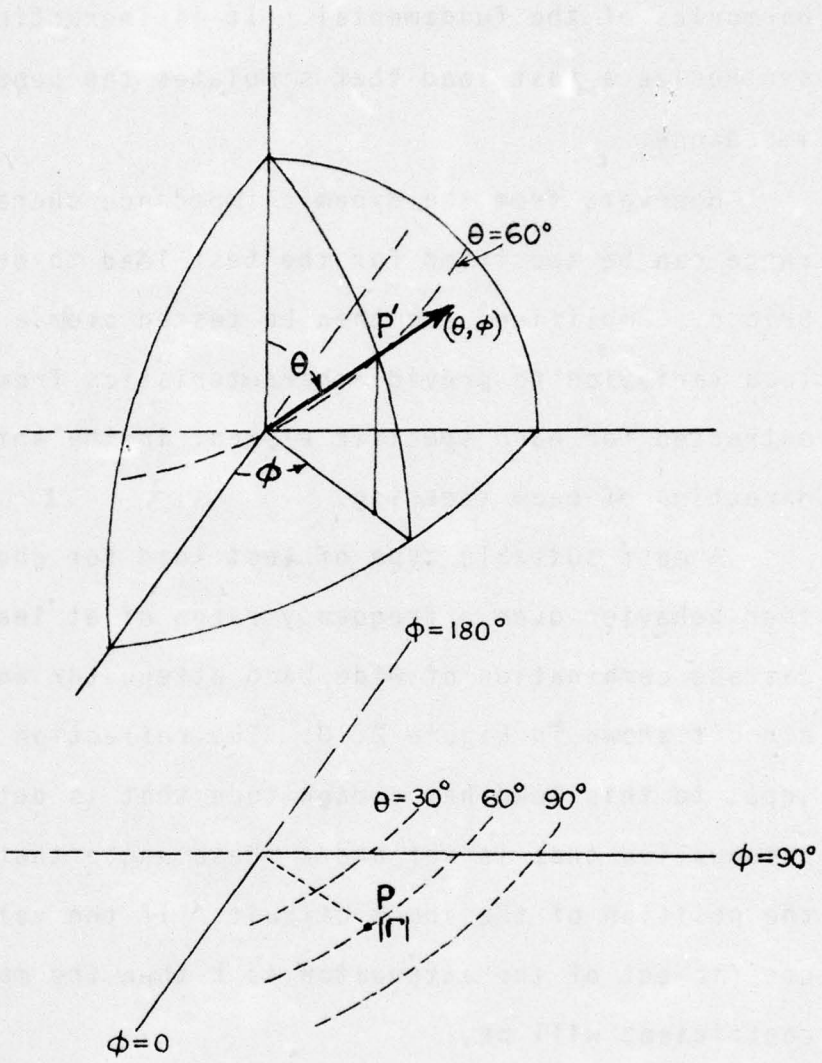

The value of $|\Gamma|$ for the direction θ,ϕ indicated is plotted on a flat sheet at the point P i.e. at the value of θ and ϕ on this sheet corresponding to the "scan angle" (θ,ϕ). Contours of constant $|\Gamma|$ are then drawn from a large number of values of $|\Gamma|$.

Figure 2.9 *Interpretation of reflection coefficient versus scan angle graphs.*

harmonics of the fundamental. It is impractical to attempt to synthesize a test load that simulates the behavior of the dynamic impedance.

However, from the dynamic impedance characteristics, a total range can be specified for the test load to be used with the bridge. Amplifiers can then be tested over a realistic range of load variation to provide characteristics from which data can be extracted for each specific element in the antenna for any direction of beam steering.

A most suitable type of test load for characterizing amplifier behavior over a frequency range of at least 3 to 1 is a cascade combination of wide band attenuator and variable short circuit shown in Figure 2.10. The reflection coefficient at the input to this load has a magnitude that is determined by the attenuation that is set and a phase angle that is determined by the position of the short circuit. If the voltage transmission coefficient of the attenuator is k then the magnitude of reflection coefficient will be,

$$|\Gamma| = +k^2$$

and the voltage standing wave ratio will be,

$$S = \frac{1 + k^2}{1 - k^2}$$

A movement of ΔL in the position of the short circuit away from the input port will change the phase of the reflection coefficient by an angle,

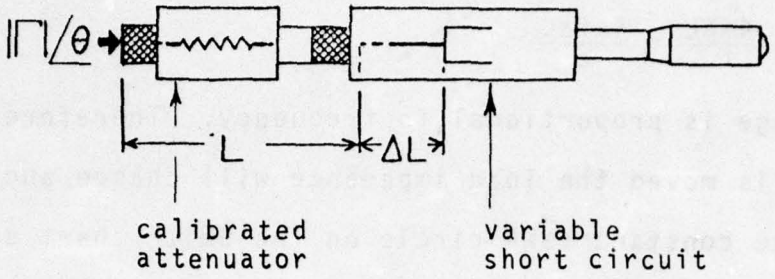

$|\Gamma| = +k^2$, determined by attenuator setting (transmission k)
$\Delta\theta = \frac{4\pi f}{c}\Delta L$, changes are determined by short circuit position.

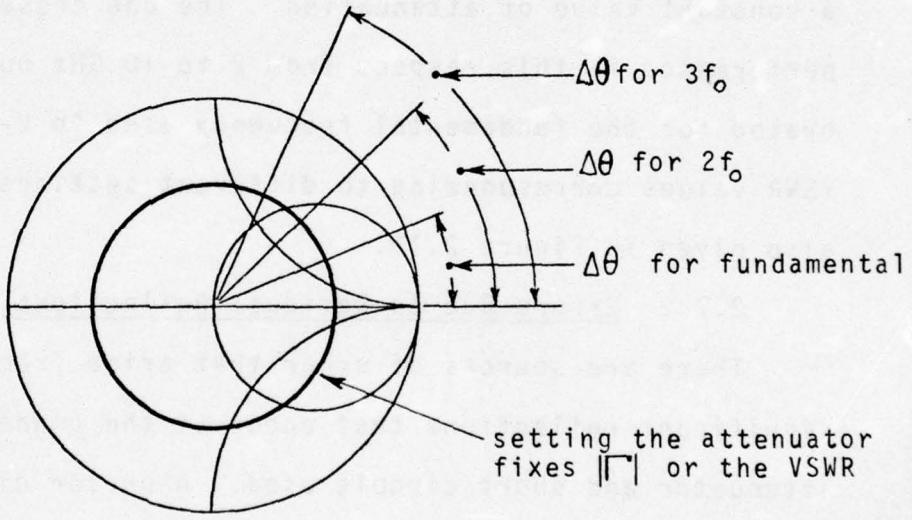

SMITH CHART

Attenuator DB	0.5	1	2	3	6	10	20
$\|\Gamma\|$	+0.89	+0.79	+0.63	+0.5	+0.25	+0.1	+0.01
VSWR	17.4	8.72	4.42	3.00	1.67	1.22	1.02

Figure 2.10 Standard load used for testing modules at points around chosen VSWR circles on the Smith chart.

$$\Delta\theta = \frac{4\pi\Delta L}{\lambda} = \frac{4\pi f\Delta L}{c}$$

The phase change is proportional to frequency. Therefore as the short circuit is moved the load impedance will change and follow the path of the constant VSWR circle on the Smith chart selected by setting the attenuator. The diagram illustrates that the angular displacements for second and third harmonics are twice and three times that for the fundamental. However, for the same VSWR circle to be followed at each frequency the attenuator must have a constant value of attenuation. The one chosen gave acceptable performance in this respect from 2 to 10 GHz but had to be calibrated for the fundamental frequency used in L-band, 1.325 GHz. VSWR values corresponding to different settings of attenuation are also given in Figure 2.10.

2.7.2 Errors Due to Residual Reflections From Connectors

There are sources of error that arise from the small but significant reflections that occur at the connectors on the attenuator and short circuit used. A phasor diagram to illustrate the effect of these reflections is given in Figure 2.11. Consider behavior at the fundamental frequency. As shown in the outline diagram in Figure 2.11, the total reflection at the input port of the load will be made up of small components from the connectors with phases determined by dimensions and frequency, and a large component from the short circuit if the attenuator is set to a low value. The large component varies in phase as the short circuit position is altered. The phasor diagram in the reflection coefficient plane is drawn on a Smith chart, AB representing the incident wave,

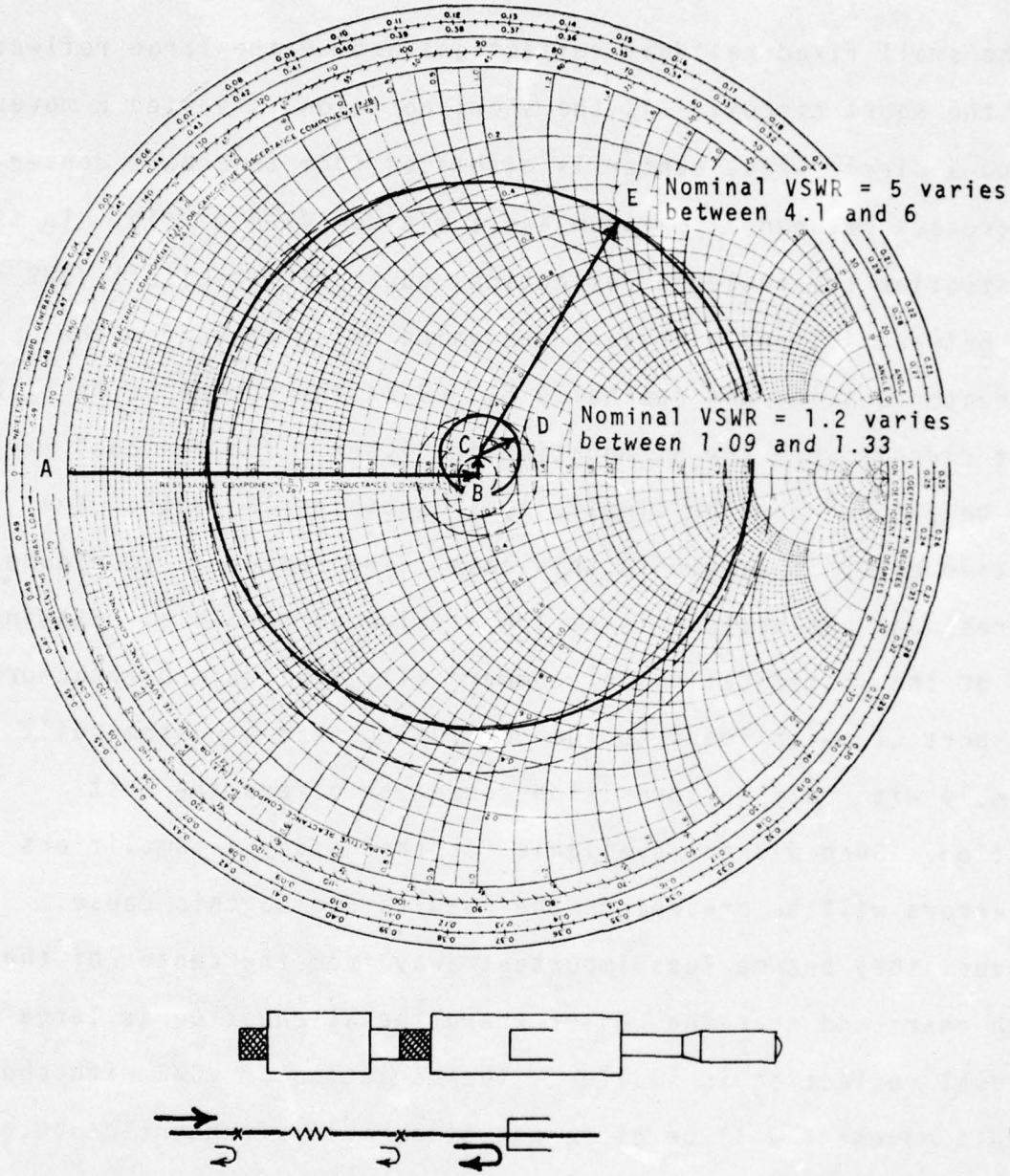

Figure 2.11 Phasor diagram of incident and reflected waves to illustrate the effect of residual unwanted reflections on the performance of the standard test load.
AB incident wave
BC residual reflection (fixed)
CD reflection from standard load for small attenuation and a specific position of the short
CE reflection from standard load for large attenuation setting.

BC the small fixed residual reflections and CE the large reflection from the short circuit. As the short position is varied E moves around a circle whose center is displaced from the chart center and crosses between a maximum and a minimum VSWR circle. In the illustration the residual reflections cause the resultant VSWR to vary between 4.1 and 6 whereas the value calculated from the attenuator setting was nominally 5. CD is the component from the short circuit when the attenuation is higher. The residual may also be altered but for simplicity is shown as CB again. The relative error is larger in this case. The remedy is to reduce the residual reflections to as low a value as possible. Examination of the specifications of commercially available attenuators and short circuits leads to the conclusion that a custom built assembly with only one precision connector offers the best solution. Such was not available for this study of amplifiers and errors will be present in the results due to this cause. However, they become less important away from the center of the Smith chart and near the center where the attenuation is large the residual reflection is smaller. The variation of VSWR with short circuit movement will be different at harmonic frequencies because the error causing residual reflection will be different.

2.7.3 Arrangements For Plotting Results as a Function of Short Circuit Position

The short circuit position is controlled by a micrometer. The micrometer is coupled via a gear reduction to a helipot as shown in the photograph of Figure 2.12. A voltage can be obtained

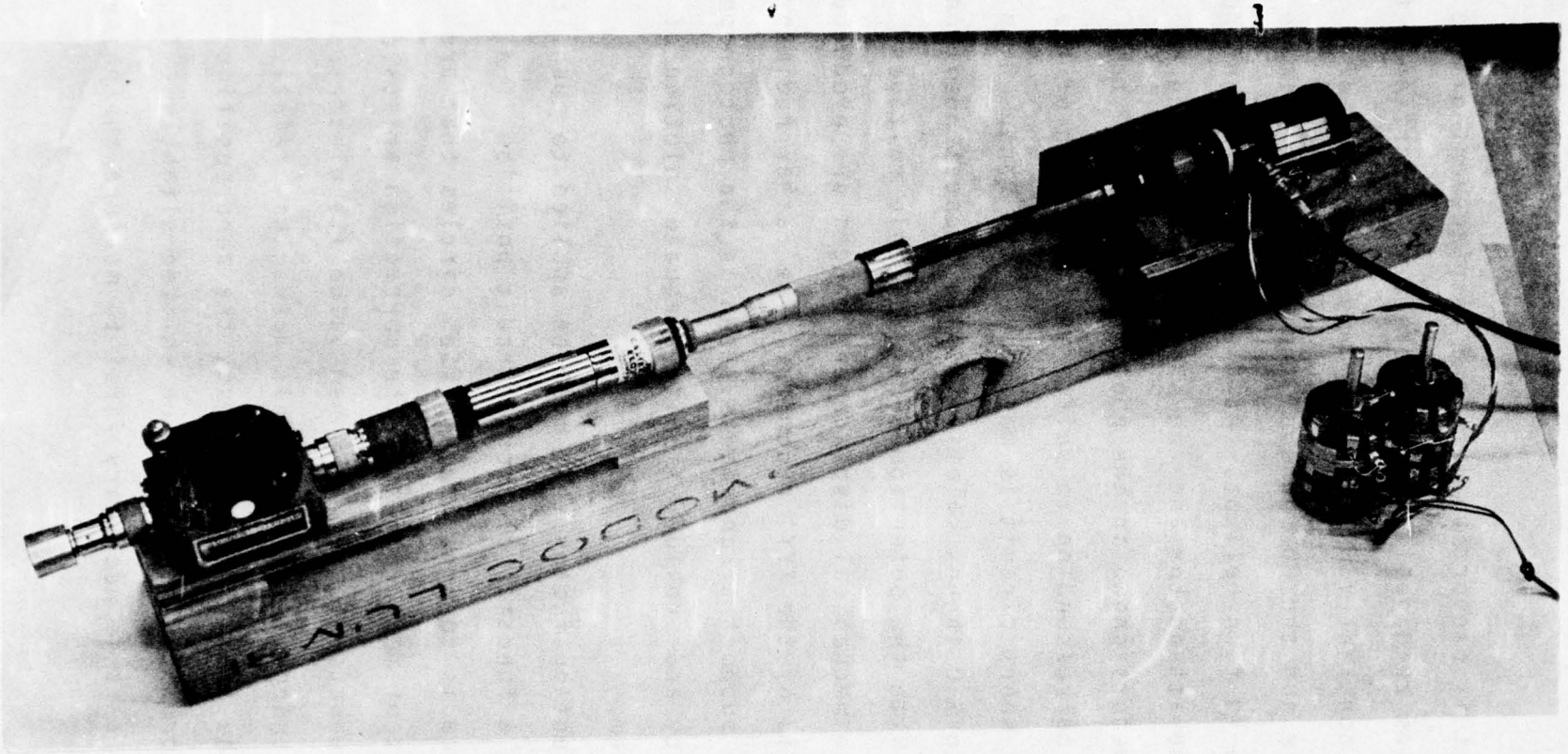

Figure 2.12 Photograph of test load for preset reflection magnitude and variable reflection angle

from the helipot that is proportional to the displacement of the short circuit from its zero position and therefore proportional to movement around the constant VSWR circle. Only two inches of movement is available and the 80 turns of the micrometer thimble cause 8 turns of the 10 turn helipot. At L-band, a line stretcher is placed between the attenuator and the short circuit. The additional potentiometers shown in the photograph are used to give voltage shifts corresponding to shifts in the length of the line stretcher. The short circuit is moved over the ranges 0 to 2, 2.5 to 4.5 and 5.0 to 7.0 inches relative to its closest position to the attenuator. With the potentiometers available voltages proportional to those mechanical displacement ranges are produced for driving the X-axis of the XYY' recorder. The rather rudimentary coupling and sliding support arrangements shown in the photograph do not impair accuracy and provide a quite adequate solution of the mechanical problem.

There is a correction factor that must be applied to quantities that are recorded as a function of short circuit position if a common phase reference is to apply to all VSWR circles that are traced out in the set of measurements. The correction arises because when the attenuator is set to a new value its electrical length will also be changed slightly. This means that relative to the output port of the amplifier under test, the zero position on the short circuit micrometer scale will be shifted slightly. To correct for this shift it is necessary first to measure the phase

behavior of the attenuator. From this behavior it is possible to calculate the quantity L in Figure 2.10 at each of the test frequencies as a function of attenuator setting and therefore VSWR. The variation over a range of two inches that is possible in short circuit position adds to this calculated length. Thus the X-axis scale on each recording can be relabelled by adding the appropriate value of L for the frequency and VSWR being used. In this way all recordings are referred to a common position on the line between the device under test and the load, namely the input to the load. The corrections are as large as 20 degrees in phase for the highest test frequencies. They depend entirely on the characteristics of the attenuator being used. Account has been taken of this correction in the work presented in later chapters of this report.

2.8 The Variations in Output Amplitude and Phase Caused By a Variations in the Standard Test Load

2.8.1 Changes in Amplitude and Phase Due to the Amplifier and Due to Load Reflection

The bridges make measurements on a precise fraction of the signal V^+ that propagates from the output of the amplifier under test to the standard test load. The reflection from that load propagates back to the amplifier port. All of the amplifiers tested have a three port circulator between the output power amplification stage and the output port. The load reflected power enters at the second port of this circulator and propagates out of the third port into a matching termination. Apart from

changes in the amplitude and phase of V^+ measured by the bridge, the load reflection also gives rise to changes in the amplitude and phase of the wave absorbed by the load compared with that incident on it. The load could be the dynamic impedance of an element of the phased array antenna in which case the absorbed wave is that which energizes the antenna and is mainly radiated and partly dissipated in antenna losses. Thus, there are amplitude and phase errors that arise due to reflection from a mismatched dynamic impedance at each antenna element.

Figure 2.13 illustrates the simple transmission line theory for calculating these effects. With a unit amplitude voltage wave incident on the load of reflection coefficient Γ_T, the resultant voltage across the load is V_t/V^+ which is different in phase from the incident wave by θ_1 degrees. The absorbed power is calculated from V_t/V^+ and will be less than that incident on the load. θ_1 is called the angle of transmission coefficient on the standard Smith chart and in Figure 2.14 lines of constant phase angle in 10 degree steps are shown. Figure 2.15 shows the proportion of the incident power absorbed as circles about the center of the Smith chart. The values are those given by the radially scaled parameter "TRANSM COEFF, P". The power loss due to reflection can be used as a decibel quantity and equi-loss contours in decibels are shown in Figure 2.16. The values are those given by the radially scaled parameter "REFL LOSS dB".

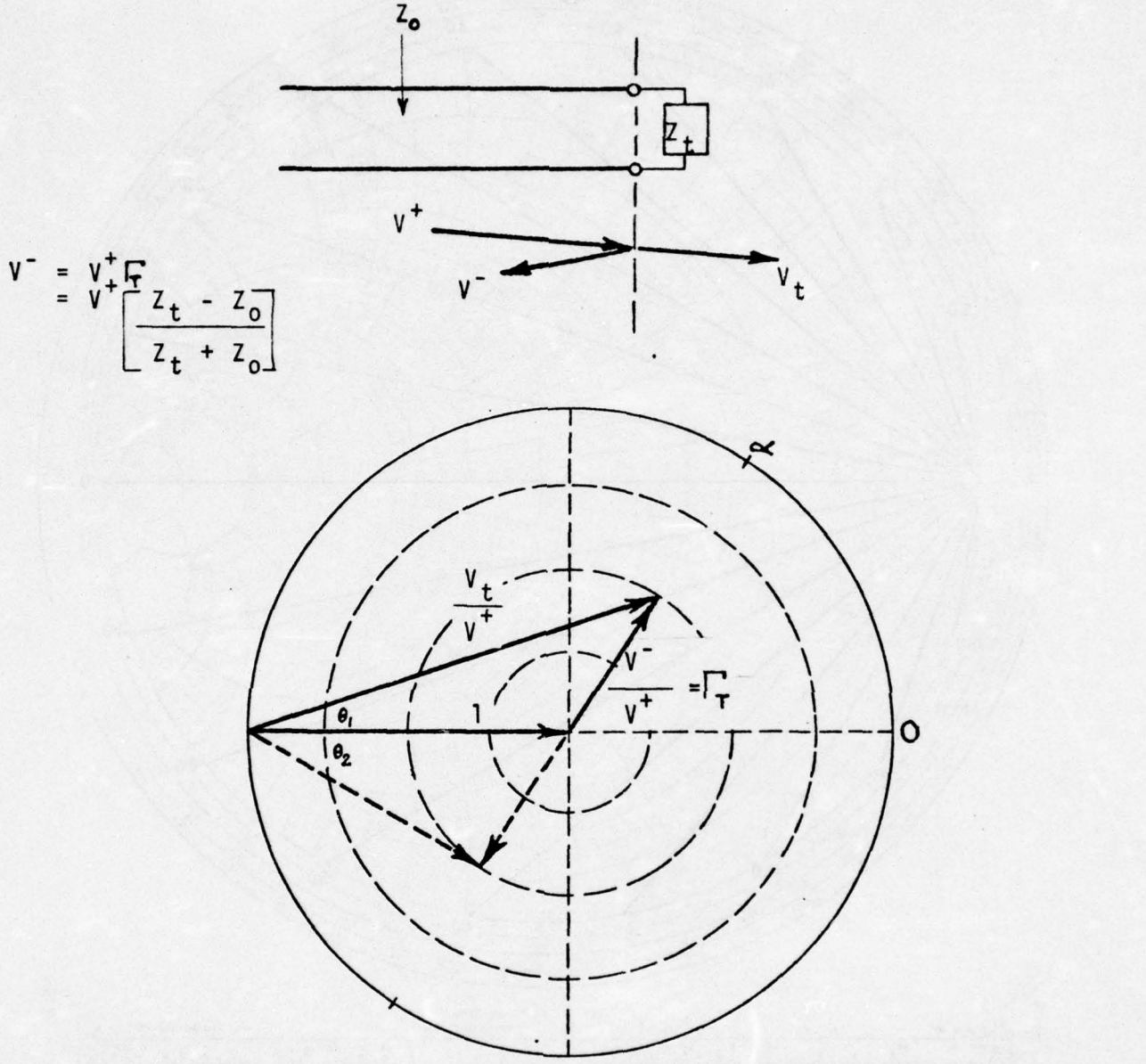

Reflection coefficient plane
(same as for Smith Chart)

Figure 2.13 The resultant voltage V_t across the load on a transmission line differs in phase and amplitude from the incident voltage wave V^+ as shown above.

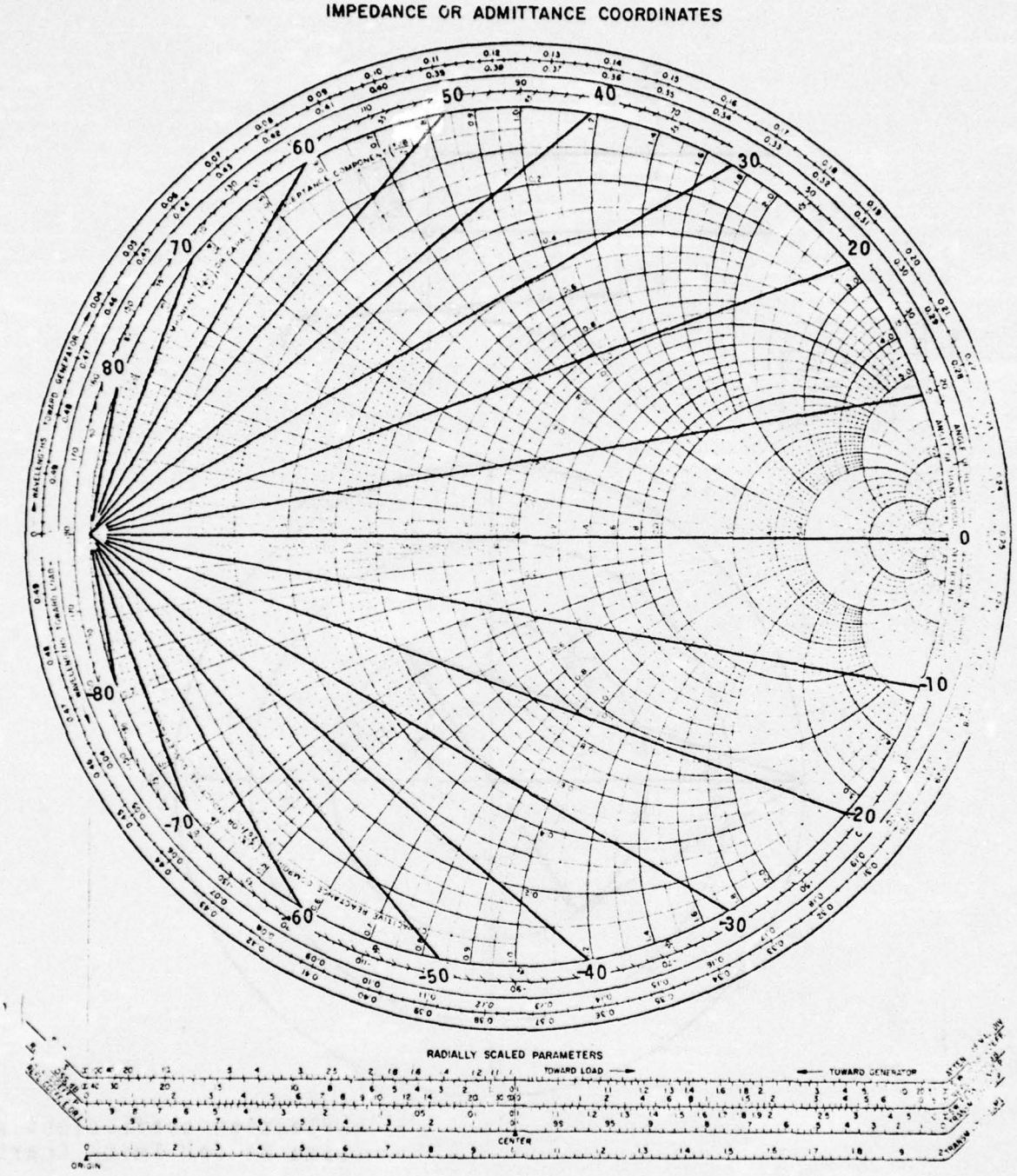

Equi-phase contours in electrical degrees.
Depends only on and assumes a passive load.

Figure 2.14 Phase of excitation of the load relative to the incident wave as a function of the load impedance.

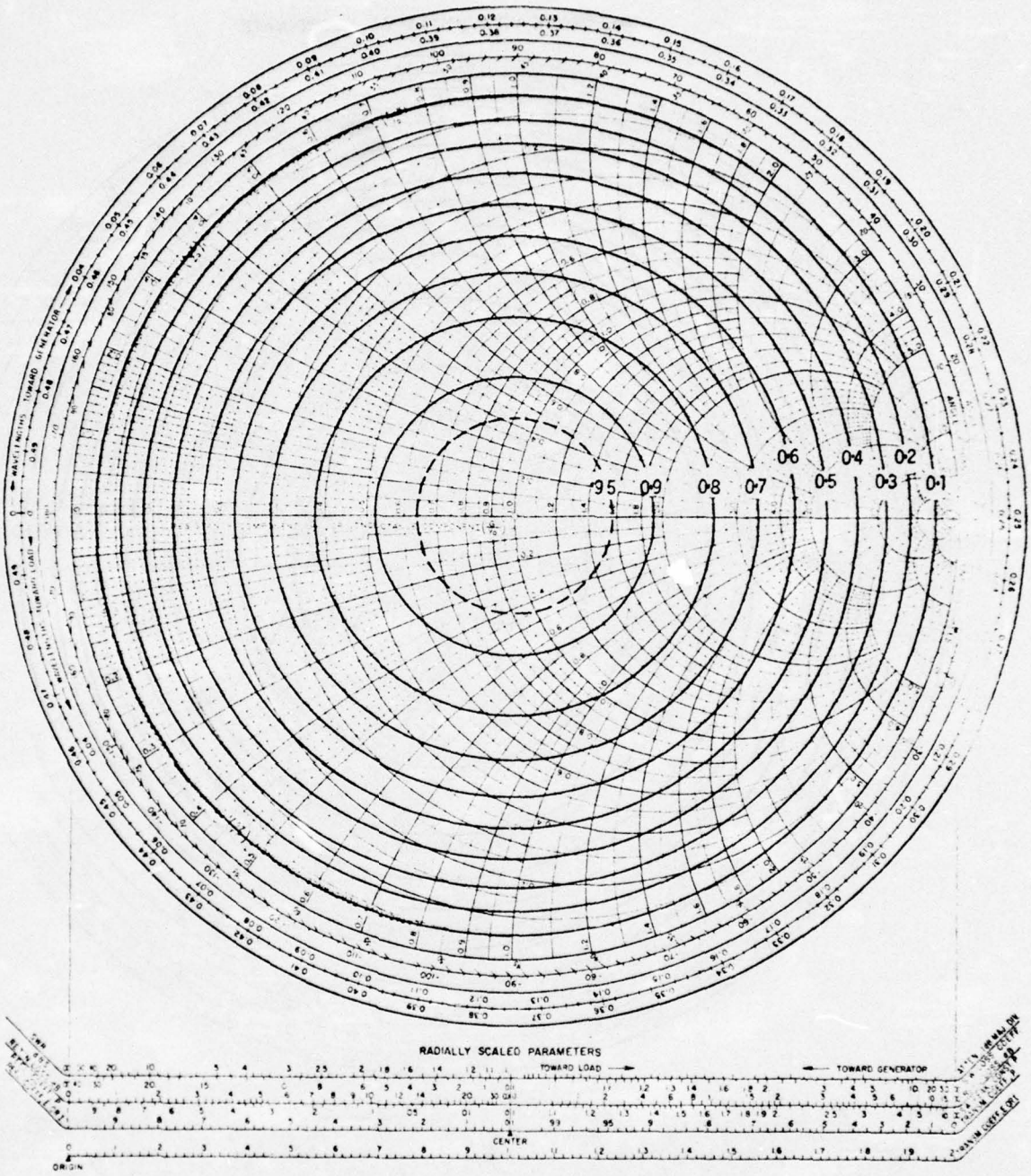

Equi-loss contours as a multiplying factor.

Figure 2.15 Effect of loss due to reflection from the load shown as a proportion of power absorbed. Power absorbed in the load (or radiated by an antenna element) is obtained by reducing the power wave (in watts) from the output port by the factor from the corresponding load impedance point on these contours.

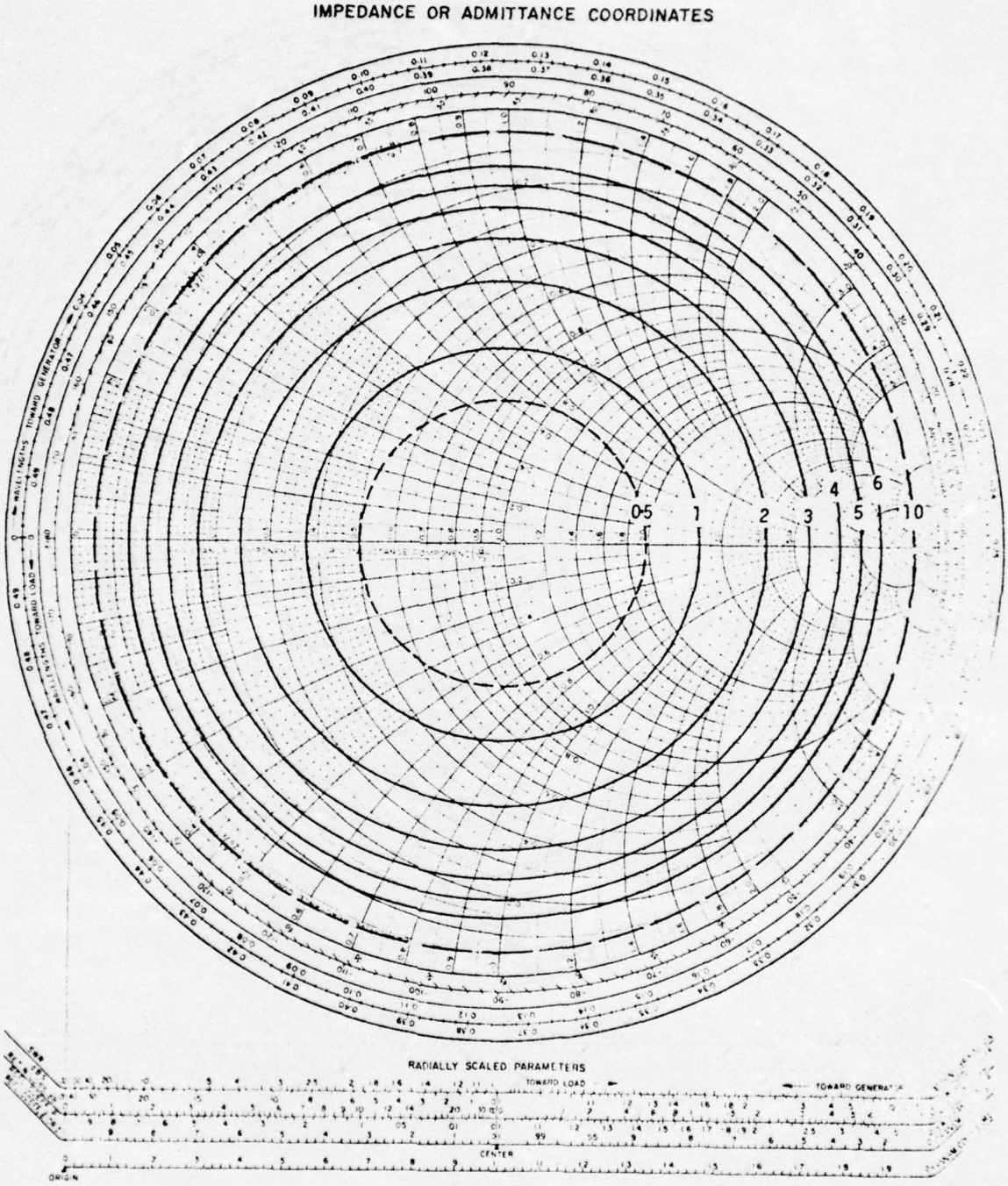

Equi-loss contours in DB (negative sign implied)

Figure 2.16 Loss in DB due to reflection from the load. Power absorbed by the load (or radiated by an antenna element) is obtained by reducing the power wave (in DB) from the output port by this reflection loss (in DB).

2.3.2 Procedure For Combining the Two Types of Amplitude and Phase Error

For phased array antennas of the type in Figure 1.1 the total amplitude and phase error will have at least two parts, one arising from reflection at the dynamic impedance of antenna elements and another arising from the effect of load reflections on the output produced by the power amplifier. The amplitude errors from these two origins are combined by multiplication of factors or addition of decibels. The phase errors cannot be combined unless the electrical distance between the reference positions for them is known, and the procedure is quite complicated as explained in the following.

Let Figure 2.13 represent the phasor diagram for position A of the variable short circuit in the standard test load. If the short circuit is moved to position B then a different phasor diagram will apply such as that shown in Figure 2.17. Each diagram has been normalized by dividing all voltages by the forward travelling wave components, V_A^+ in the first case and V_B^+ in the second case. Because of this the two diagrams cannot be combined to yield the quantities that we seek. From experimentally determined results presented in later chapters, in general V_B^+ will differ in both amplitude and phase from V_A^+. With the bridge assemblies the amplitudes of V_A^+ and V_B^+ can be measured and the change in phase of V_B^+ from V_A^+ can also be measured. From that data a combined phasor diagram can be constructed as illustrated in Figure 2.18. It is simply a matter of scaling Figures 2.13 and 2.17 according to the relative voltages of V_A^+ and V_B^+ and super-

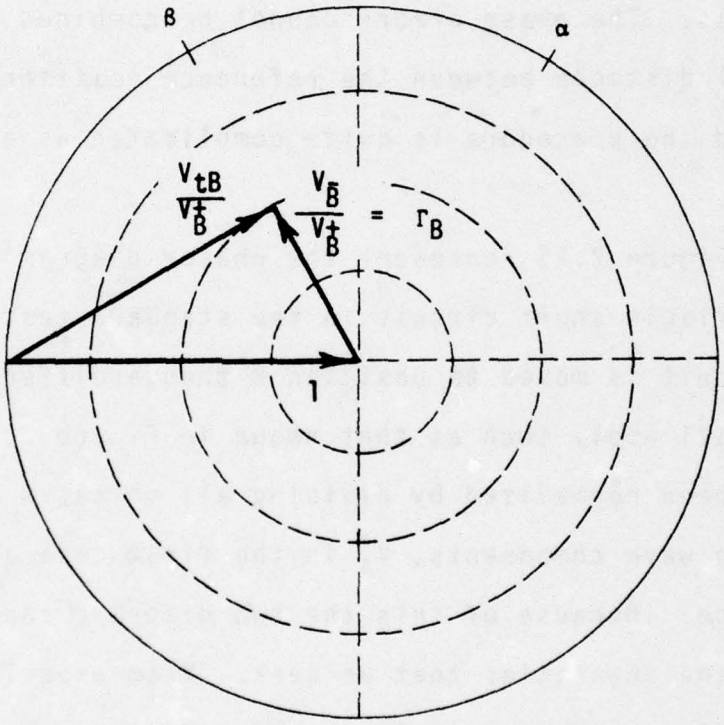

Reflection coefficient plane
(same as for Smith chart)

Figure 2.17 The resultant voltage V_{tB} across the standard test load for the case where the short circuit is moved to position B from position A to which Figure 2.13 applies.

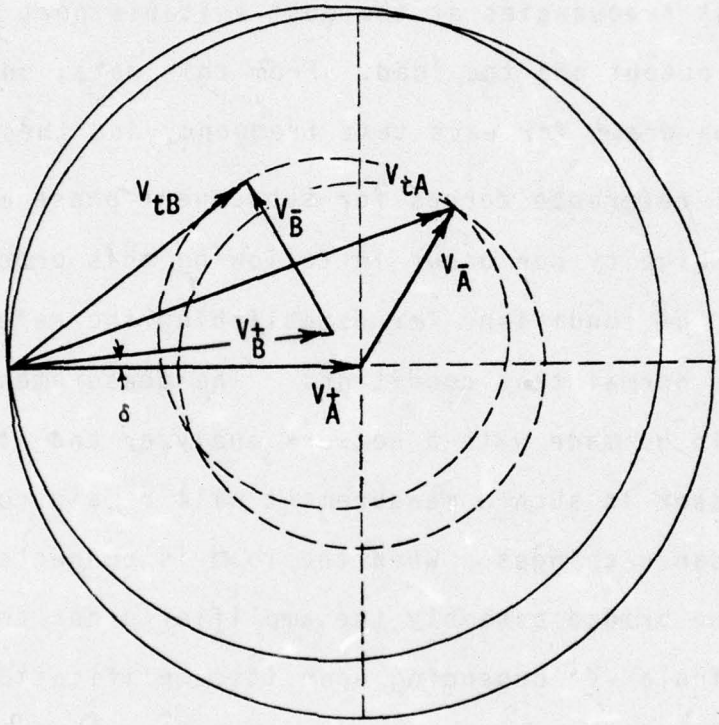

Figure 2.18 The combined phasor diagram of incident, reflected and transmitted voltages for positions A and B of the short circuit in the standard test load

imposing these diagrams with the correct angles between V_A^+ and V_B^+.

A reference zero for all phase quantities must be defined. One way in which it may be done is as follows. With the standard test load set for the largest VSWR to be used and the short circuit set to zero on its scale, the load impedance is measured at all test frequencies at the most suitable port between the amplifier output and the load. From this data, one phasor diagram can be drawn for each test frequency and these can be used as the set of reference zeroes for subsequent phase measurements.

An ambiguity can occur in following this procedure and it arises in the conditions for establishing the reference zero compared with normal test conditions. The measurement of load impedance would be made with a network analyzer and it is assumed that the V^+ phasor in such a measurement will remain constant if the load impedance changes. When the load is connected to the test path in the bridge assembly the amplifier under test will produce some particular V^+ depending upon its amplification and total electrical length for the load conditions. So the reference zero will be at a specific point in the range of behavior of the amplifier and it will be imposed by the load and the port position that are chosen. Changing the load for defining the reference zero will alter V^+ for the test amplifier but not for the network analyzer used to establish the reference zero. Hence, apparently different results may be obtained depending upon the reference zero definition.

Note that neither the path to the null detector nor the reference signal, considered as a phasor, enter into the above problem. It is as well that they do not because an additional ambiguity exists as to the precise position where the test and reference signals first cancel. This is because they are combined in a hybrid in which coupling of the signals into a common path occurs over a length that is significant compared with a wavelength. If the resultant in that path through the coupling region that becomes the null path is examined in detail, it changes progressively from one of the signals to a zero in a monotonically decreasing way. The first point in the line where a zero appears is difficult to locate exactly and is a significant distance inside the device from the physical connectors on the hybrid.

The procedure of obtaining data by bridge balancing, extracting from it phase changes in V^+ as a function of mismatch and then combining these changes with phase changes at reflection using the phasor diagram method explained above, is a long and tedious procedure. In the results presented in the following chapters the changes in amplitude and phase of V^+ is emphasized. Time has not allowed all of those results to be combined with the data contained in Figures 2.14 to 2.16. The detailed calculations necessary to produce accurate contours over the Smith chart would be lengthy and repetitious. However, the worst case for given values of antenna element dynamic impedance can be quickly estimated using Figures 2.14 to 2.16 and corresponding charts of

amplitude and phase data for V^+ for the amplifier under consideration. Such a procedure should be satisfactory for the purposes of this study.

CHAPTER 3

STUDIES OF L-BAND MICROWAVE BIPOLAR TRANSISTOR AMPLIFIER MODULES

3.1 Description of the L-Band Modules Studied (Ref. (3 to 7).)

One of the two solid state transceiver modules evaluated with the L-band bridge assembly is shown in Figure 3.1. It is a hermetically sealed unit with a multipin connector for power supplies and control signals and two OSM coaxial connectors for microwave signals. A block diagram which schematically shows the microwave functions that are performed between the two microwave ports is given in Figure 3.2. In the transmit condition control signals switch the channel switch, designated CS, and the transmit-receive switch, TR, to the T position. An input signal of at least 30 mW in the frequency range 1.265 to 1.39 GHz is fed via the input port and then via a 4-bit phase shifter, PS, to a 3-stage preamplifier PR. The output from the preamplifier is divided to drive two transistors in the first stage of the power amplifier, PA. The output from each of these transistors is divided so that four transistors are driven in the second and final stage. After combining, approximately 60 watts peak pulse power with a maximum pulse length of 1.5 milliseconds and a maximum duty factor of 0.3 is available at the output. The overall gain of the pre- and power amplifiers is about 33 dB. The output passes via a 3-port circulator, CC, to the output port and thence to the antenna element. Any reflections from the antenna will

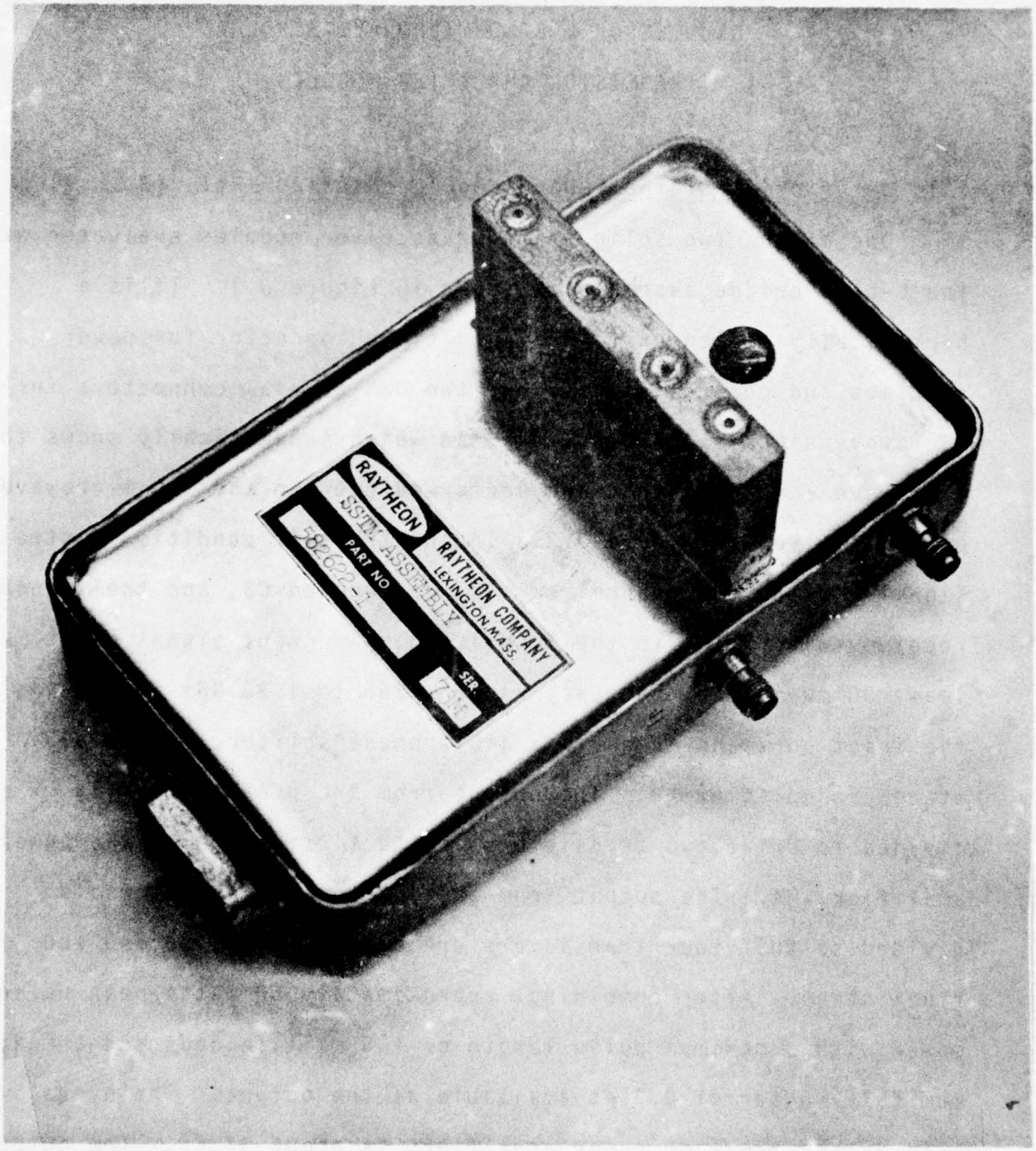

Figure 3.1 Photograph of L-band transceiver module

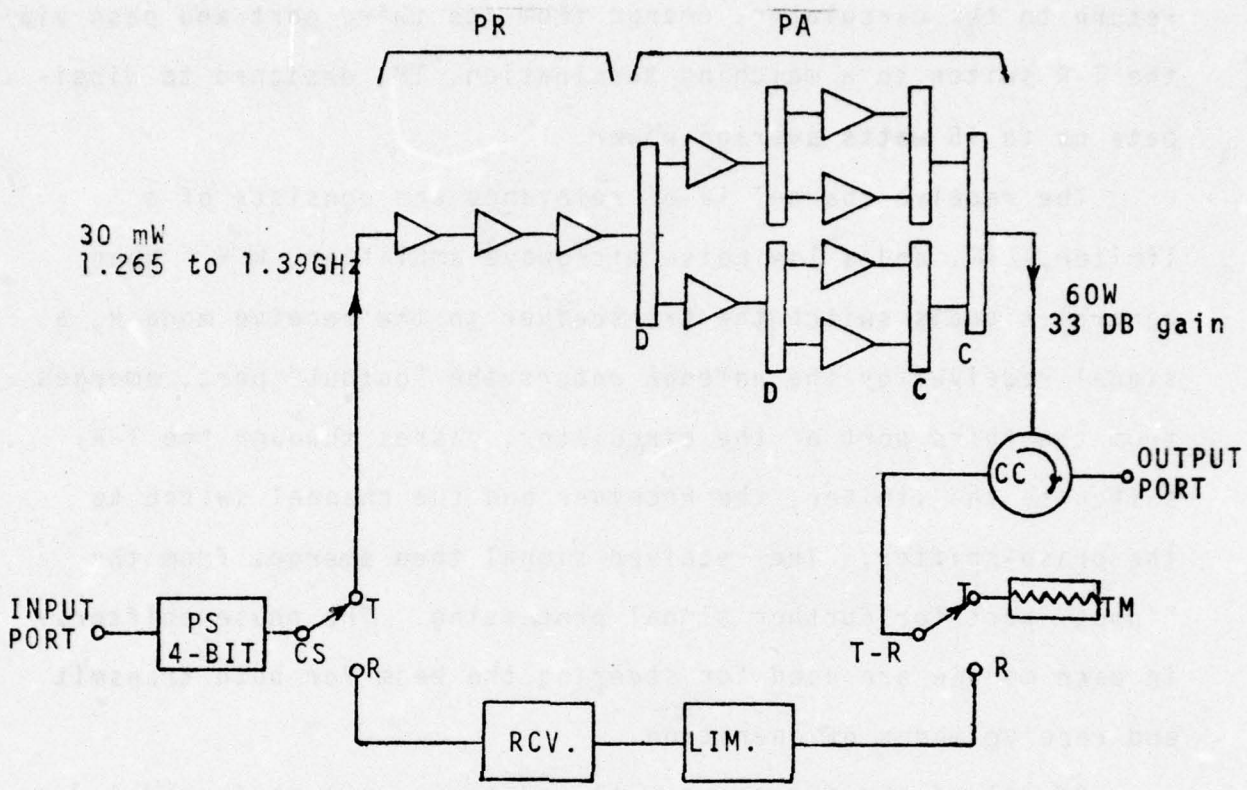

Figure 3.2 Block diagram of L-band amplifier unit incorporating

PS	4-bit digital phase shifter
CS	channel switch
PR	3 stage preamplifier
PA	2 stage class C power amplifier with power dividers (D) and combiners (C)
CC	circulator
TR	transmit-receive switch
TM	termination for reflections under transmit conditions shown
LIM	limiter for received signals
RCV	low noise microwave receiver amplifier

return to the circulator, emerge from its third port and pass via the T-R switch to a matching termination, TM, designed to dissipate up to 15 watts average power.

The receive channel is of relevance and consists of a limiter, LIM, and a low noise microwave amplifier, RCV. When control signals switch the transceiver to the receive mode R, a signal received by the antenna enters the "output" port, emerges from the third port of the circulator, passes through the T-R switch to the limiter, the receiver and the channel switch to the phase-shifter. The received signal then emerges from the "input" port for further signal processing. The phase shifters in each module are used for steering the beam for both transmit and receive modes of operation.

If all of the functions outlined above were performed in an ideal way then,

(i) the circulator and the termination on the T-R switch would prevent mismatch of the output load from affecting the power flowing out of the power amplifier

(ii) There would be no harmonic components of the input present in the output of the power amplifier

(iii) the output would remain constant during the on period of the pulsed operation.

In the experimental results that follow it is found that,

(i) the outflow power is dependent on the load

(ii) there are harmonic components in the outflow power and these also are dependent on the load

(iii) significant measurable changes in the output occur during the pulse.

It is evident that the modules are not ideal but it is not possible to specifically indicate which of the many functions performed within the hermetically sealed box contribute most to the behavior that is observed.

3.2 Input Drive and Response Characteristics

Correct bias and control voltages for operating these modules were obtained from reports describing their design, development and performance (6,7). Signal drive requirements of the modules were established from plots of power flow to a matched load as a function of input incident power at closely spaced frequencies throughout the specified passband for the modules. The plots for the module designated as serial number 73M (SN73M) are shown in Figure 3.3 and exhibit the pronounced non-linear relationship between outflow and incident power that is characteristic of class C operation. The threshold incident power necessary for any output to appear depends upon frequency. The effect of this is to yield a bandpass response characteristic that is wider for higher incident power levels as shown in Figure 3.4. The power reflected at the amplifier input was also monitored with item 6 in Figure 2.2 and response characteristics in terms of absorbed input power could be obtained. They do not differ significantly from those of Figure 3.4. Similar results were obtained for the second module SN29M.

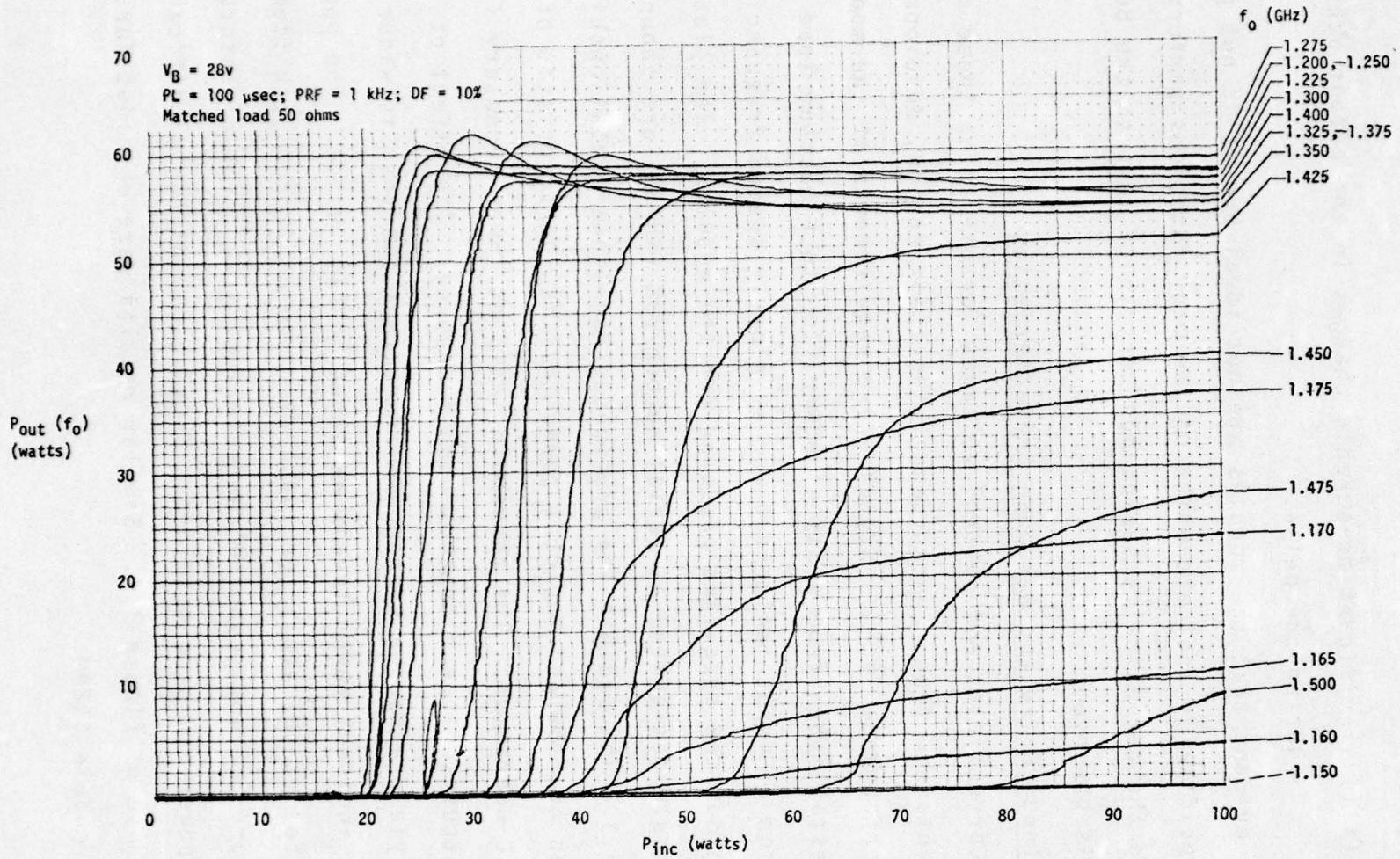

Figure 3.3 Power outflow versus power incident characteristics for L-band amplifier SN73M for various excitation frequencies

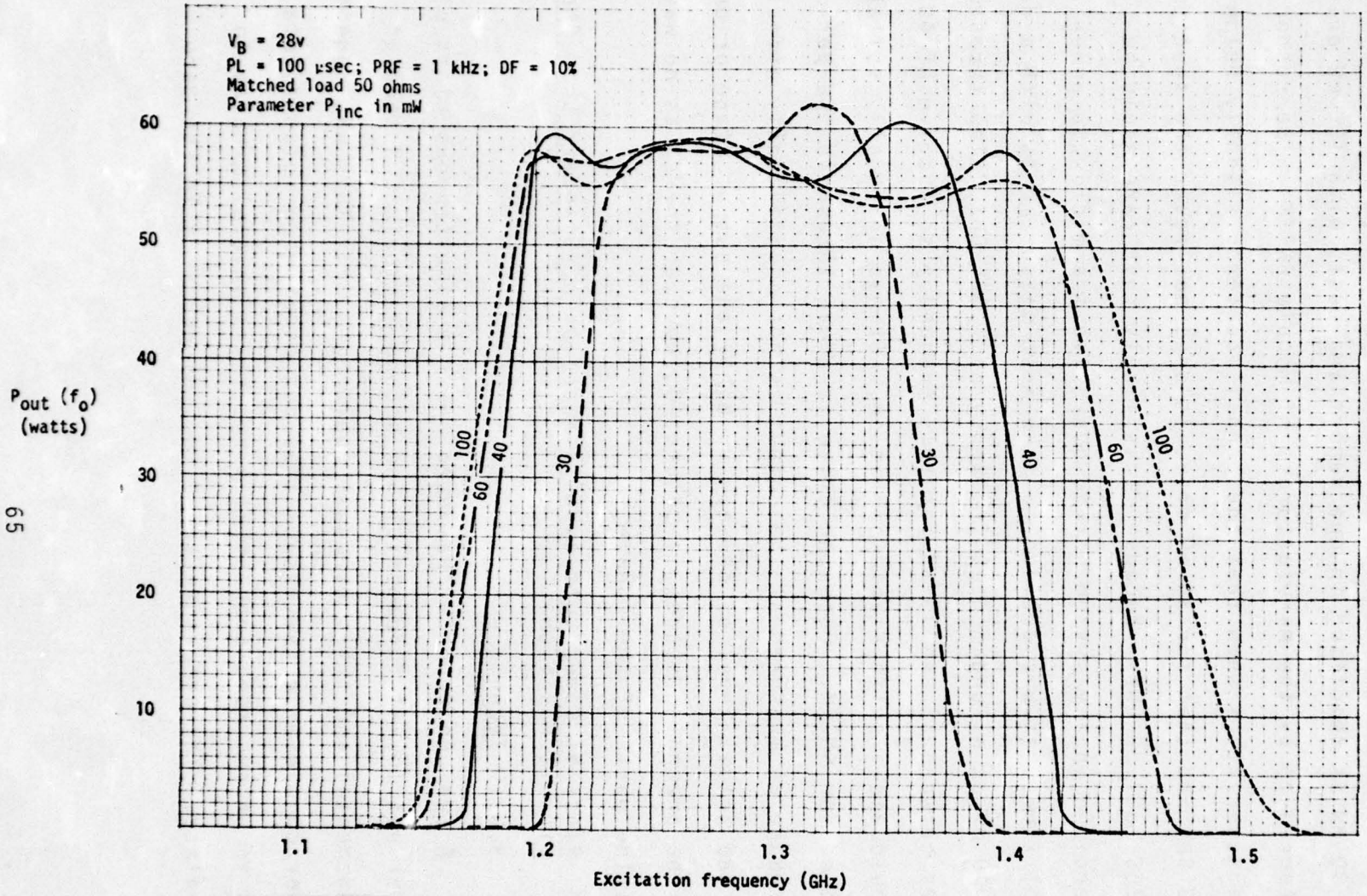

Figure 3.4 Frequency response characteristics for various excitation power levels for L-band amplifier SN73M

An ambiguity regarding the drive requirements of these modules exists in the reports referred to above in that a drive of 30 mW is specified in one report and tests with 100 mW drive referred to by the manufacturers of module SN73M. The response characteristics show that the band is centered slightly below 1.3 GHz and that for 30 mW drive it does not cover the specified 1.265 to 1.39 GHz. Because it is likely that care would be exercized in any system not to overdrive the microwave power amplifiers, it was decided to make most measurements with a drive of 40 mW at a fundamental frequency of 1.325 GHz. The threshold lies between 22 and 30 mW for this frequency so a drive of 40 mW should yield quite stable operation. It was an equally suitable choice for SN29M. Once the drive is above threshold the performance as measured at the output is not significantly affected by the actual level of drive. Probably the output stage or one of the preceding stages is saturated, however there was no way of testing parts of the module.

3.3 Plots of Power Outflow as a Function of Standard Load Short Circuit Position

3.3.1 Technique

A two pen recorder was used so that simultaneous plots of power outflow at fundamental and second harmonic and then at fundamental and third harmonic could be made. This was done in order to minimize the errors that can occur when related data has to be recorded sequentially and takes several minutes to complete. The errors referred to include drift in the zero

settings on power meters, selective amplifier and recorder and drift or variations in the gain of the selective amplifier and the recorder.

The selective amplifier was used to measure the harmonic outputs because it was expected that these could fall well below the smallest level that can be accurately measured with a power meter. The selective amplifier was that contained in a standing wave ratio meter. This imposed a restriction on operating conditions in the following way. The amplifier is tuned to 1 kHz and is designed to amplify the envelope obtained by detection of a microwave signal that is amplitude modulated at 1 kHz. In these studies the microwave signals are all pulse modulated so a pulse repetition frequency of 1 kHz had to be used. The selective amplifier responds to the fundamental in the envelope pulse train produced by the detector. A low level detector is used and the signal incident on it is kept small so that the output from the selective amplifier is proportional to the microwave power incident on the detector.

The harmonic level relative to the fundamental is established by an attenuator substitution method. A tunable bandpass filter of known insertion loss is used to pass either the harmonic or the fundamental to the detector and selective amplifier combination. The gain of the amplifier is held fixed and when measuring the fundamental, an accurately known attenuation is introduced to reinstate the level on the amplifier to that obtained when measuring the harmonic. In this way detector and amplifier

handle the same level of signal in each case and thus the accuracy of measurement of relative level is not influenced by either item.

3.3.2 Typical Power Plots

Actual power plots for the fundamental and second harmonic are reproduced in Figure 3.5 and for the fundamental and third harmonic in Figure 3.6. The same operating conditions apply to all of these plots which taken together comprise the amplitude data for SN73M when presented with loads having a nominal VSWR of 5.8. The breaks in the plots arise from limitations in the apparatus used for obtaining the X-axis voltage for the recorder. These limitations were explained in detail in section 2.7.3.

The plot of power outflow at the fundamental frequency, $P_{out}(fo)$, appears from both Figures to be repeatable to an accuracy of about one percent. The variations in level are periodic and correspond to the load impedance at the fundamental frequency being varied around the complete VSWR circle on the Smith chart. In a separate calibration the actual VSWR is higher for the fundamental frequency because of the test load attenuator characteristic. Data from that calibration is as follows:

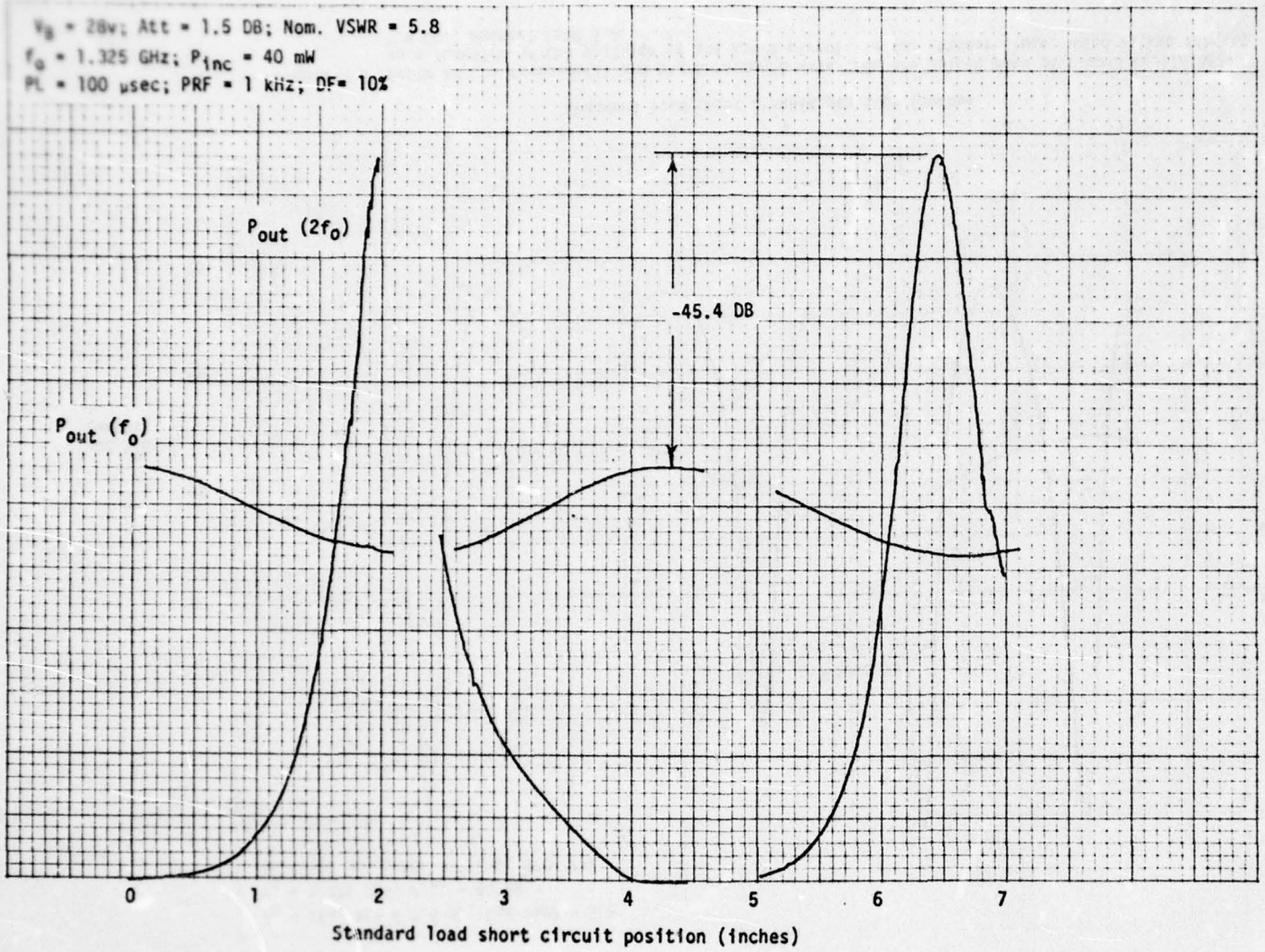

Figure 3.5 Power of the fundamental and second harmonic wave from the output port of L-band module SN73M as a function of the position of the short circuit in the standard load. Load attenuator set 1.5 DB. Nominal VSWR 5.8.

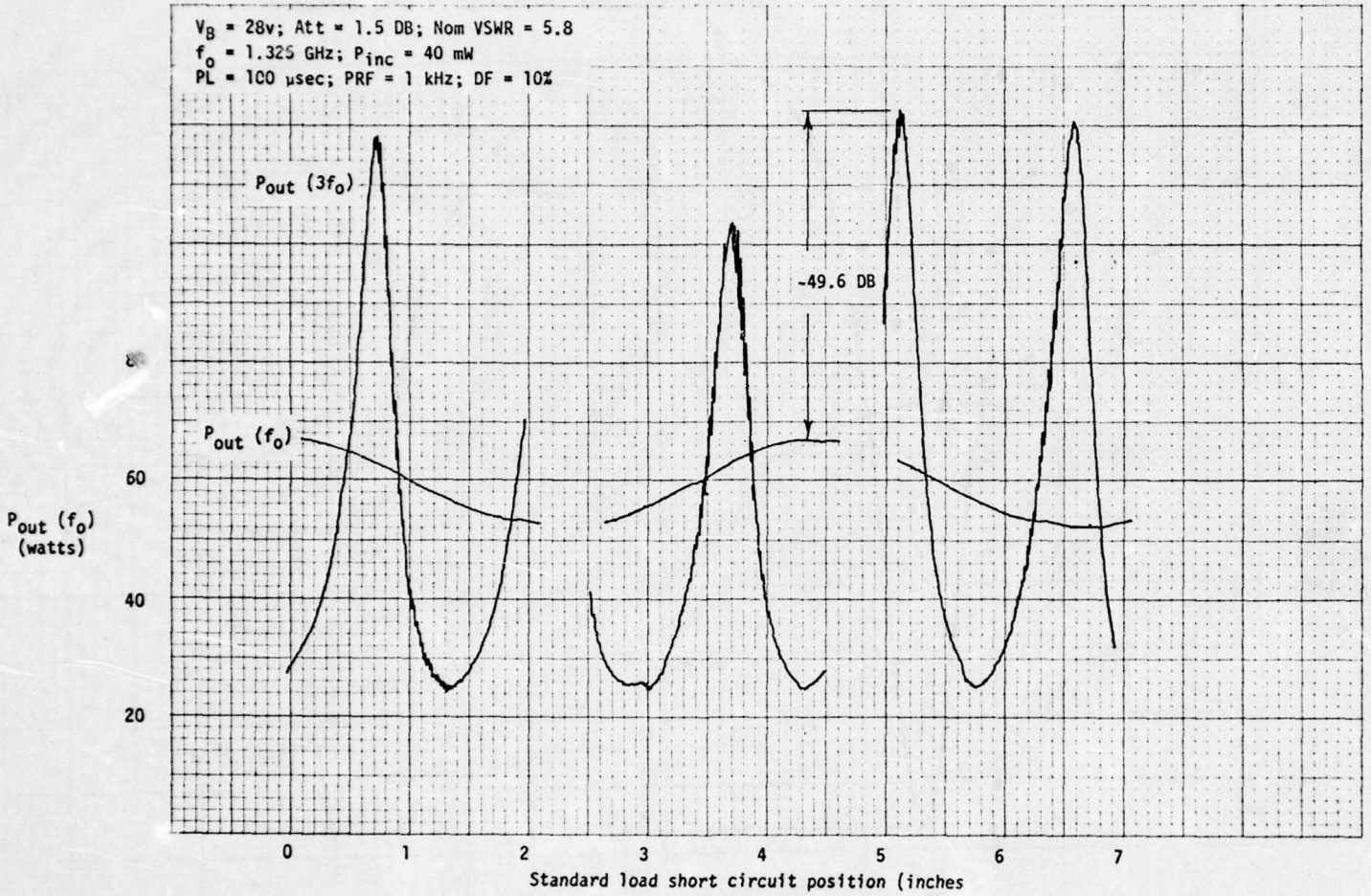

Figure 3.6 Power of the fundamental and third harmonic wave from the output port of L-band module SN73M as a function of the position of the short circuit in the standard load. Load attenuator set 1.5 DB. Nominal VSWR 5.8.

ATTENUATOR SETTING DB	NOMINAL VSWR	VSWR AT fo = 1.325 GHz	VSWR AT 2fo = 2.65 GHz	VSWR AT 3fo = 3.975 GHz
1.5	5.8	8.5	5.8	5.8
2.0	4.4	6.5	4.4	4.4
2.5	3.6	5.4	3.6	3.6
3.0	3.0	4.6	3.0	3.0
5.0	1.93	3.0	1.9	1.9
8.0	1.37	2.0	1.4	1.4
10.0	1.22	1.7	1.2	1.2
16.0	1.05	1.35	1.1	1.1
20.0	1.02	1.25	-	-

It is evident from these plots that an actual load VSWR of 8.5 is not prevented by the circulator from affecting the fundamental outflow power from the amplifier. A maximum change of $\pm$10 percent about the average value occurs. This is small compared with the power loss due to reflection at the mismatched load.

The power outflow at the second harmonic shows much larger variations in amplitude. The plot in Figure 3.5 is on a relative power scale and the amplitude variation is well in excess of 30 dB. The peak level of second harmonic is 45.4 dB below the peak level of fundamental outflow. One other prominent feature of this plot is that the variation in second harmonic level has the same periodicity as the variations in the fundamental. This means that the variations in outflow at second harmonic are caused by the variations in the load impedance presented at fundamental frequency and not the impedance at second harmonic. This point will be discussed further when complete data plots on

Smith charts are presented in the next section.

The plot of power outflow at the third harmonic in Figure 3.6 also shows amplitude variations. The range is not as great as for second harmonic, the maximum level relative to the maximum level of fundamental is 49.6 dB down, but there are positions of the load short circuit such that the third harmonic level can be greater than the second harmonic, e.g., 0.7 inches. The period of the variations is one third of that for the fundamental and indicates that these variations are caused by the changes in load impedance at the third harmonic frequency not the fundamental. The differences in the levels of successive maxima in Figure 3.6 are due to the variations in VSWR that arise from residual reflections from connectors as explained in section 2.7.2. Other plots for lower values of VSWR show that the peak decreases rapidly with decreasing VSWR. With the short circuit set to the 3.7 inch position the resultant VSWR is less than 5.8 and this accounts for the lower level of the harmonic.

The power plots for module SN29M are presented in Figures 3.7 and 3.8 for comparison with those for module SN73M in Figures 3.5 and 3.6. It will be noted that overall features of the plots are similar, that power levels differ somewhat and that the positions of the test load short circuit at which peaks occur are also different. It can be concluded that the gain of the amplifiers, the mechanisms that produce harmonics and the overall insertion electrical lengths of the modules are slightly different.

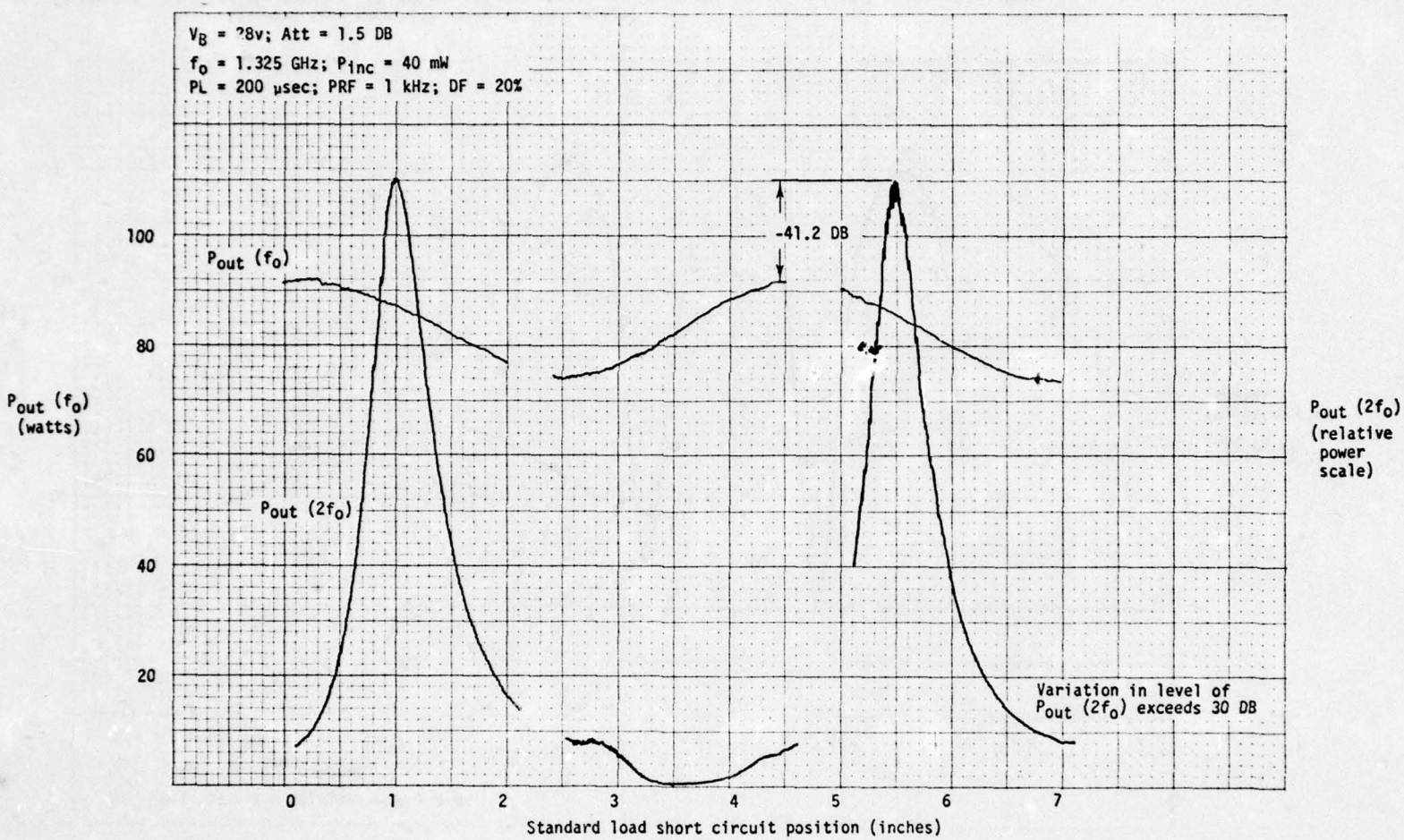

Figure 3.7 Power of the fundamental and second harmonic wave from the output port of L-band module SN29M as a function of the position of the short circuit in the standard load. Load attenuator set 1.5 DB.

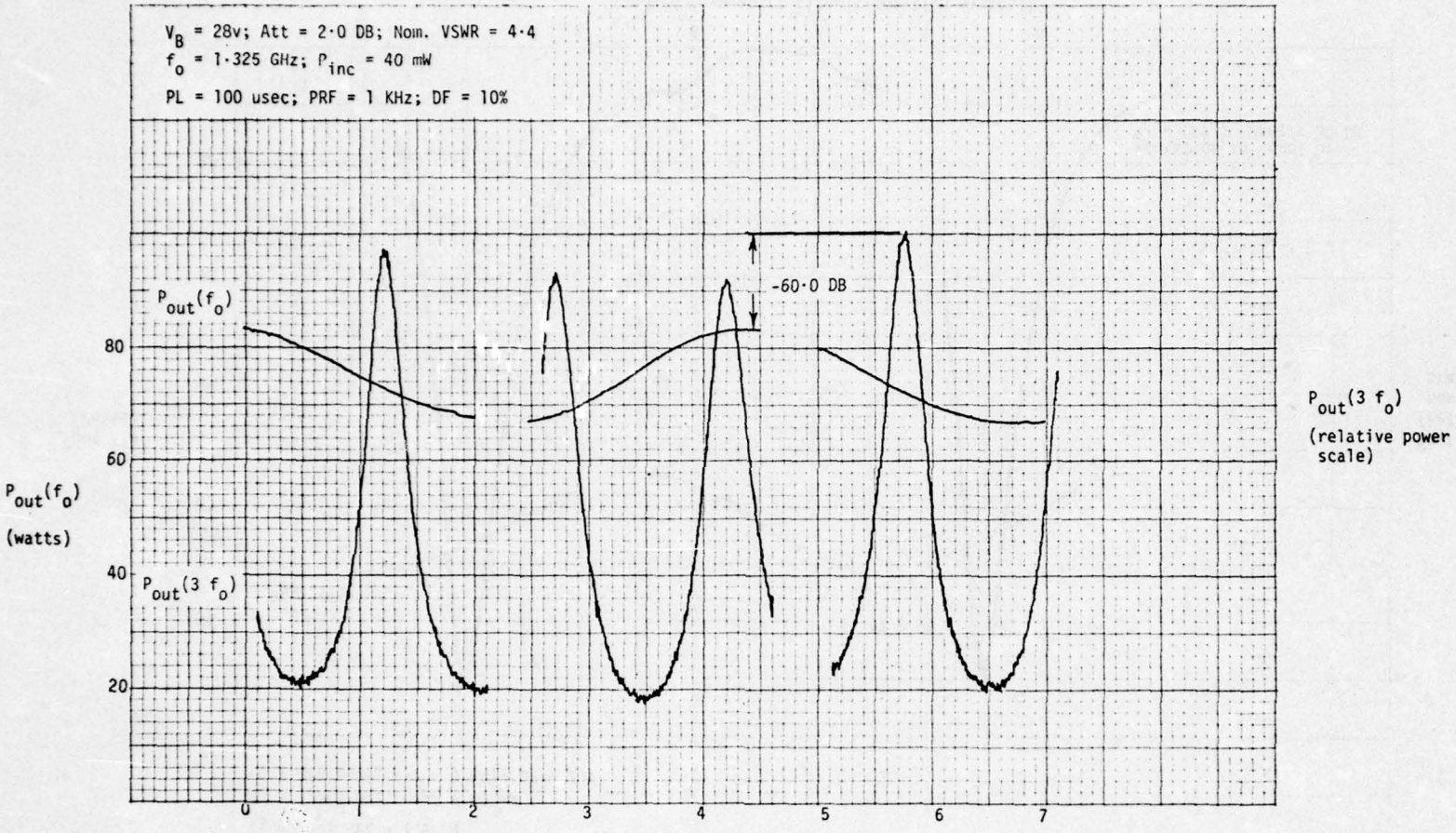

Figure 3.8 Power of the fundamental and the third harmonic wave from the output port of L-band module SN29M as a function of the position of the short circuit in the standard load. Load attenuator set 2·0 DB. Nominal VSWR 4·4.

To illustrate that the apparatus is usable down to nominal VSWR's that might be swamped by residual reflections from connectors in the standard test load, Figure 3.9 shows plots for SN29M with a nominal VSWR of 1.05. Variations in both the fundamental and the second harmonic power levels are clearly evident and accurately reproducible with variation of the position of the test load short circuit.

All of the large number of plots that were made for the two modules cannot be presented but the information contained in them is presented in an integrated form as contours on the Smith chart in the next section.

3.3.3 Results as Equi-Power Contours on Smith Charts

From a complete family of plots of power outflow for suitably chosen values of VSWR, equi-power contours can be constructed on a Smith chart. For L-band module SN73M Figures 3.10, 3.11 and 3.12 are the equi-power contours at fundamental, second and third harmonics. The coordinates for the first two sets of results are the real and imaginary parts of the load impedance at the fundamental frequency. For the third set, the load impedance at the third harmonic applies. The attenuator setting yields a lower value of attenuation at the fundamental frequency than at the harmonics, as already explained in section 3.3.2, and so the contours in the first two sets of results extend over a larger diameter region of the Smith chart than in the third set of results.

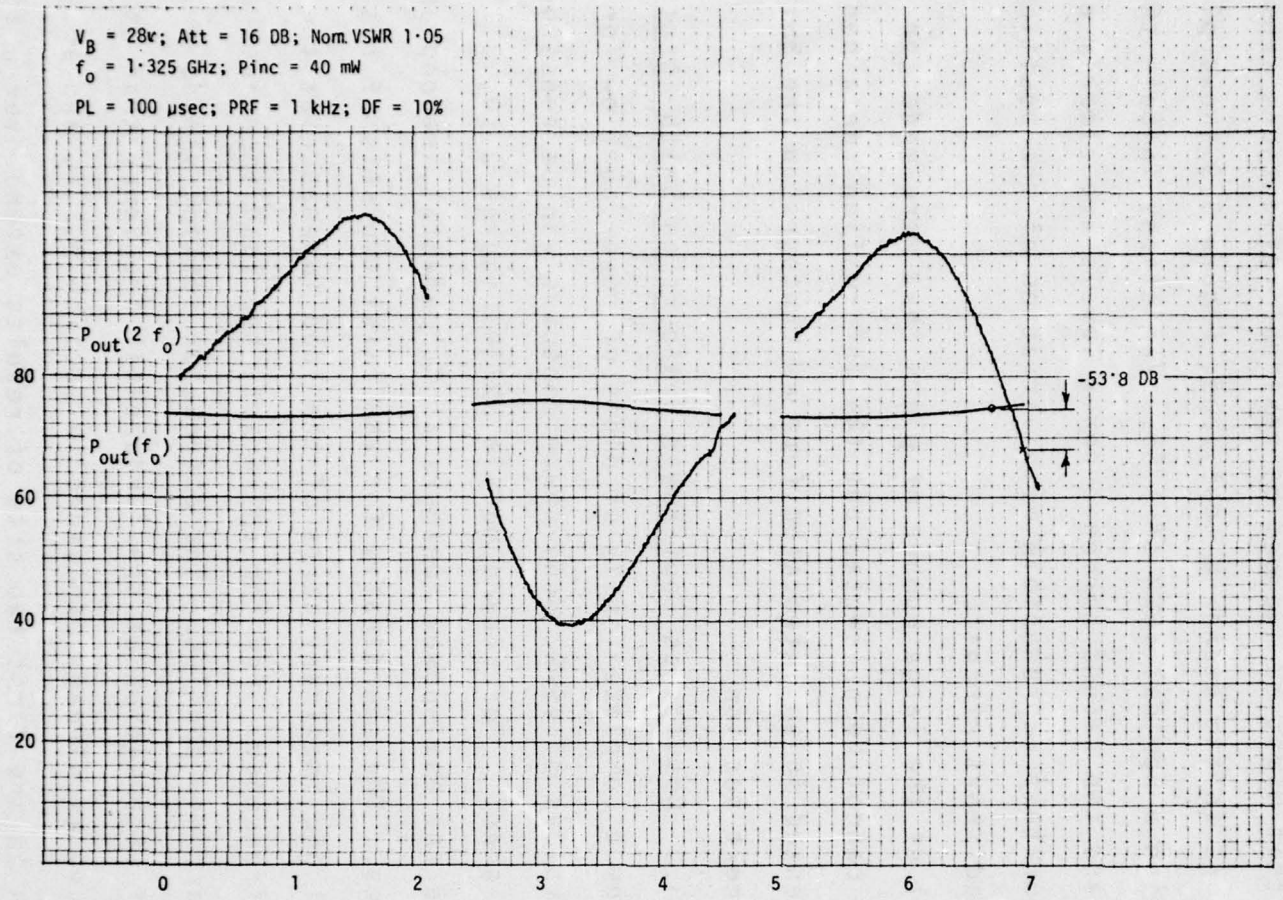

Figure 3.9 Power of the fundamental and second harmonic wave from the output port of L-band module SN29M as a function of the position of the short circuit in the standard load. Load attenuator set 16 dB. Nominal VSWR 1·05.

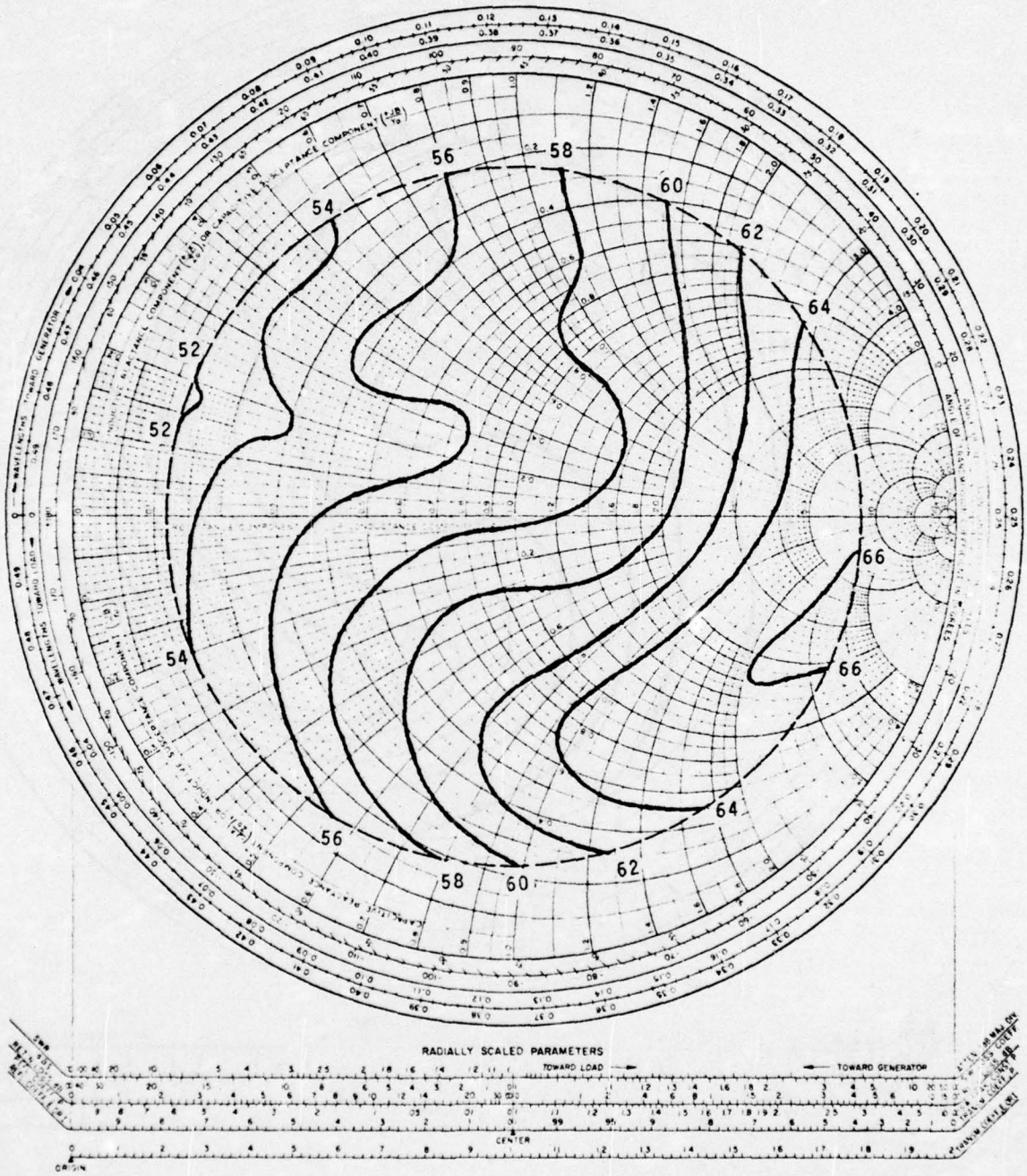

Equi-power contours in watts.
Signal frequency 1.325 GHz. Incident power 40 mW peak.
Signal pulse length 100 microsecs. PRF 1kHz. DF 10%.

Figure 3.10 Power of fundamental wave from the output port of L-band module SN73M as a function of the load impedance at the fundamental.

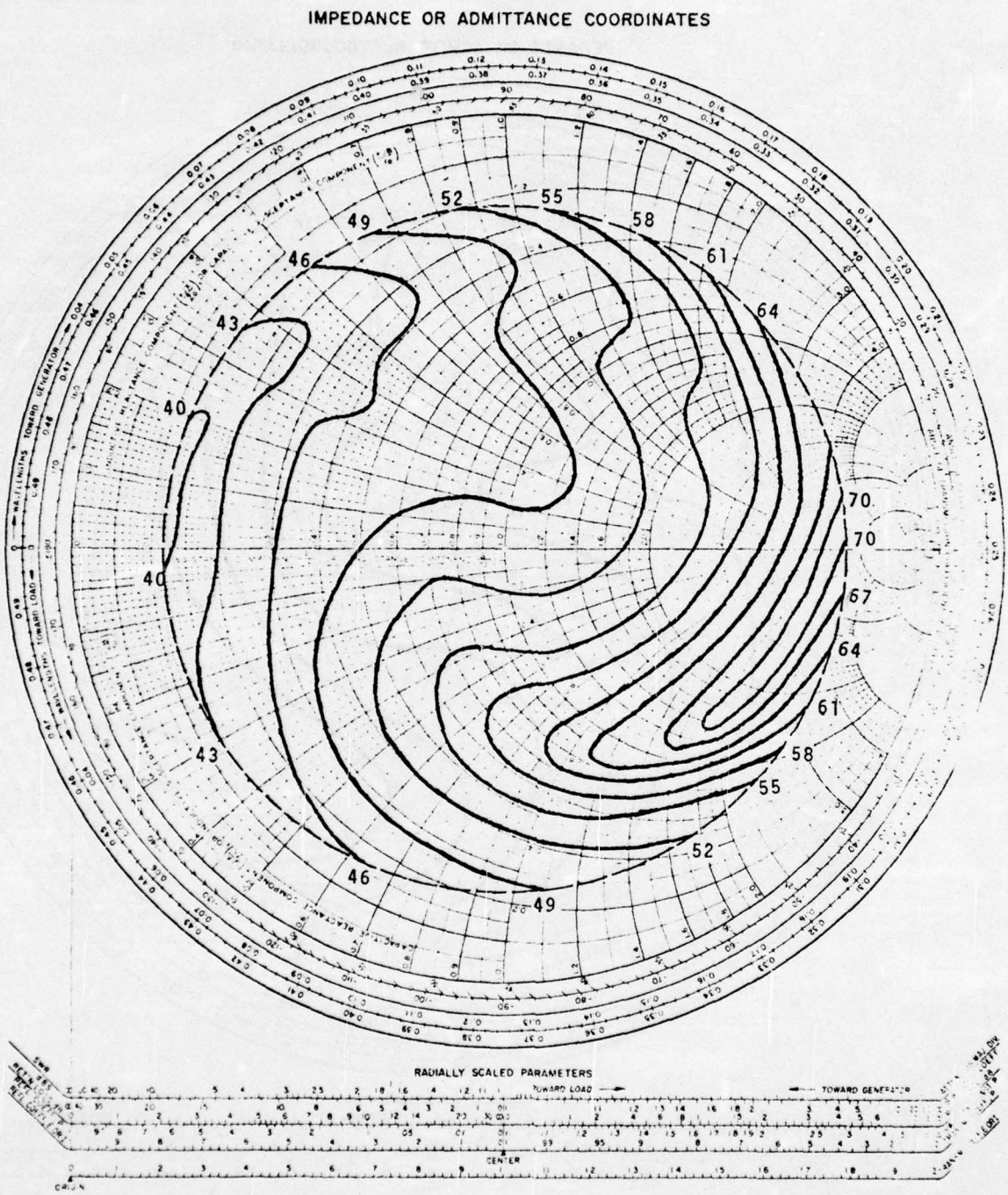

Equi-power contours in DB below fundamental.
Signal frequency 1.325 GHz. Incident power 40 mW peak.
Signal pulse length 100 microsecs. PRF 1kHz. DF 10%.

Figure 3.11 Power of second harmonic wave from the output port of L-band module SN73M as a function of the load impedance at the fundamental.

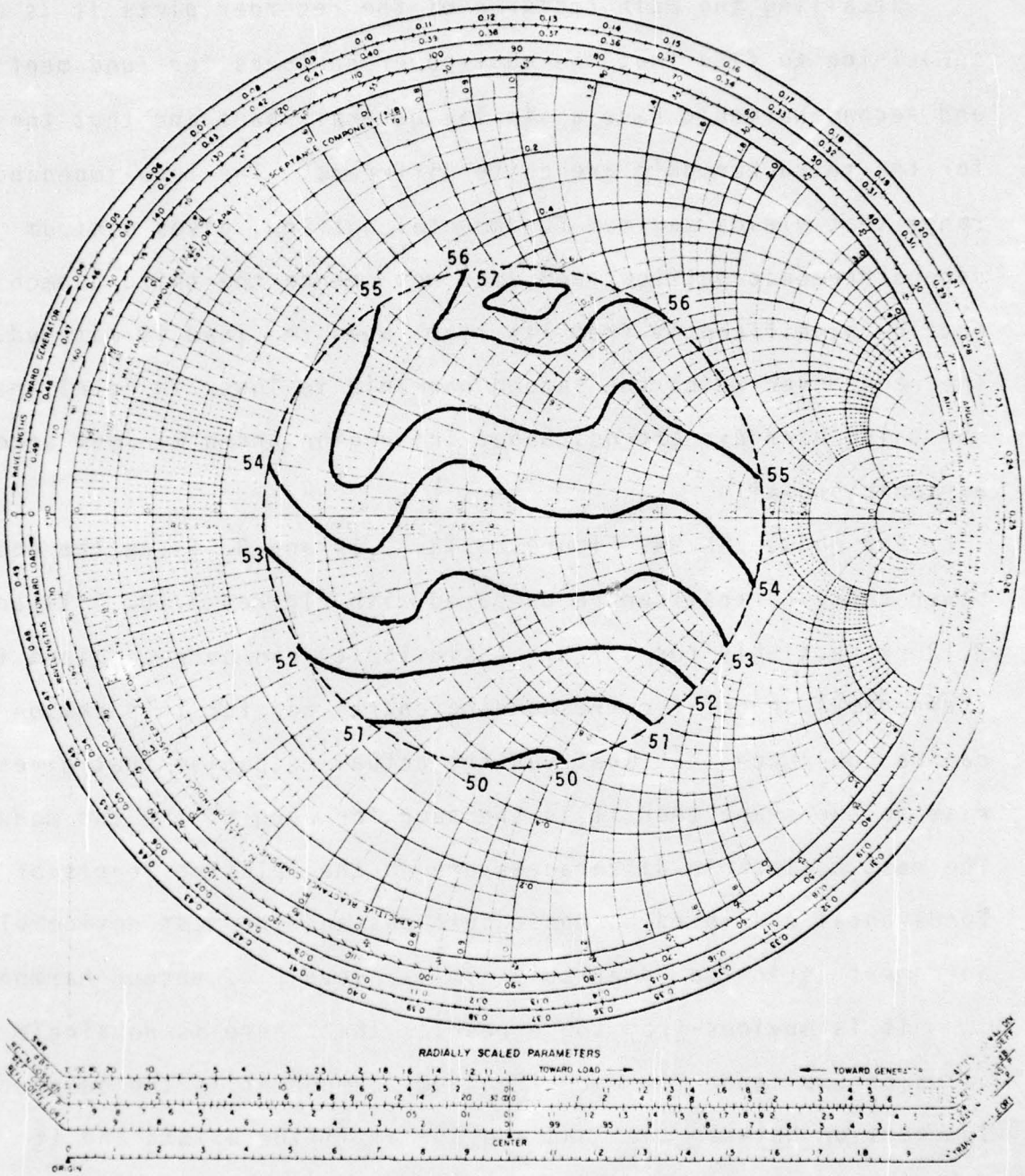

Equi-power contours in DB below fundamental.
Signal frequency 1.325 GHz. Incident power 40 mW peak.
Signal pulse length 100 microsec. PRF 1kHz. DF 10%.

Figure 3.12 Power of third harnonic (3.975 GHz)wave from the output port of L-band module SN73M as a function of the load impedance at the third harmonic.

Recalling the main features of the recorder plots it is not surprising to find that the equi-power contours for fundamental and second harmonic have a similar general shape and that those for the third harmonic are quite different. The load impedance range that yields maximum fundamental outflow, gives minimum second harmonic outflow, and does not change the third harmonic outflow significantly from its level when the load is matched. The range over which the second harmonic is lower in level than the third harmonic extends about the region where minimum second harmonic prevails.

For module SN29M, Figures 3.13, 3.14 and 3.15 are the equi-power contours that can be compared with Figures 3.10, 3.11 and 3.12 respectively for SN73M. A similarity can be recognized in the general shape of corresponding charts and for this reason it can be concluded that whatever the actual mechanism that gives rise to the shape then it is the same for each of the two modules. The most noticeable differences are in the relative levels of fundamental and third harmonic outflows and the most noticeable agreement is in the remarkably similar levels of second harmonic.

It is obvious from these results that there is no single value of amplitude for each frequency component in the output. Interaction between the load and the amplifier exists and it results in variations in the amplitude of components that is large for the second harmonic, moderate for the third harmonic and small for the fundamental.

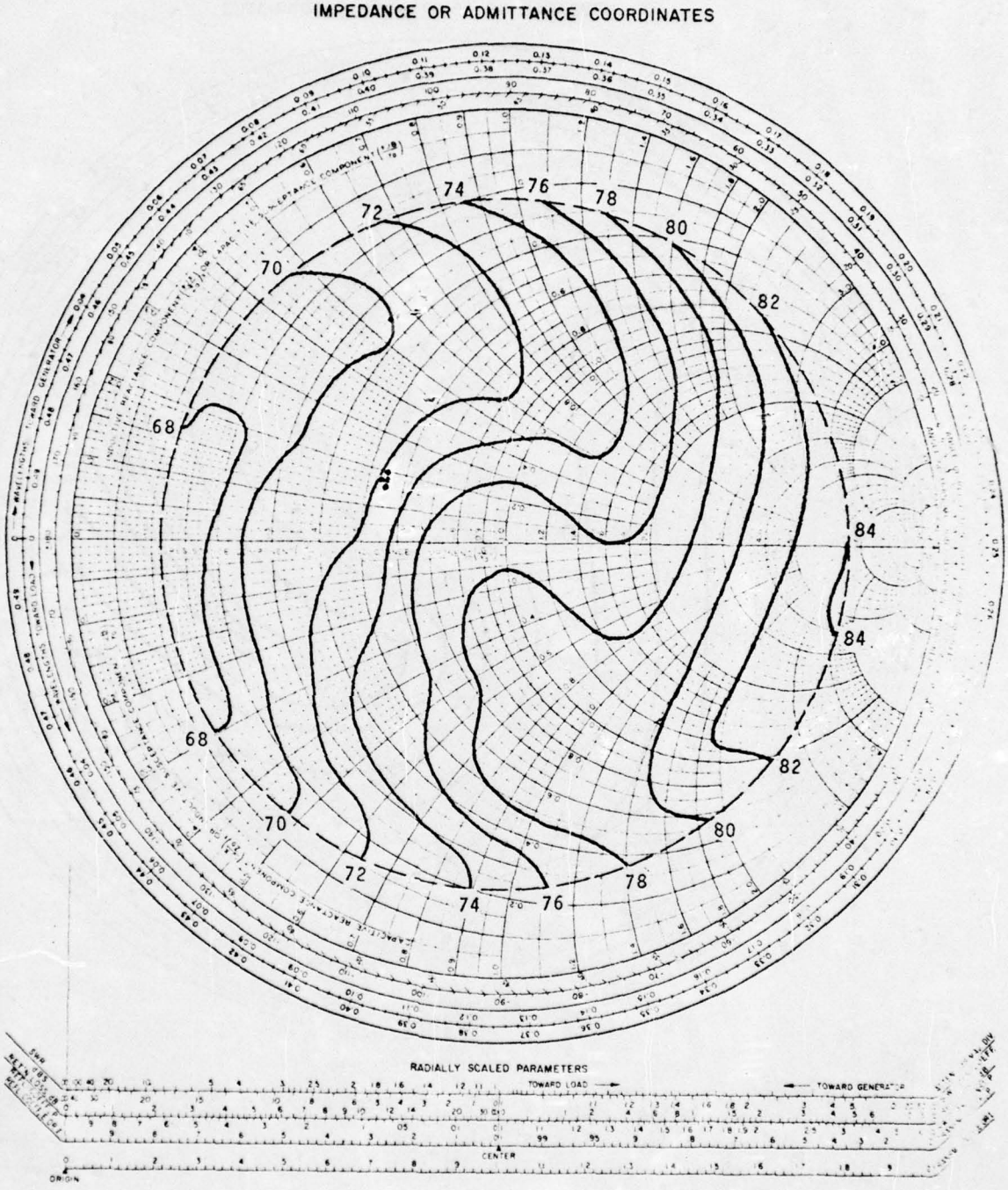

Equi-power contours in watts.
Signal frequency 1.325 GHz. Incident power 40 mW peak.
Signal pulse length 100 microsecs. PRF 1kHz. DF 10%.

Figure 3.13 Power of fundamental wave from the output port of L-band module SN29M as a function of the load impedance at the fundamental.

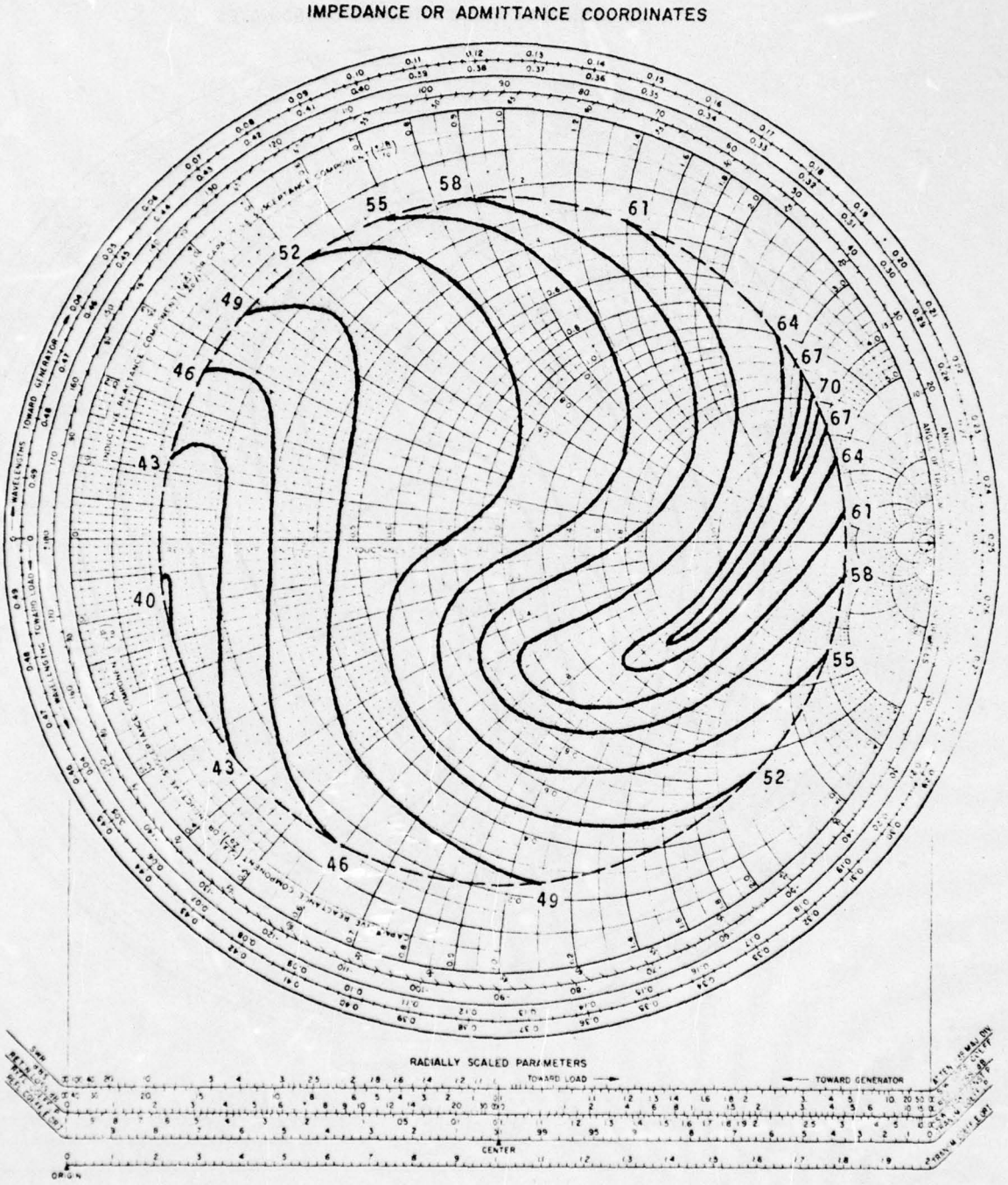

Equi-power contours in DB below fundamental.
Signal frequency 1.325 GHz. Incident power 40 mW peak.
Signal pulse length 100 microsecs. PRF 1kHz. DF 10%.

Figure 3.14 Power of second harmonic wave from the output port of L-band module SN29M as a function of the load impedance at the fundamental.

AD-A032 130 SYRACUSE UNIV N Y DEPT OF ELECTRICAL AND COMPUTER E--ETC F/G 9/5
SOLID STATE ARRAY STUDIES RELEVANT TO OTP REGULATIONS. PART 1. --ETC(U)
AUG 76 D W GRIFFIN F30602-75-C-0121
UNCLASSIFIED RADC-TR-76-241-PT-1 NL

2 OF 3
AD
A032130

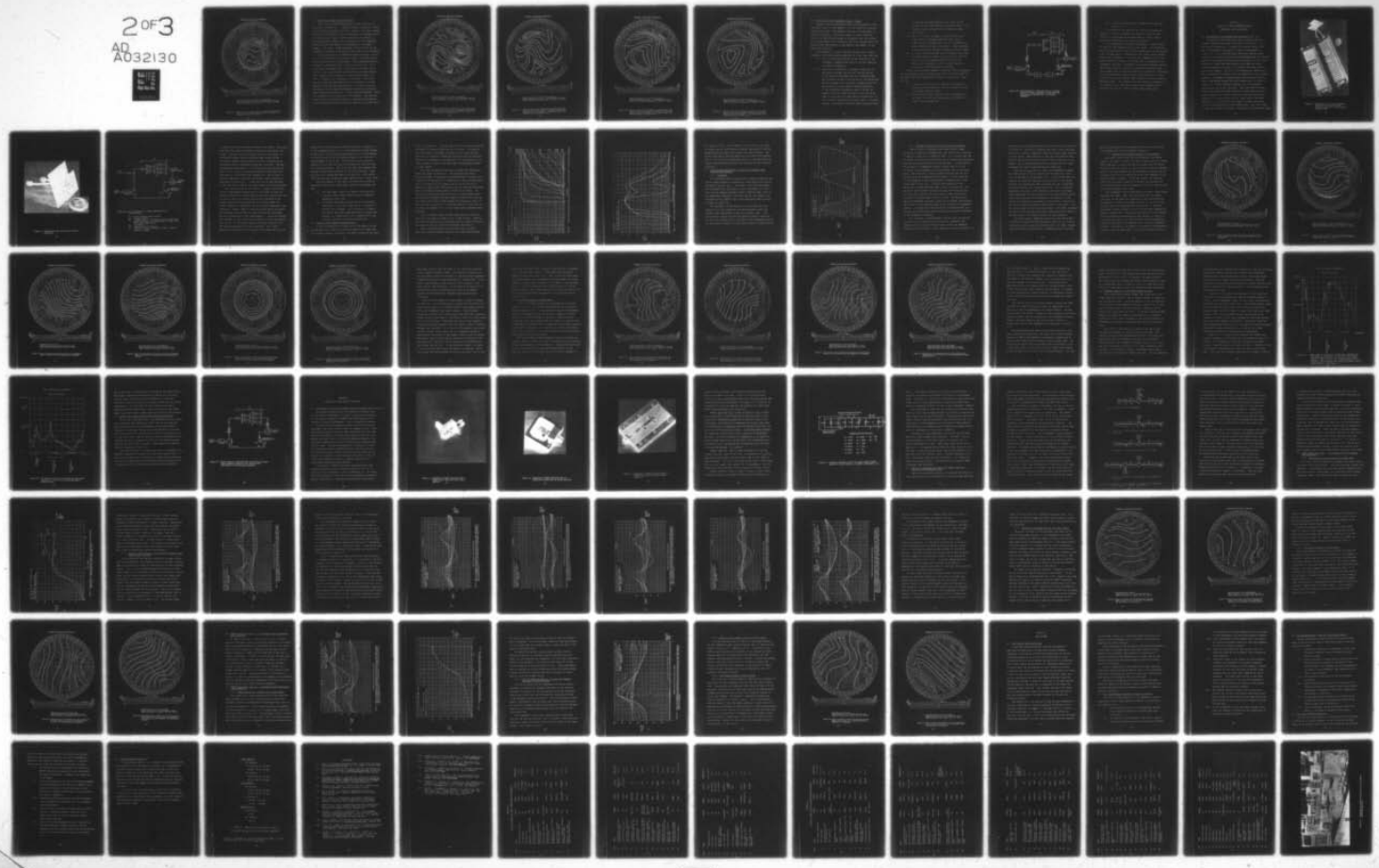

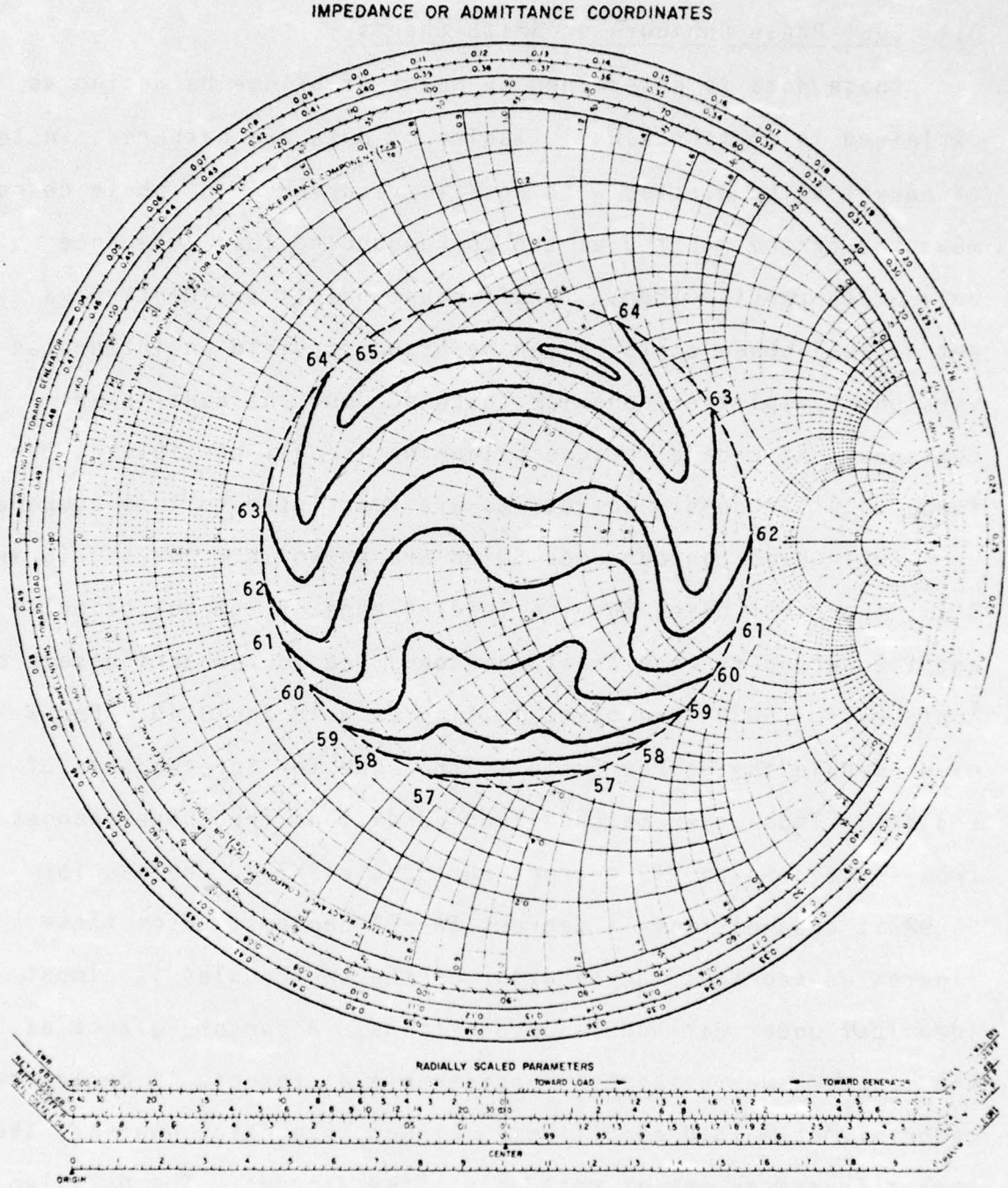

Equi-power contours in DB below fundamental.
Signal frequency 1.325 GHz. Incident power 40 mW peak.
Signal pulse length 100 microsecs. PRF 1kHz. DF 10%.

Figure 3.15 Power of third harmonic (3.975 GHz) Wave from the output port of L-band module SN29M as a function of the load impedance at the third harmonic.

3.4 Equi-Phase Contours on Smith Charts

Phase data is determined by means of bridge balancing as explained in section 2.6. Tables of data are gathered, instead of curves being plotted with an XYY' recorder. The phase changes measured can be plotted at the corresponding load impedance point on a Smith chart. Then, if sufficient points are plotted, a set of equi-phase contours can be drawn to yield an integrated version of amplifier behavior to complement the equi-power contours. At L-band, bridge balancing is only possible at the fundamental frequency so results are restricted to this component.

Equi-phase contours for SN73M are shown in Figures 3.16 and 3.17, the first being for the leading edge of the output pulse and the second for the trailing edge. The corresponding sets of contours for SN29M are given in Figures 3.18 and 3.19. For a given module the degree scale is the same for the two sets of results. Thus under matched load conditions the phase changes from -3 degrees to +19 degrees for module SN73M, whereas for SN29M it changes from -3 degrees to +18 degrees. From these figures we see that the behavior of the two modules is almost identical under matched load conditions. A cursory glance at the contours would suggest considerable difference in behavior under mismatch load conditions. Closer inspection however, shows that differences are at most only a few degrees. The detailed features cannot be explained without a more detailed knowledge of various possible effects within the module as discussed below.

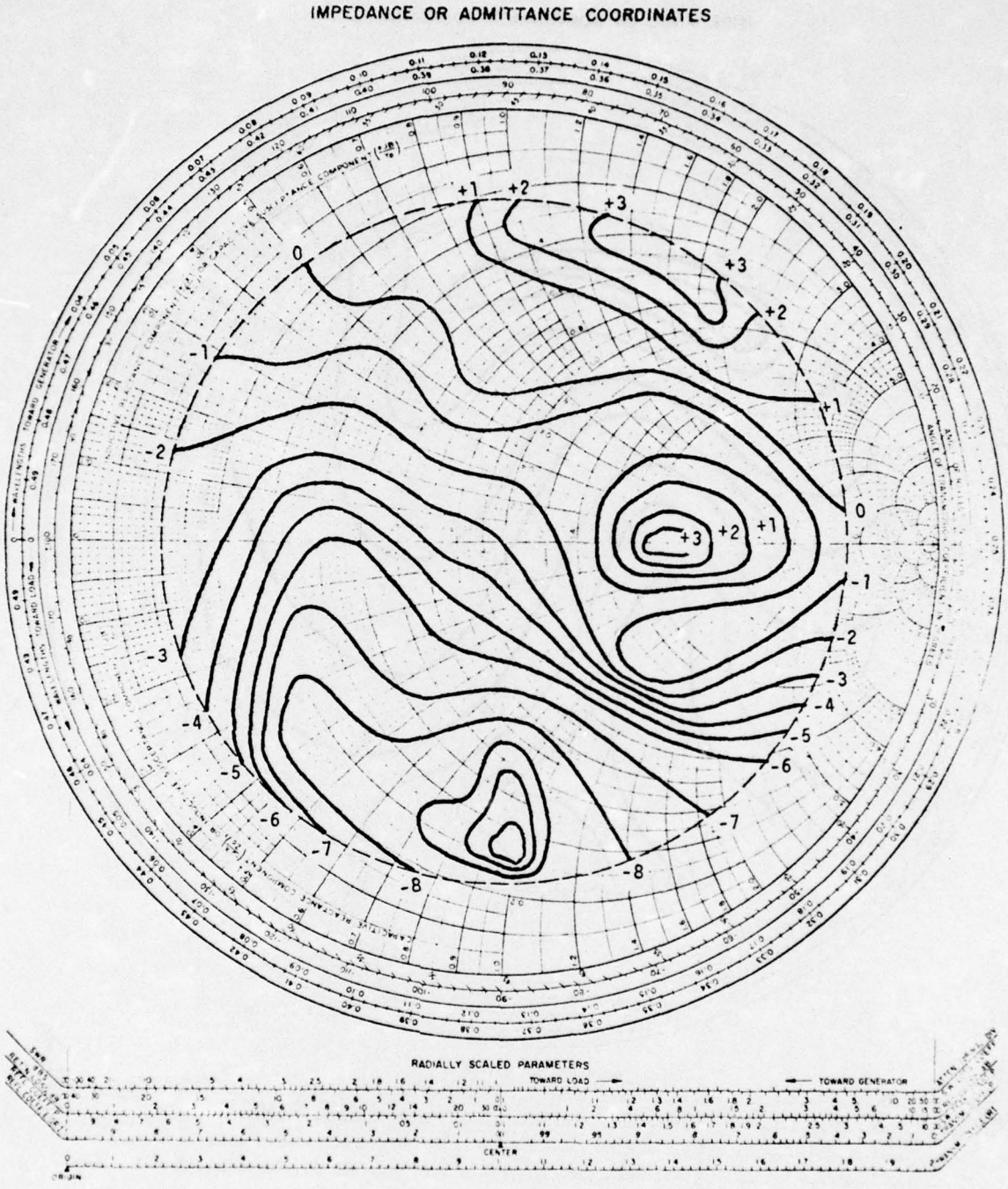

Equi-phase contours in electrical degrees.
Signal frequency 1.325 GHz. Incident power 40 mW peak.
Signal pulse length 100 microsecs. PRF 1kHz. DF 10%.

Figure 3.16 Relative phase of the fundamental wave from the output port of L-band module SN73M as a function of the load impedance at the fundamental. Measurement made at the leading edge of the output pulse.

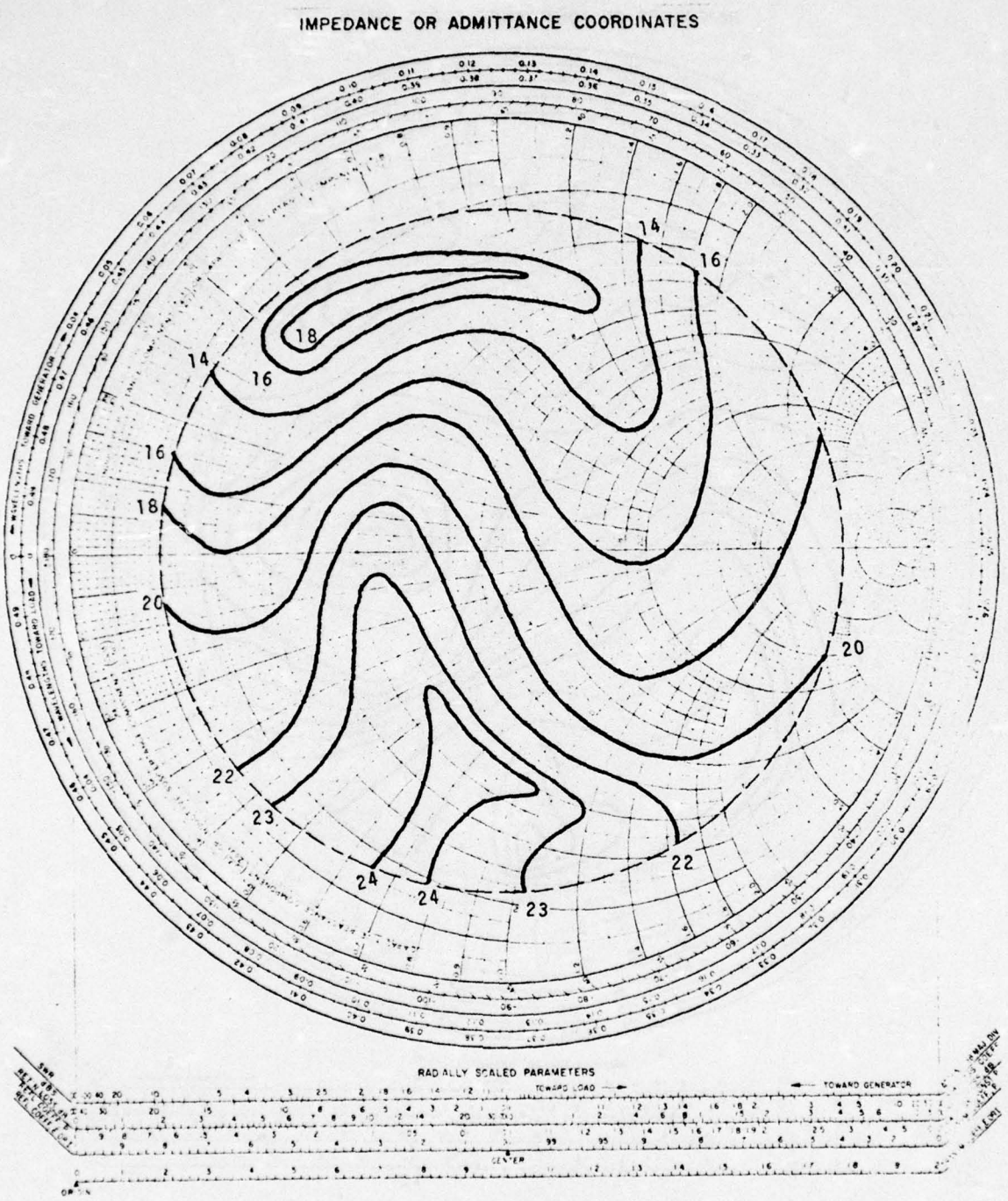

Equi-phase contours in electrical degrees.
Signal frequency 1.325 GHz. Incident power 40 mW peak.
Signal pulse length 100 microsecs. PRF 1kHz. DF 10%.

Figure 3.17 Relative phase of the fundamental wave from the output port of L-band module SN73M as a function of the load impedance at the fundamental. Measurement made at the trailing edge of the output pulse.

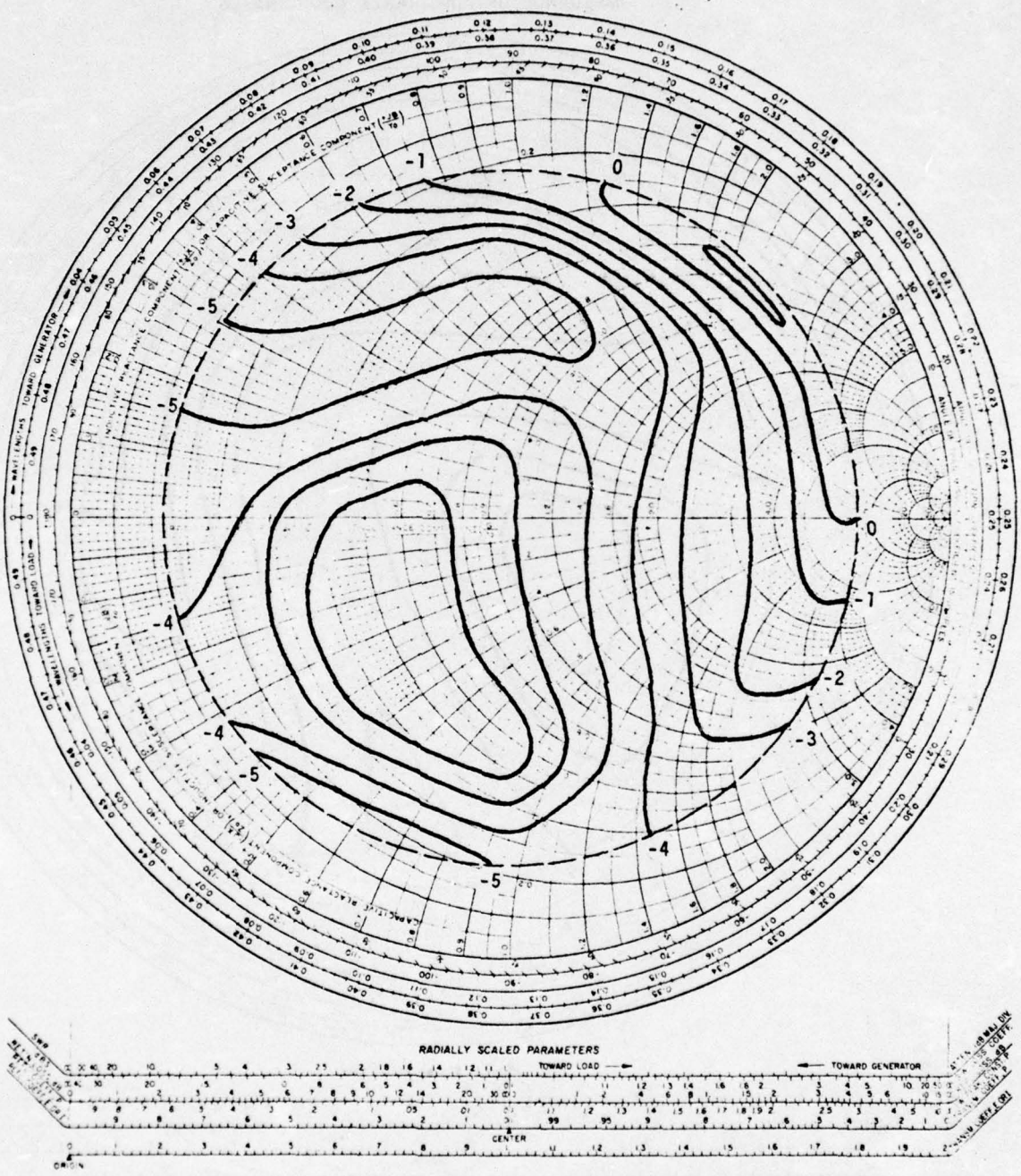

Equi-phase contours in electrical degrees.
Signal frequency 1.325 GHz. Incident power 40 mW.
Signal pulse length 100 microsecs. PRF 1kHz. DF 10%.

Figure 3.18 *Relative phase of the fundamental wave from the output port of L-band module SN29M as a function of the load impedance at the fundamental. Measurement made at the leading edge of the output pulse.*

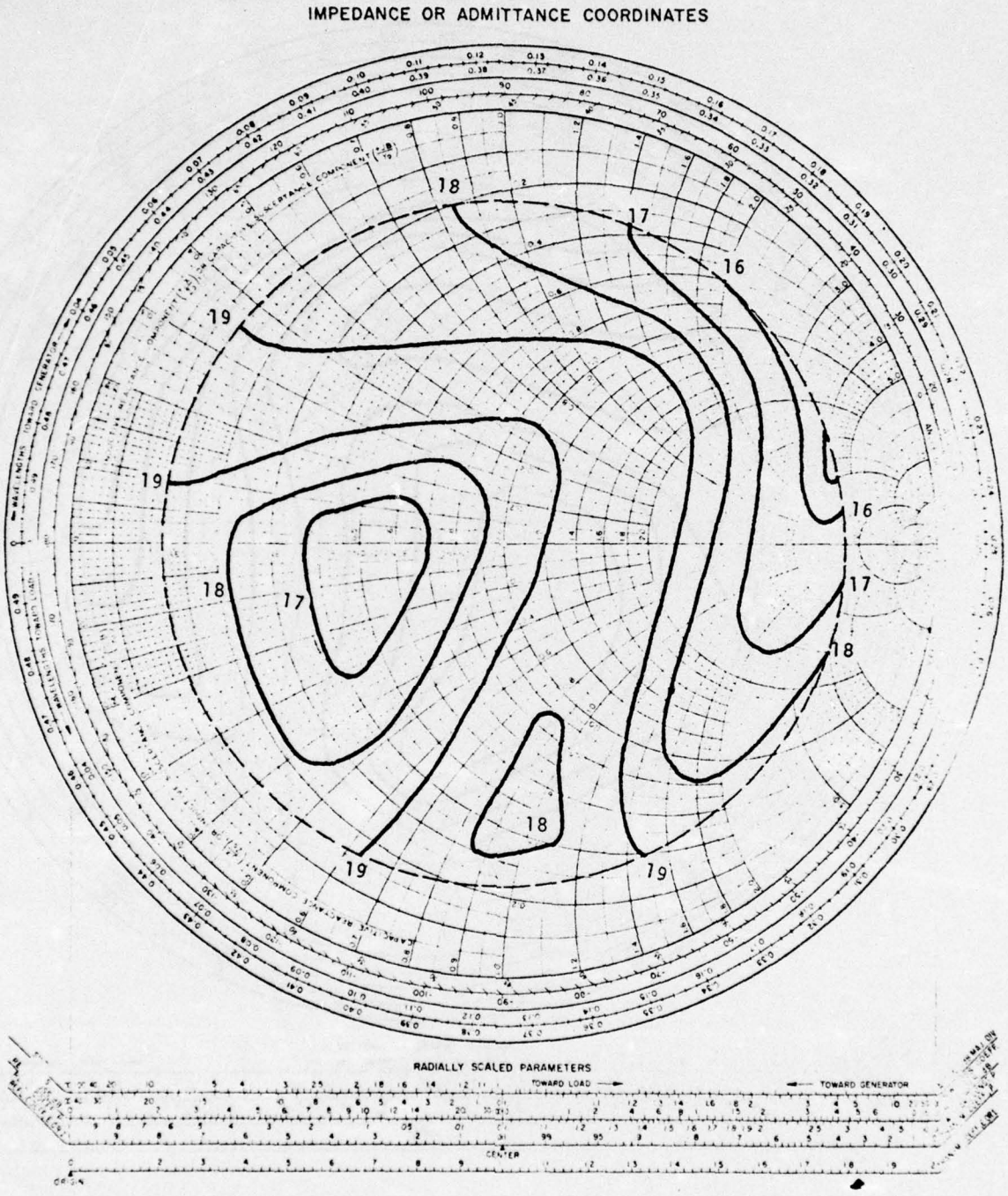

Equi-phase contours in electrical degrees.
Signal frequency 1.325 GHz. Incident power 40 mW.
Signal pulse length 100 microsecs. PRF 1kHz. DF 10%.

Figure 3.19 Relative phase of the fundamental wave from the output port of L-band module SN29M as a function of the load impedance at the fundamental. Measurement made at the trailing edge of the output pulse.

3.5 Effects That Could Determine Contour Shapes

Because it was not possible to make any measurements on the individual parts of these modules, it is not possible to explain the detailed shape of the contours obtained from measurement of overall performance. There are a number of points about the function of the different stages in the module that are relevant to its performance and discussion of them is a starting point for gaining some understanding of the behavior that appears in the Smith chart contours.

The following is a list of the more obvious ways in which components within the module may perform in a less than ideal way.

(i) the circulator will provide finite isolation in the fundamental frequency band and will be less effective at harmonic frequencies

(ii) there will be some level of leakage through the T-R and channel switches and this will be more serious in the transmit mode when high level microwave power may be present at the T-R switch due to load reflection. Any such leakage will constitute a feedback path from the output port to the input of the pre-amplifier. If the attenuation through this path is 60 dB, for example, then the signal fed back will be only 27 dB lower in level than the input and in voltage terms it will be about 5 percent of the input level. T-R switch leakage is designed so that with total reflection from

the antenna the power incident on the input to the limiter will not reach receiver degradation level. The limiter allows a maximum of 50 milliwatts to reach the receiver

(iii) the first of the five stages of amplification used under transmit conditions operates under class A conditions and the rest under class C. Variations in output loading will cause variations in input impedance of these relatively low gain microwave amplifier stages

(iv) to isolate load variations from the output of the final microwave amplifier stage not only must the circulator have low reverse leakage properties but also the termination connected via the T-R switch should be as close to reflection-free as practical.

Taking the above points together, additional signal components can be expected on the input and output lines of the pre-amplifier and power amplifier respectively as shown in Figure 3.20. These will be,

(i) a reverse travelling set of components (fundamental, second and third harmonics) from the circulator to the final power amplifier stage

(ii) an additional forward travelling set of components on the input line from the channel switch to the first stage of the pre-amplifier

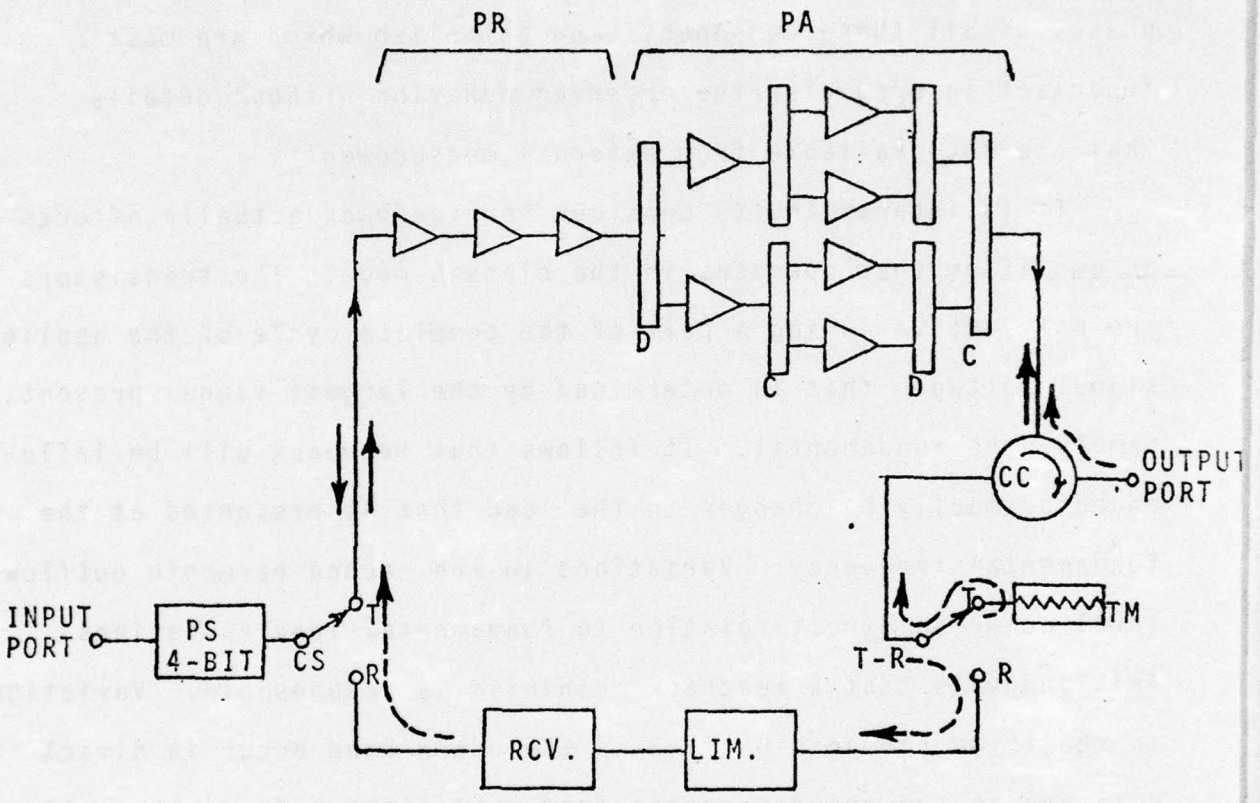

Figure 3.20 Block diagram of L-band amplifier unit showing additional signal components arising from load reflection and imperfections in microwave components

(iii) a reverse travelling set of components on the same line as (ii).

It is impossible to determine the relative magnitude and phases of all these components and establish which are most important in producing the observed behavior without details that are not available from external measurements.

It is interesting to consider how feedback actually affects an amplifier that operates in the class C mode. The transistors are only active during a part of the complete cycle of the applied signal voltages that is determined by the largest signal present, namely, the fundamental. It follows that feedback will be influenced primarily by changes in the load that is presented at the fundamental frequency. Variations in the second harmonic outflow level occur in direct relation to fundamental load variations. This suggests that a feedback mechanism is responsible. Variations in the third harmonic outflow on the other hand occur in direct relation to the third harmonic load variations and are of smaller amplitude range. This suggests that the mechanism responsible is an interaction with the output stage through leakage and re-reflection around the "load-circulator-output-stage" path.

CHAPTER 4

STUDIES OF S-BAND MICROWAVE BIPOLAR TRANSISTOR AMPLIFIER MODULES

4.1 Description of the S-Band Modules Studied (Ref. 8,9)

The overall S-band transceiver module assembly that was studied, comprised the three items shown in Figure 4.1. It is described in reference 3. Two amplifier modules drive an element of the antenna array which is shown in more detail in Figure 4.2. It is a crossed dipole which will radiate either linearly or circularly polarized waves depending upon the relative phasing of the output from each amplifier module. The amplifier modules are fitted with OSM connectors for input and output microwave signals and a multi-pin connector for power supplies and control signals. The unit is not hermetically sealed but it was not practical to attempt tests on subsections of the internal assembly. A schematic diagram showing the microwave functions that are performed between the two microwave ports is shown in Figure 4.3. In the transmit condition, the T-R and channel switches are set to the T position. Pulse modulated microwave input at the relatively high level of 0.5 watts and in the frequency range 3.1 to 3.5 GHz, enters the input port and passes through a 3 bit phase shifter to the input stage of the power amplifier. The output from that stage is divided to provide drive for two transistors in the second stage. The final stage is made up of three transistors so the output from the second stage

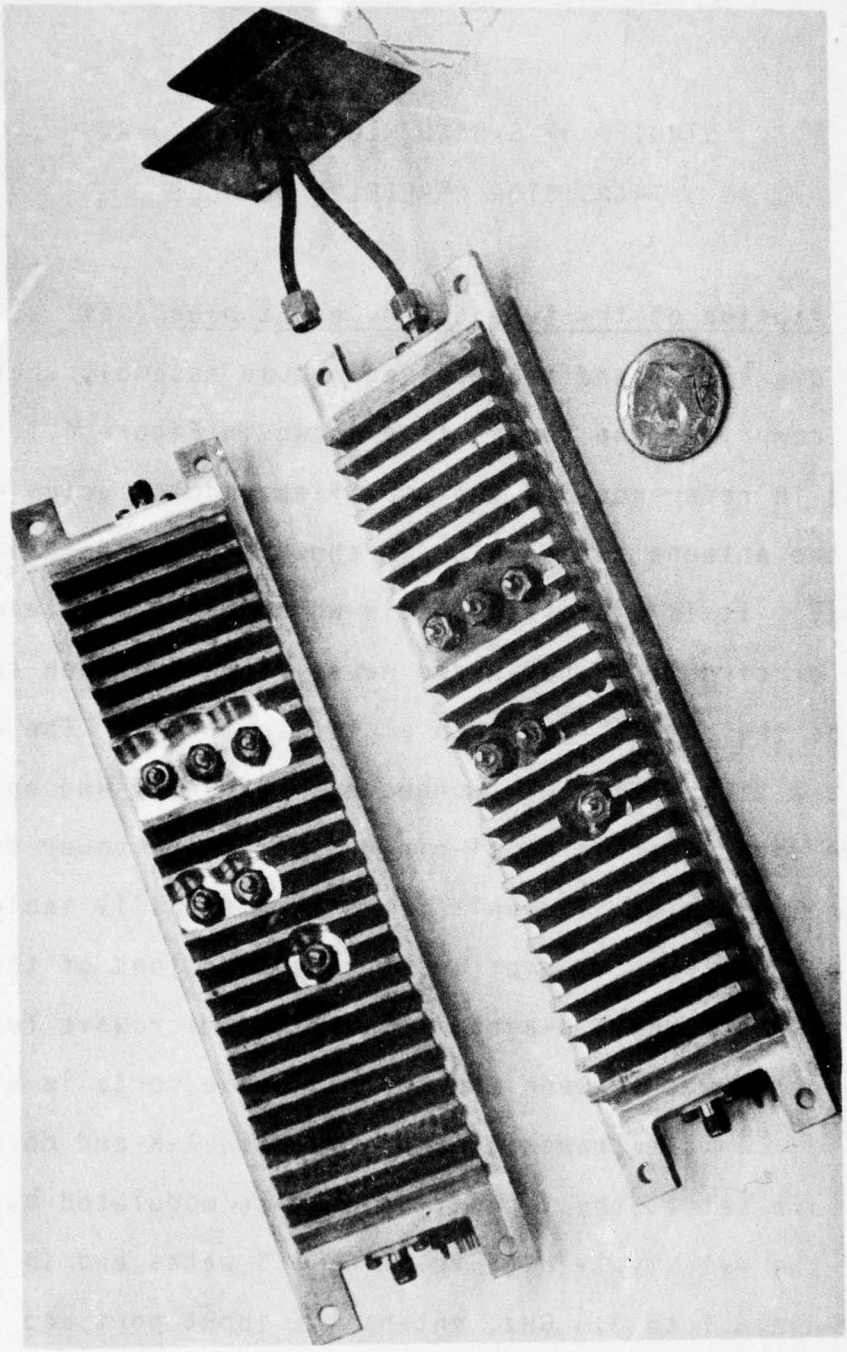

Figure 4.1 Photograph of the S-band transceiver module assembly comprising two amplifier units and a crossed dipole antenna element

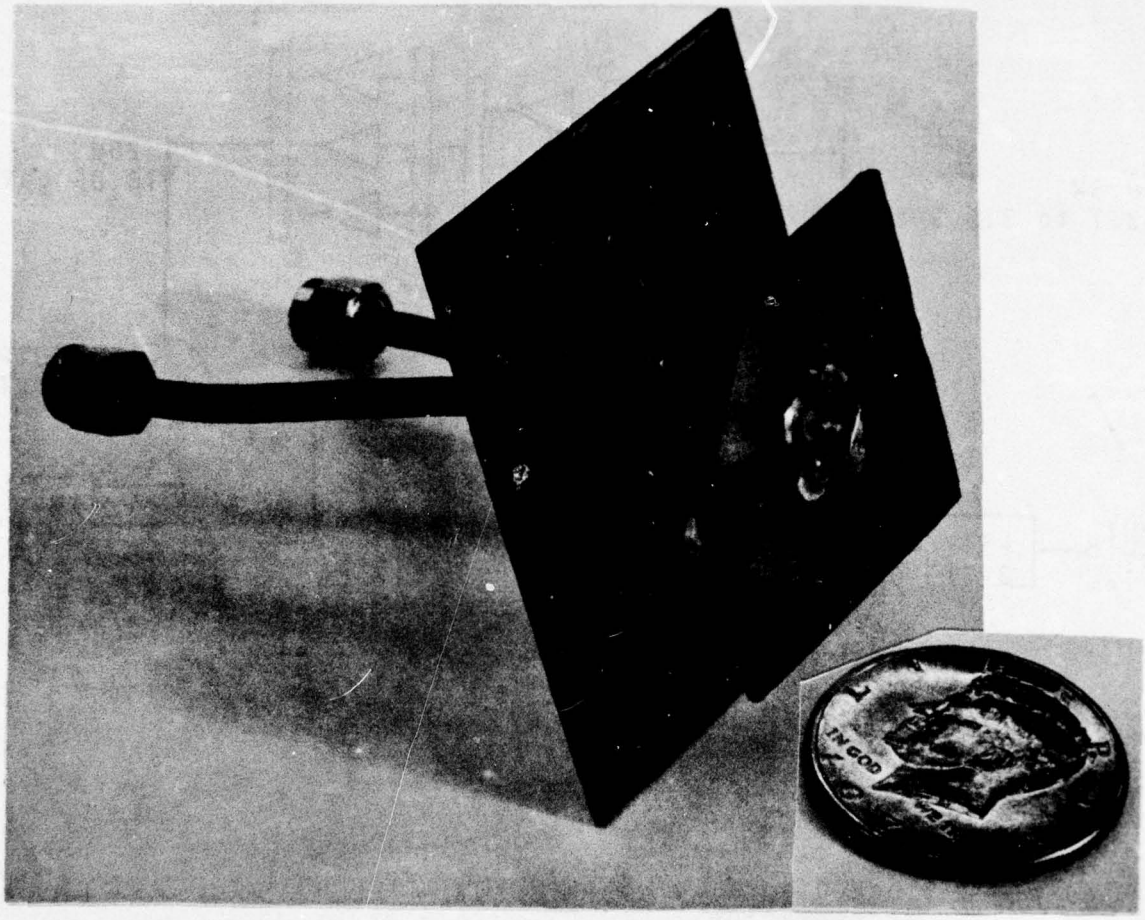

Figure 4.2 Photograph of the crossed dipole antenna - bowtie type

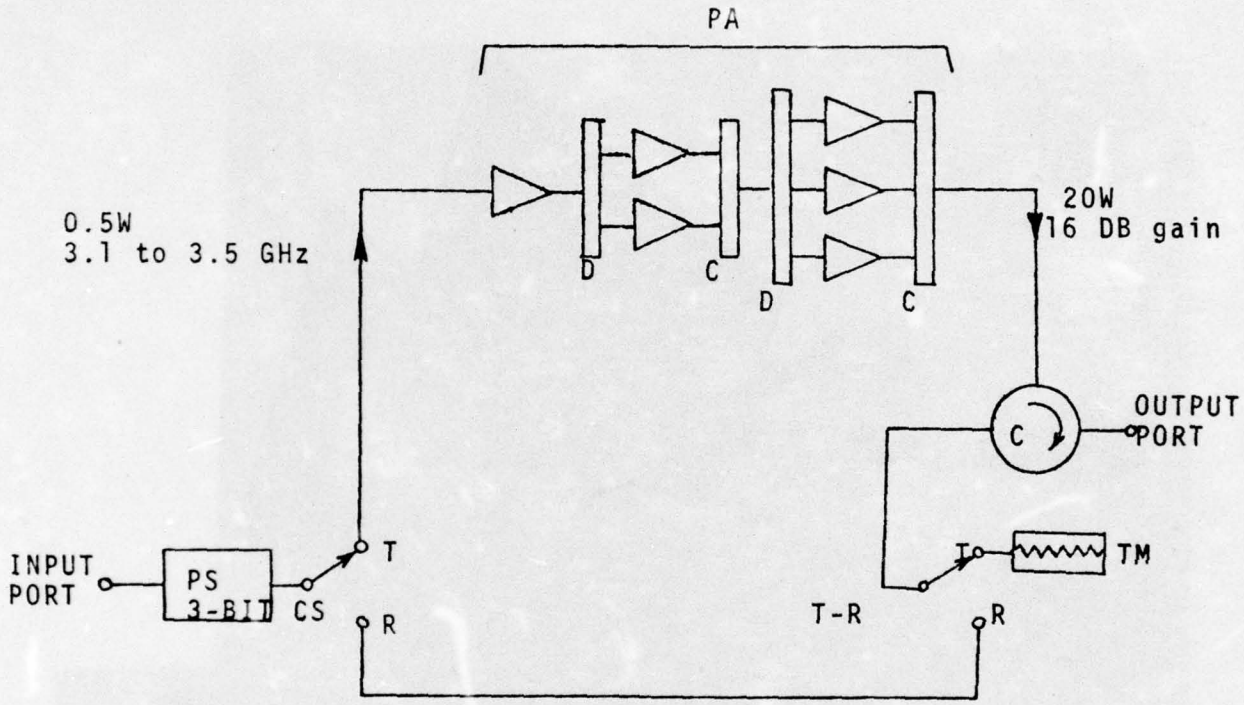

Figure 4.3 Block diagram of S-band amplifier unit incorporating

PS 3-bit digital phase shifter
CS channel switch
PA 3-stage class C microwave bipolar transistor power amplifier including power dividers (D) and power combiners(C)
CC circulator
TR transmit-receive switch
TM termination for reflections under transmit condition shown

is combined and then divided into three drive signals. The output from the final stage is nominally 20 watts and the overall gain 16 dB. It passes via the circulator to one of the dipoles in the antenna element and any reflected power returns to the circulator, emerges from the third port and is absorbed by the termination that is connected through the T-R switch. The maximum operating pulse width is 1 millisecond and the maximum duty cycle is 10%. Most of the tests performed on these amplifiers were done at a pulse repetition frequency of 1 kHz to permit a selective amplifier to be used for harmonic level recording as explained in section 3.3.1. A duty cycle of 10% was used most of the time and as a result the pulse length was 100 microseconds.

The receive channel in this module is simpler than the one in the L-band modules because there is no limiter or amplifier. Received signals pass via the circulator to the R position on the T-R switch, then via a coaxial line to the R position on the channel switch and then through the 3-bit phase shifter for signal processing in other parts of the receiver connected to the input port. Because there is no receiver gain within the module and the power amplifier has less gain than the pre- and power amplifier combination in the L-band module, it can be anticipated that feedback is less likely to be a problem in the S-band module provided the T-R and channel switches give good isolation from the receive path when set in the T position. Small signal measurements were made from the output to the input port with the

amplifier set in the transmit condition as shown in Figure 4.3. In the fundamental band 3.1 to 3.5 GHz attenuation varied between 44 and 52 dB, in the second harmonic band 6.2 to 7.0 GHz between 30 and 55 dB and in the third harmonic band 9.3 to 10.56 GHz it varied between 33 and 48 dB. These are not precise values of insertion loss of the path back to the amplifier input but they are a close indication. The values are lower than expected and probably reflect the limitations of the S-band switches. They may also give a reason why there is no amplifier in the coaxial line receiver path and why the power amplifier gain is only 16 dB.

Two other aspects of this amplifier module that relate to the state of the art on S-band power transistor development are that

(i) the input power cannot be allowed to rise more than 2 dB above the 0.5 watt operating level, otherwise damage may result, and

(ii) the VSWR on the output line of any one of the power transistors in the final stage may not rise above 2:1 without risk of damage. The circulator will reduce the VSWR of any given mismatched load by a factor that depends in a complex way on its isolation and on the residual reflection from the termination TM.

4.2 Input Drive and Response Characteristics

In order to determine the signal drive requirements of the S-band amplifiers a series of plots were made of the power flow to a matched load as a function of the power incident on the input

port of the amplifier. This was done at closely spaced frequencies throughout the passband specified for the module. In addition, plots were made of the power reflected from the input so that behavior as a function of absorbed input power could be obtained. Because this refinement is not essential for the purposes of this study, results in terms of incident power are presented throughout this chapter.

Plots for the amplifier with serial number 145, designated SN145, are shown in Figure 4.4. The pronounced non-linear relation between incident power and outflow power indicates class C operation in the amplifier. Manufacturer's tests involved drive levels of either 0.4 or 0.5 watts and in view of the risk of damage that could result from overdriving, no tests were performed with an incident microwave power in excess of 0.5 watts. The threshold incident power that gives rise to output depends upon the excitation frequency and the response characteristics derived from these plots exhibit large changes with increasing levels of drive as seen in Figure 4.5. From these results a drive level of 0.5 watts was adopted for all of the studies with mismatched load conditions.

Plots of outflow versus incident power were also made with transistor bias supply voltages of 26, 27 and 28 volts. Performance improves steadily with increasing bias so a level of 28 volts was chosen for the more detailed mismatched load studies.

Similar features appear in the outflow versus incident power plots and the response characteristics that were obtained

Figure 4.4 Power outflow versus power incident characteristics for S-band amplifier SN145 for various excitation frequencies.

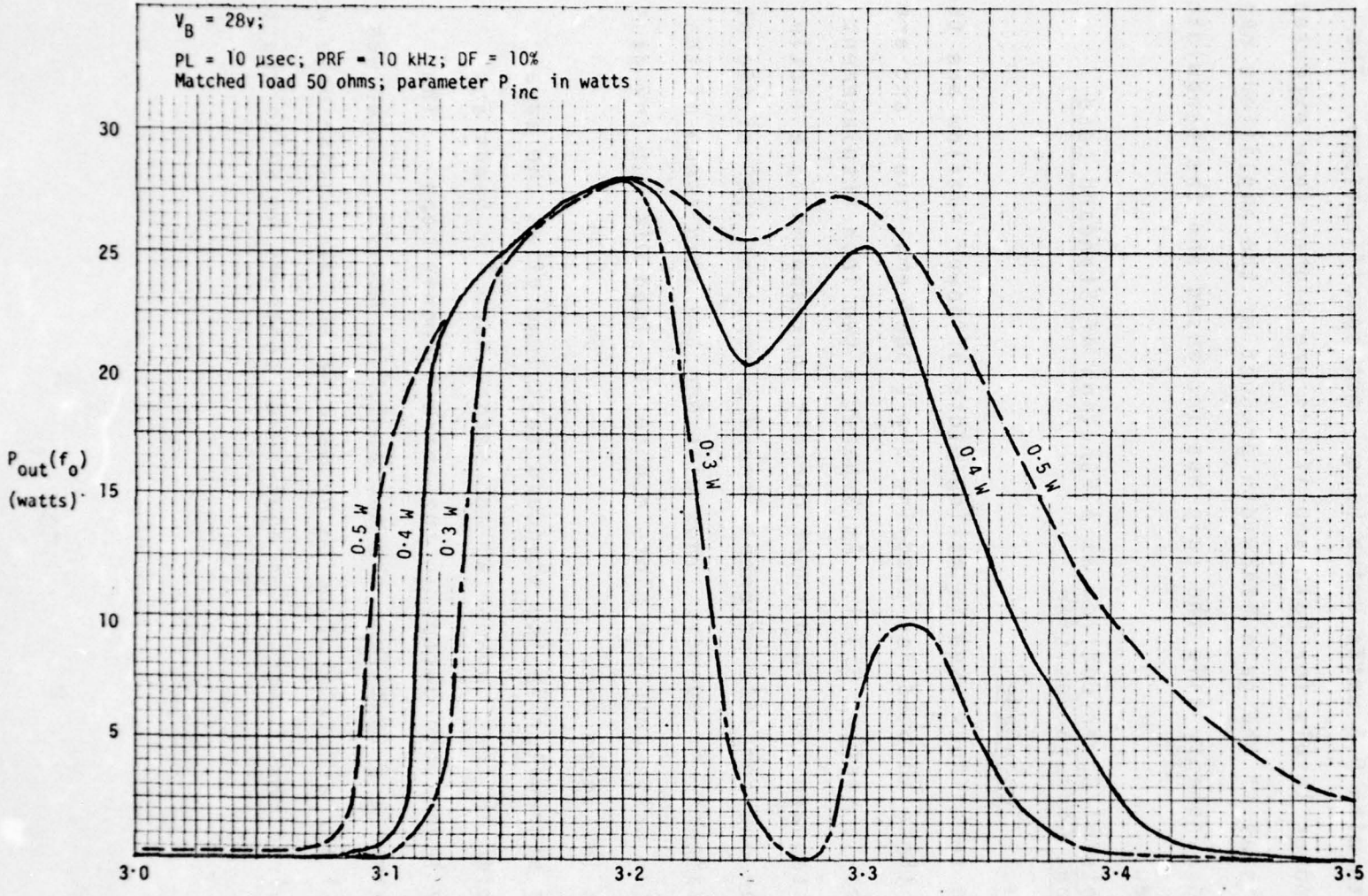

Figure 4.5 Frequency response characteristics for various excitation power levels for S-band amplifier SN145.

for amplifier SN99. As with SN145, a drive level of less than 0.4 watts gave an unsatisfactory response characteristic and the bandwidth with 0.5 watts drive barely met specifications. The output power levels for both amplifiers are higher than expected and it is as if the gain bandwidth product of the amplifiers has remained constant while the gain has increased and the bandwidth decreased.

4.3 Plots of Power Outflow as a Function of Standard Load Short Circuit Position

4.3.1 Technique

The techniques used in making plots of power outflow are the same as those adopted for studying the L-band amplifiers and are presented in section 3.3.1. At S-band, a two inch displacement of the standard test load short circuit corresponds to a little more than one complete movement around a constant VSWR circle at the fundamental frequency. Thus with one two inch sweep of the micrometer drive complete plots can be obtained without any gaps as shown in Figure 4.6.

The attenuator in the standard test load gives the same attenuation in the fundamental and second harmonic bands and slightly lower attenuation in the third harmonic band The third harmonic output from the two amplifier modules tested was too small for accurate plots to be made so the attenuator data was not required for constructing equi-power contours on Smith charts.

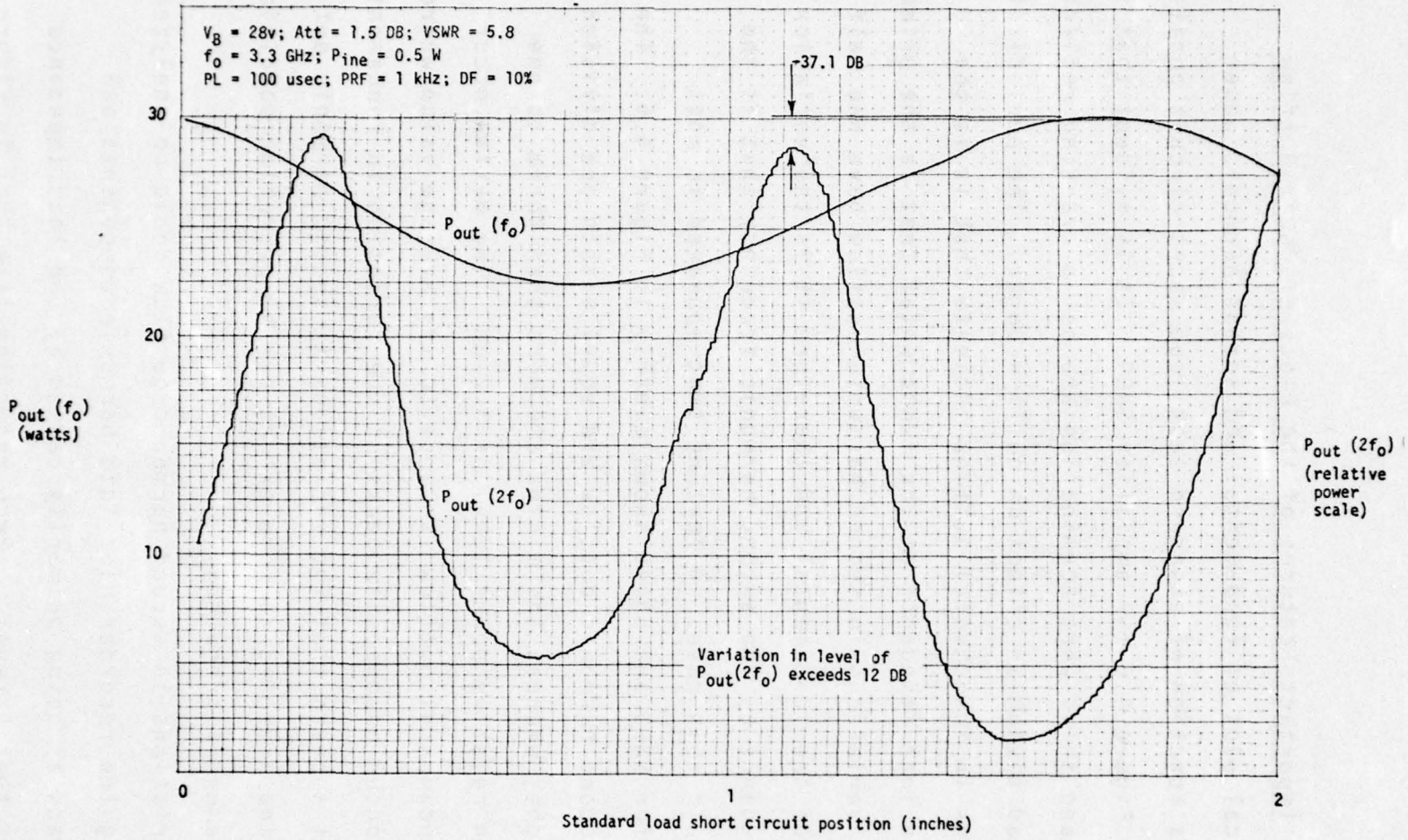

Figure 4.6 Power of the fundamental and the second harmonic wave from the output port of S-band module SN99 as a function of the position of the short circuit in the standard load. Load attenuator set 1.5 DB, nominal VSWR = 5.8.

4.3.2 Important Features of the Plots of Power Outflow

A typical plot of fundamental and second harmonic power outflow as a function of standard test load short circuit position is shown in Figure 4.6 for amplifier SN99. It is evident that the circulator and third port termination are not preventing reflections from the load having an effect on outflow power. The periodicity of variations in fundamental outflow indicate that it is the variation in load impedance at the fundamental that is the prime cause. The variations in second harmonic outflow have one half the period of the fundamental and therefore it is the variation in load impedance at the second harmonic frequency that is the prime cause in this case. A feature that appeared in most recordings for SN99 and SN145 shows clearly in Figure 4.6. The maxima of second harmonic outflow are equal within one division in fifty eight, whereas the minima are more than three to one different in relative power level or 5.2 dB. The maxima occur when the fundamental outflow is close to its average value whereas the minima occur on opposite peaks of the variation in fundamental outflow. It appears that the variations in second harmonic outflow are being affected to some extent by the operating conditions at the fundamental frequency.

The variations in second harmonic outflow could be analyzed by resolving the recorder plot into harmonic components and regarding each as being primarily caused by the load impedance variation at that harmonic. Each recording like that in Figure 4.6

would have to be analyzed and then using the families of sinusoidal variations as a function of standard load short circuit position the results could be integrated in the form of equi-power contours on Smith charts. There would be a chart for each periodic term found in the original family of plots of which Figure 4.6 is one member. Limits to the time and effort available for this study prevented this type of detailed analysis being done.

Each plot of $P_{out}(2fo)$ in a family was inspected to choose the range of short circuit position that included the largest ratio of maximum to minimum power flow. It was assumed that this range of variation was caused by load variations at the second harmonic only and data was then extracted and used to determine equi-power contours on a single Smith chart. Such a procedure suppresses variations at the fundamental period and attributes larger amplitudes to the variations at the second harmonic period. These sources of error are recognized in the analysis of the results but there would be analytical difficulties in making use of a more accurate and complex interpretation of the plots. This will be discussed in the concluding chapter. The simpler procedure of analysis that has been used yields a good overview of behavior and data that is sufficiently accurate for most purposes.

The third harmonic components produced by each module were 57 decibels or more below the fundamental level and could not be plotted accurately enough to yield meaningful equi-power contours There was evidence of periodicity in otherwise noisy recordings

that indicated that the third harmonic outflow varies with the load impedance at the third harmonic frequency.

4.3.3 Results as Equi-Power Contours on Smith Charts

Equi-power contour plots for the fundamental and second harmonic are shown in Figures 4.7 and 4.8 respectively for S-band module SN99 and in Figures 4.9 and 4.10 respectively for SN145. The coordinates for Figures 4.7 and 4.9 are the real and imaginary parts of the load impedance at the fundamental frequency and for Figures 4.8 and 4.10 the same parts of the load impedance at the second harmonic frequency. All of the contours are contained within the same maximum VSWR circle because the standard test load attenuator gave the same attenuation from 3 to 7 GHz for any given setting amongst those used.

The fundamental outflow from SN145 varies over a wider range than that from SN99. Apart from this point there is overall similarity in the shape and orientation of the characteristics. To emphasize the effect that power loss due to reflection from the load has on the appearance of the absorbed (or radiated) equi-power contours Figures 4.11 and 4.12 have been prepared for amplifier module SN99. The contours of Figure 4.11 are obtained by point-by-point multiplication of the contours of Figure 4.7 with those of Figure 2.15. The reflection effect predominates and gives the contours the appearance of a family of concentric circles. The effect of the module in providing a load dependent forward travelling power wave is to displace the near-circular

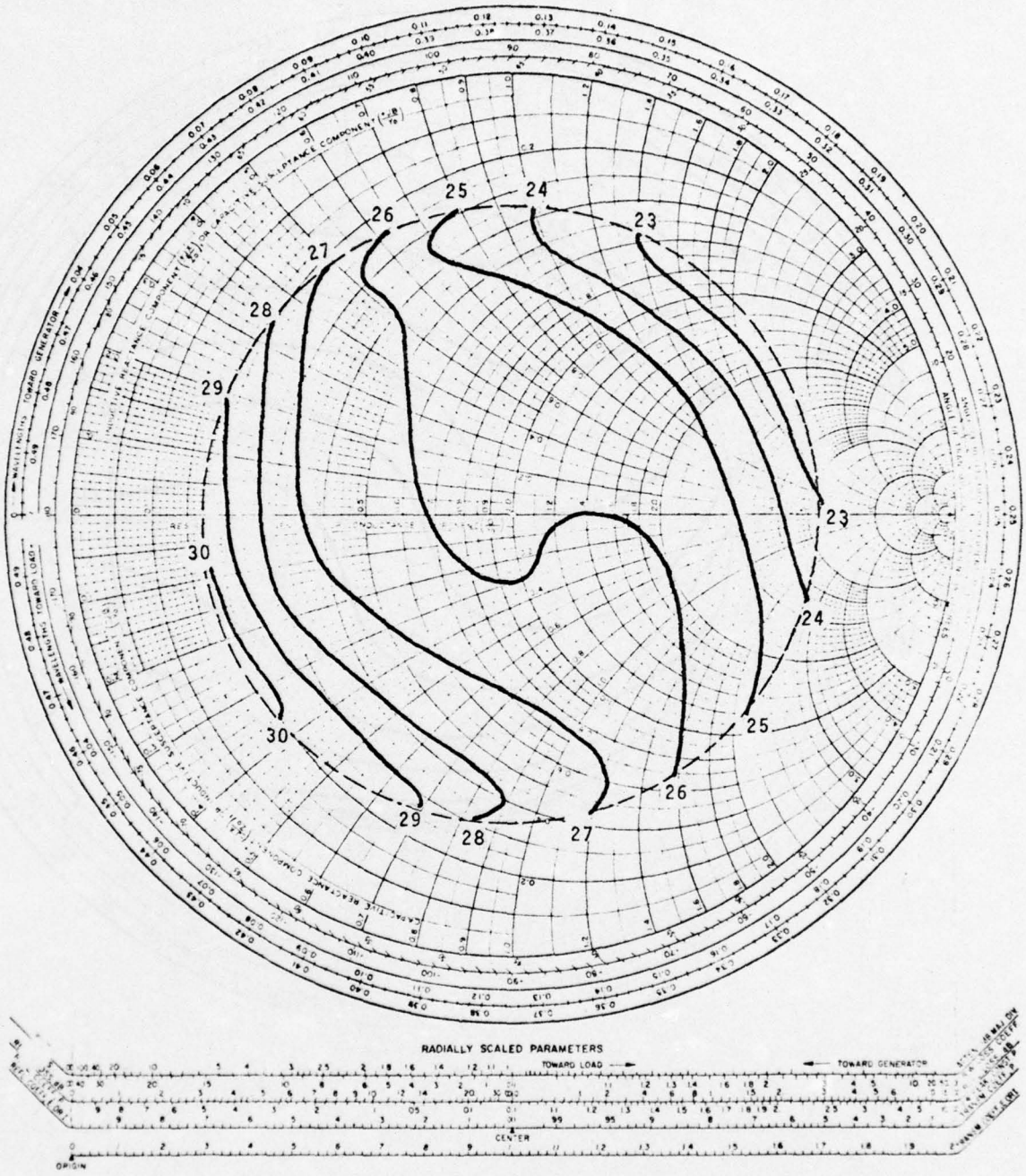

Equi-power contours in watts.
Signal frequency 3.30 GHz. Incident power 0.5 W peak.
Signal pulse length 100 microsecs. PRF 1kHz. DF 10%.

Figure 4.7 Power of fundamental wave from the output port of S-band module SN99 as a function of the load impedance at the fundamental.

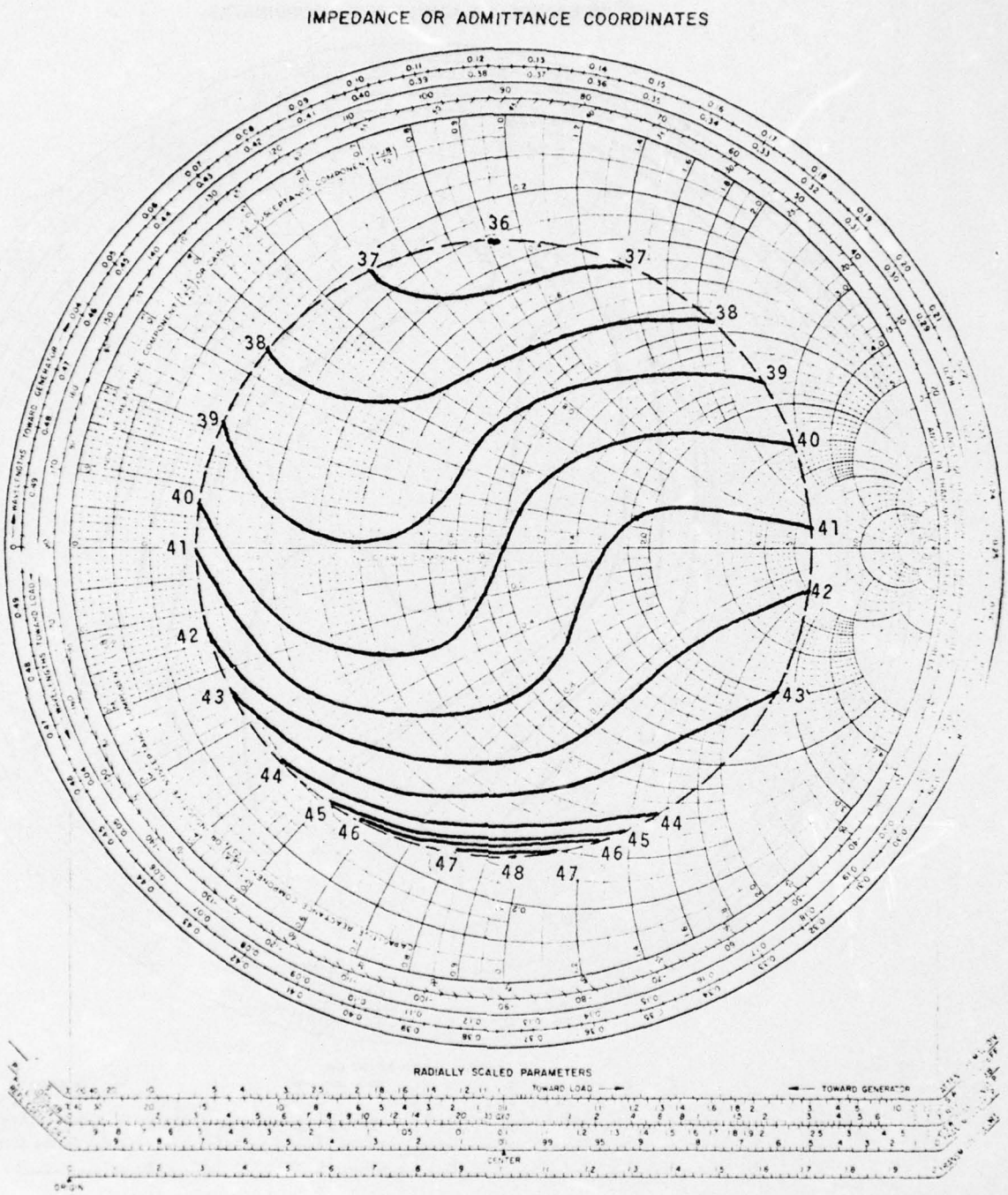

Equi-power contours in DB (below fundamental)
Signal frequency 3.30 GHz. Incident power 0.5 W peak.
Signal pulse length 100 microsecs. PRF 1kHz. DF 10%.

Figure 4.8 Power of second harmonic wave from the output port of S-band module SN99 as a function of the load impedance at the second harmonic (6.60 GHz)

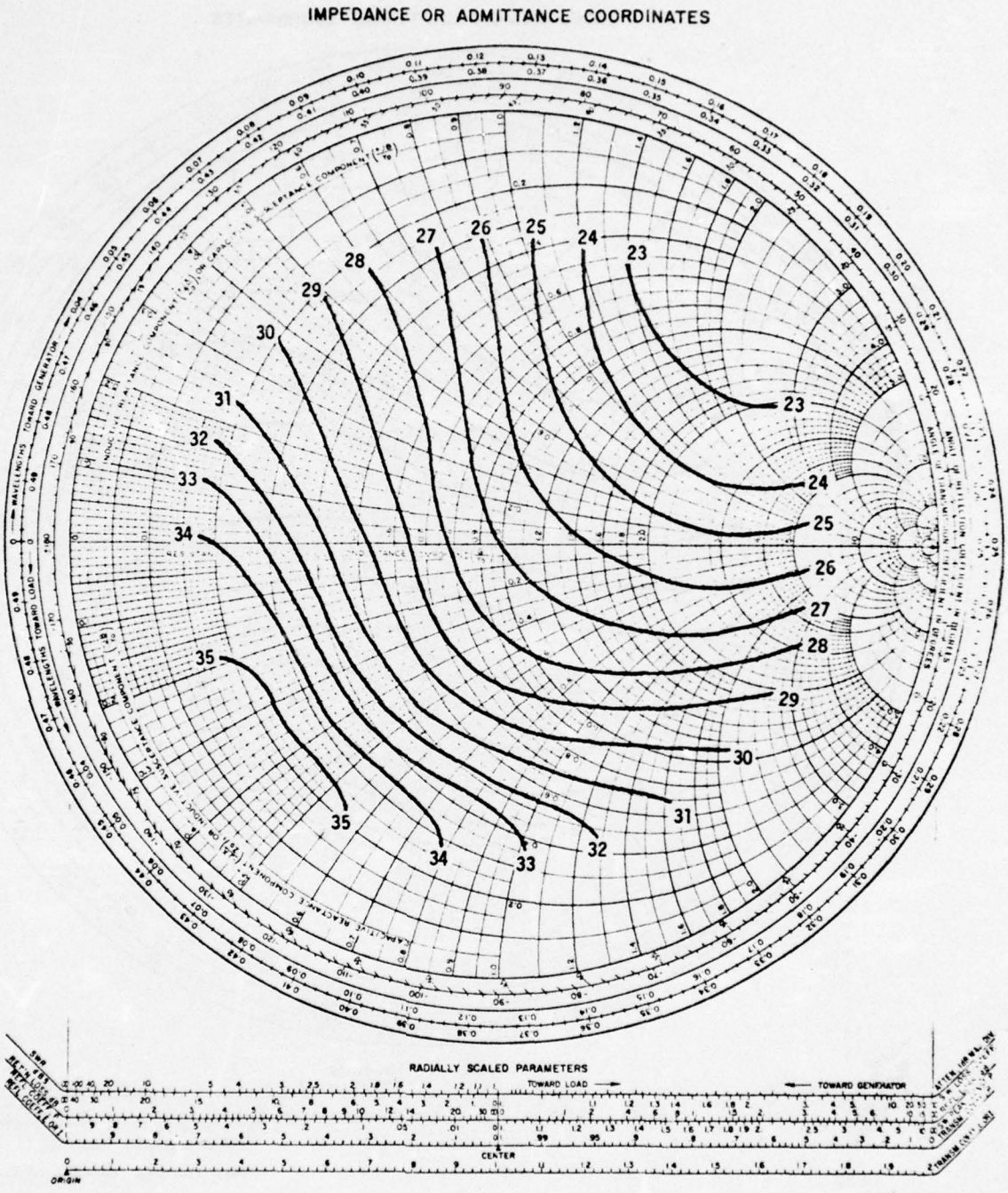

Equi-power contours in watts.
Signal frequency 3.30 GHz. Incident power 0.5 W peak
Signal pulse length 100 microsecs. PRF 1 kHz. DF 10%

Figure 4.9 Power of fundamental wave from the output port of S-band module SN145 as a function of the load impedance at the fundamental

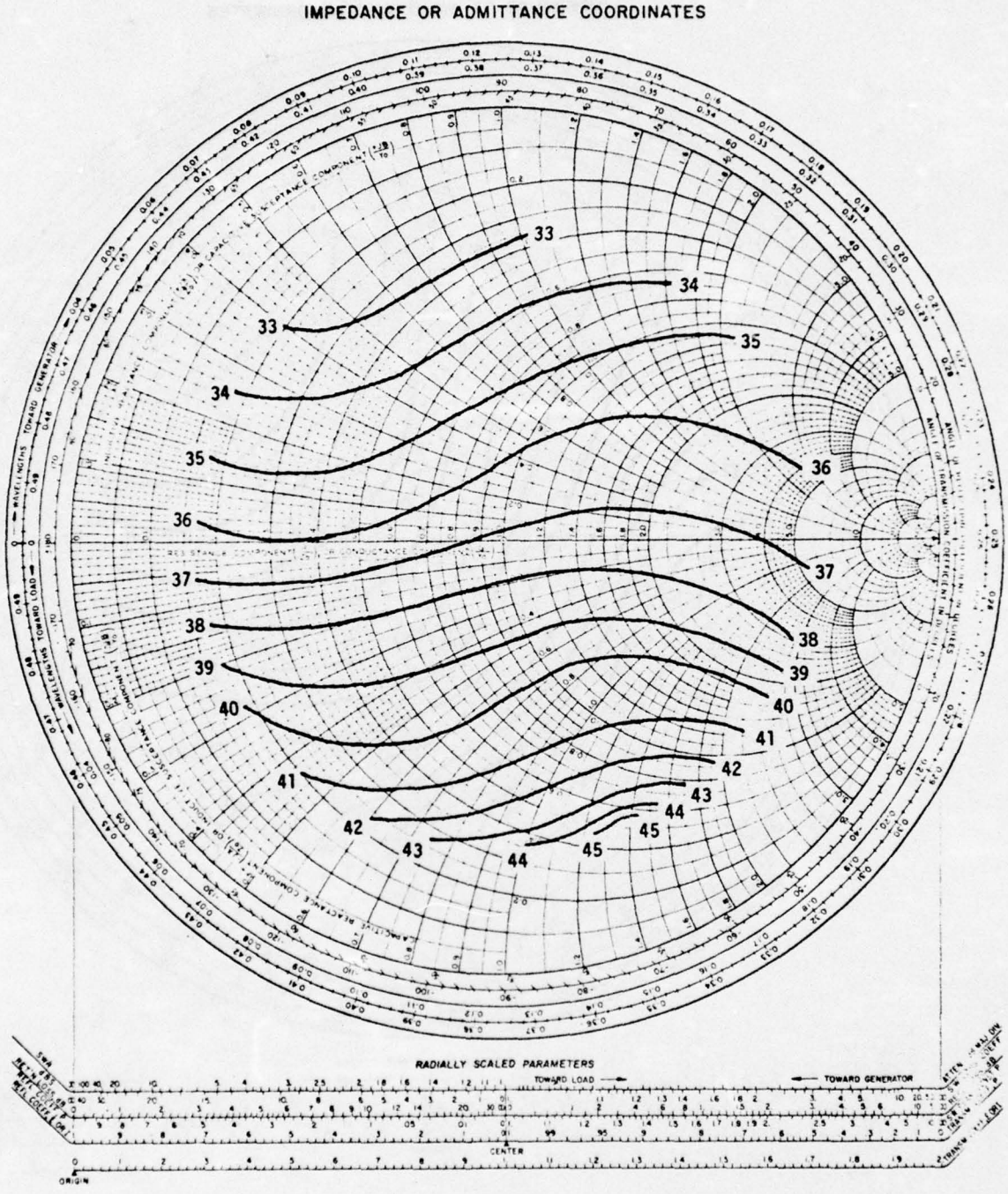

Equi-power contours in DB (below fundamental)
Signal frequency 3.30 GHz. Incident power 0.5 W peak
Signal pulse length 100 microsecs. PRF 1 kHz. DF 10%

Figure 4.10 Power of second harmonic wave from the output port of S-band module SN145 as a function of the load impedance at the second harmonic (6.60 GHz)

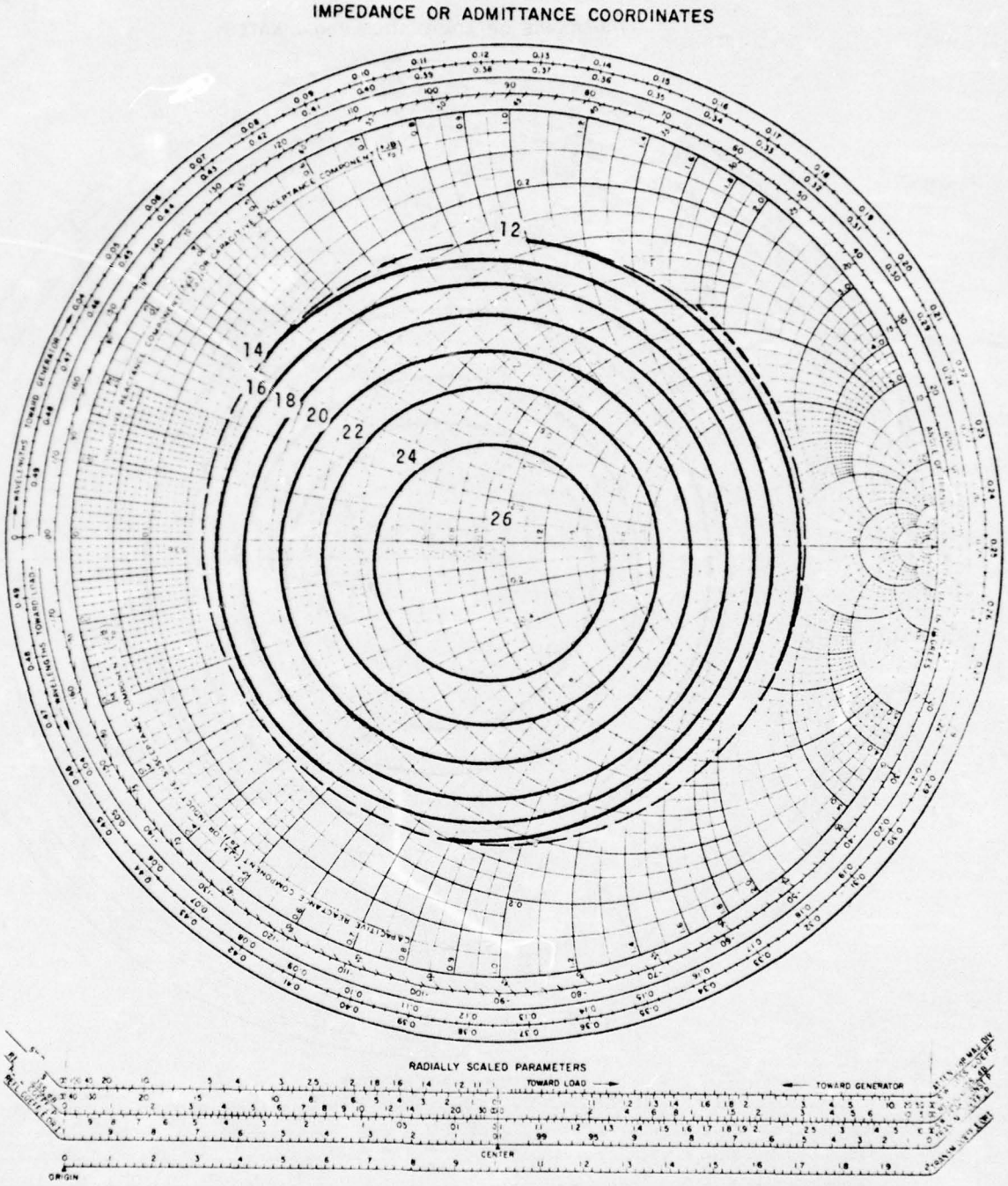

Equi-power contours in watts.
Signal frequency 3.30 GHz. Incident power 0.5 W peak.
Signal pulse length 100 microsecs. PRF 1kHz. DF 10%.

Figure 4.11 Power of fundamental absorbed by the load (or radiated by an antenna element) from S-band module SN99 as a function of the load impedance at the fundamental.

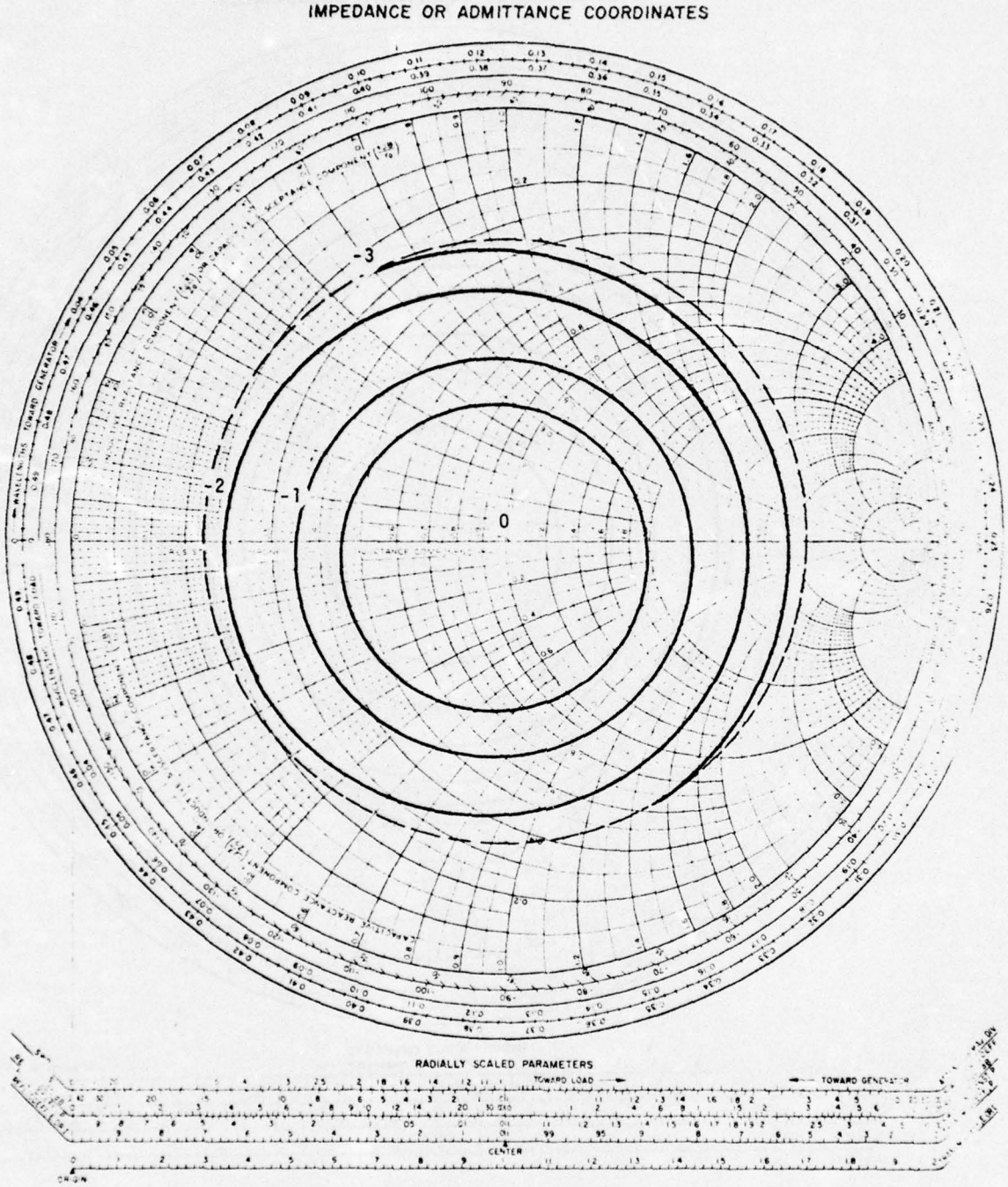

Equi-power contours in DB below 26 W peak.
Signal frequency 3.30 GHz. Incident power 0.5 W peak.
Signal pulse length 100 microsecs. PRF 1kHz. DF 10%.

Figure 4.12 Power of fundamental absorbed relative to the available power from S-band module SN99 as a function of the load impedance at the fundamental.

equi-power contours from the center of the Smith chart and give each a slightly different center. The contours of Figure 4.12 are equi-power contours of absorbed (or radiated) power expressed in decibels relative to power absorbed by a matched load. If the VSWR is approximately 2 then about one half a decibel is loss mainly due to load reflection. If the contours on Figure 4.7 or 4.9 were more closely spaced then the effect of the module behavior on the absorbed (or radiated) power would be more pronounced.

Second harmonic behavior of each module is shown in Figures 4.8 and 4.10 and is characterized by contours that are similar in shape to each other and if rotated through ninety degrees are not unlike the fundamental equi-power contours. These features correspond to stability in relative positions and close connection between relative amplitudes in the original plots of outflow versus short circuit position. Throughout the range of load impedance variation the second harmonic level from SN145 is about 3 decibels stronger than from SN99. It is unwise to draw general conclusions from the results of two modules but to a reasonable degree of approximation the pattern of equi-power contours could be assumed the same for each of these modules tested and the harmonic level represented as a deviation from an average level determined for the matched load position. If the radiating element is a dipole a large reflection coefficient and VSWR can be expected. While this reduces the radiated power by causing reflection loss it also

means that the actual level of harmonic radiated may lie anywhere in a 10 dB range for a VSWR of 5 and depend upon the dynamic impedance around that VSWR circle. Thus, unlike the effect that the module behavior has on fundamental radiated power, at second harmonic it has a strong influence if load VSWR is high and phase varies. This is an important result from the point of view of providing data at each antenna element in an array with the aim of calculating the radiation characteristics of the array at the second harmonic.

4.4 Equi-Phase Contours on Smith Charts

To plot equi-phase contours at the fundamental and second harmonic for each of two modules the bridge has to be balanced about two hundred times. It was decided to make all measurements on the leading edge of the pulse and not to repeat all of the results for the trailing edge of the pulse. Phase variation during the pulse under matched load conditions is a quantity that is measured by the manufacturer. Comparison of equi-phase contours for each end of the pulse, as is possible at L-band with Figures 3.16, 3.17, 3.18 and 3.19, would be interesting but the additional labor could not be fully justified.

The relative phase of the fundamental outflow from SN99 and SN145 are shown in Figures 4.13 and 4.15 respectively as a function of the load impedance at the fundamental. Compared with the match condition the mismatch can cause the insertion phase of the amplifier module to vary as much as plus or minus 15 degrees if

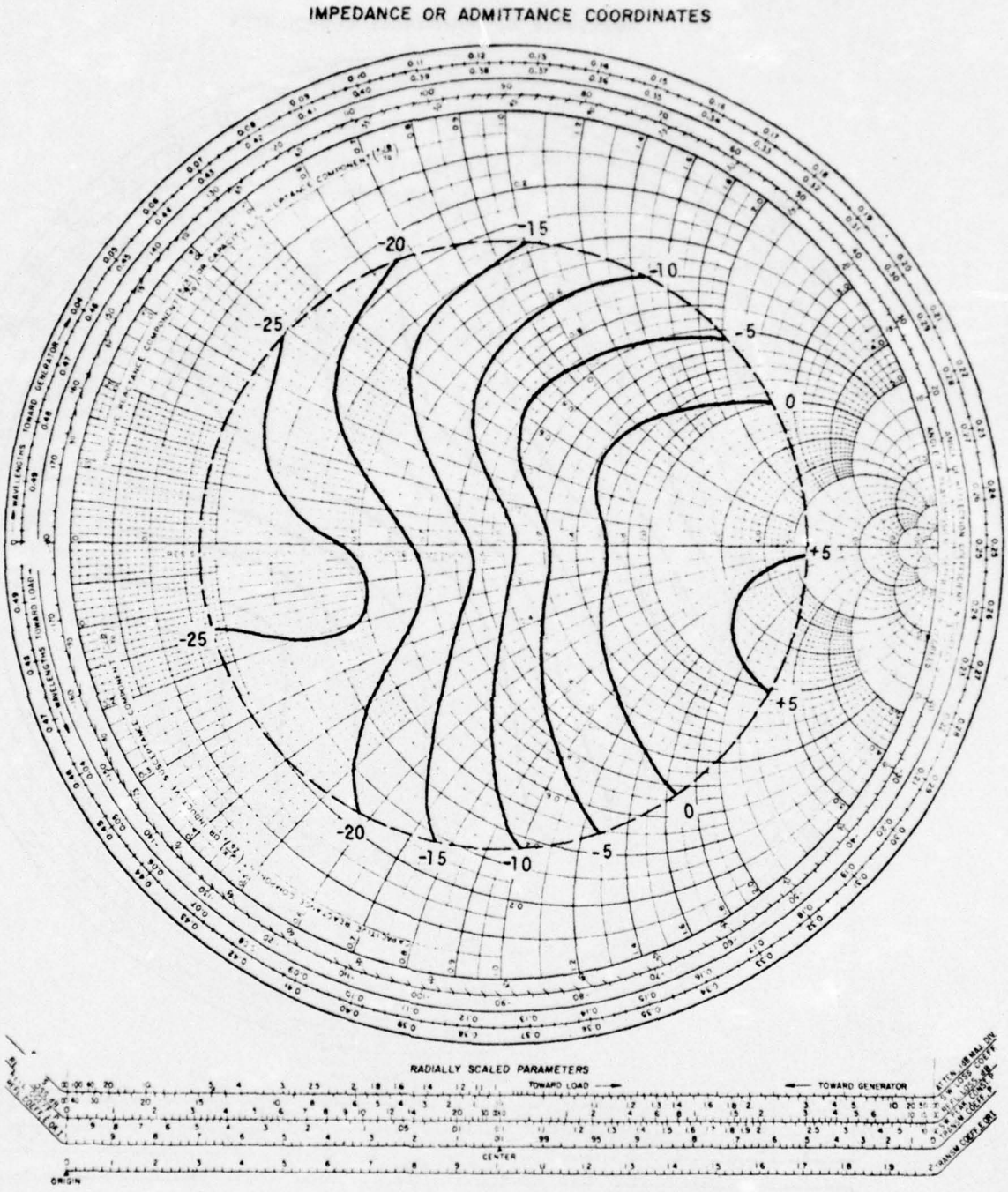

Equi-phase contours in electrical degrees.
Signal frequency 3.30 GHz. Incident power 0.5 W peak.
Signal pulse length 100 microsecs. PRF 1kHz. DF 10%.

Figure 4.13 Relative phase of the fundamental wave from the output port of S-band module SN99 as a function of the load impedance at the fundamental.

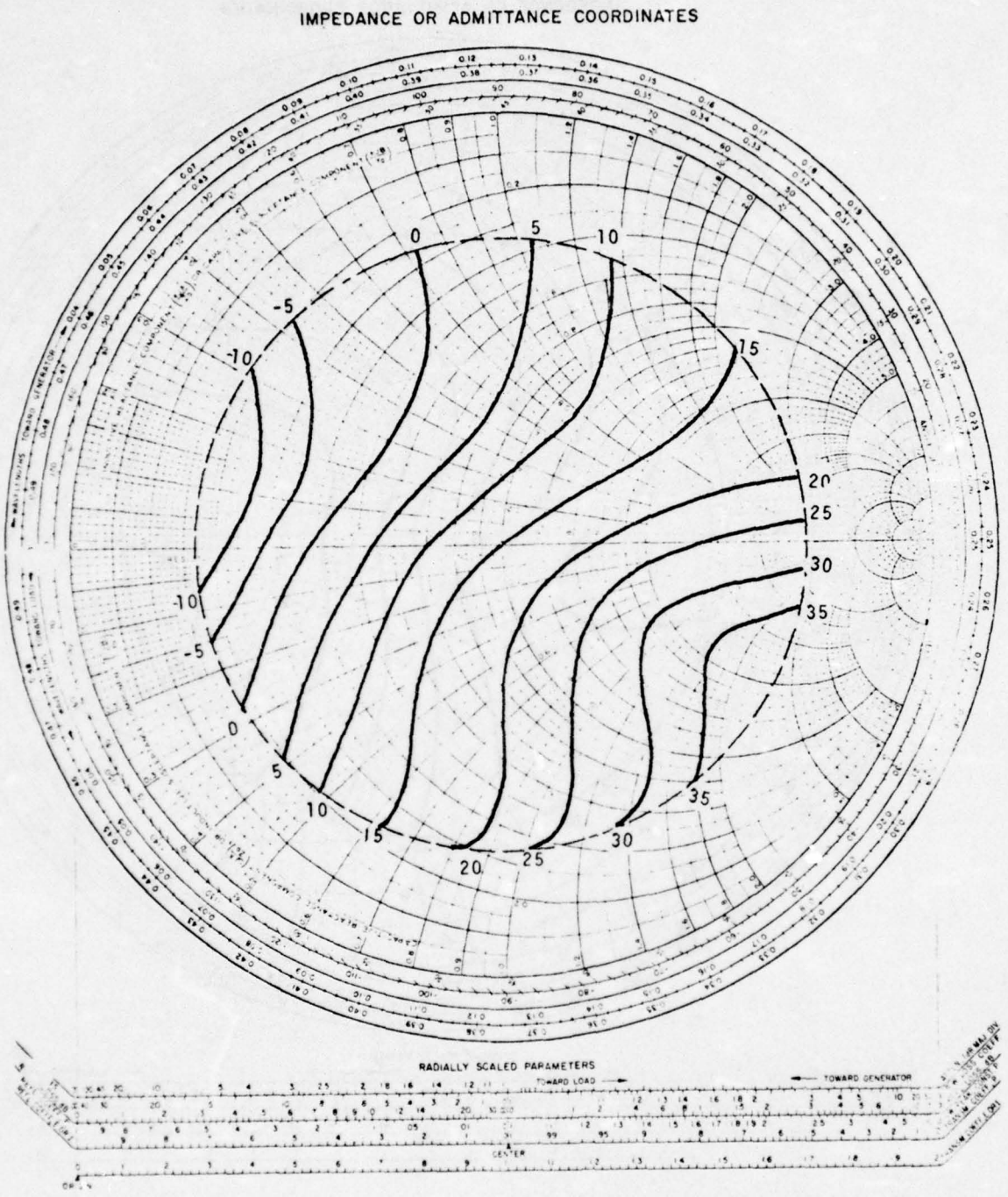

Equi-phase contours in electrical degrees.
Signal frequency 3.30 GHz. Incident power 0.5 W peak.
Signal pulse length 100 microsecs. PRF 1kHz. DF 10%.

Figure 4.14 Relative phase of the second harmonic wave from the output port of S-band module SN99 as a function of the load impedance at the second harmonic (6.60 GHz).

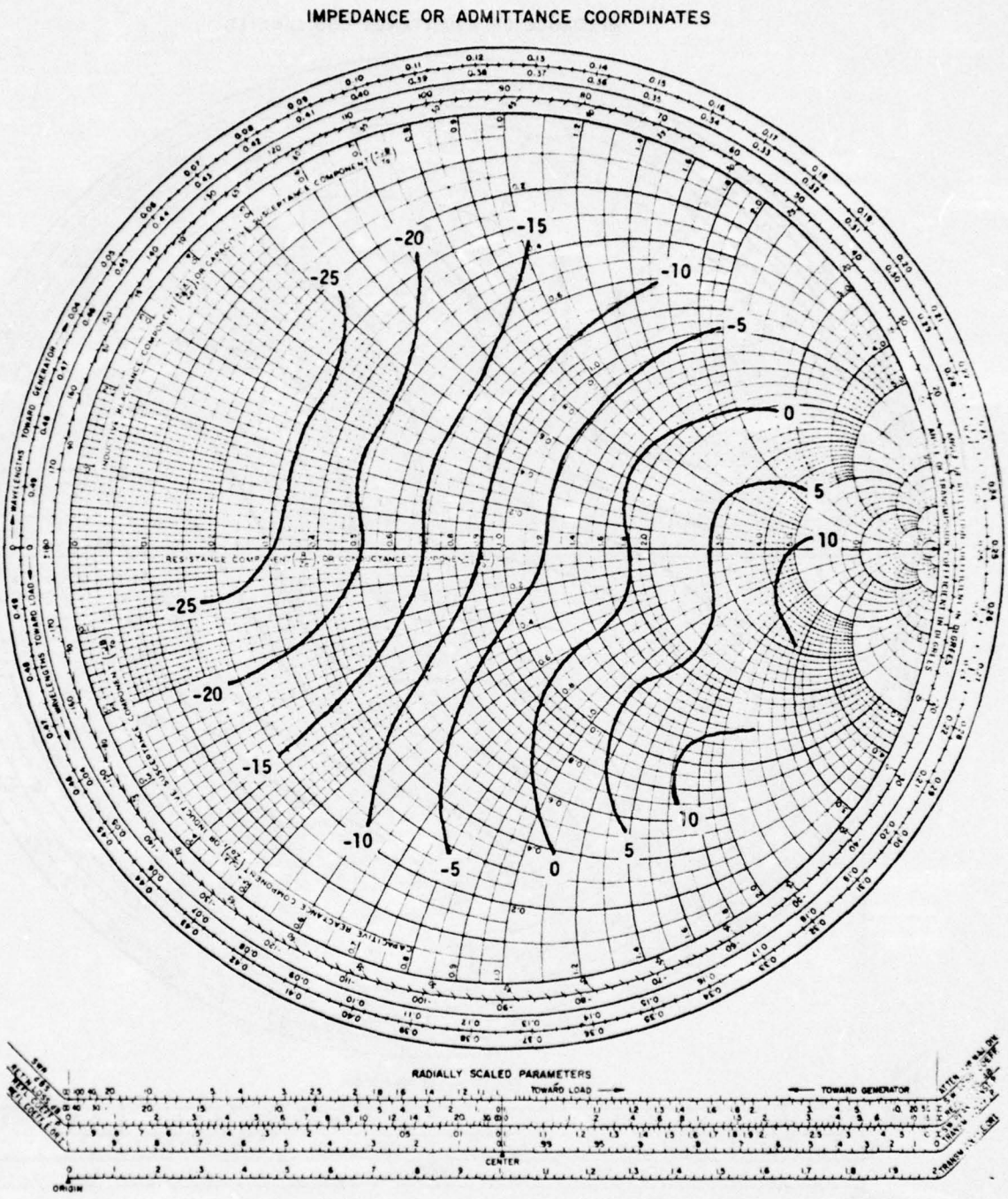

Equi-phase contours in electrical degrees
Signal frequency 3.30 GHz. Incident power 0.5 W peak.
Signal pulse length 100 microsecs. PRF 1 kHz. DF 10%

Figure 4.15 Relative phase of the fundamental wave from the output port of S-band module SN 145 as a function of the load impedance at the fundamental

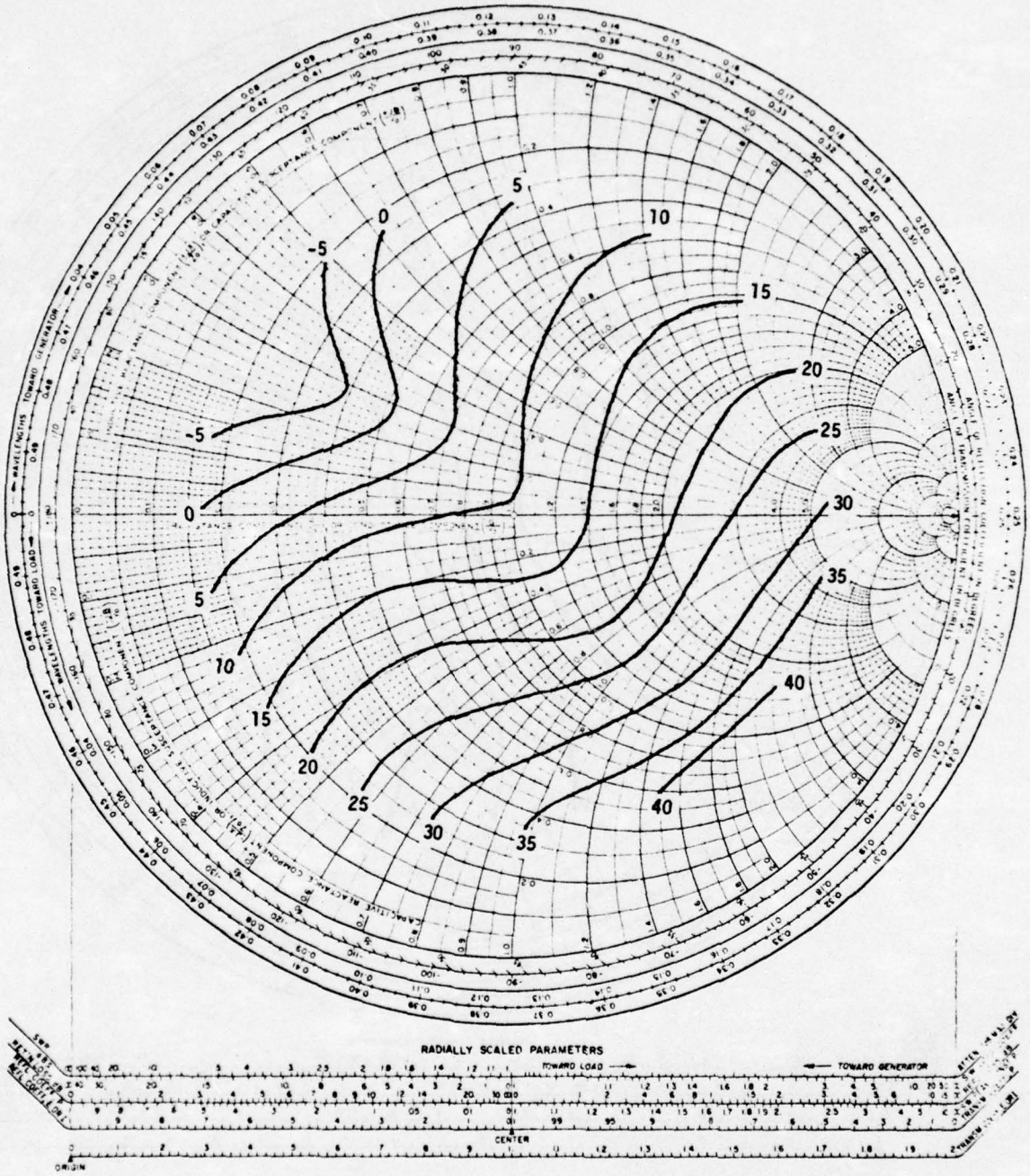

Equi-phase contours in electrical degrees.
Signal frequency 3.30 GHz. Incident power 0.5 W peak.
Signal pulse length 100 microsecs. PRF 1 kHz. DF 10%

Figure 4.16 Relative phase of the second harmonic wave from the output port of S-band module SN 145 as a function of the load impedance at the second harmonic (6.60 GHz)

the load VSWR reaches 5. There is good similarity between the characteristics. An interesting feature is that the rate of variation of phase with changing load impedance is greatest near the center of the chart for changes in the resistive part and is least for changes in the reactive part. These observations depend entirely on the reference port for the measurements which in this case was the output connector on the module. To account for these observations a detailed analysis of mechanisms responsible for the effect would be necessary and was beyond the scope of the study.

The relative phase of the second harmonic outflow from SN99 and SN145 are shown in Figure 4.14 and 4.16 respectively as a function of the load impedance at the second harmonic. The equi-phase contours are similar in shape for the two modules and are not greatly different from the appearance of the fundamental contours. However, the phase range for the second harmonic outflow is greater than that for the fundamental and approaches a factor of 2 to 1.

The contributions that these effects that originate in the module may make to phase errors are likely to be quite different, because the VSWR of the antenna at fundamental frequency may be close to unity and at second harmonic it may be quite large. The results show clearly that a large VSWR does not necessarily give a large phase error; in fact the electrical length of the module may be the same as that at match for a chosen frequency. The same

remark applies to the phase error that arises from reflection as shown in Figure 2.14. The simplest thing that can be done with this data as a first step is to determine the worst possible error that can occur by adding the largest phase deviations found on a chosen VSWR circle on Figure 2.14 and the same VSWR circle on a set of equi-phase contours for the module being considered.

4.5 Impedance Behavior of the S-Band Module Antenna

The crossed dipole antenna element that forms part of the S-band module of Figure 4.1 and is shown in detail in Figure 4.2 was available for tests. With the behavior of the two amplifiers as a function of load impedance now known in detail, it is relevant to examine some of the main features of behavior of the antenna that loads these amplifiers. The dynamic impedance under phased array operation cannot be determined but the isolated element will have a major influence on the relative behavior at fundamental and harmonic frequencies that occurs in the phased array.

Each dipole is energized via a coaxial line and a balun configuration between the radiating arms and the small rear reflector plate produces balanced excitation of the dipole arms. Ideally the radiating elements should have zero reflection coefficient over the fundamental frequency range 3.1 to 3.5 GHz, and unity reflection coefficient at all other frequencies that may appear in the amplifier output. Measurements were made on the antenna with an Automatic Network Analyzer. The two connectors

on the antenna were connected to the analyzer so that the reflection coefficient looking into the input line and the transmission characteristics from the energized dipole to the second dipole and through to its feeder line could be measured. Since the dipoles are cross-polarized they should be isolated from each other and the insertion loss from one connector on the antenna to the other should be large.

Figure 4.17 is a graph of the magnitude of the reflection coefficient at the energized port over the frequency range 2 to 12 GHz. In the fundamental range, 3.1 to 3.5 GHz, the reflection coefficient varies from 0.20 to 0.27, in the second harmonic range, 6.2 to 7.0 GHz, it varies from 0.48 to 0.89 and in the third harmonic range, 9.3 to 10.5 GHz, it varies from close to an ideal match to 0.65. A simple center-fed half wave dipole can be expected to present a high input impedance to the second harmonic and a low input impedance to the third. The bow-tie shape will yield broader band behavior but it is evident from the measurements that better harmonic characteristics in the form of higher reflection coefficient values would be an improvement.

Figure 4.18 is a graph of the insertion loss between the coaxial connectors on the antenna over the frequency range 2 to 12 GHz. It is adequate over both the fundamental and second harmonic frequency ranges but falls to as low as 4 decibels in the third harmonic range where the reflection coefficient is near zero. Thus, any third harmonic power fed to one dipole is partly

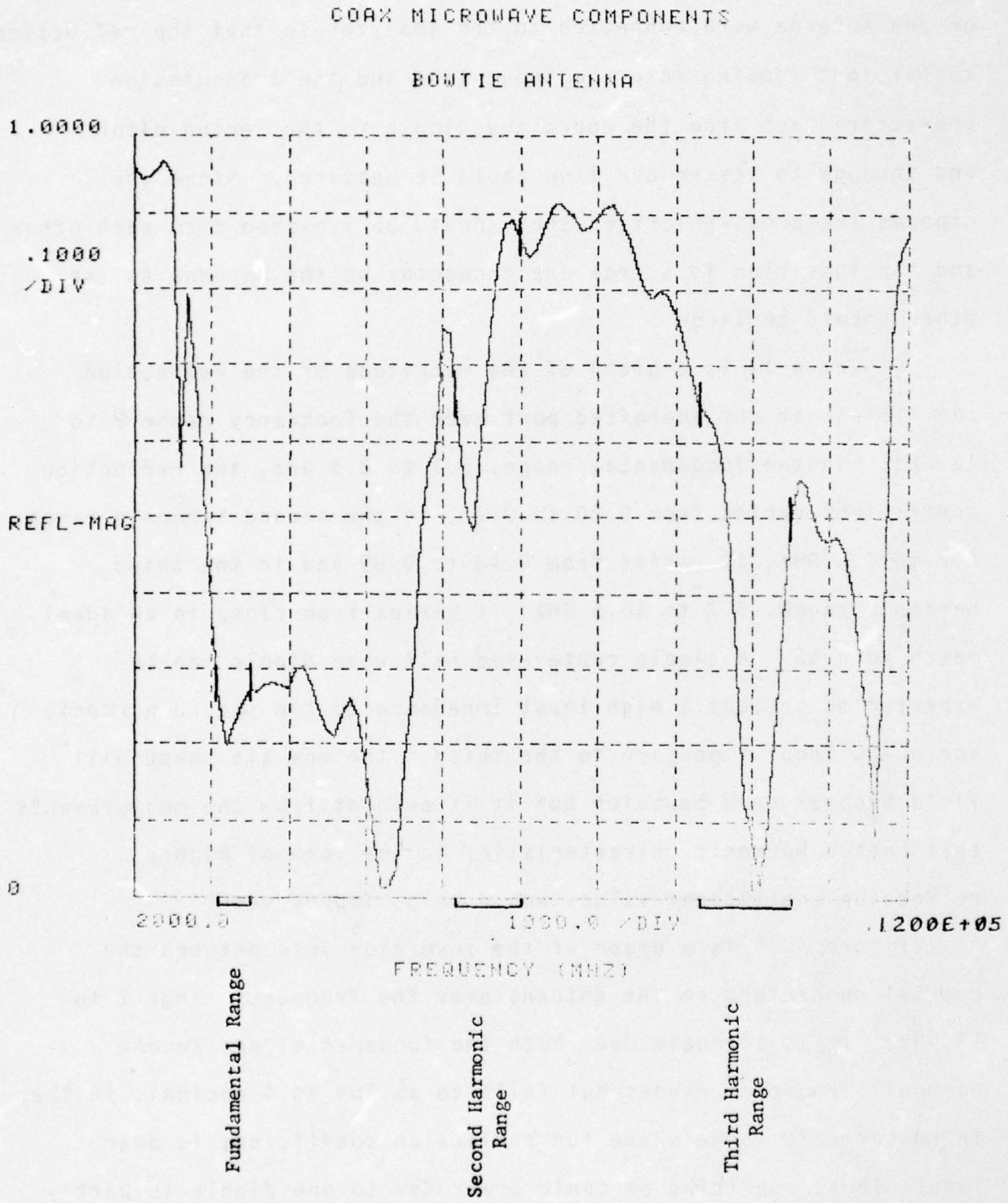

Figure 4.17 Magnitude of reflection coefficient measured at the input to one dipole of the bow-tie crossed dipole element used in the S-band phased array antenna. The port for the second dipole was terminated with a matched load and the element tested under anechoic conditions.

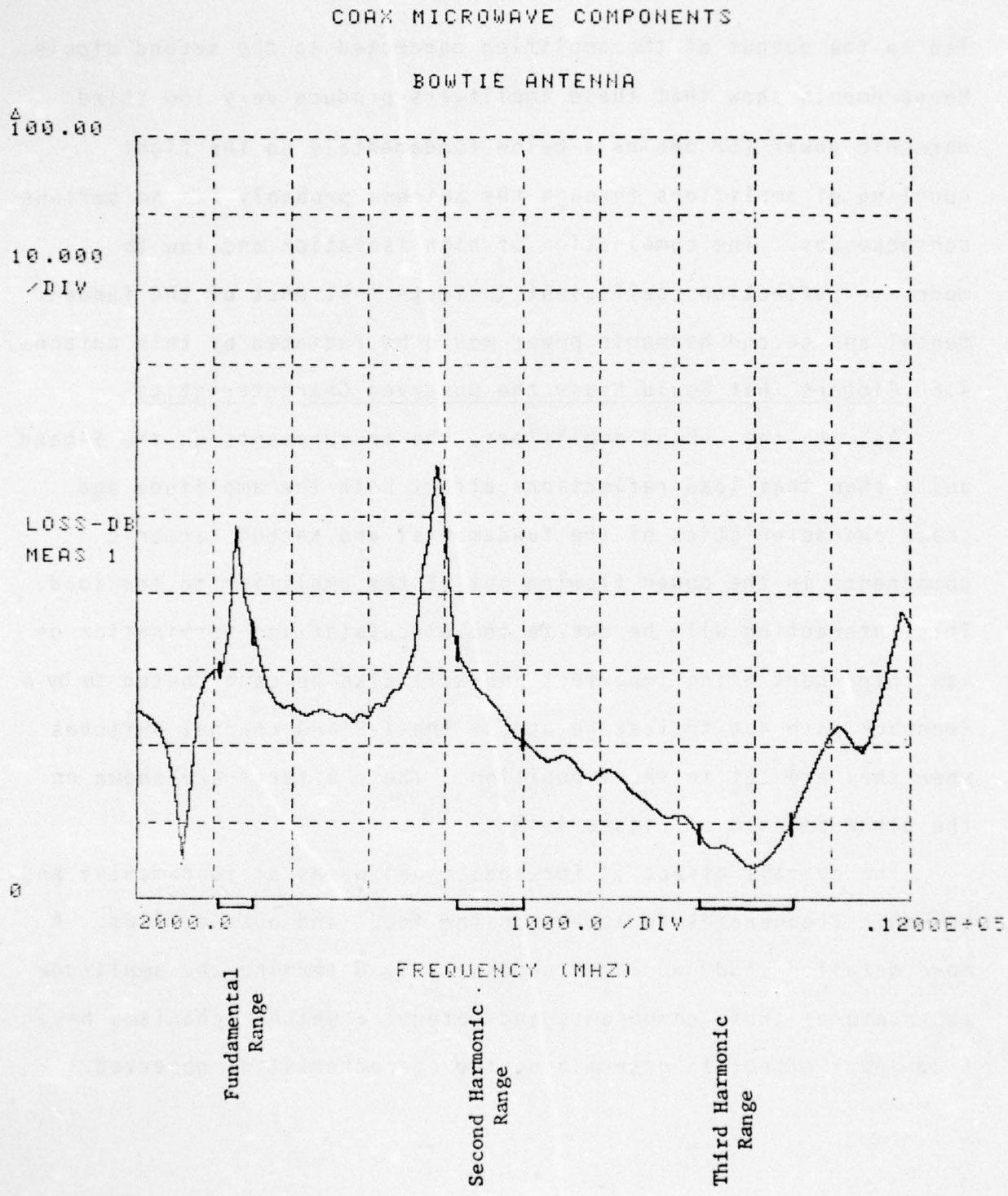

Figure 4.18 The measured insertion loss between the two coaxial connectors on the bow-tie type crossed dipole antenna element

fed to the output of the amplifier connected to the second dipole. Measurements show that these amplifiers produce very low third harmonic power (57 decibels below fundamental) so the tight coupling of amplifiers through the antenna probably has no serious consequences. The combination of high isolation and low to moderate reflection coefficient indicate that most of the fundamental and second harmonic power would be radiated by this antenna.

4.6 Factors That Could Cause the Observed Characteristics

As with the L-band amplifiers, the measurements on the S-band units show that load reflections affect both the amplitude and phase characteristics of the fundamental and second harmonic components in the power flowing out of the amplifier to the load. This interaction will be due to the circulator and termination on its third port being imperfect and will also be contributed to by a feedback path due to leakage across the T-R and channel switches when they are set in the T position. These effects are shown on the block diagram of Figure 4.19.

The overall effect is for additional waves at fundamental and harmonic frequencies to appear on the input and output lines. A more detailed study would be necessary to determine the amplitude and phase of these components and determine which mechanisms have a dominant effect in determining the characteristics observed.

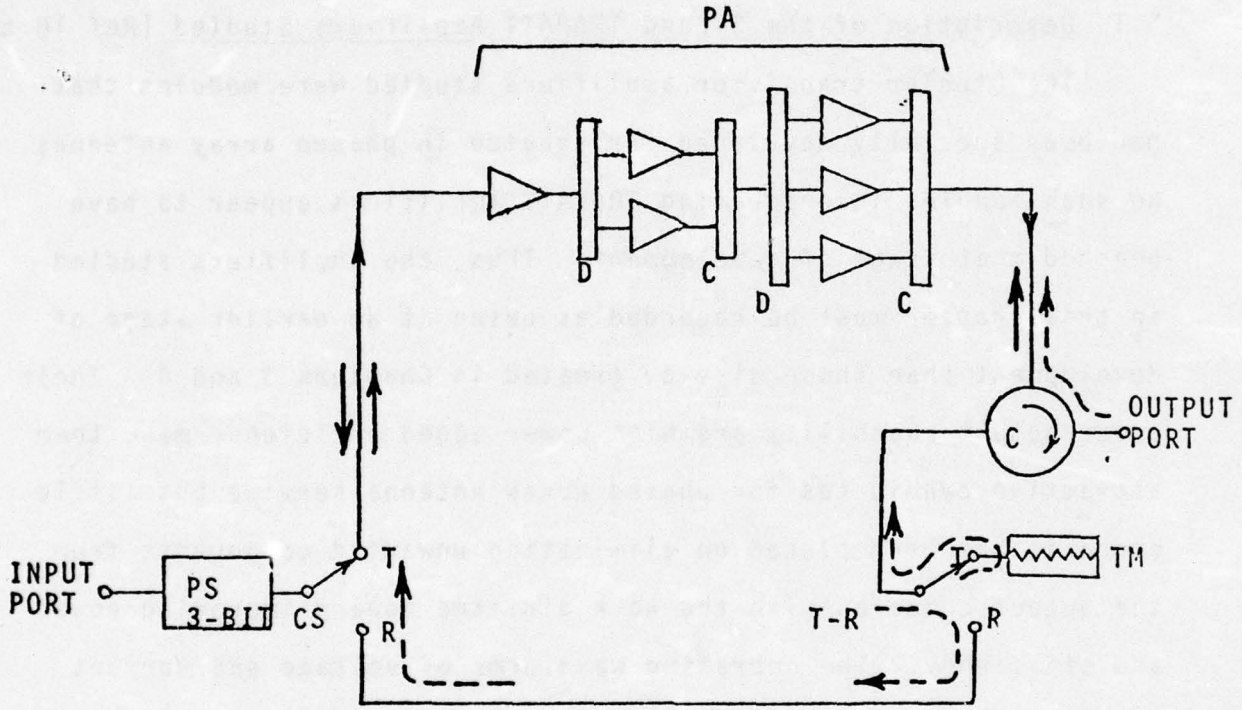

Figure 4.19 Block diagram of S-band amplifier unit showing the extra signal components caused by load reflection and imperfections in the microwave components

CHAPTER 5

STUDIES OF S-BAND TRAPATT AMPLIFIERS

5.1 Description of the S-Band TRAPATT Amplifiers Studied (Ref 10 to 14)

The bipolar transistor amplifiers studied were modules that had been specially developed for service in phased array antennas. No such modules incorporating TRAPATT amplifiers appear to have reached that stage of development. Thus, the amplifiers studied in this chapter must be regarded as being at an earlier stage of development than those already treated in Chapters 3 and 4. Their power output capability and high power added efficiency make them attractive candidates for phased array antenna service but little emphasis has been placed on eliminating unwanted components from the output compared with the work directed toward improving power and efficiency. The operating waveforms of voltage and current have high level harmonic components and for efficient operation at the desired output frequency quite restrictive conditions are placed on the impedance versus frequency characteristic that the circuit must present to the diode. Several theoretical and experimental studies have been reported.

The particular TRAPATT amplifiers studied with the S-band harmonic balancing bridge are shown in Figures 5.1 to 5.3. A report on their development is given in Reference 10. All three are lumped element type amplifier circuits designed by systematic computer experiments to determine the combination of equivalent

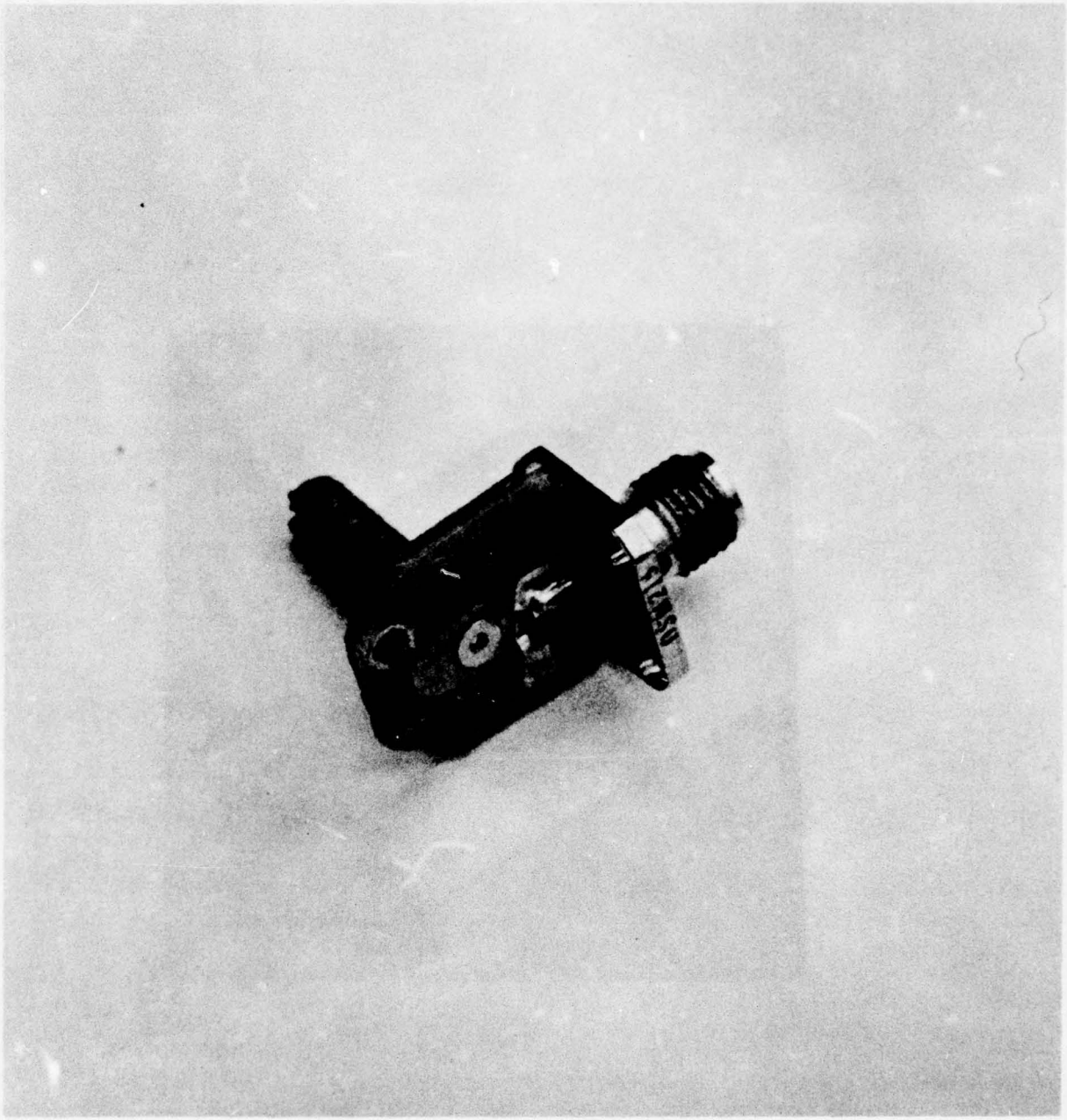

Figure 5.1 Photograph of TRAPATT amplifier Type I - lumped circuit type with single tuning capacitor

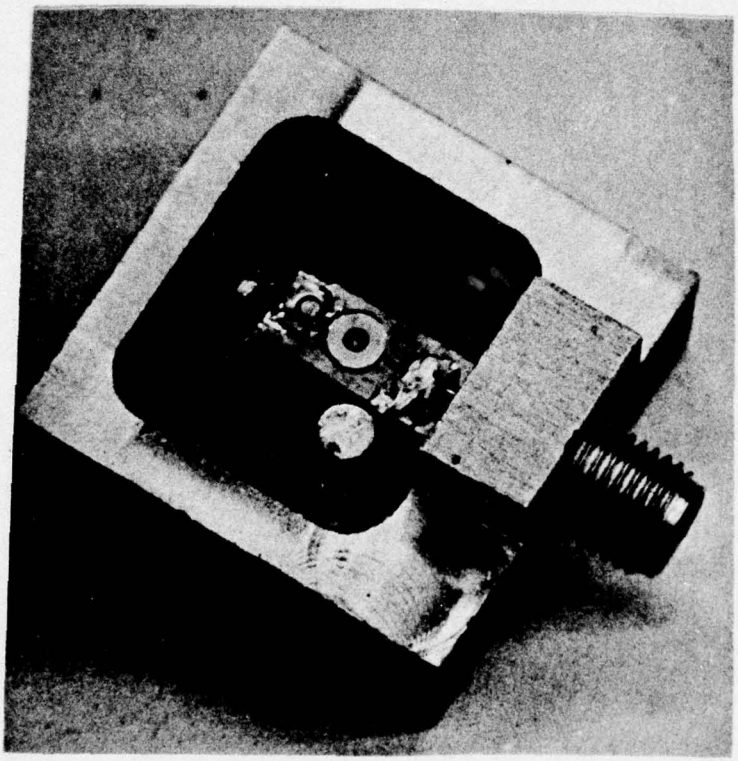

Figure 5.2 Photograph of TRAPATT amplifier Type II - lumped circuit type with two tuning capacitors

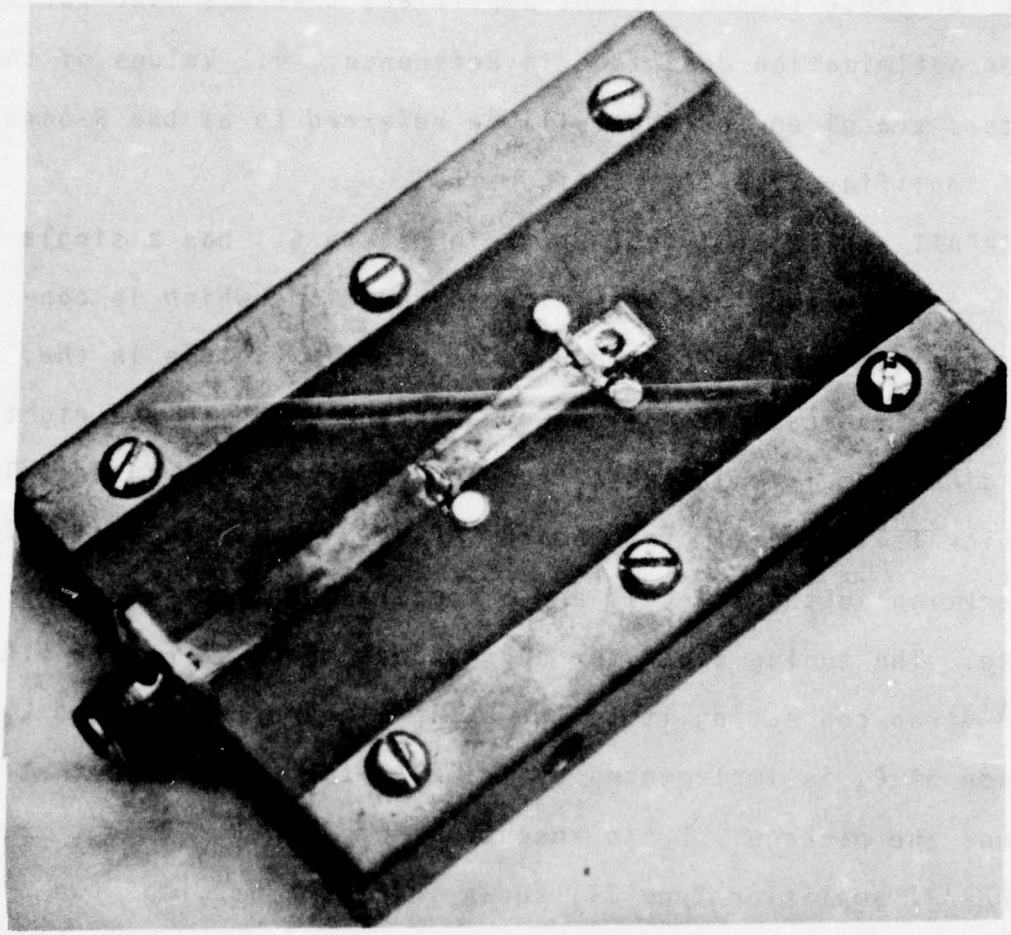

Figure 5.3 Photograph of TRAPATT amplifier Type III - lumped circuit type with three tuning capacitors

circuit values that would give optimum performance with the particular diodes to be used. Figure 5.4 is the equivalent circuit for these lumped element amplifiers that was used for the computer optimization described in Reference [10]. Values of the parameters are given for what will be referred to as the S-band TRAPATT amplifier Type III of Figure 5.3.

TRAPATT amplifier Type I shown in Figure 5.1 has a single tuning capacitor in close proximity to the diode which is contained in a replaceable package and is clearly visible in the photograph. The capacitor is underneath the strap to the right of the diode and is adjustable from the reverse side of the 1/16 inch thick Tellite dielectric board. Five diodes were available for operation in this circuit and a comparison of performance was made. The tuning capacitor corresponds to C_3 in Figure 5.4 and the strap connecting it to the strip line corresponds to L_4. Variation of C_4 is implemented by trimming the strip line that surrounds the package. C_5 is absent.

TRAPATT amplifier Type II, shown in Figure 5.2, has two timing capacitors close to the diode, corresponding to C_3 and C_4, and both are adjustable from the reverse side to that shown in the photograph. This unit is the same as the Type I circuit apart from C_4 and a rugged frame support for all components. The five diodes that were available could be operated in either circuit.

TRAPATT amplifier Type III shown in Figure 5.3 has a third adjustable capacitor C_5 placed a distance θ_1 from capacitors C_3

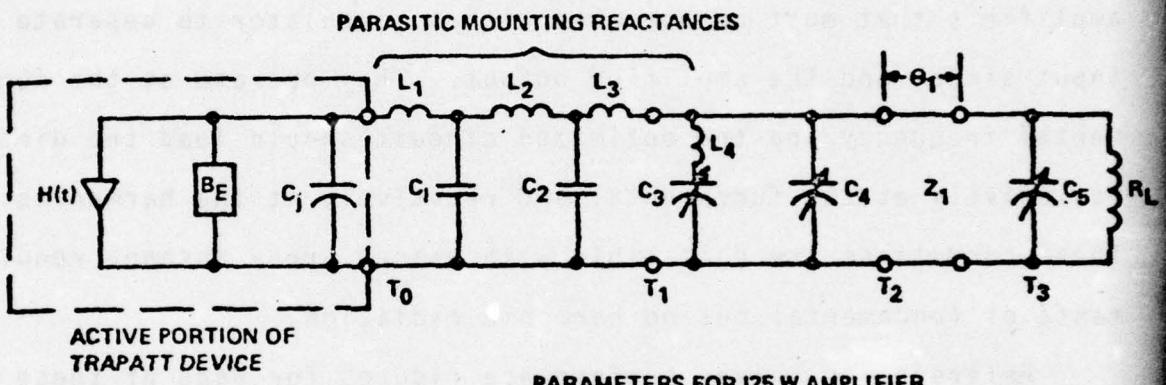

PARAMETERS FOR 125 W AMPLIFIER

C_j = 4.0 p F	C_3 = 2.2 p F	V_B = 80V
L_1 = .58 nH	L_4 = .30 nH	I_{dc} = 6A
C_1 = .249 pF	C_4 = .30 pF	
L_2 = .084 nH	Z_1 = 50 Ω	
C_2 = .045 pF	θ_1 = .86"	
L_3 = .254 nH	C_5 = 1.4 pF	

Figure 5.4 Schematic equivalent circuit of lumped-element TRAPATT amplifier circuits (Grace M., Kroger H. and Potter C. N.)

and C_4. The diode is fixed in the circuit and the mounting parasitic reactances are different from those for the packaged diode. The diode is a larger area and therefore larger capacitance diode, and C_5, placed approximately a quarter wavelength away, serves an impedance matching function at the fundamental frequency.

All three types of amplifier are single-port reflection-type amplifiers that must be operated with a circulator to separate the input signal and the amplified output. They operate at the fundamental frequency and the optimized circuit should load the diode resistively at the fundamental and reactively at the harmonics. These conditions are compatible with phased array antenna requirements of fundamental but no harmonic radiation.

Reference 10 gives performance figures for each of these amplifiers under matched load conditions. The Type I and II units operated at 3.2 GHz with a gain of 6 decibels and a -1 decibel bandwidth of 0.3 GHz. Peak output power was 50 to 60 watts for a 1 microsecond pulse width and a duty factor of 0.001. The Type III amplifier using larger area diodes operated at 3.1 GHz with a gain of 5 decibels and a -1 decibel bandwidth of 0.2 GHz. Peak output power was 100 to 125 watts. No figures are given for harmonic levels in the output nor for behavior under mismatched load conditions.

5.2 Choice of Components for Measuring TRAPATT Amplifier Behavior With Mismatched Loads

There are precautions necessary in measuring the effect of load reflection on the performance of a reflection type amplifier

compared with making similar measurements on multi-stage microwave transistor power amplifiers. The precautions arise from the basic requirement that the reflection-type amplifier operate with a circulator to separate the incident and amplified signals.

Four alternative equipment arrangements that may be used are shown schematically in Figure 5.5. The first arrangement, Figure 5.5(a) requires the minimum number of components. The TRAPATT amplifier TA is connected via a bias tee BT to the single three port circulator C. The input signal from S is controlled by attenuator LS and monitored at the directional coupler DC. The power outflow is monitored by the second directional coupler that precedes the standard test load containing attenuator AP and adjustable short circuit SC. This arrangement is unsatisfactory for two reasons. Firstly, the bias tee is not reflection-free or loss-free. Losses reduce the usable gain of the amplifier and reflections alter the load actually presented to the TRAPATT amplifier. The second reason why the arrangement is unsatisfactory is that the standard test load reflection is transmitted by the three-port circulator back to the signal source with little loss. Unless the source assembly is very well matched this return signal will be partially reflected and combine with the primary input signal. Thus, load reflections will give rise, in this way, to significant variations in the power from the output port but they will be due to effects external to the reflection amplifier and the circulator. Part of the input is provided by the output

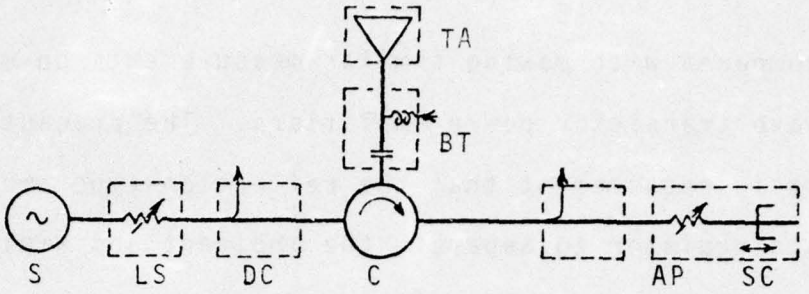

(a) Minimum number of components

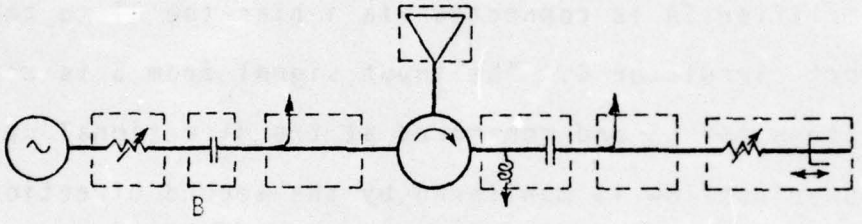

(b) Extra DC blocker required-uncertain load due to bias tee.

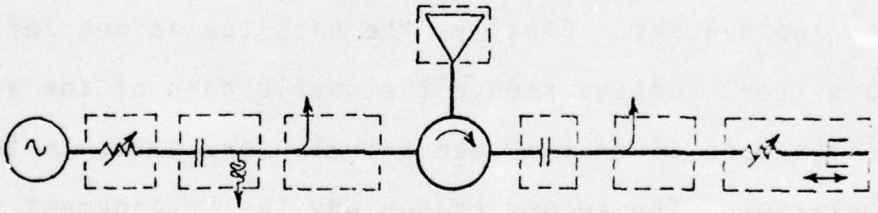

(c) Reflections via the source due to bias tee.

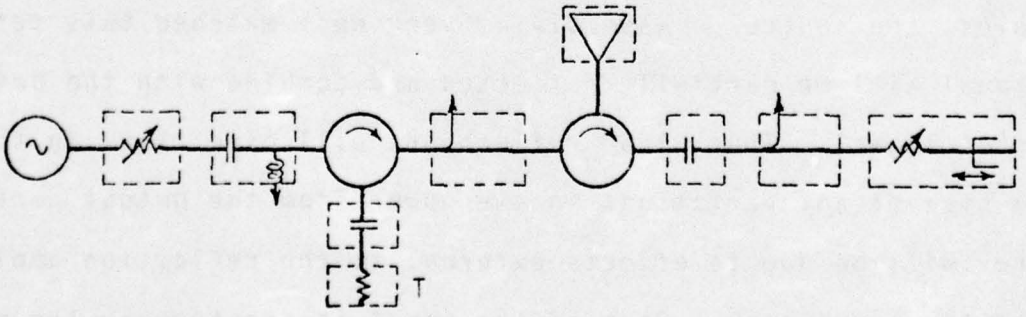

(d) Extra circulator minimises effect of external reflections.

Figure 5.5 Schematics of alternative arrangements for measuring the performance of TRAPATT amplifiers.

of the amplifier and as the phase of the load reflection is altered through 360 degrees the output passes through one maximum and one minimum. With power TRAPATT amplifiers having a gain of about 5 dB extreme mismatch conditions would have to prevail at both the load and the source for the losses to be less than the gain and self-sustained oscillation to develop. However, the output power variations are quite large and it is not possible from such a simple arrangement to determine, how sensitive power TRAPATT amplifiers are to load reflection components that return along the output line, as distinct from those that affect the input signal.

Figure 5.5(b) and (c) show two other arrangements that include one circulator. The bias tee is removed from between the TRAPATT and the circulator and placed either in the output line or the input line. In both cases an additional DC blocker B has to be included in the assembly. The objection to the first rearrangement is that the bias tee introduces uncertainty as to the load at the circulator port. In the second rearrangement source reflections may be made worse by the bias tee in that line.

Monitoring the incident wave at the input port of the circulator as the standard test load is varied around a constant VSWR circle gives an accurate indication of whether re-reflection feedback from the source is occurring. An assembly is required in which re-reflection feedback is negligible. Then the study amounts to discovering what effects arise when practical

circulators are used and a reduced amplitude version of the standard test load reflection reaches the TRAPATT amplifier by leakage through the circulator.

Figure 5.5(d) shows the most satisfactory arrangement that could be devised for this study. A second circulator is introduced between the source and the amplifier circulator immediately before the directional coupler used for monitoring the incident input signal. Residual reflections along the path between the amplifier circulator and the termination T on the second circulator were kept so low that the return loss for the resultant of these components was significantly greater than the leakage of the amplifier circulator. With the latter component dominant, a study of the sensitivity of the TRAPATT amplifier to load reflection in a well engineered situation has been made using the recording technique explained in section 3.3.1. If source re-reflection cannot be reduced satisfactorily, then the merits of recording become doubtful because, to hold the incident input wave constant, point by point measurements would have to be made.

5.3 TRAPATT Amplifier Type I - Performance Under Mismatched Load Conditions

5.3.1 Power Outflow as a Function of Incident Power

An initial test was conducted to determine the output versus input behavior of the amplifier. This was done under matched load conditions. Simultaneous plots were made of the fundamental and the second harmonic output powers as a function of the incident fundamental power. The results are shown in Figure 5.6 and

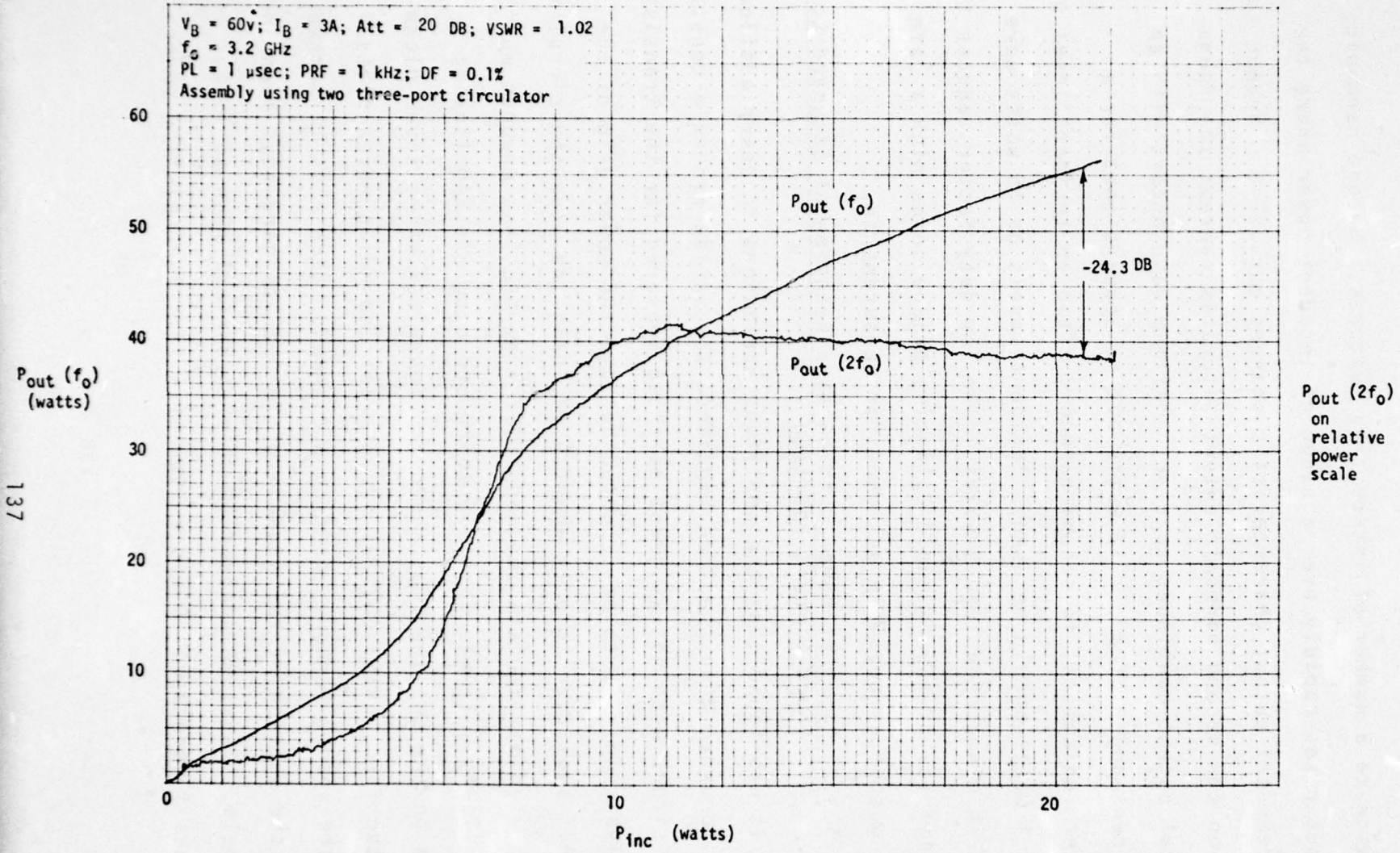

Figure 5.6 Power outflow at fundamental and second harmonic versus incident power for S-band TRAPATT amplifier Type I. Load attenuator set 20 DB, nominal VSWR = 1.02

illustrate a number of interesting features. Second harmonic output rises rapidly over a range of incident power where the fundamental output characteristic changes curvature. Beyond this region the second harmonic output saturates whereas the fundamental output continues to rise. Maximum gain occurs with an incident power of about 10 watts but it appears that for a better fundamental to second harmonic ratio an incident level of 3 or 4 watts should be used. Incident levels of 15 watts were used in mismatched load studies. The low duty factor reduces the sensitivity of the harmonic balancing bridge so as high a safe peak output as possible was used for measurements.

5.3.2 Plots of Power Outflow as a Function of Standard Load Short Circuit Position

It was found that the amplitude variations in power outflow that occurred when the load impedance was varied around a constant VSWR circle were not as great as those measured for the transistor modules. This is to be expected because the power gain of the TRAPATT amplifier is only about 5 decibels and also the circulator being used may isolate the amplifier from the load changes more effectively. It was possible to record complete families of plots on the one sheet as shown in Figure 5.7 where seven plots for the fundamental outflow and the corresponding seven plots for the second harmonic outflow are shown. Each plot is marked with the setting of the attenuator in the standard test load in decibels. Thus, 20 denotes 20 dB or a nominal VSWR of 1.02, whereas 1 denotes 1 dB and a VSWR of 8.72. The relative power

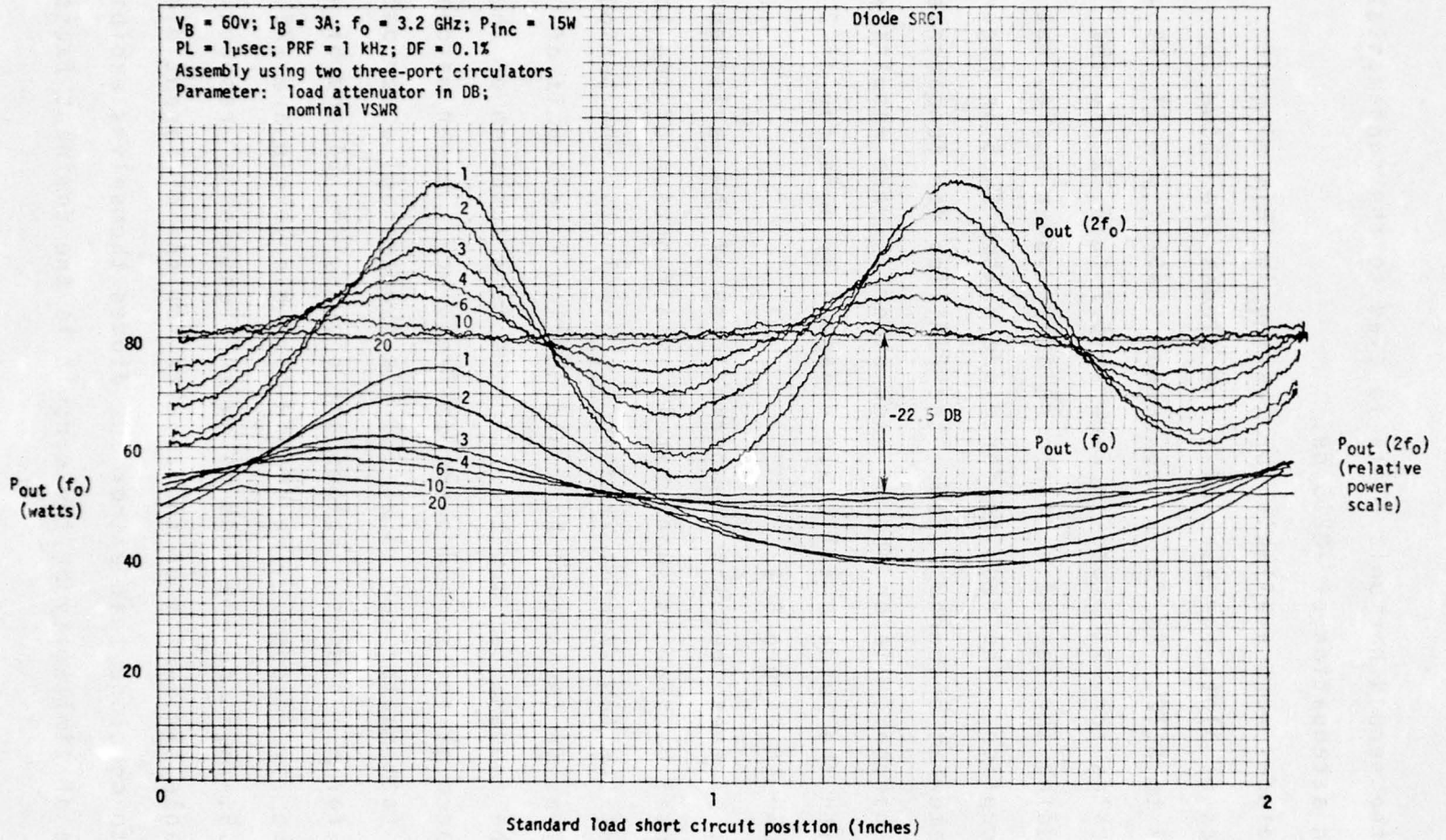

Figure 5.7 Power of the fundamental and second harmonic wave from the output port of S-band TRAPATT amplifier Type I as a function of the position of the short circuit in the standard load. Load attenuator setting is the parameter. Results are for diode number SRC1. Second harmonic power scale is the same for Figures 5.7 to 5.12.

scale for the second harmonic plots is tied to the fundamental level by an attenuation of -22.5 dB.

Five diodes were available for testing in this circuit. The families of plots for each of these diodes are shown in Figures 5.7 to 5.12. As far as equipment stability will allow the axis scales for all plots in Figures 5.7 to 5.12 are the same, including the second harmonic relative power scale, but for one exception. The results for diode number SRC5 in Figure 5.11 are somewhat obscured because the families for fundamental and second harmonic lie on top of each other. These results were repeated with the fundamental scale expanded by a factor of 2 and are shown in Figure 5.12.

In all of these results the periodicity of the variations in fundamental outflow is such that it is a function of the load impedance at the fundamental frequency. Similarly, the period of the variations in the second harmonic outflow is one half of that for the fundamental and therefore it is a function of the load impedance at the second harmonic frequency. Under matched conditions (attenuator set to 20 dB) the fundamental power output is similar for all diodes. Values are 52, 55, 49, 54 and 51 watts peak for the five diodes. The second harmonic levels are -22.5, -23.9, -27.5,-23.6 and -24.7 dB below the fundamental respectively. The remarkable similarity of the results for the different diodes leads one to conclude that either the diodes themselves exhibit this degree of similarity or the circuit is the dominant factor

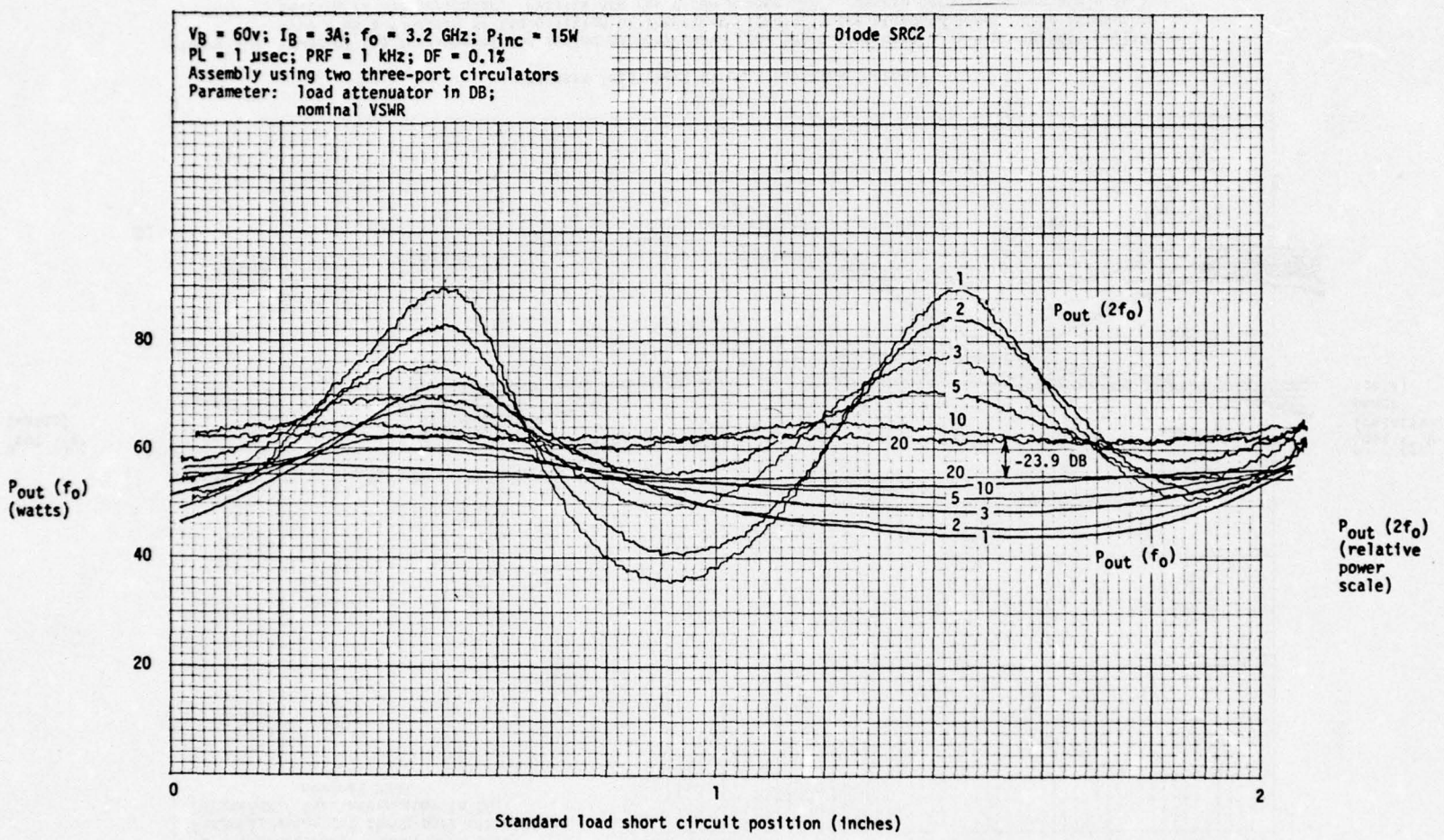

Figure 5.8 Power of the fundamental and second harmonic wave from the output port of S-band TRAPATT amplifier Type I as a function of the position of the short circuit in the standard load. Load attenuator setting is the parameter. Results are for diode number SRC2. Second harmonic power scale is the same for Figures 5.7 to 5.12.

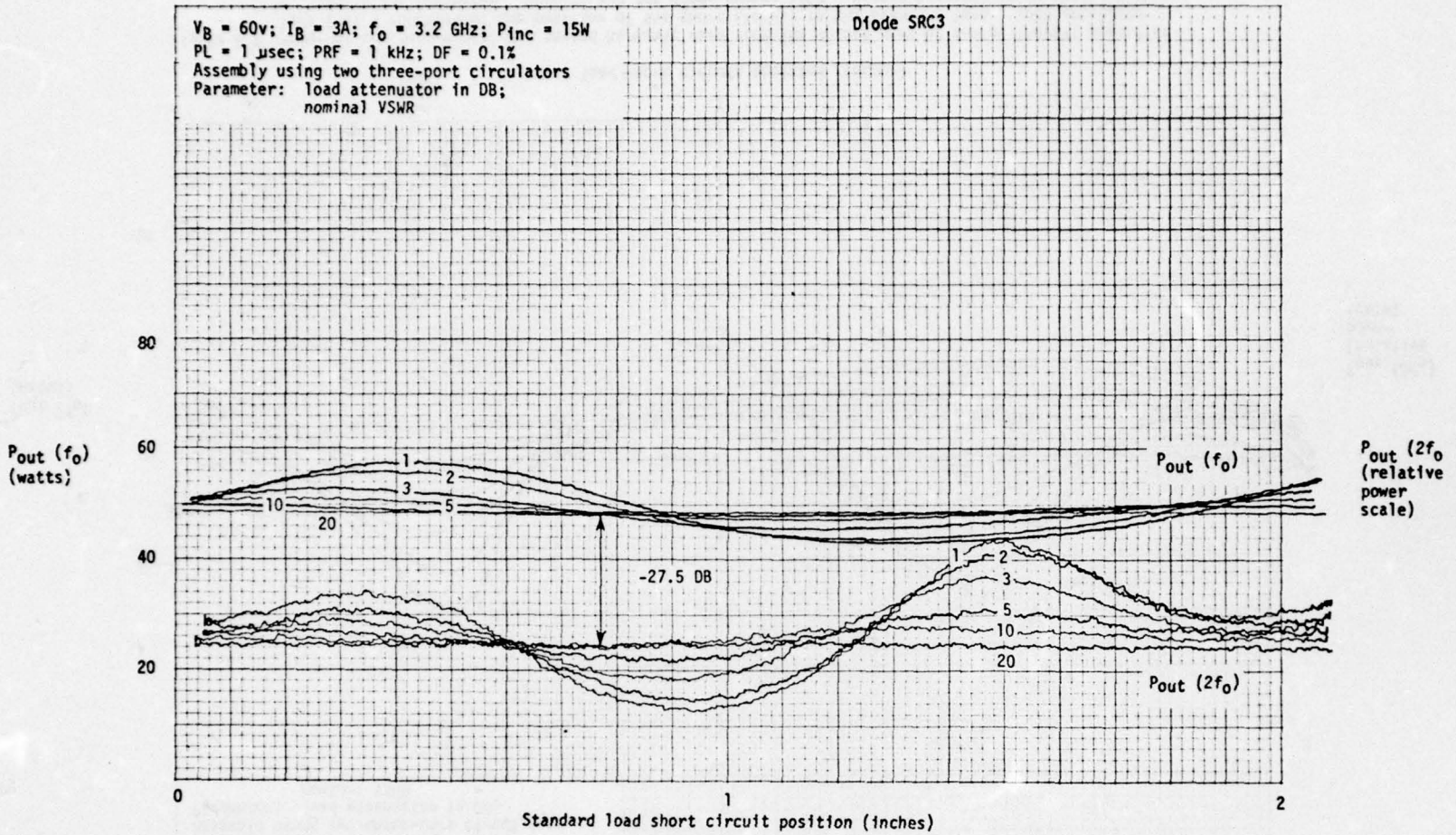

Figure 5.9 Power of the fundamental and second harmonic wave from the output port of S-band TRAPATT amplifier Type I as a function of the position of the short circuit in the standard load. Load attenuator setting is the parameter. Results are for diode number SRC3. Second harmonic power scale is the same for Figures 5.7 to 5.12.

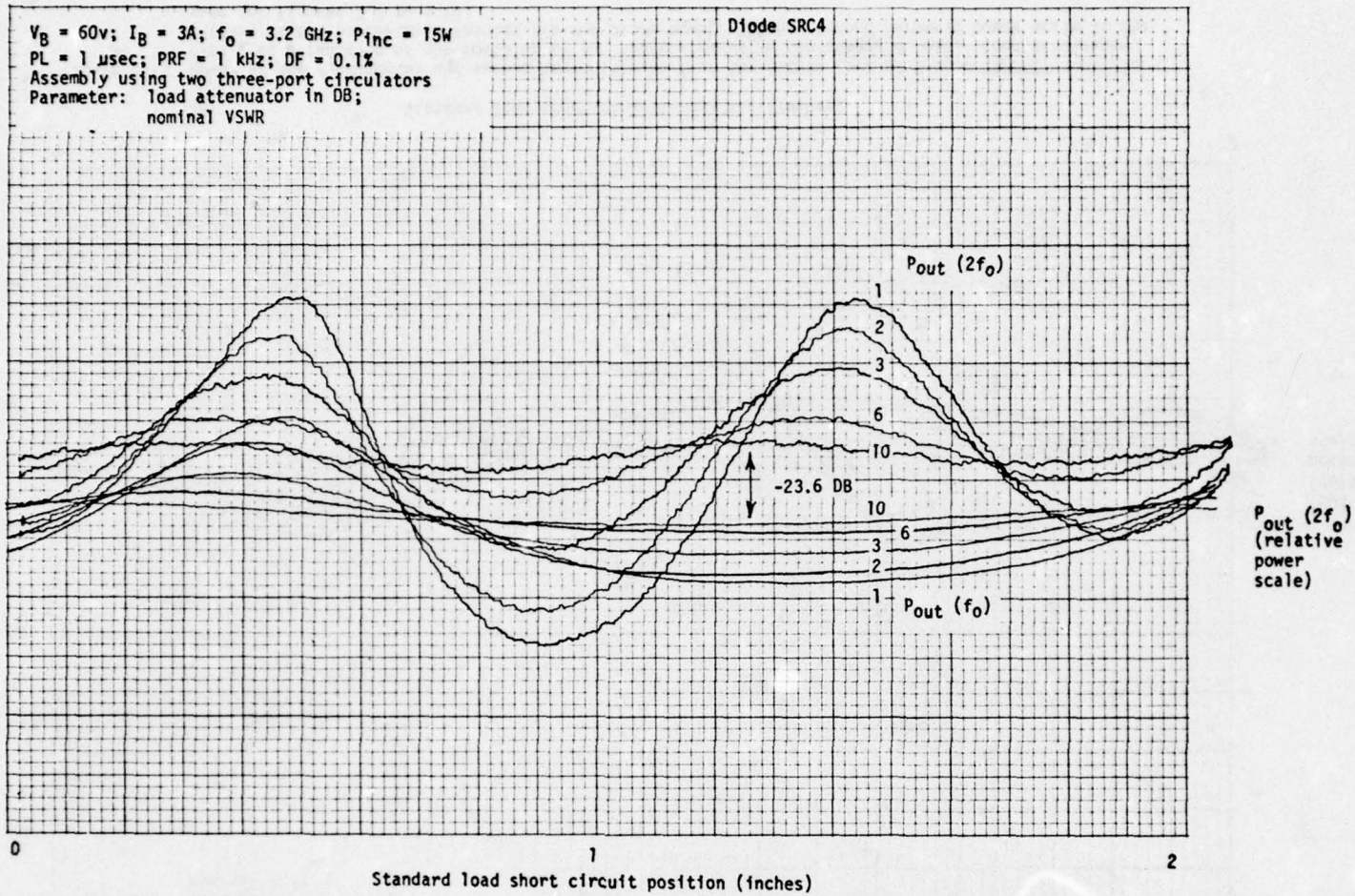

Figure 5.10 Power of the fundamental and second harmonic wave from the output port of S-band TRAPATT amplifier Type I as a function of the position of the short circuit in the standard load. Load attenuator setting is the parameter. Results are for diode number SRC4. Second harmonic power scale is the same for Figures 5.7 to 5.12.

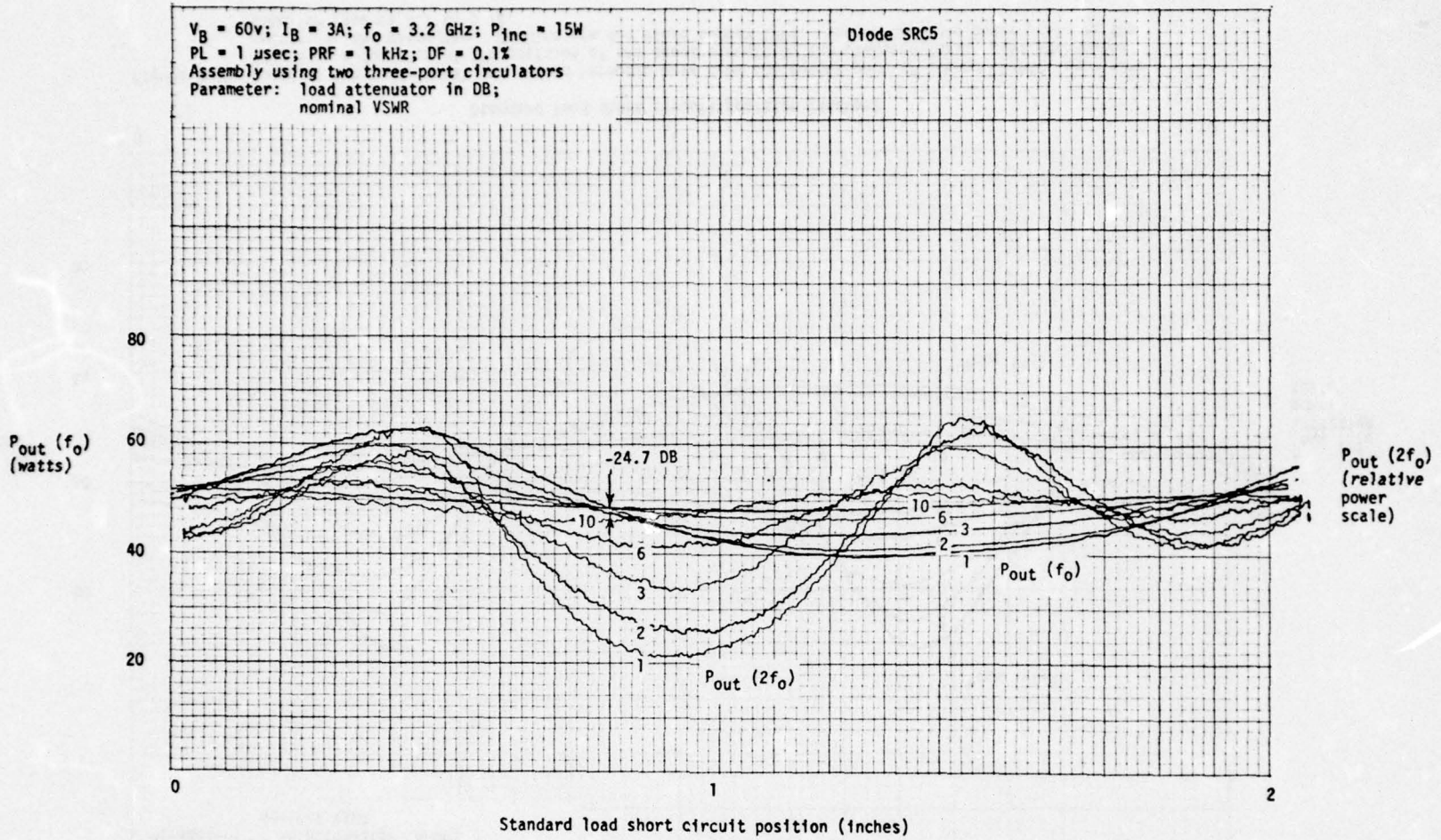

Figure 5.11 Power of the fundamental and second harmonic wave from the output port of S-band TRAPATT amplifier Type I as a function of the position of the short circuit in the standard load. Load attenuator setting is the parameter. Results are for diode number SRC 5. Second harmonic power scale is the same for Figures 5.7 to 5.12.

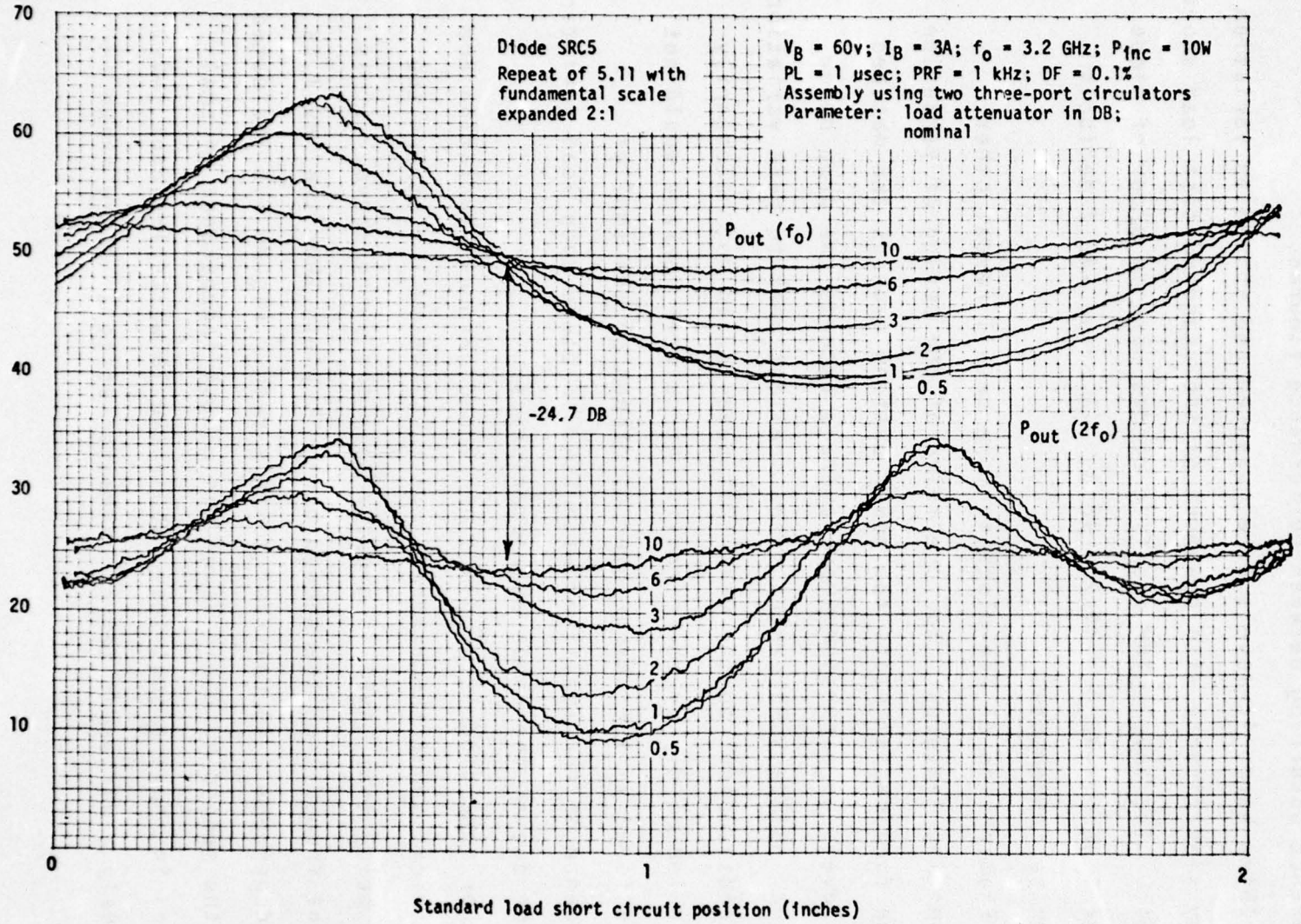

Figure 5.12 Power of the fundamental and second harmonic wave from the output port of S-band TRAPATT amplifier Type I as a function of the position of the short circuit in the standard load. Load attenuator setting is the parameter. Results are for diode number SRC5 and only differ from Figure 5. in that the P_{out} (f_o) scale is altered to separate the plots. Second harmonic power scale is the same for Figures 5.7 to 5.12.

and will tolerate differences between diodes without as great a difference occurring between performance figures.

Third harmonic levels were measured and showed no variation of any significance with movement of the standard test load short circuit. The levels for the five diodes were in order of diode number 1 to 5; -42.0, -44.7, -48.8, -43.2 and -46.7 decibels below the fundamental.

Examination of the plots in more detail reveal other interesting features. For one third of the period of variation of the fundamental plots the power outflow exceeds the matched load level and excursion above average exceeds the drop below average. Diode SCR3 exhibits the smallest peak to peak variation and lends support to the view that behavior is not necessarily controlled mainly by the circuit. Circulator leakage would not have altered in the change over of diodes so the smaller dependence of the amplifier with SCR3 in place upon load variations must be due to the diode characteristics.

For some diodes the plots of second harmonic variation are symmetrical about the matched load level while for others the swing below that level is greater than the swing above. It is evident from all of the second harmonic plots that the level is load dependent. In contrast to this result Figure 5.6 indicated that the second harmonic level was almost independent of small changes in input signal level about the 15 watts incident level. Obviously a different set of characteristics to those shown in

Figure 5.6 would result if a mismatched load were used. It is essential to carefully match the output load to obtain accurate response characteristics for amplifiers that react sensitively to load mismatches.

5.3.3 Results as Equi-Power Contours on Smith Charts

The plots in Figure 5.7 for diode SRC1 have been used to construct equi-power contours for the fundamental and second harmonic outflows and these are shown in Figures 5.13 and 5.14. When compared with corresponding plots for L- and S-band bipolar transistor modules it is evident that the ratio of maximum to minimum fundamental power outflow is similar for all amplifiers. However, the range of variation of second harmonic outflow is much small for the TRAPATT than for the transistor amplifiers. The level is higher, but as will be seen when the Type III amplifier results are presented, there is reason to believe that harmonic output levels can be reduced by circuit design.

The reason for the smaller variation in harmonic outflow may well be due to the inherent operation of the TRAPATT. The harmonic voltage level trapped within the circuit lumped at the diode terminals is known to be high for efficient TRAPATT operation. Also the coupling at the second harmonic between that circuit and the load must be low. Hence, irrespective of the performance of the circulator at the second harmonic frequency the load variations will only produce a small variation in the trapped second harmonic voltage. This line of reasoning and the experimental results suggest that it may be easier to make accurate prediction of

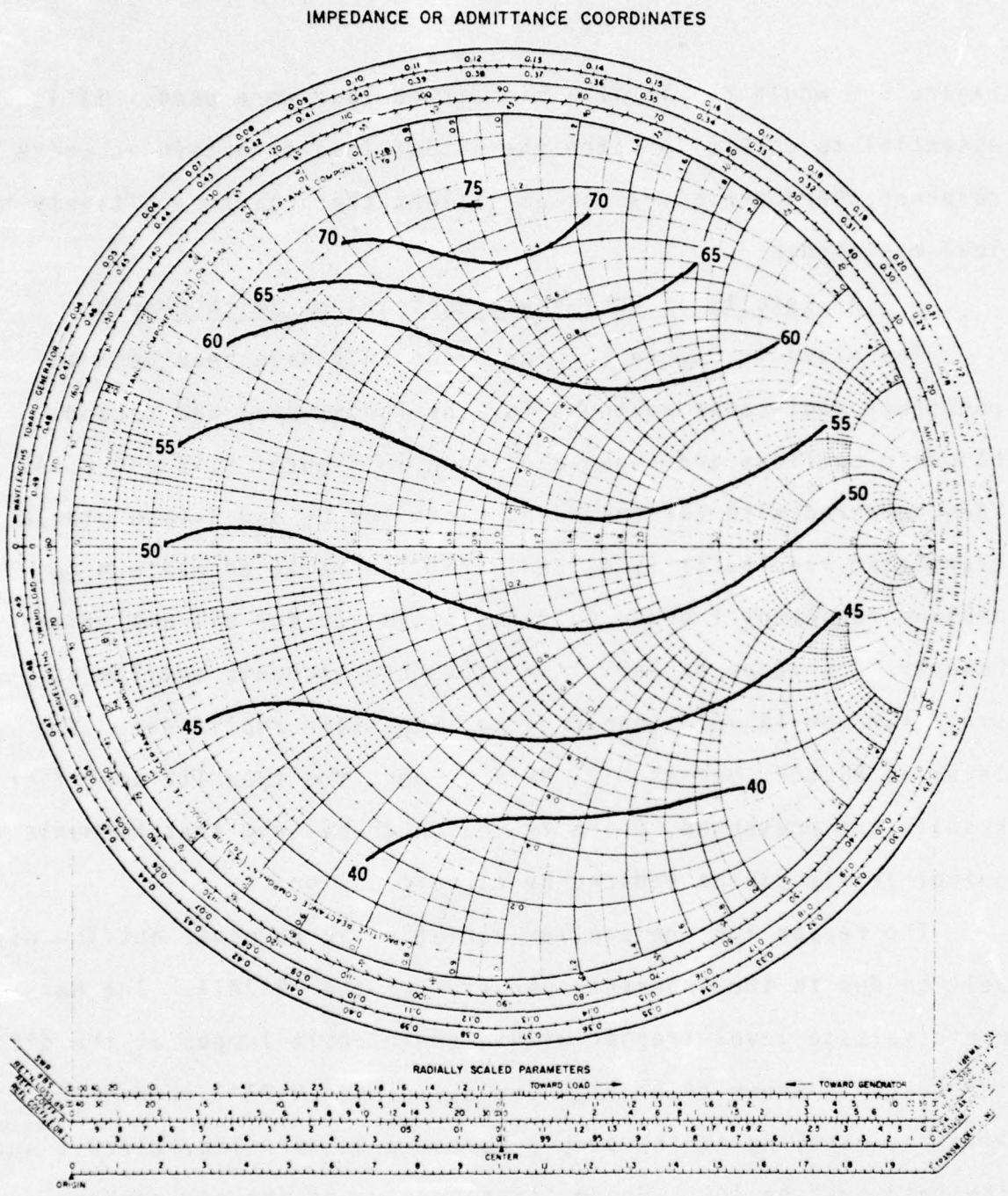

Equi-power contours in watts.
Signal frequency 3.2 GHz. Incident power 15 W peak.
Signal pulse length 1.0 microsecs. PRF 1 kHz. DF 0.1%.

Figure 5.13 Power of fundamental wave from the output port of S-band TRAPATT amplifier Type I with diode SRC1 as a function of the load impedance at the fundamental.

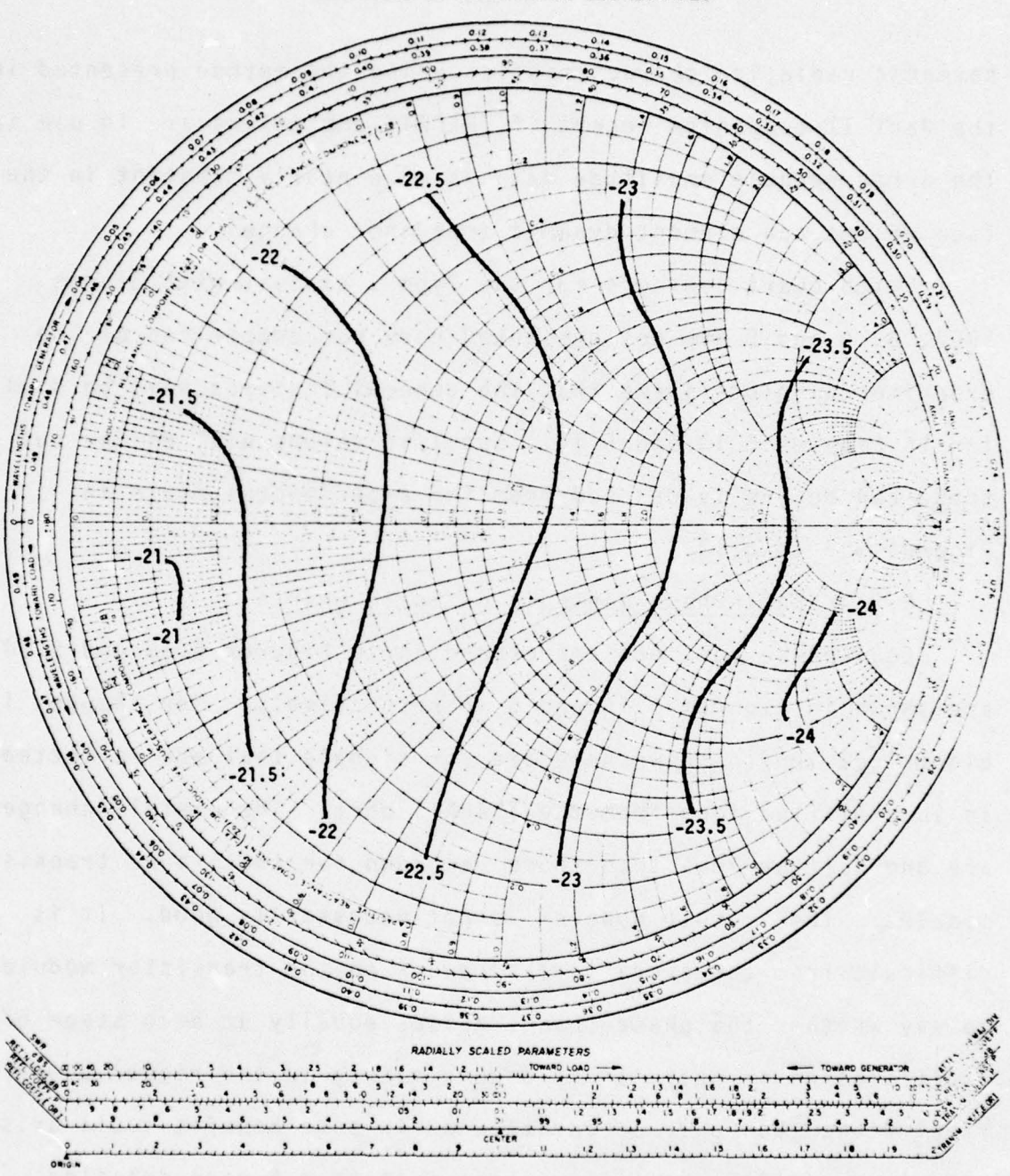

Equi-power contours in DB below fundamental.
Signal frequency 3.2 GHz. Incident power 15 W peak.
Signal pulse length 1.0 microsecs. PRF 1 kHz. DF 0.1%.

Figure 5.14 Power of second harmonic wave from the output port of S-band TRAPATT amplifier Type I with diode SRC1 as a function of the load impedance at the second harmonic.

harmonic radiation characteristics using the method presented in the Part II companion report if TRAPATT amplifiers are in use in the array because amplitude data is more nearly constant in the face of antenna element dynamic impedance change.

Smith chart contours for the Type I circuit with diodes SRC2, 3, 4 and 5 are not presented here but comparison of the experimental plots shows that the general features will be similar to Figures 5.13 and 5.14. Specific values will differ but these can be easily deduced from the experimental plots in Figures 5.8 to 5.12.

5.3.4 Equi-Phase Contours on Smith Charts

Equi-phase contours corresponding to Figures 5.13 and 5.14 are shown in Figures 5.15 and 5.16 respectively. The changes in electrical length shown here are for signals that are reflected in an amplified form from the TRAPATT port. The overall changes are one half or less than those recorded for the S-band transistor modules. This result however is not necessarily good. It is difficult from the overall measurement on the transistor module to say whether the phase change arises equally at each stage of amplification or not. If it occurs mainly in the higher power final stage then on a comparative basis some benefit could arise by using a TRAPATT amplifier stage instead. A more detailed study is desirable before firm conclusions regarding such a comparison can be drawn.

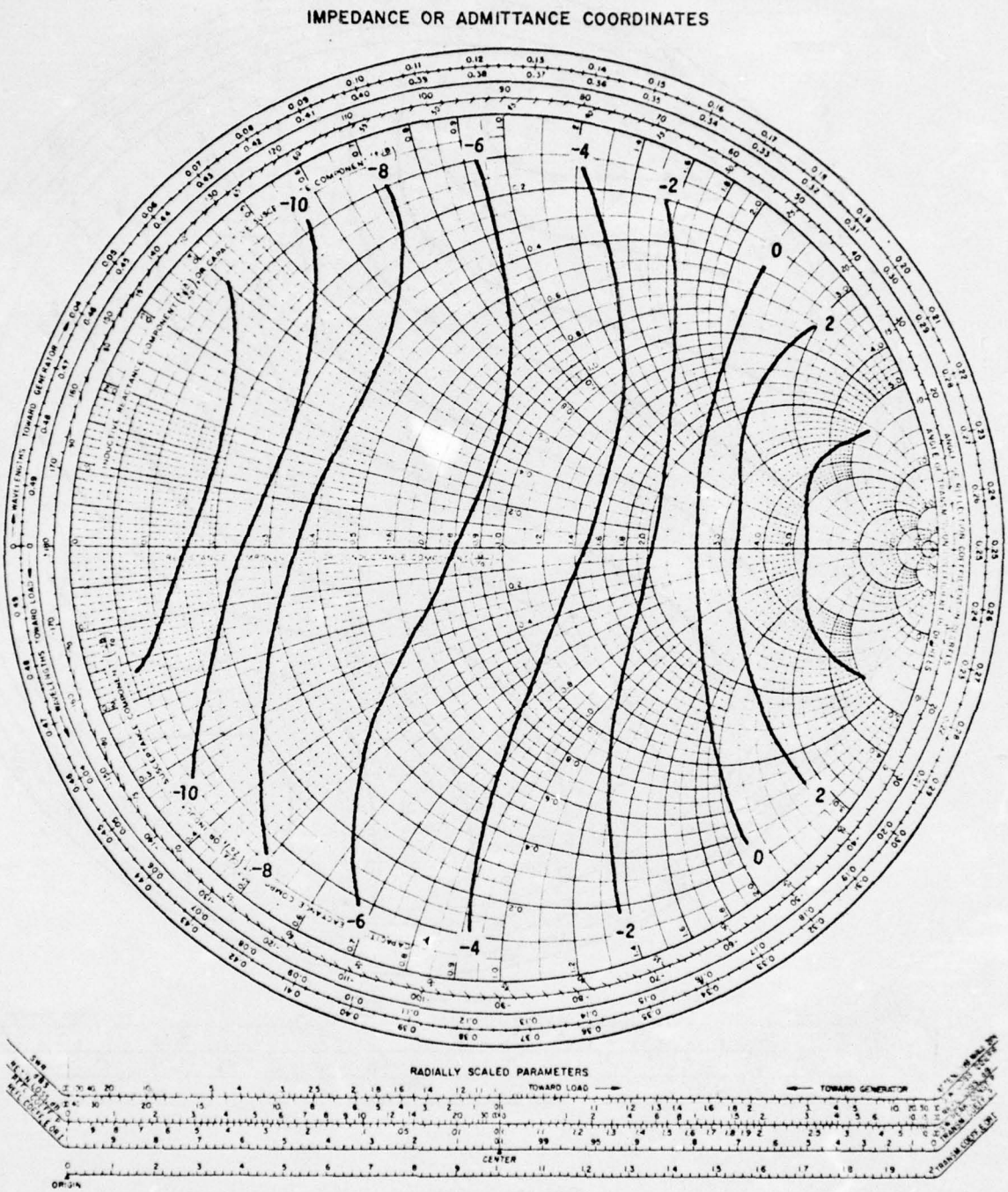

Equi-phase contours in electrical degrees.
Signal frequency 3.20 GHz. Incident power 15 W peak.
Signal pulse length 1.0 microsecs. PRF 1 kHz. DF 0.1%.

Figure 5.15 Relative phase of the fundamental wave from the output port of S-band TRAPATT amplifier Type I with diode SRC1 as a function of the load impedance at the fundamental.

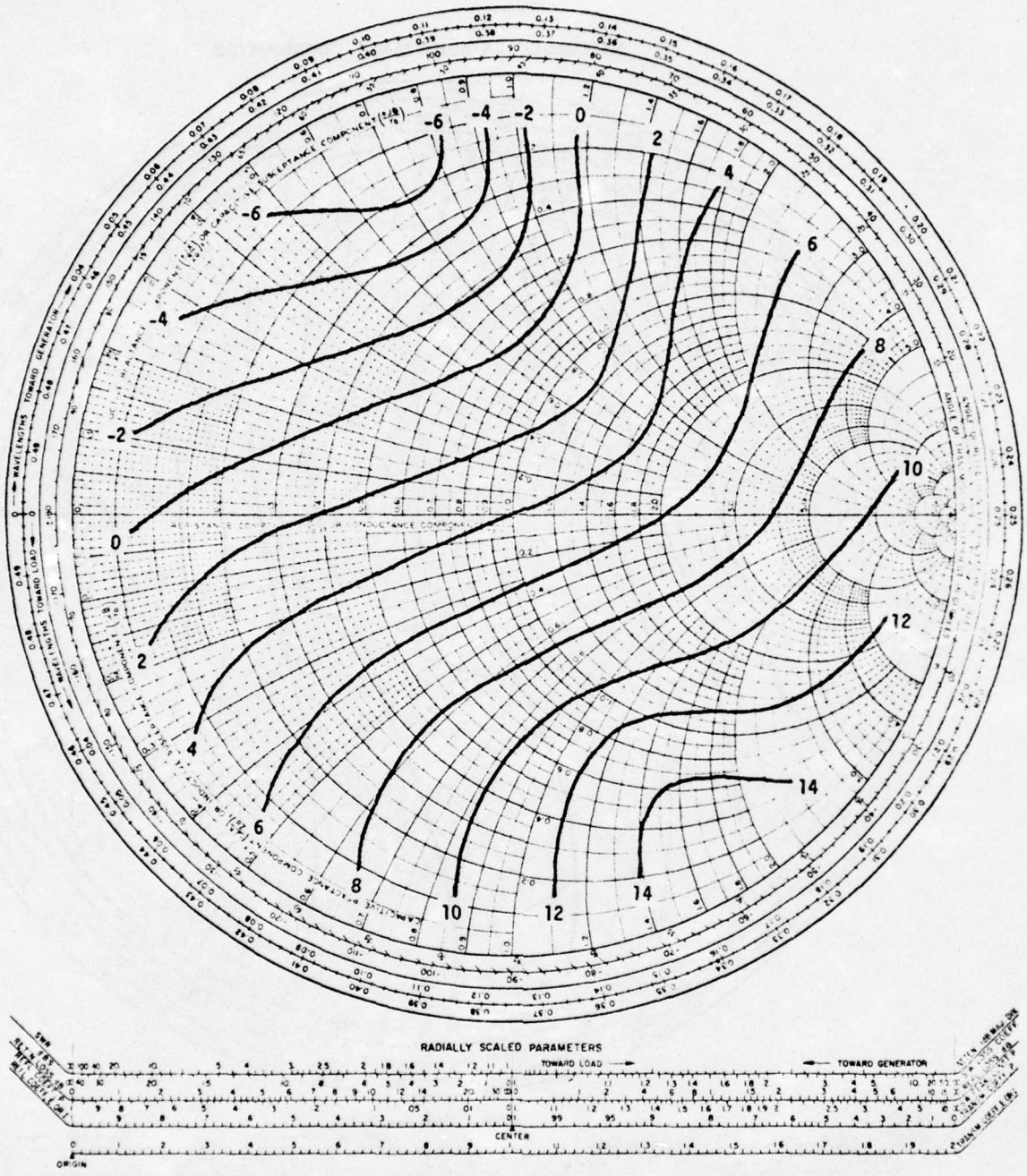

Equi-phase contours in electrical degrees.
Signal frequency 3.20 GHz. Incident power 15 W peak.
Signal pulse length 1.0 microsecs. PRF 1 kHz. DF 0.1%.

Figure 5.16 Relative phase of the second harmonic wave from the output port of S-band TRAPATT amplifier Type I with diode SRC1 as a function of the load impedance at the second harmonic (6.40 GHz).

5.4 TRAPATT Amplifier Type II - Performance Under Mismatched Load Conditions

As noted in section 5.1, the Type II circuit is almost identical with Type I the only significant electrical difference being an adjustable capacitor corresponding to C_4 in the equivalent circuit of Figure 5.4. Comparison of the power outflow plots of Figure 5.17, which are for diode SRC1 in the Type II circuit, with those of Figure 5.7, which are for the same diode in the Type I circuit, shows that the performance is similar. The second harmonic level is slightly higher and undergoes slightly larger variations in amplitude. An instability is evident over the range 0.5 to 0.8 inches in the range of travel of the short circuit. This was sensitive to the setting of capacitor C_4 and with perserverance could probably be eliminated. The third harmonic level was independent of the load short circuit position and was -40.8 decibels below fundamental.

5.5 TRAPATT Amplifier Type III - Performance Under Mismatched Load Conditions

5.5.1 Power Outflow as a Function of Incident Power

The output versus input characteristics of the amplifier under matched load conditions were measured to begin with. Equipment limitations prevented the recommended input level of 30 watts being applied. Plots of power outflow at fundamental and second harmonic as a function of incident power up to 22.5 watts are shown in Figure 5.18. The remarkable result is that at the highest input and therefore output level the second harmonic was 51 decibels below the fundamental and the third harmonic was

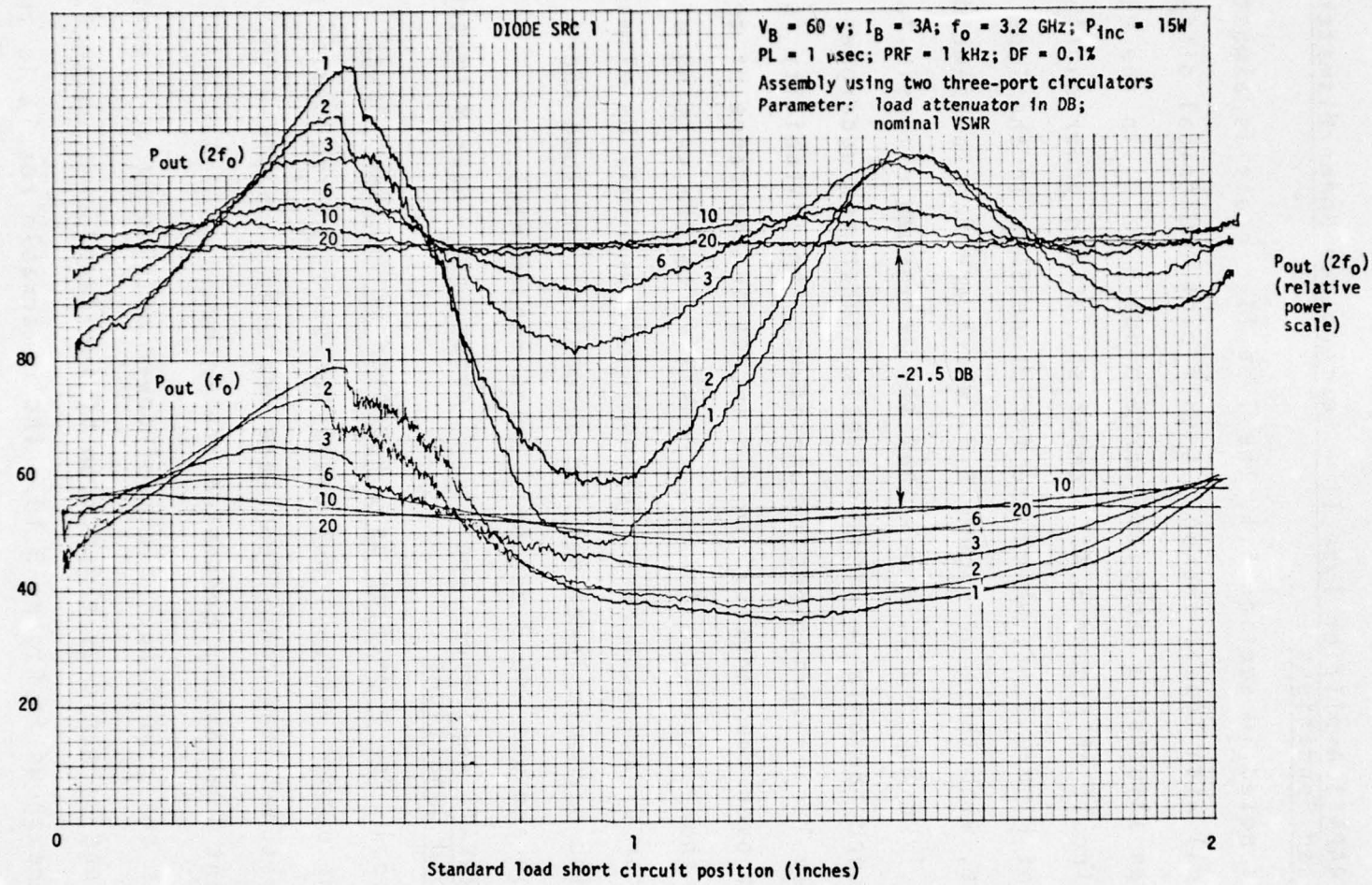

Figure 5.17 Power of the fundamental and second harmonic wave from the output port of S-band TRAPATT amplifier Type II as a function of the position of the short circuit in the standard load. Load attenuator setting is the parameter. Results are for diode number SRC 1. Second harmonic power scale is the same as for Figures 5.7 to 5.12.

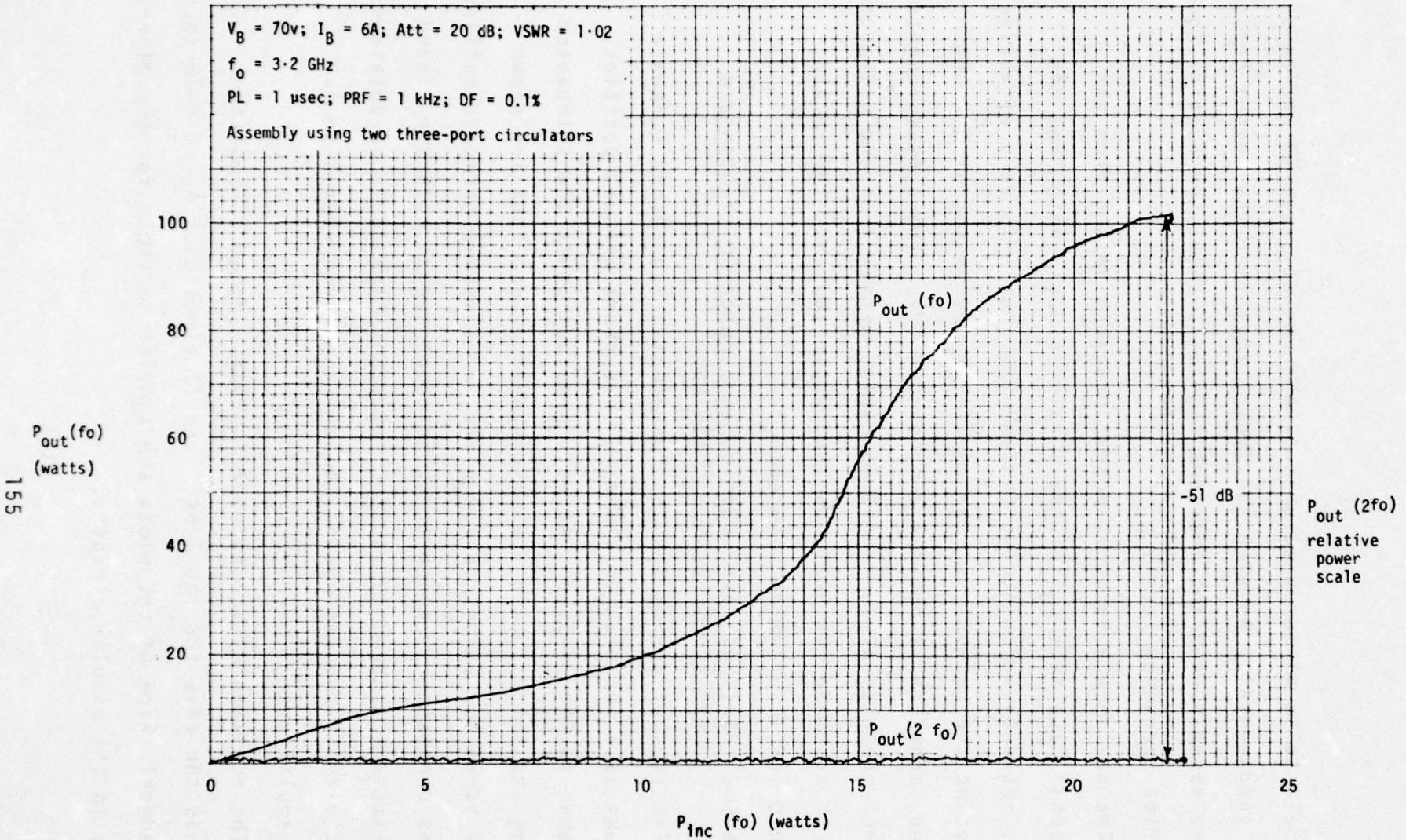

Figure 5.18 Power outflow at fundamental and second harmonic versus incident power for S-band TRAPATT amplifier Type III. Load attenuator set 20 DB, nominal VSWR = 1.02

too small to be measured accurately and was at least 56 decibels below fundamental. As with the Type I amplifier the output begins to rise rapidly when the incident signal is about one half of the specified operating level.

The negligible harmonic output probably arises from the additional capacitor C_5, placed a quarter wavelength from the diode, not only matching the fundamental, but also very effectively reflecting the harmonics. The amplifier was tested at 3.2 GHz and the bandwidth is nominally about 0.2 GHz. These measurements were not repeated at various frequencies within the band although a search was made for settings that would increase the second harmonic level but without success.

5.5.2 Plots of Power Outflow as a Function of Standard Load Short Circuit Position

Families of curves for the fundamental and second harmonic outflows as a function of standard load short circuit position are shown in Figure 5.19. As with previous plots the attenuator setting and in this case the corresponding load VSWR are shown as the parameter values on the plots. The second harmonic outflow remains consistently close to noise level and no accurate record of variations related to short circuit position could be obtained. Sensitivity is reduced by the low duty cycle of operation for these amplifiers.

The fundamental varies over a greater range of amplitude than was the case for the Type I and II circuits. Apart from that the general shape of the plots are similar to those for the other diodes in the simpler circuits.

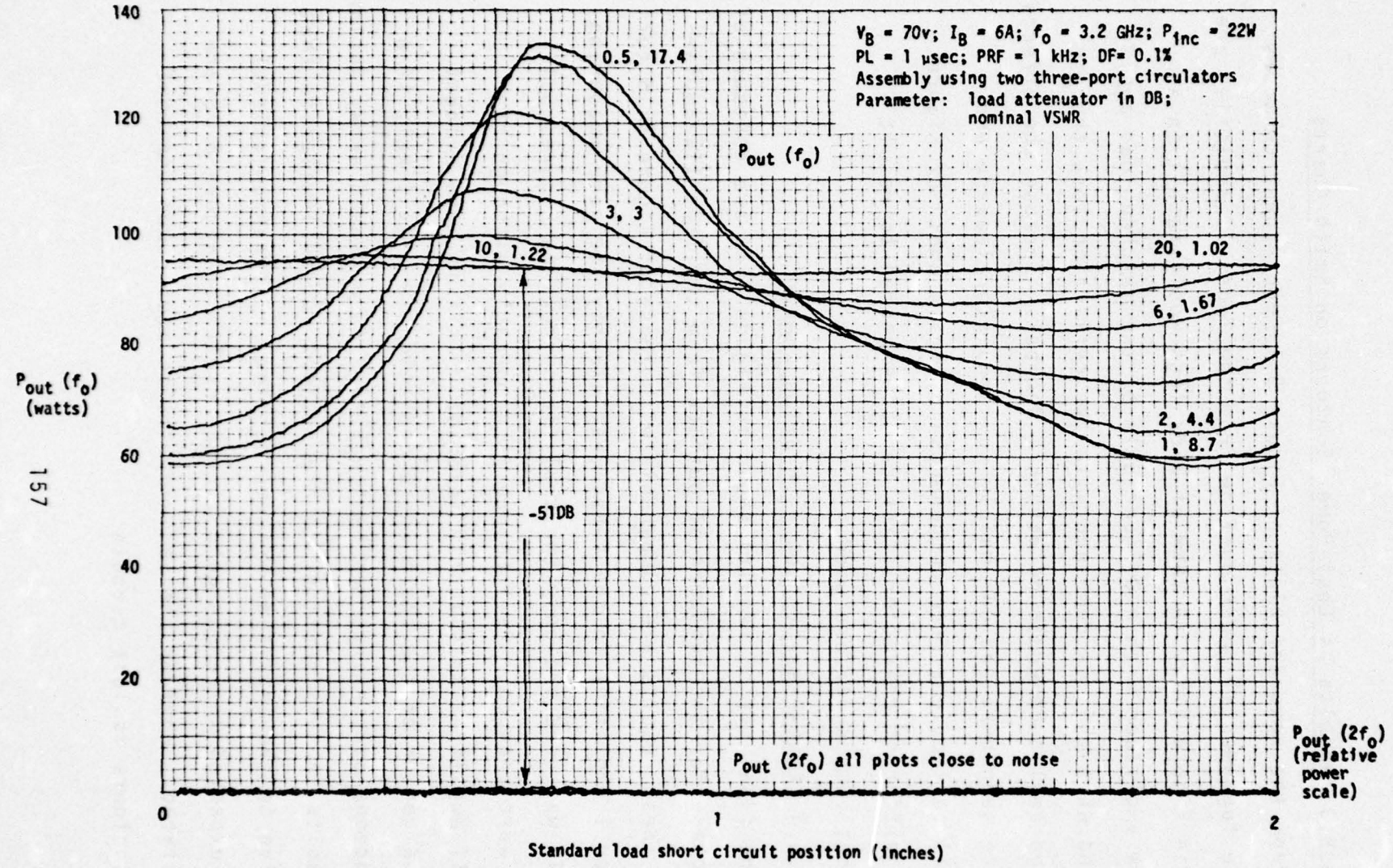

Figure 5.19 Power of the fundamental and second harmonic wave from the output port of S-band TRAPATT amplifier Type III as a function of the position of the short circuit in the standard load. Load attenuator setting is the parameter.

5.5.3 Results as Equi-Power Contours on Smith Charts

From the recorder plots of Figure 5.19 equi-power contours for the fundamental power outflow from the Type III amplifier are shown in Figure 5.20. A VSWR of 2 or less would result in an outflow amplitude within 0.5 decibels of the matched load amplitude and when this is combined with the reflection loss the radiated amplitude would be within 1 decibel. Because the effects that are seen here are due mainly to circulator leakage and residual reflections from components in the assembly of Figure 5.5(d) different characteristics can be expected to result if different components are used.

5.5.4 Equi-Phase Contours on Smith Charts

The final set of results shown in Figure 5.21 are contours of equal phase for the fundamental outflow from the Type III amplifier. These results are comparable with those of Figure 5.15 for the Type I amplifier in the sense that exactly the same measuring assembly was used and only the amplifiers shown in Figures 5.1 to 5.3 were changed. Performance is comparable although the Type III amplifier is slightly inferior. This is more evident near the center of the chart where operation is most likely if a good antenna performance has been achieved in a phased array design. The results in this section 5.5 are subject to the limitation that the drive to the amplifier is somewhat low. The harmonic level can be expected to remain good if the results of Figure 5.18 are extrapolated. Whether the same applies to equi-power and equi-phase contours is less certain.

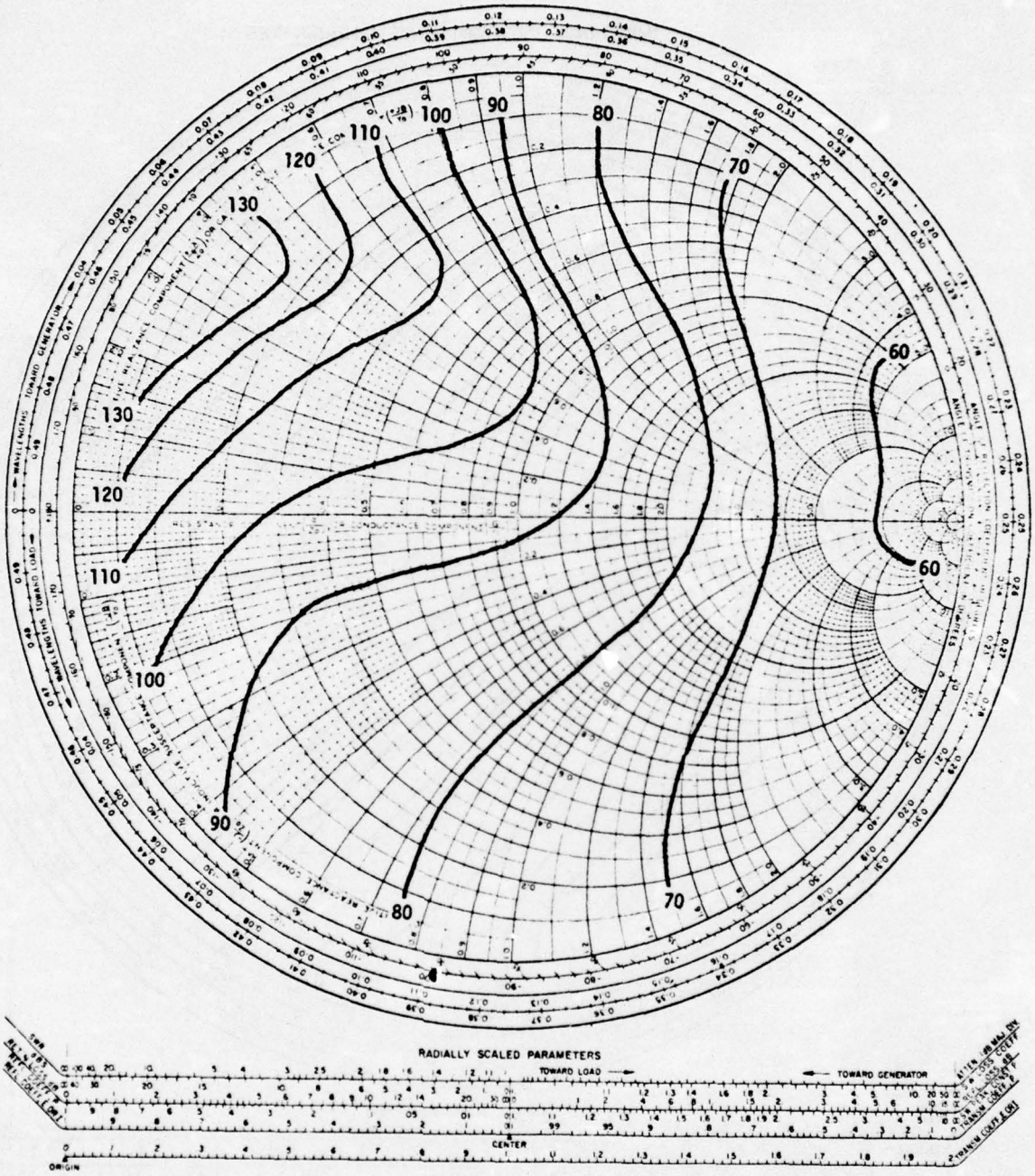

Equi-power contours in watts.
Signal frequency 3.20 GHz. Incident power 22 W peak.
Signal pulse length 1.0 microsecs. PRF 1 kHz. DF 0.1%

Figure 5.20 Power of fundamental wave from the output port of S-band TRAPATT amplifier Type III as a function of the load impedance at the fundamental

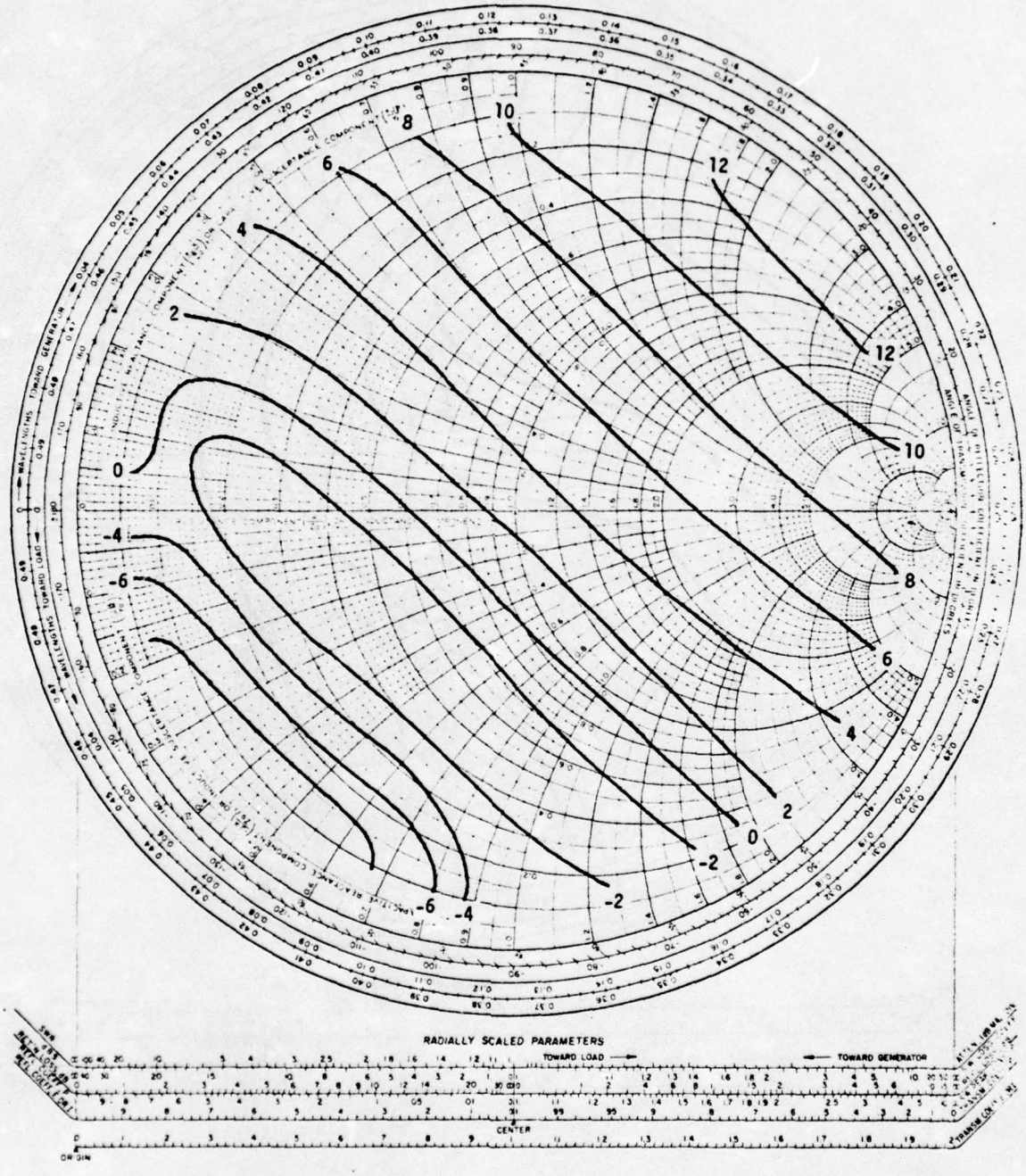

Equi-phase contours in electrical degrees.
Signal frequency 3.20 GHz. Incident power 22 W peak.
Signal pulse length 1.0 microsecs. PRF 1 kHz. DF 0.1%

Figure 5.21 Relative phase of the fundamental wave from the output port of S-band TRAPATT amplifier Type III as a function of the load impedance at the fundamental

CHAPTER 6

CONCLUSIONS

6.1 The Harmonic Balancing Bridge

It has been demonstrated that accurate measurement of amplitude and phase data of harmonically related frequency components in the output from microwave amplifiers can be made. The method appears to be the only satisfactory one if large differences in level exist between the amplitudes to be measured. With careful choice and calibration of components commercially available units can be assembled to form a harmonic balancing bridge that will function satisfactorily over the band 2 to 12 GHz. A useful feature of the bridge is that the amplifier under test can be investigated with accurately known mismatched loads and the behavior obtained in terms of variations in the amplitude and relative phase of the wave that is generated at the output and propagates toward the load. Thus, effects arising in the amplifier are separated from those arising from the wave absorbed by the load being different from that incident on it due to the reflection process.

The versatility of the harmonic bridge has been extended by devising a technique for plotting amplitude variations of the frequency components flowing out of the amplifier as a function of the varying phase of a constant magnitude load reflection. The family of plots that result from different tests with different reflection magnitudes have been used to present amplitude behavior

as equi-power contours on a Smith chart whose coordinates are those of the load impedance that is primarily related to the amplitude variations observed.

Bridge balancing at the fundamental and then each harmonic in rising order is a manual process that makes studies of phase behavior time consuming. The technique in determining an accurate balance has been developed but no simple way of automatically determining the balance appears practical without a sacrifice of accuracy.

The full capability of the bridge has not been exploited extensively because the third harmonic levels in the amplifiers studied was near the noise level or did not vary significantly with change in the phase of the load reflection.

This type of bridge and its use for studying microwave amplifiers appears to be original insofar as the behavior that has been found was previously unknown and exhibits a number of surprising features.

6.2 The L-Band Bipolar Transistor Transceiver Modules

The effect of load variations on the components from the output port of the L-band transceiver modules is surprising in the following ways,

(i) significant variations in the fundamental outflow occur indicating imperfect isolation from load variations

(ii) variations of second harmonic level over a range in excess of 30 decibels may occur and they are related

to variations of the load impedance that is presented at the fundamental, not the second harmonic frequency

(iii) large variations of third harmonic level also occur and these are related primarily to the load impedance at the third harmonic frequency

(iv) there are load conditions that can give rise to a state such that the third harmonic level exceeds the second harmonic

(v) reflection losses at the antenna for each frequency component are dependent on the dynamic impedance presented by the elements at each frequency, notwithstanding the fact that amplitude variations in the incident wave may depend upon impedance at another frequency. This makes specification of the input data for calculations of the radiation patterns of driven element phased array antennas a more complex problem than was originally thought.

(vi) two separate sources of phase error can be distinguished, one arising in the module and affecting the wave incident on the antenna and the other due to the wave absorbed by the antenna being different from the incident wave

(vii) various mechanisms arising from module design limitations and component imperfections are responsible for the complex behavior observed.

6.3 The S-Band Bipolar Transistor Transceiver Modules

Similar conclusions to those drawn in the L-band studies apply to the results of tests on the S-band bipolar transistor transceiver modules.

(i) significant variations in fundamental outflow occur indicating imperfect isolation between load and amplifier output.

(ii) large variations in second harmonic outflow may occur. They are primarily related to variations of the second harmonic load impedance but some dependence on variations in the fundamental load impedance can be seen in the recordings

(iii) third harmonic levels are too low to be studied accurately

(iv) specification of input data for calculation of the radiation patterns at fundamental and second harmonic depend upon a knowledge of the dynamic impedance at each element in the array

(v) two separate sources of phase error can be distinguished one arising in the module and other at the antenna element due to reflection

(vi) various mechanisms can be contributors within the module to the behavior observed at the output.

6.4 The S-Band TRAPATT Amplifiers

The results of measurements of TRAPATT amplifier performance are found to be closely dependent on the circulator and other items in the assembly used to bias, energize and monitor behavior.

If care is taken to eliminate what can otherwise be dominant effects originating from the choice of external components, a measure of real TRAPATT limitations are possible. From the results of this study the following conclusions are drawn,

(i) the microwave circuit requirements for sustaining TRAPATT operation are compatible with requirements for suppressing harmonic components from appearing in the output

(ii) circuit requirements also lead to low coupling between the load impedance and the harmonics trapped in the diode circuit and as a result variations in the amplitude of harmonic outflow due to load variations are small or negligible

(iii) fundamental outflow variations with load variations can be comparable to those that occur in microwave transistor modules

(iv) specification of amplitude and phase data for calculations of radiation patterns should be a less complex task than for bipolar transistor module driven array elements

(v) choice of optimum components to use in association with the single port TRAPATT amplifier must be regarded as a major problem where tight specifications may be a difficult problem to solve at reasonable cost.

6.5 Simple Summary of Results

For convenience Table 6.1 is a summary of the amplitude levels encountered in all of the amplifiers tested. It is presented in as simple a way as possible to indicate the levels of the components flowing out of the module and the range over which they may vary if the load presents a VSWR of 3.0. It will be realized that they are distilled from the more detailed picture of behavior contained in the large number of Smith chart plots presented in the report.

It will be seen that they provide a basis for an optimistic view that solid state amplifiers driving elements of phased array antennas will be able to meet OTP requirements for radar operation. A more detailed statement is presented in the Part II companion report to this study.

L BAND MODULES

2nd Harmonic

-50 dB (-47 to -65 dB)

-54 dB (45 to -67 dB)

3rd Harmonic

-54 dB (-50 to -57 dB)

-61 dB (-58 to -66 dB)

S BAND MODULES

2nd Harmonic

-40 dB (-38 to -43 dB)

-37 dB (-34 to -41 dB)

3rd Harmonic

<-60 dB (<-60 dB)

<-60 dB (<-60 dB)

TRAPATT DEVICE

2nd Harmonic

-51 dB

3rd Harmonic

<-60 dB

TABLE 6.1 Second and Third Harmonic Levels Of Some Microwave Solid State Devices (Matched*)

*Figures in parentheses indicate levels with VSWR = 3.0 and variable angle of reflection coefficient.

REFERENCES

(1) Staff of the Sperry Research Center, "Electronic Scanning," Sperry Engineering Review, Vol. 18, Number 4, Winter 1965.

(2) Blake, Carl, "Design, Performance and Cost Considerations For Solid State Arrays," Phased Array Antennas, Oliner, AA, and Knittel, G.H. (Editors), Artech House, (1972 Dedham, Mass.).

(3) Herskowitz, Gerald J. and Schilling, Ronald B. (Editors), Semiconductor Device Modelling For Computer-Aided Design, (McGraw-Hill, 1972), Chapter 3, Harrison, R.G., "Large-Signal Microwave Frequency Transistor Modelling."

(4) Johnson, Joe, (Editor), "Solid Circuits," Communication Transistor Company, Application Book 2.2.8.0A.

(5) Poole, Walter E., "Microwave Power Chip Carriers," Res. and Dev. Tech. Report, ECOM-0008-F, Final Report, February 1974.

(6) Noel, Philip L, "Integrated Solid-State Transceiver," Res. and Dev. Tech. Report, ECOM-0083-2, Semi-Annual Report, 15 April 70 to 14 October 71, Pub. May 1972.

(7) Rosen, D.E., et al, "Integrated Solid-State Transceiver," Res. and Dev. Tech. Report, ECOM-0121-4, Final Report, January 71 to August 73, Pub. January 1974.

(8) Hanley, G., Viola, R. and Koegler, P., "Solid State S-Band Transmit/Receive Module," 1974 IEEE G-MTT International Microwave Symposium, June 12-14, 1974, Georgia Institute of Technology, Atlanta, Georgia.

(9) Lazar, Stephen, "Solid State Power Amplifiers For S-Band Phased Array Radar," Microwave Systems News, Feb/Mar 1975.

(10) Grace, M., Kroger, H. and Potter, C.N., "S-Band Amplifier," Research Report SRRC-RR-75-10, Sperry Research Center, Final Report 11 Feb to 14 Mar 1975.

(11) Kroger, H., Potter, C.N., Grace, M.I., Pratt, H., Bozler, C., Cox, N.W., Gsteiger, K.E., Hill, G.N. and Rucker, C.T., "High Average Power TRAPATT Devices," 1973 Proc. Cornell Biennial Conference, p. 371-380.

(12) Kroger, Harry and Grace, Martin I., "TRAPATT Amplifier," RADC-TR-74-261, Final Report, January 1975. AD# A005680.

(13) Grace, M.I., Potter, C.N., Kroger, H. and Pratt, H.J., "TRAPATT Amplifier For Phased Arrays," RADC-TR-73-409, Final Report, February 1974. AD# 777602/4GI.

(14) Grace, M.I., Kroger, H. and Pratt, H., "TRAPATT Amplifier For Phased Arrays," RADC-TR-73-26, Interim Report, March 1973. AD# 760545.

(15) Fong, T.T. and Ying, R.S., "Solid State Amplifier For Spread Spectrum Communications," RADC-TR-75-56, Final Report, February 1975. AD# A007789.

(16) Kawamoto, H., Prager, H.J., Allen, E.L. and Mikenas, V.A., "Advances in High-Power, S-Band TRAPATT-Diode Amplifier Design," Microwave Jl., 17, p. 41-44, 1974 February.

(17) Rosen, A., Kawamoto, H., Prager, H.J., Liu, S.G., and Paglione, R.W., "S-Band Amplifier - TRAPATT," Res. and Dev. Tech. Report, ECOM-72-0213-F, Final Report, 15 June 72 to 14 Dec 73, Pub. August 1974.

APPENDIX 1

LIST OF ITEMS IN THE L-BAND BRIDGE ASSEMBLY

ITEM	NAME	MAKER	MODEL	SERIAL	BANDWIDTH
1	Microwave oscillator	HP	8690B	507-01137	1-2,2-4
2	PIN modulator	HP	8714A	351-00253	0.8-2.4
3	TWT amplifier	HP	489A	811-01207	1-2
4	Wavemeter, absorption type	FXR	N410A	1167	1-4
5	Directional coupler, 10 dB coaxial	Narda	3042B-10	03049	0.92-2.2
6	Bidirectional coupler, 20 dB coaxial	Narda	3022	274	1-4
7	Device under test (DUT)	See report	-	-	-
8	Directional coupler, 30 dB coaxial	Narda	3002-30	759	0.95-2
9	Attenuator, fixed coaxial 10 dB pad unit	Narda	766-10	05743	DC-12
10	Bidirectional coupler, 20 dB cozxial unit	Narda	3022-20	274	0.95-4
11	Filter, bandpass variable preselector type	FEL	30D105500	F096007	2-4
12	Detector, low level sensitive crystal type	AEL	3101A	1128	DC-12

ITEM	NAME	MAKER	MODEL	SERIAL	BANDWIDTH
13	Attenuators, precision substitution type	HP	8492A	0482,1030, 1058	DC-18
14	Reflection test unit	HP	8741A	810-00313	0.1-2
15	Termination, matched 50 ohm coaxial unit	HP	908A	1	DC-12
16	Attenuator, variable calibrated coaxial unit	Merrimac	AU26A1NC1	212	2-12
17	Line stretcher, 50 ohm coaxial unit	GR	874-LK20	1	0.1-5
18	Short circuit, variable micrometer setting unit	Gen Micro-wave Corp.	N906-1	124	DC-12
19	Attenuator, variable calibrated coaxial unit	Microlab/ FXR	AV-90N	73	1-5
20	Hybrid, coaxial type 3 dB coupler	Narda	3032	653	0.95-2
21	Directional coupler, 10 dB coaxial unit	Narda	3042B-10	03045	0.92-2.2
22	Detector low level sensitive crystal type	AEL	3101A	1165	DC-12
23	Delay line, coaxial cable type	Lab made	-	-	DC-10
24	Termination, matched 50 ohm coaxial unit	HP	909A	132	DC-12
25	Thermistor mount	HP	478A	18510	0.01-12.4

ITEM	NAME	MAKER	MODEL	SERIAL	BANDWIDTH
26	Thermistor mount	HP	478A	18677	0.01-12.4
27	Power meter	HP	431B	451-05394	n.a.
28	Power meter	HP	431B	451-06467	n.a.
29	SWR meter, (used as selective amplifier)	HP	415D	331-00788	n.a.
30	XYY' recorder	Honeywell	540	1320B/F71	n.a.
31	Spectrum analyzer	HP	141T/8555A	-018431 -03947	.01-18
32	Oscilloscope	Tektronix	321	3077	n.a.
33	Helipot and mechanical coupling (500 ohms)	Lab made	-	-	n.a.
34	Power supply for helipot	Lambda	LH119AFM	G1788	n.a.
35	Power supply, dual regulated	Lambda	LPD-422A-FM	363007	n.a.
36	Power supply, dual regulated	Trygon	DL40-1	A67556	n.a.

APPENDIX 2

LIST OF ITEMS IN THE S-BAND BRIDGE ASSEMBLY

ITEM	NAME	MAKER	MODEL	SERIAL	BANDWIDTH
1	UHF signal generator	HP	616A	2234	1.75-4.25
2	PIN modulator	HP	8732A	502-00352	1.3-4.5
3	Directional coupler, 10 dB coaxial	Narda	3003-10	04090	2-4
4	TWT amplifier	Alto Scientific	20C2.0-4.0Q35	1387	2-4
5	Wavemeter, absorption type	HP	536A	331	1-4
6	Filter, bandpass coaxial type	HP	8431A	120	2-4
7	Hybrid, coaxial type 3 dB coupler	Narda	3033	583	2-4
8	Hybrid, coaxial type 3 dB coupler	Narda	3033	472	2-4
9	Attenuator, variable calibrated coaxial unit	Arra	3-6414-20	162	2-4
10	Directional coupler 20 dB coaxial	Narda	3003-20	08136	2-4
11	Directional coupler	Narda	3003-20	08132	2-4
12	Device under test (DUT)	See report	-	-	-

ITEM	NAME	MAKER	MODEL	SERIAL	BANDWIDTH
13	Directional coupler 30 dB coaxial	Narda	3003-30	1056	2-4
14	Reflection test unit	HP	8742A	740-00152	2-12.4
15	Attenuator, variable calibrated coaxial unit	Merrimac	AU26A1NC1	212	2-12
16	Short circuit, variable micrometer setting unit	Gen. Microwave Corp.	N906-1	124	DC-12
17	Termination, matched 50 ohm coaxial unit	HP	909A	77	DC-12
18	Directional coupler 10 dB coaxial unit	Narda	3044-10	09058	4-8
19	Attenuator, variable calibrated coaxial unit	Merrimac	AU26A1NC1	207	2-12
20	Hybrid, coaxial type 3 dB coupler	Narda	3034	80	4-8 (Coupling acceptable 2-11)
21	Switch, single pde six position coaxial type	TRW Electronics	CON6AB	H6511	2-12
22	Filter, bandpass coaxial type	HP	8431A	28	2-4
23	Filter, bandpass coaxial type	HP	8435A	21	4-8
24	Filter, bandpass coaxial type	HP	8436A	73	8-12

ITEM	NAME	MAKER	MODEL	SERIAL	BANDWIDTH
25	Delay line, coaxial cable type	Lab made	-	-	DC-12
26	Reflection test unit	HP	8741A	810-00168	0.1-2 (line stretcher usable to 5 GHz)
27	Termination, matched 50 ohm coaxial unit	HP	909A	132	DC-12
28	Directional coupler 20 dB coaxial unit	Narda	3003-20	08135	2-4
29	Attenuator, variable calibrated coaxial unit	Arra	4414-40	248	2-4
30	Directional coupler 10 dB coaxial unit	Narda	3003-10	10001	2-4
31	Attenuator, variable calibrated coaxial unit	Arra	3-6414-20	235	2-4
32	Directional coupler 20 dB coaxial unit	Narda	3003-20	8138	2-4
33	Attenuator, fixed coaxial pad unit	Narda	766-3	05006	DC-12
34	TWT amplifier	Alfred	562A	1522	4-8
35	Directional coupler, 30 dB coaxial unit	Narda	3045C-30	20018	7-12.4
36	Filter, high pass coaxial unit	Microwave Assoc.	F335-UPM	84	5-12.4

ITEM	NAME	MAKER	MODEL	SERIAL	BANDWIDTH
37	Directional coupler, 10 dB coaxial unit	Narda	3044B-10	03013	3.7-8.3
38	Filter, band separation coaxial unit	Melabs	X-122	2	4-12,4-7.5,7.5-12
39	Wavemeter, absorption type	FXR	N414A	263	3.95-11
40	Transmission test unit	HP	8740A	712-00467	DC-12.4
41	Directional coupler, 10 dB coaxial unit	Narda	3004-10	783	4-10
42	Attenuator, variable calibrated coaxial unit	Arra	3-6414-20	234	1-9
43	Hybrid, coaxial type 3 dB coupler	Narda	3035	09001	7-11
44	Termination, matched 50 ohm coaxial unit	Bird	80F	1807	DC-12
45	Attenuator, fixed coaxial pad unit 3 dB	Narda	766-3	04639	DC-12
46	Wavemeter, absorption type	FXR	N414A	315	3.95-11
47	S-parameter test unit	HP	8746B	1142A00257	0.5-12.4
48	Directional coupler, 10 dB coaxial unit	Narda	3004-10	782	4-10
49	Attenuator, variable calibrated	Microlab/ FXR	AJ-210N	4	0.25-8

ITEM	NAME	MAKER	MODEL	SERIAL	BANDWIDTH
50	Thermistor mount	HP	478A	18510	0.01-12.4
51	Thermistor mount	HP	478A	18677	0.01-12.4
52	Thermistor mount	PRD	N6284	264	0.01-12.4
53	Power meter	HP	431B	451-05394	n.a.
54	Power meter	HP	431B	451-06467	n.a.
55	Power meter	HP	431B	301-02685	n.a.
56	Pulse generator	Rutherford	B7F-S	F960	n.a.
57	Modulator	HP	8403A	523-00273	n.a.
58	Oscilloscope	HP	141A	620-00255	n.a.
59	Spectrum analyzer	HP	141T/8555A	-01843/ -03947	.01-18
60	Milliammeter, clip-on DC type	HP	428B	601-03750	n.a.
61	Power supply, dual regulated	Lambda	LPD-422A-FM	363007	n.a.
62	Power supply, dual regulated	Trygon	DL40-1	A67556	n.a.
63	Pulsed bias supply	Velonex	570	453	n.a.
64	Helipot and mechanical coupling (500 ohms)	Lab. made	-	-	n.a.
65	Power supply for helipot	Lambda	LH119AFM	G1788	n.a.
66	XYY' recorder	Honeywell	540	1320B/F71	n.a.

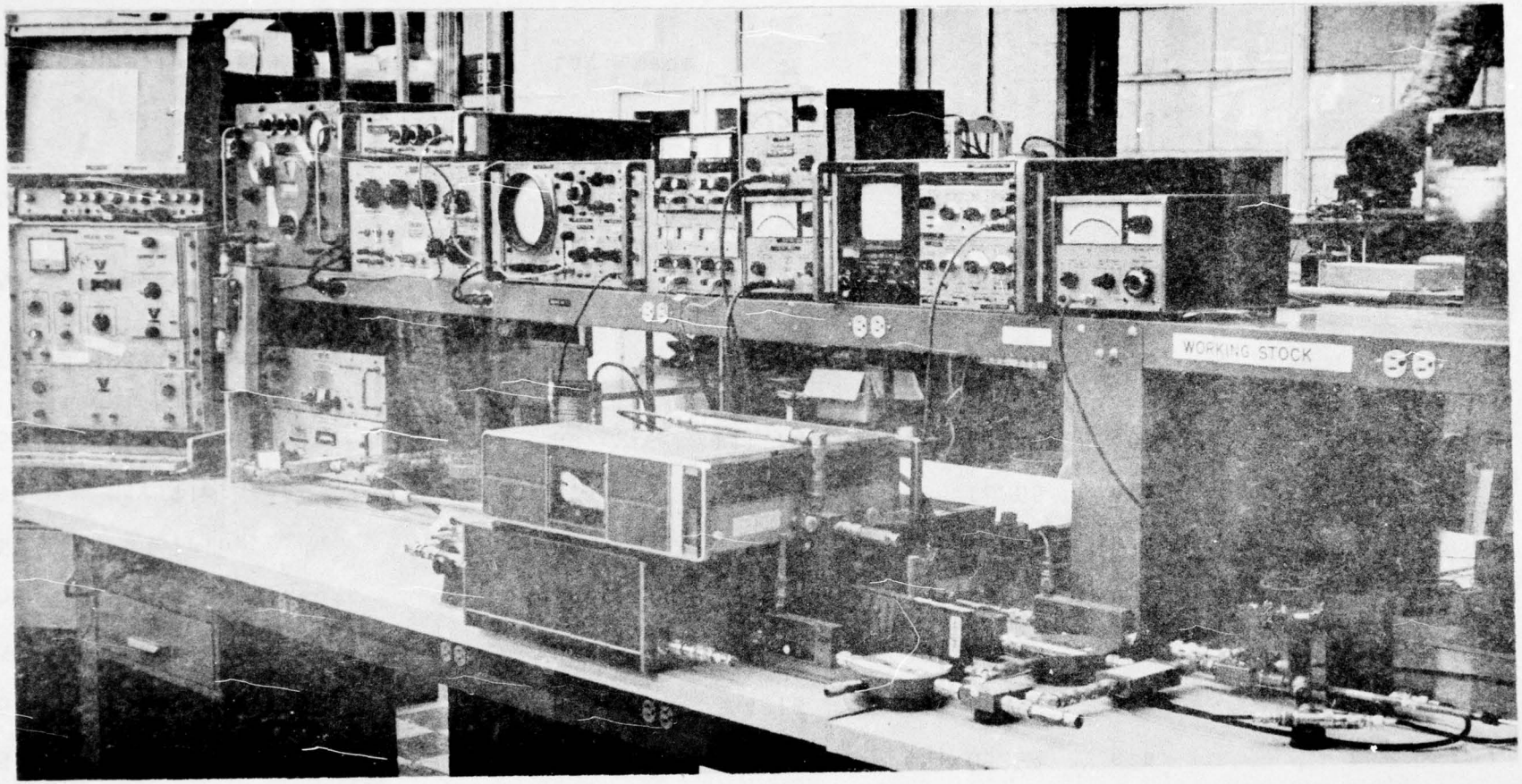

Figure A2.1 Photograph of S-band bridge assembly with harmonic balancing capability

AD-A032 130 SYRACUSE UNIV N Y DEPT OF ELECTRICAL AND COMPUTER E--ETC F/G 9/5
SOLID STATE ARRAY STUDIES RELEVANT TO OTP REGULATIONS. PART 1. --ETC(U)
AUG 76 D W GRIFFIN F30602-75-C-0121
UNCLASSIFIED RADC-TR-76-241-PT-1 NL

3 OF 3
AD
A032130

END

DATE
FILMED
1-77

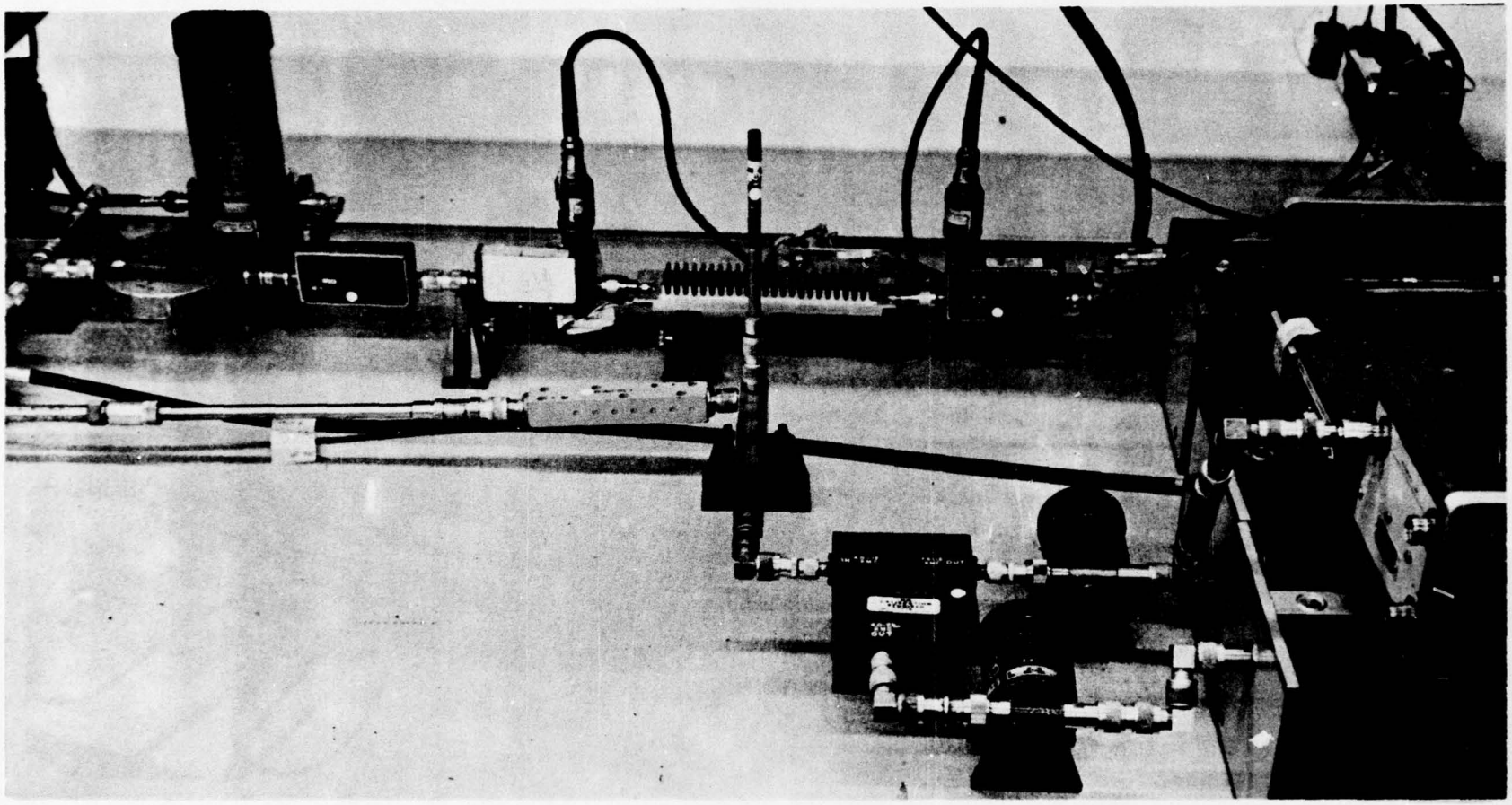

Figure A2.2 Photograph of S-band bridge assembly - the four paths, device under test, fundamental reference and second and third harmonic reference path

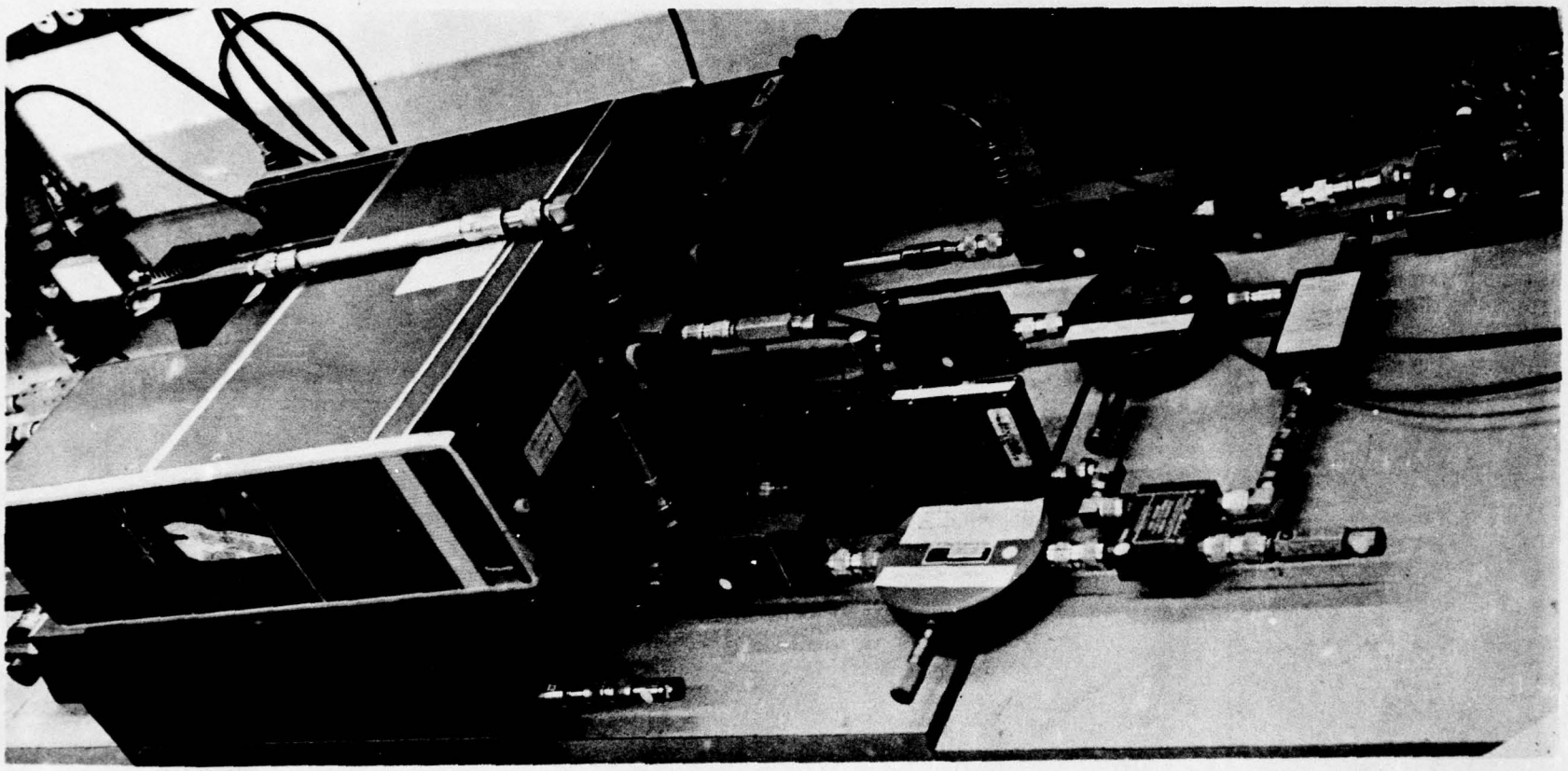

Figure A2.3 Photograph of S-band bridge assembly - balancing line stretchers and attenuators and signal combining arrangements

APPENDIX 3

Review of

MULTIPLE FREQUENCY EFFECTS

IN

IMPATT and TRAPATT

AMPLIFIERS

June 1975

Stephen T. Kowel

Department of Electrical and Computer Engineering
Syracuse University
Syracuse, N.Y. 13210

I. Introduction

Our purpose here is to survey the literature in order to determine what is known about multiple frequency effects in IMPATT and TRAPATT amplifiers operating in the GHz range. After a brief introduction concerning the nature of IMPATT and TRAPATT modes, we will review the nature of multiple frequency effects, and then offer some conclusions.

To begin with, most of the results that are described in the literature relate to idealized large signal computer simulations. Efforts to compare these results with experimental evidence is complicated by the great variability among devices obtained in spite of the best manufacturing efforts, the profound effect of mounting structures, and the great number of variables to be controlled.

Since its inception the avalanche diode, as a microwave device, has received a great deal of attention, and many significant advances have been made concerning power output, efficiency, frequency range, fabrication and evaluation techniques, and other properties.

Avalanche diodes have been fabricated so far in Si, Ge, and GaAs. Due to the basic phenomena involved in the generation of negative conductance in this device, almost any semiconductor material can, in principle, be employed for realizing an avalanche-diode oscillator. This results in a great deal of flexibility in the choice of a material as compared to the Gunn effect, for example, which is limited to a few materials. The desirable parameters which are important in determining the suitability of a particular material are the following:[1]

1) A high saturated drift velocity of the carriers
2) A high energy gap and low and equal ionization rates
3) A high thermal conductivity
4) Availability, reliability, and ease of forming a junction

It is therefore possible that other materials may be found which have a combination of properties which are more desirable than the three materials mentioned.

A great deal of flexibility also exists in the formation of a junction. Junction formation can be achieved through 1) diffusion, 2) Schottky barrier, 3) ion implantation, and 4) epitaxial growth.

II. Physical Explanation of IMPATT Diode Operation

An understanding of the dynamic operating characteristics of IMPATT diodes can be obtained best by considering the operation of a Read diode[1]. The structure, field distribution, and current waveforms for a reverse-biased Read diode are shown in Fig. 1. The Read diode consists of two regions: a narrow avalanche region (p-region) in which carrier multiplication by impact ionization occurs, and a drift region (intrinsic region) in which the carriers drift at saturated or field-independent velocities and where no impact ionization occurs.

The negative resistance or conductance of a Read diode is attributed to a phase shift between the current through the diode and the voltage across it. This phase shift consists of two components. There is a phase delay of the current caused by the avalanche multiplication process and by the finite transit time of the holes drifting through the drift region. The phase delay caused by the avalanche process results from the condition that the rate of generation of electron-hole pairs in the avalanche region is proportional to both the electric field and the density of electrons and holes that are already present. If a small RF voltage of sufficiently high frequency is assumed to be superimposed along with a dc voltage near breakdown across the

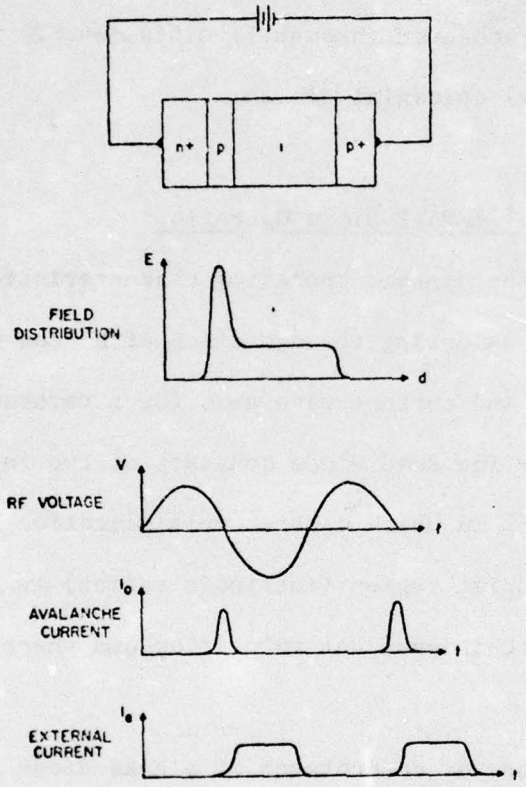

Fig. 1. Read-diode waveforms [1].

diode, the rate of generation of electron-hole pairs will exceed the rate at which the pairs leave the avalanche region. Thus both the density of carriers and the current will grow exponentially with time as long as the RF and dc voltages add to give a total field above breakdown. When the RF voltage changes sign and subtracts from the dc voltage, causing the field to fall below breakdown, the generation rate starts decreasing, causing the current to decrease. Thus the current generated by the avalanche process will have its maximum when the RF field goes through zero. Thus, as shown in Fig. 1, the avalanche process contributes a 90° inductive phase lag to the current generated in the avalanche region. This current is then injected into the drift region of the diode. The current induced in the external circuit by this charge, drifting through the drift region at a saturated drift velocity, is shown at the bottom of Fig. 1. Thus the fundamental component of the external current is more than 90° out of phase with the RF voltage causing the resistance or conductance of the diode to be negative. In order for the diode to operate as a stable oscillator, the negative conductance of the diode must decrease with increasing RF voltage. The RF voltage across the diode will grow until the admittance of the diode is balanced by the admittance of the diode mount and microwave circuit. The diode will oscillate at a frequency and RF voltage level where the diode admittance is equal and of opposite sign to the circuit admittance.

There are several important effects which must be included in this explanation. First, there is the effect of the space charge of the carriers. As mentioned previously, the current in the diode consists primarily of holes which will cause the electric field to decrease behind them and to increase in front of them as they drift across the drift region. As the holes are

generated in the avalanche region and injected into the drift region, they cause the field in the avalanche region to be depressed. The depression of the field by the space charge of the holes causes the field to drop below the breakdown level before the RF voltage does. Therefore, the phase lag of the current due to the avalanche process is decreased. If the RF voltage is held constant and the dc current is increased, which means the space charge in the diode is increased, the field in the avalanche region will drop below the breakdown level earlier in the cycle. Thus, the phase lag of the current will decrease with increasing dc current and constant RF voltage. Conversely, if the dc current is held constant but the RF voltage is increased the phase lag of the current is increased.

The additional phase delay needed for negative conductance is caused by the transit time of the holes. The effect of the transit time on the frequency range of operation can be easily understood by assuming that the current generated in the avalanche region is generated in a sharp pulse. The exact time in the cycle that this pulse is generated will be a function of the dc current and the RF voltage as discussed previously. For a given diode the transit time remains constant but the phase delay decreases with decreasing frequency. At a sufficiently low frequency the phase delay of the transit time plus the phase lag of the avalanche process are not sufficient to have the fundamental component of the external current lag the RF voltage by more than 90°. Therefore, below a certain cutoff frequency the conductance of the diode becomes positive. As can be seen from the effect of the RF voltage on the phase lag in the avalanche process, the conductance will be negative at lower frequencies for larger RF voltages. However, for these frequencies the diode will not be a self-starting oscillator since the small-signal conductance is positive. As the dc current is increased, the cutoff frequency is increased

due to the effect of the current on the phase lag in the avalanche process.

The Read diode is a convenient structure for analytical purposes and for obtaining a physical understanding of IMPATT diodes, but it is difficult to construct. The p-n junction is easier to fabricate but much more difficult to analyze. In the p-n junction the avalanche region and drift region are not separated, but rather carriers are generated while they are drifting through an appreciable portion of the diode. Also, both electrons and holes take part in the conduction process rather than just one type of carrier. Thus, it is not possible to separate the two phase-delay components as in the Read diode. However, the mechanisms causing the phase delay between the voltage and the current in IMPATT diodes are still the transit time and the avalanche process.

Small-signal results predict the range of current and frequency in which an IMPATT diode will oscillate if placed in the proper resonant circuit. These results also indicate the magnitude of the maximum negative conductance which can be generated by the diode. However, no data on power output, efficiency, and other important effects can be obtained since IMPATT diodes are nonlinear devices and the space-charge distribution under large-signal conditions is much different from the small-signal case.

A large-signal analysis was performed by Evans and Haddad[2] where, in addition to the assumptions made by Read, they assumed a small transit angle in the drift region. With this assumption they were able to obtain closed-form solutions for the equations and thus several important nonlinear properties of the device could be predicted, even though qualitatively, without resorting to extensive computer calculations. This model is also very well suited for studying self-oscillating frequency converters and other nonlinear phenomena which may otherwise be prohibitive to investigate with more exact analyses.

Blue[3] used a Read-type diode for a large-signal analysis in which the field in the avalanche region was independent of position and the space-charge effects within the avalanche region were neglected. The numerical techniques employed for solving the equations which were obtained by this analysis produced an efficient and inexpensive computer program. Results[4] of an analysis of this type for a Si Read diode in which the avalanche region is 1 μm wide and the drift region is 4 μm wide are shown in Fig. 2. The results show the effect of RF voltage on the admittance and the lower cutoff frequency. Scharfetter and Gummel[5] have developed a computer program for obtaining a numerical solution to the basic equations which govern the operation of the avalanche diode. They have attempted to make their model as exact as possible by including carrier generation and recombination due to impact ionization and defects, respectively, and the variation of mobility as a function of electric field and doping density. They have also assumed that these effects are not equal for both electrons and holes and have included the effect of the microwave circuit on the diode in which it is placed. Their program is presumed to give the most accurate and detailed solution for the large-signal operating characteristics of IMPATT diodes. However, the amount of computer time necessary for its execution is prohibitive for any detailed study of the effect of different diode parameters on its operating characteristics. A large-signal analysis was developed by Greiling et al[6], in which IMPATT diodes with any doping profile could be analyzed. Though not all of the physical parameters included by Scharfetter and Gummel were included in this analysis, it does give good physical results for the large-signal operating characteristics of IMPATT diodes. The amount of computer time required for execution is such that it is also possible to use the analysis to study the effect of different diode parameters on the operating characteristics.

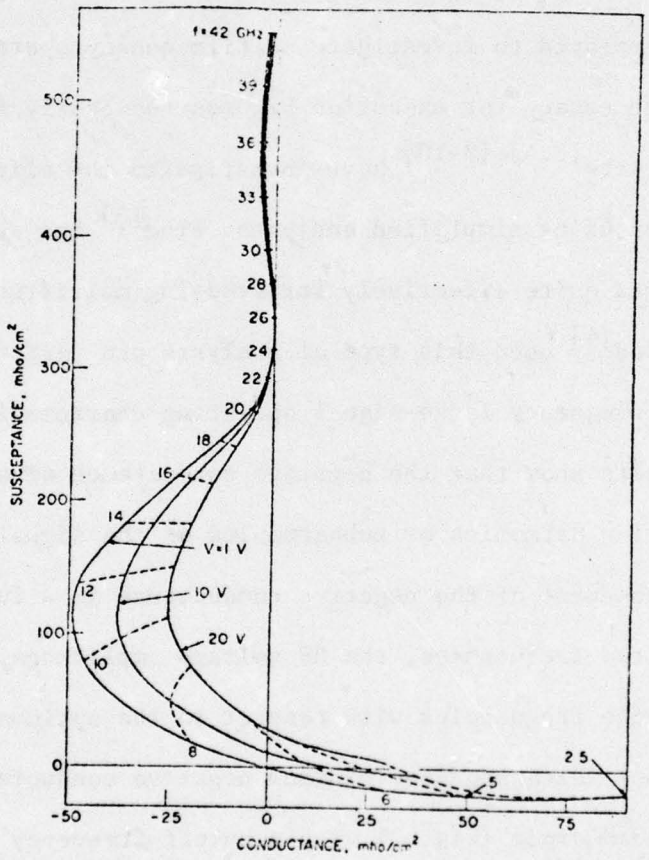

Fig. 2. RF admittance of a Si diode, $V_{RF} = V \sin \omega t$, $I_{dc} = 500$ A/cm^2; Schroeder and Haddad [4].

The results obtained from this analysis and a comparison with experimental results are presented in a recent paper[7].

III. Multifrequency Effects

Because of the broad-band negative resistance and the nonlinearities, IMPATT diodes operate under multifrequency as well as single-frequency conditions. Although the analyses of Scharfetter and Gummel[3] and Greiling and Haddad[7] can be employed to investigate multifrequency operation, the amount of computer time necessary for execution becomes too costly for a detailed study. Several workers[3,4],[8-10] have investigated the effect of multifrequency operation using simplified analyses. Blue[3] has shown that his analysis can be used quite effectively for studying multifrequency operation. Schroeder and Haddad[4] used this type of analysis and performed an extensive study of the multifrequency large-signal operating characteristics of Read diodes. These results show that the negative conductance of a Read diode can be enhanced by having harmonics or subharmonics of the signal frequency present. This enhancement of the negative conductance is a function of the phase between the two frequencies, the RF voltage amplitudes, and the relative value of the frequencies with respect to the optimum operating frequency (frequency which produces minimum negative conductance). It was shown that for a Read diode (Fig. 2) with a cutoff frequency around 7 GHz and an optimum operating frequency of 11 GHz, the diode could oscillate with significant output power at 5 GHz if a properly phased oscillation at 10 GHz were present. This is due to waveshaping of the RF voltage across the diode which causes an additional phase delay in the generation of the current in the avalanche process. Under single-frequency operation at 5 GHz the total phase delay of the avalanche process and the transit time is not enough for

the fundamental current to be more than 90° out of phase with the RF voltage. However, by adding the second harmonic of the signal frequency with the proper phase it is possible to generate a waveform which causes the RF field in the avalanche region to go through zero at a much later time in the cycle and thus increase the phase delay of the avalanche process. This additional phase delay is enough for the conductance to become negative. Therefore, the phase angle between the fundamental and harmonic RF voltages is an important parameter in determining the negative conductance of the diode. It was also shown that it is possible to degrade the performance of the diode with certain phase angles.

Figure 3 summarizes the results of this analysis for harmonic and subharmonic tuning. The power density is plotted as a function of frequency for two-frequency modes where the harmonic ratio is two and a single-frequency operation curve is plotted for comparison. The phase angle is chosen to provide maximum output power at the designated frequency while maintaining negative conductance at both frequencies. The single-frequency curve is dashed below 7 GHz because the small-signal conductance is positive there.

The curve labeled second-harmonic tuning shows the power output obtainable at the fundamental with an equal amplitude second harmonic present. The improvement is greatest at frequencies below the optimum transit-time frequency and it is possible to obtain power output comparable to and even slightly greater than that attained at the optimum single-frequency point. The second-harmonic tuning curve extends below the avalanche frequency, indicating that it is possible to obtain power from the diode at frequencies below the single-frequency operating range. However, for frequencies above the optimum 11 GHz the power improvement is small and for frequencies from

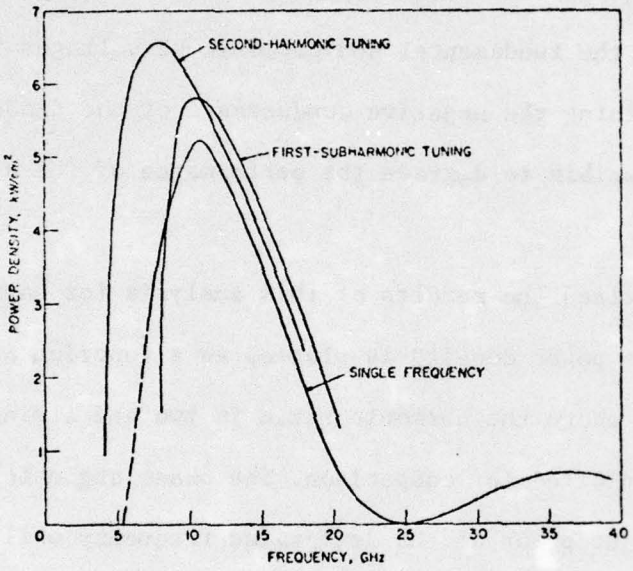

Fig. 3. Optimum power output for a Si Read diode under various operation conditions; $V_{RF} = 20 \sin(\omega_2 t + \Psi)$, $J_{dc} = 500$ A/cm^2; Schroeder and Haddad [4].

12 to 20 GHz better performance is obtained using first-subharmonic tuning.

The first subharmonic tuning curve shows that there is little improvement below 11 GHz, but that in the frequency range from 11 to 20 GHz some improvement can be obtained. In particular, at 20 GHz the improvement attainable is nearly 100 percent although the power is not so large as at the optimum single-frequency point. These results were also compared to more realistic diode structures and good agreement was obtained[11]. Also, these theoretical results were found to be in good agreement with experimental results reported by Swan[12].

IV. Basic Principles of Operation and Characteristics of the TRAPATT Mode

In 1967 Prager et al[13] observed experimentally high-efficiency operation of avalanche diodes under pulsed conditions. Due to the low frequency of operation (considerably less than the transit-time mode) and the 60-percent efficiency which was higher than IMPATT theory predicted, they referred to it as the "anomalous mode".

Using the experimental voltage waveforms of an oscillating Ge diode in a computer simulation, Scharfetter et al[14] developed a physical explanation and detailed description of this mode of operation. Their simulation showed that when the large-signal limits of IMPATT operation were exceeded, a low-frequency high-efficiency mode could exist.

In IMPATT operation, as the RF voltage increases, several effects limit the performance of this mode. First, the effect of a large space charge on the field in the drift region increases the field in front of the pulse high enough for impact ionization to occur. Also, for large space charge the field behind the pulse is depressed so that the drift velocity of some of the carriers will drop below saturation and will be trapped in this low-field region for a short time. Both the generation and trapping of carriers in the

drift region change the transit angle and degrade the performance of the diode. The space charge of the pulse will also depress the field in the avalanche region and decrease the phase delay produced by the avalanche process. This in effect also changes the transit angle and degrades the performance.

Scharfetter et al[14] showed that when these limits were exceeded by having a large RF voltage at the IMPATT frequency and large current densities, the following events occur. A large overvoltage at the IMPATT frequency (approximately twice the breakdown voltage) generates a large space charge in the avalanche region which depresses the field almost to zero behind it and increases it in front of the carriers to a high enough level to cause impact ionization. In Figure 4 the different waveforms are shown for an instant in time in the cycle. In Figure 4(a), the hole and electron current densities are large enough to reduce the field almost to zero at the left edge of the diode and increase it on the right to cause avalanching. This avalanche region or zone traverses the diode leaving behind it an electron-hole plasma trapped in the low field. The carriers in the diode which are moving at low-field-dependent velocities are then removed by space-charge-limited flow. In Figure 4(b) the terminal current and voltage are plotted. The large overvoltage due to the IMPATT oscillations is reduced to a small value as the avalanche zone traverses the diode and fills it with a plasma. The current which is almost all particle current during the low-field state is large, whereas as the plasma is removed the particle current is reduced and the terminal current becomes mostly displacement current. As is shown by the voltage and current waveforms, the current is large when the voltage is small and vice versa; thus, this current-voltage (I-V) relationship leads to a very efficient mode. For lower current densities it is possible for the

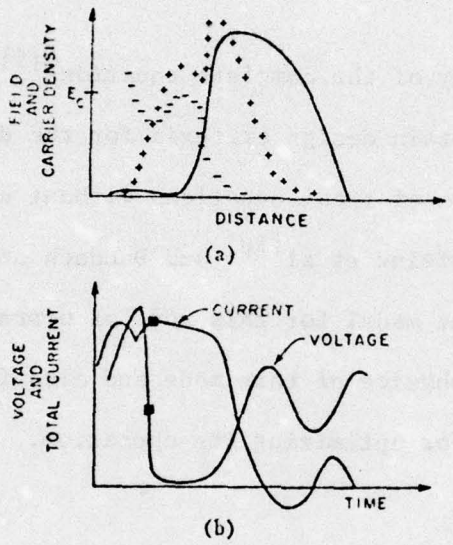

Fig. 4. TRAPATT waveforms. (a) Field and carrier density. (b) Terminal voltage and current, Evans [15].

avalanche zone not to travel through the entire length of the diode. This depends on the magnitude of the space-charge field and that due to the doping profile. Under these conditions the efficiency can be low (less than 1 percent) even though the diode is in the trapped-plasma avalanche triggered transit (TRAPATT) mode.

Because of the complexity of the complete equations[5] describing this mode it is not feasible to obtain design criteria for the diode or the circuit by a detailed solution of these equations without using a prohibitive amount of computer time. Clorfeine et al[16] and DeLoach and Scharfetter[17] developed a simple and elegant model for this mode of operation which is useful in understanding the physics of this mode and also for obtaining approximate design criteria for optimizing its operation.

V. Noise

Some representative data for FM noise performance of IMPATT oscillators are given in Figure 5 with that of an X-13 klystron for comparison. All data have been reduced to an equivalent 100-Hz bandwidth. The FM noise has been expressed as an rms frequency deviation, Δf_{rms}, in accordance with conventional practice. The rms frequency deviation is related to the FM noise power for small modulation index by the equation[18]

$$\Delta f_{rms} = f_m \frac{P_{SB}}{P_0}$$

where

P_{SB} = double sideband FM power

P_0 = the power of the oscillator

It should be noted in interpreting Figure 5 that the loaded Q factor of the oscillator affects noise performance. The following relation for the

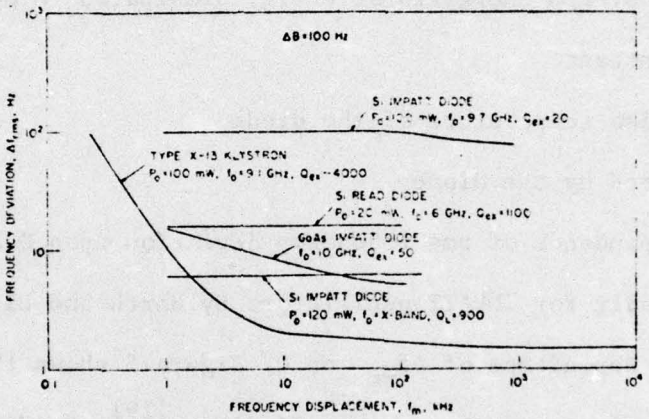

Fig. 5. Comparison of FM noise data for IMPATT-mode oscillators[1].

rms frequency deviation of a negative-conductance oscillator may be deduced from

$$\Delta f_{rms} = \frac{f_o}{Q_L} \quad \frac{kT(\Delta B)}{P}$$

where

Q_L = 2π times the stored energy/total energy dissipated in one cycle

k = Boltzmann Constant

T = Effective noise temperature of the diode

P = Power generated by the diode

The inverse dependence of rms frequency deviation upon Q has been verified experimentally for IMPATT oscillators by Harth and Ulrich[38]. Bearing in mind the dependence of Δf_{rms} on Q, Figure 5 shows that GaAs appears to be better in FM noise performance than Si diodes[19]. Ge diodes seem to be better in this respect than Si also[20], although the data are not shown in the figure since detailed results are not available.

Some representative AM noise data for IMPATT oscillators are given in Figure 6. The reported data have been reduced to double sideband noise-to-carrier ratios in a 100-Hz bandwidth. The effect of Q on AM noise is usually found to be much less important than for FM, especially for frequencies close to the carriers. For GaAs diodes operated at high current densities attained only under pulse bias especially low AM noise-to-carrier ratios are obtained, i.e. more than -145 dB at 1-MHz displacement[21].

There are circuit techniques for further reducing IMPATT oscillator noise which have been experimentally demonstrated. FM noise may be reduced by the use of a stalo cavity or by injection phase locking to a source which has low FM noise, while AM noise performance can be improved by optimizing the bias network impedance[1].

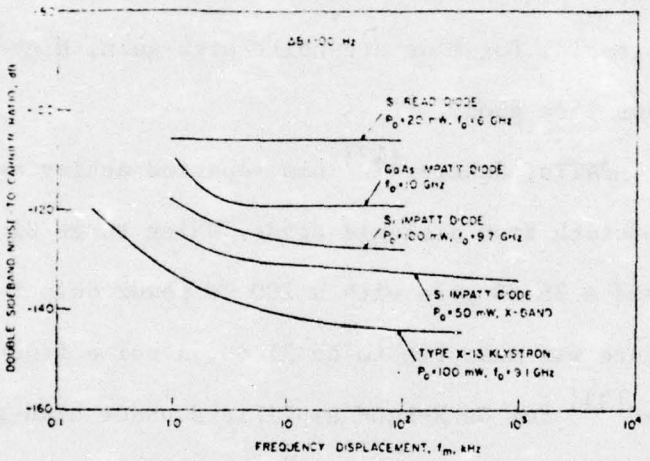

Fig. 6. Comparison of AM noise data for IMPATT-mode oscillators[1].

VI. IMPATT Amplifiers

IMPATT Diodes can also be employed in microwave amplifiers. IMPATT amplifiers have been realized in Si, Ge, and GaAs diodes using a circular-coupled reflection-type amplifier circuit. The saturated power output and dc to RF conversion efficiency at high drive levels are comparable to that obtained from the same diode operated as an oscillator. The noise figures currently reported for IMPATT amplifiers are in the range from 20 to 40 dB. While this type of noise performance may prohibit their use as low-noise preamplifiers, the potential for moderate-noise high-gain, high-power output amplifiers seems very good.

Using Si X-band IMPATTs, Scherer[22] has reported achieving a 13-dB gain over a 1-GHz bandwidth from a single diode. Using three Si diodes in cascade he has achieved a 36-dB gain with a 200-mW power output at 10 GHz. The overall noise figure was measured to be 31 dB. A noise figure of 30 dB has also been reported[23] for Ge X-band amplifiers under high-gain conditions; this is some 6 to 10 dB lower than that usually observed in Si diodes of similar structure.

A GaAs X-band amplifier has been reported by Baranowski et al[19] which gives small-signal gains of 10 to 30 dB with noise figures as low as 20 dB. Thus, at present, GaAs diodes used as amplifiers or oscillators provide better noise performance than Si diodes.

It has been demonstrated by Midford and Bowers[24] that an IMPATT diode can be fabricated for use as a traveling-wave amplifier, in contrast to the more conventional lumped negative-conductance reflection-amplifier approach. Several other schemes exist where discrete diodes may be employed for traveling-wave amplifier applications. These include coupled cavities, a loaded microstrip line on a ferrite substrate and a loaded slow-wave structure

or filter network.

Hoefflinger et al[25] reported amplification in the TRAPATT mode. They achieved this by tuning the amplifier circuit to establish a transit-time frequency oscillation and suppress all subharmonics; they then observed stable reflection gain at several of the subharmonics. At 1.3 GHz, a high-power gain of 12 dB resulting in a dc to RF conversion efficiency of 25 percent was observed[26].

Preliminary results for TRAPATT avalanche diodes indicate that the TRAPATT amplifier is quite noisy[1].

VII. Multifrequency and TRAPATT Oscillations

One circuit used to obtain CW oscillation in the TRAPATT mode employs a coaxial line, approximately 60 cm. long, with five tuning slugs, in which the diode is mounted[1]. The object in tuning is to place one slug close to the diode to tune the IMPATT frequency and use the remaining four slugs to form a low-pass filter located at approximately $\lambda/2$ of the TRAPATT frequency from the diode[27].

Several Ge diodes have been operated in the TRAPATT mode in this circuit and did display the TRAPATT mode but the maximum efficiency observed was 8 percent. Several other Ge diodes which were strongly punched through at breakdown exhibited the TRAPATT mode at much higher efficiencies.

When the TRAPATT mode was obtained, the spectrum analyzer displayed, in addition to the fundamental frequency (402.3 MHz), the second, third, and fourth harmonics. The relative magnitude of the harmonics, while always present, could be made comparable to that of the fundamental by altering the characteristics of the low-pass filter formed by the tuning slugs, but they were always present. In addition, probing the circuit between the diode and

the low-pass filter revealed the presence of transit-time range signals which were always harmonically related to the fundamental, for instance the 25th, 26th, and 27th harmonics[1].

It was noted that, for diodes which displayed the TRAPATT mode, the exact position of the tuning slugs was not critical to obtain the TRAPATT mode, although obtaining optimum efficiency required a moderate amount of tuning.

In addition to the simple harmonic generation effect, two other significant problems exist in TRAPATT oscillators[28]. One is "front end jitter", a random time delay between the application of diode current and the onset of rf oscillation. The jitter (which may be 40 nsec. or more) is thought to stem from the random nature of the inception of the IMPATT mode, which generally triggers the TRAPATT mode[28].

The other difficulty is "multimoding", a variation of up to 1 MHz in the frequency of oscillation. Often one of the modes will "break up", generating a burst of noise. This phenomena is highly temperature dependent. Careful tuning is thus essential to obtain "clean" results[28].

TRAPATT amplifiers for phased arrays have been developed recently[29]. They continue to suffer from many of the same problems (noise, multimoding, jitter, harmonics). Here the mounting structures (microstrip) are critical. Careful adjustment to control second and third harmonics is necessary to effect large gain[29], but these harmonics pose a problem in that they are undesirable in the radiated energy.

A recent review of the TRAPATT mode for oscillators and amplifiers reveals that these problems are somewhat less significant for use in amplifiers[30]. While these problems are circuit controllable, the variation from device to device is quite great, requiring careful tuning for each device.

VIII. Multifrequency Operation

Modes of multifrequency operation other than TRAPATT exist which are frequently observed. One such mode involves the presence of harmonic or subharmonic signals in the IMPATT frequency range. Such harmonics are almost unavoidably present in the large-signal operation of an avalanche diode in the IMPATT mode. Depending on the circuit impedance level at the harmonic frequency, the effect of the presence of harmonics on the fundamental frequency performance may be negligible, helpful, or deleterious as just discussed. The effect of harmonic tuning in the IMPATT mode was first observed experimentally by Swan[12] and has subsequently been studied by others[3,4,9,10,11,31].

Another kind of multifrequency operation results from the broadband negative conductance of an IMPATT diode. It is possible, depending on the circuit, to load the diode lightly at several different frequencies within the IMPATT range. When this occurs with small RF amplitudes, the nonlinearities of the avalanche diode resulting from the nature of the ionization process and from modulation of the depletion-layer capacitance (for nonpunch-through diode structures) cause frequency mixing to occur. The mixing properties open up a wide range of interesting applications. Avalanche diodes have been operated as self-oscillating frequency converters and parametric amplifiers[1].

An example of the sort of multifrequency oscillations attainable is shown in Haddad et al[1] of the X-band portion of the output spectrum of a nonpunch-through Si diode. The circuit used was the TRAPATT circuit described previously. Output power was measured at 255 MHz corresponding to an efficiency of about two percent. Signals were also present at the second, third, and fourth harmonics and also the ninth, tenth, and eleventh harmonics of 255 MHz.

The Z-band transit-time signals shown in the photograph were detected with a probe close to the diode followed by a 6.5 GHz high-pass filter. The photograph is somewhat deceptive since each signal frequency is represented several times due to mixing with different harmonics of the analyzer's local oscillator. Nevertheless, the X-band frequencies were carefully measured and found to consist of signals at 11.086 GHz $\pm$ n x 255 MHz, where n varies from zero to six. It was concluded that the mode is a complicated mixing phenomena, rather than TRAPATT, since the transit-time signals are not harmonically related to the ultra-high frequency (UHF) signal.

IX. Conclusions

Multiple frequency effects are quite profound in IMPATT and TRAPATT mode devices. Indeed, these are a family of such effects, such as harmonic generation, harmonic input tuning, multimoding and mode breakup, spurious noise, and jitter.

Recent work indicates that many of these effects can be minimized or indeed utilized in a controlled fashion, as in the case of harmonic input tuning. Except for the pure harmonic effects associated with the fundamental nonlinearities, the basis of the other effects is not well understood. These effects are not predicted by the computer models, and so are likely due to nonuniformities of temperature, charge densities and current densities.

While these problems remain, it will be hard to predict whether IMPATT and TRAPATT devices will be satisfactory from a number of design standpoints, especially the generation of low harmonic content. Because low harmonic content has not been an area of concern, little quantitative data can be found to offer firmer conclusions beyond the need for direct experimental effort on assembled subsystems.

REFERENCES

[1] G.I. Haddad, P.T. Greiling, and W.E. Schroeder, "Basic Principles and Properties of Avalanche Transit-Time Devices", IEEE Trans. on Microwave Theory and Techniques, vol. MTT-18, No. 11, pp. 752-772, November 1970.

[2] W.J. Evans and G.I. Haddad, "A Large-Signal Analysis of IMPATT Diodes", IEEE Trans. Electron Devices, vol. ED-15, pp. 708-717, October 1968.

[3] J.L. Blue, "Approximate Large Signal Analysis of IMPATT Oscillators", Bell Syst. Tech. J., vol. 48, pp. 383-396, February 1969.

[4] W.E. Schroeder and G.I. Haddad, "Effect of Harmonic and Subharmonic Signals on Avalanche-Diode Oscillator Performance", IEEE Trans. Microwave Theory Tech. (Correspondence), vol. MTT-18, pp. 327-331, June 1970.

[5] D.L. Scharfetter and H.K. Gummel, "Large-Signal Analysis of a Silicon Read Diode Oscillator", IEEE Trans. Electron Devices, vol. ED-16, pp. 64-77, January 1969.

[6] P.T. Greiling, G.I. Haddad, and R.J. Lomax, "Large-Signal Analysis of Avalanche-Diode Oscillators with Various Doping Profiles and Materials", presented at the IEEE Device Res. Conf., Rochester, N.Y., June 1969.

[7] P.T. Greiling and G.I. Haddad, "Large-Signal Equivalent Circuits of Avalanche Transit-Time Devices", IEEE Trans. Microwave Theory Tech., vol. MTT-18, No. 11, pp. 842-853, November 1970.

[8] B. Hoefflinger, "Recent Development on Avalanche Diode Oscillators", Microwave J., vol. 12, pp. 101-115, March 1969.

[9] C.A. Brackett, "Characterization of Second-Harmonic Effects in IMPATT Diodes", presented at the Avalanche Diode Workshop, New York, N.Y., December 1969.

[10] K. Mouthaan, "Two-Frequency Operation of the Avalanche Transit-Time Oscillator", Proc. IEEE (Letters), vol. 58, pp. 510-512, March 1970.

[11] W.E. Schroeder, "Nonlinear Properties of IMPATT Devices", RADC-TR-72-267, October 1972. **AD# 751974.**

[12] C.B. Swan, "IMPATT Oscillator Performance Improvement with Second-Harmonic Tuning", Proc. IEEE (Letters), vol. 56, pp. 1616-1617, September 1968.

[13] H.J. Prager, K.K.N. Chang, and S. Weisbrod, "High-Power High-Efficiency Silicon Avalanche Diodes at Ultra High Frequencies", Proc. IEEE (Letters), vol. 55, pp. 586-587, April 1967.

[14] D.L. Scharfetter, D.J. Bartelink, H.K. Gummel, and R.L. Johnston, "Computer Simulation of Low-Frequency High-Efficiency Oscillation in Germanium", presented at the IEEE Solid-State Device Res. Conf., Boulder, Colo., June 1968.

[15] W.J. Evans, "Circuits for High-Efficiency Avalanche-Diode Oscillators", IEEE Trans. Microwave Theory Tech., vol. MTT-17, pp. 1060-1067, December 1969.

[16] A.S. Clorfeine, R.J. Ikola, and L.S. Napoli, "A Theory for the High-Efficiency Mode of Oscillation in Avalanche Diodes", RCA Rev., vol. 30, pp. 397-422, September 1969.

[17] B.C. DeLoach, Jr., and D.L. Scharfetter, "Device Physics of TRAPATT Oscillators", IEEE Trans. Electron Devices, vol. ED-17, pp. 9-21, January 1970.

[18] M. Schwartz, Information Transmission, Modulations, and Noise. New York: McGraw-Hill, 1959.

[19] J.J. Baranowski, V.J. Higgins, C.K. Kim, and L.D. Armstrong, "Gallium Arsenide IMPATT Diodes", Microwave J., vol. 12, pp. 71-76, July 1969.

[20] R.L. Rulison, G. Gibbons, and J.G. Josenhaus, "Improved Performance of IMPATT Diodes Fabricated from GE", Proc. IEEE (Letters), vol. 55, pp. 223-224, February 1967.

[21] P.A. Levine, "Ultralow Noise in Pulsed GaAs Avalanche Diode Oscillators", Proc. IEEE (Letters), vol. 58, pp. 494-495, March 1970.

[22] E.F. Scherer, "A Multistage High-Power Avalanche Amplifier at X Band", IEEE J. Solid-State Circuits, vol. SC-4, pp. 396-399, December 1969.

[23] E.F. Scherer, "Investigations of the Noise Spectra of Avalanche Oscillators", IEEE Trans. Microwave Theory Tech., vol.MTT-16, pp. 781-788, September 1968.

[24] T.A. Midford and H.C. Bowers, "A Two-Port IMPATT Diode Traveling-Wave Amplifier", Proc. IEEE (Correspondence), vol. 56, pp. 1724-1725, October 1968.

[25] B. Hoefflinger, C.P. Snapp, and L.A. Stark, "High-Efficiency Avalanche-Resonance Pumped Amplification", Electron. Lett., vol. 5, pp. 43-45, February 1969.

[26] B. Hoefflinger, C.P. Snapp, and L.A. Stark, "High-Efficiency Avalanche-Resonance Pumped Amplification", IEEE J. Solid-State Circuits, vol. SC-4, pp. 391-395, December 1969.

[27] D.E. Iglesias and W.J. Evans, "High-Efficiency CW IMPATT Operation", Proc. IEEE (Letters), vol. 56, p. 1610, September 1968.

[28] A.S. Clofeine and H.J. Prager, "High Power TRAPATT Devices", AFAL-TR-72-251, September 1972. AD# 905566L.

[29] M.I. Grace, C.N. Potter, H. Kroger, and H.J. Pratt, "TRAPATT Amplifier for Phased Arrays", RADC-TR-73-409, February 1974. AD# 777602/4GI.

[30] W.R. Curtice and J.J. Risco, "High-Power High Efficiency Sources", AFAL-TR-74-190, August 1974.

[31] T.P. Lee and R.D. Standley, "Frequency Modulation of a Millimeter-Wave IMPATT Diode Oscillator and Related Harmonic Generation Effects", Bell Syst. Tech. J., vol. 48, pp. 143-161, January 1969.